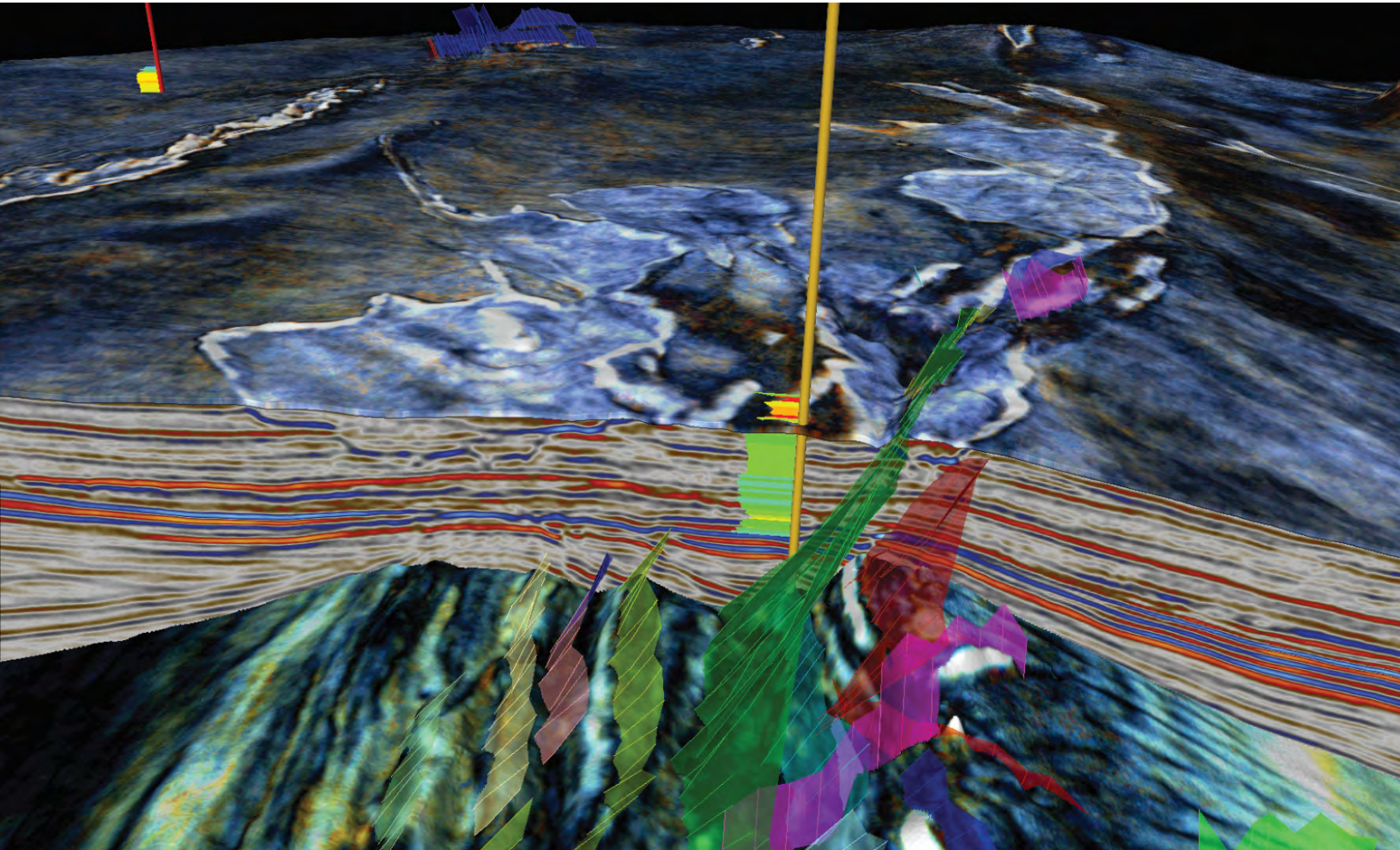


Technical University of Denmark

Department of Civil Engineering



Integrated seismic geomorphological analysis of syn- and post-depositional fluid migration features in the Chalk Group of the Danish North Sea

Doctoral thesis

April 2018

Florian W.H. Smit

Integrated seismic geomorphological analysis of syn- and post-depositional fluid migration in the
Chalk Group of the Danish North Sea

A dissertation presented
by
Florian Walther Harald Smit
to
The Department of Civil Engineering
in partial fulfilment of the requirements
for the degree of
Doctor of Philosophy
in the subject of
Geology

Technical University of Denmark
Kongens Lyngby, Denmark

April 2018

PhD thesis

University:	Technical University of Denmark (DTU)
Name of department:	Department of Civil Engineering / Centre for Oil and Gas – DTU
Author:	Florian W.H. Smit
Title:	Integrated seismic geomorphological analysis of syn- and post-depositional fluid migration in the Chalk Group of the Danish North Sea
Subject description:	This thesis deals with documenting and predicting seismic-scale chalk facies for reservoir characterization and exploration purposes, based on integration of seismic geomorphology, geochemistry, and petrography.
Academic advisor	Dr. Mikael Lüthje
External advisors	Prof. Lars Stemmerik (Copenhagen University) Dr. Frans van Buchem (Maersk Oil and Gas / Halliburton)
Submitted:	30/4/2018
Cover illustration	First documentation of seismic-scale diagenetic geobodies in the Chalk Group. This example occurs above the Ryan Anticline in the southernmost Danish Central Graben, and illustrates the integrated seismic geomorphological methodology. From Smit <i>et al.</i> (2018)



Remember to look up at the stars and not down at your feet.

Try to make sense of what you see and wonder about what makes the universe exist.

Be curious. And however difficult life may seem, there is always something you can do and succeed at.

It matters that you don't just give up.

– Stephen Hawkins

Acknowledgements

I would like to thank several people who made this PhD project possible and successful. First of all, my supervisors Lars Stemmerik, Mikael Lüthje, and Frans van Buchem for providing academic guidance and technical discussions throughout the project that facilitated interesting new insights in chalk. Frans is specially thanked for helping design the project during my employment at Maersk Oil and Gas (now Total), and Lars for helping to host this PhD at the then newly formed Danish Hydrocarbon Research and Technology Centre (DHRTC). Mikael is specially thanked for guiding and supporting through the administrative part of the PhD. Fellow colleagues at DHRTC (Michael Welch, Jesper Holst, Solomon Seyum, Frederick Amour, and Lars Simonsen) are kindly thanked for interesting technical discussions. Kresten Anderskov and Nicolas Thibault at Copenhagen University are kindly thanked for their collaboration.

Colleagues at Total are kindly thanked for always interesting technical discussions, for sharing insights, and for providing the opportunity to present the work, which helped to materialize the ideas further. Warm thanks go out to Peter Hillock, Govert Buijs, Niels Schødt, Ingelise Schmidt, Anette Uldall, Andrew Hoover, Katherine Lauriks, Peter Gelting, and Michael Hertle. Thomas Blume is kindly thanked for providing access to the SEM facility at Baltikavej.

Peter Swart and Gregor Eberli are greatly thanked for providing the opportunity to do clumped isotope analysis on chalks at the Stable Isotope Laboratory (SIL) at the Rosenstiel School of Marine and Atmospheric Sciences (RSMAS), University of Miami. These six months of working together in the Laboratory, having interesting technical discussions, and being part of the SIL staff, was a real personal and academic highlight. Philip Staudigel is especially thanked for his patience and guidance with the seismic interpreter who wanted to do clumped isotope analysis. Amel Saied, Sevag Mehterian, Sharm Giri, Megan Smith, and Evan Moore (RSMAS) are all thanked for their warm welcome.

I like to thank my family in the Netherlands (Jaap, Tineke, Esther, and grandmas Tjaaktje Scholte and Jitske Lotterman) for their support and patience with their ‘lost (grand)son’ abroad. You’ll see more of me now, I promise.

Finally, this PhD would not have been successful without my dearest Ellen Keerd, who not only kept my mind sane during these busy years and provided a cosy place to call home, but also continuously inspired me to optimism, and to create and execute initiatives. “Everything is possible. The first step is to establish that something is possible, then probability will occur” – Elon Musk. That’s the spirit! Suur aitäh Ellen!

English summary

Integrated seismic geomorphological analysis of the Upper Cretaceous and Lower Paleocene Chalk Group of the Danish Central Graben has led to critical new insights into seismic-scale heterogeneities related to syn-sedimentary fluid/gas and/or post-burial migration of fluids, and improved the understanding of the multi-phased fluid migration history. The thesis consists of one published article, two submitted manuscripts, and one manuscript in preparation for submission. A summary is given in the synopsis chapter.

Integration is achieved both in terms of scales and disciplines by combining seismic geomorphology, stratigraphy, petrophysics, petrography, and geochemistry (including clumped isotope analysis), to seismic chalk facies. Seismic geomorphology provides palaeoreconstructions of the seafloor from 3D seismic data, which then act as a spatial context for integration with well data. For the first time, clumped isotope analysis is applied to chalk from the North Sea Basin to study closed- and open-system diagenesis in relation to seismic-scale heterogeneities.

The aim of the integrated methodology is to arrive at a geological understanding of seismic-scale features observed on the palaeoseafloors. By interpreting a 'stack' of palaeoseafloor reconstructions, interlinkage between geological features might be present, which shines light on the geological evolution within the area of interest. This prepares for integration with other basin-scale trends, such as tectonic evolution and thermal maturity of major source rocks. We call this approach integrated seismic geomorphology, and have applied it to the Chalk Group. Though based on geophysical, petrophysical, petrographical, and geochemical data, the geological interpretation of the features forms the backbone of the methodology.

Key results of this thesis are (a) the revision of the 'Seismic Chalk Paradigm' in terms of the nature and origin of the seismic heterogeneities observed in the chalk, and (b) a much improved

understanding of the phased migration of basin fluids and their impacts on the chalk deposits.

The seismic chalk paradigm is subdivided into two main categories: 1) syn-depositional features and processes; 2) post-depositional features and processes. The syn-depositional features include the previously known pelagic chalks (1.A), bottom current activity features (1.B), and slope failure (1.C). With this study, we add seismic-scale gas venting features that form as a result of explosive releases of gas-bearing fluids (giant and mega pockmarks, 1.D1), and from seepage (seep carbonates, 1.D2). These features are described in depth in *Chapter III and IV (Papers 2 and 3)*. The gas venting features occur on top of inverted Campanian structures that formed the highest parts of the Late Cretaceous basin, are underlain by inverted deeply rooted Late Jurassic faults, which offset large successions of organic-rich mudstones. These features thus reflect syn-depositional fluid expulsion episodes during chalk deposition, and point to the interlinkage between basin morphology, faults, and source rock maturity.

The post-depositional features include known but refined faulted/fractured chalks (2.A), and the addition of seismic-scale diagenetic geobodies (2.B). These features are described in depth in *Chapter II (Paper 1)*. A combination of recently developed methods of image processing of seismic data and swarm intelligence made it possible to visualize near sub-seismic faults and fractured zones. Secondly, by integrating petrographic and geochemical proxies, seismic-scale diagenetic geobodies have been recognized for the first time in the Chalk Group. The extent and 3D architecture of the geobodies are controlled by contrasts in permeability/porosity and reflect the occurrence of formation tops, and feeder fault system. It therefore provides important new insights in fluid migration pathways through the Chalk Group.

Clumped isotope analysis (*Chapter V, Paper 4*) revealed that most chalks show a positive correlation between precipitation temperature and fluid $\delta^{18}\text{O}$ value (increasing with temperature), which reflects the preferential uptake of the lighter ^{16}O into the crystal lattice with increasing temperature, while

the heavier ^{18}O remains in the formation fluid. It is interpreted to reflect closed-system diagenetic behaviour (c.f. Swart *et al.* 2016). Outliers that are anomalously hot and have negative $\delta^{18}\text{O}$ values, are interpreted to reflect open-system diagenetic behaviour, and occur in veins and in surrounding narrow zones of high permeability and porosity, such as in fault damage zones. These data, coupled to seismic geomorphological palaeoreconstructions, provide important insights in the fluid migration history and diagenesis within the Chalk Group. It shows that most of the chalk experienced normal burial diagenesis, even in areas where extra-formational fluids migrated. Given the extremely low matrix permeability of chalk it is not a huge surprise that most diagenesis is in closed systems and open-system diagenesis is limited to narrow zones along high permeability fairways and areas with high pressure gradients.

Apart from the stratigraphic variation, the geographical variation in the expression of these venting events has also been documented. A predictive model is proposed that explains the occurrence or absence of gas venting features and seismic-scale diagenesis, based on basin-wide source rock potential and maturity. Gas venting features occur on Late Cretaceous basinal highs (dictated by Campanian inversion) where thermogenic and/biogenic sources for gas-bearing fluids were present, as well as inverted Late Jurassic faults. Seismic-scale diagenesis occurred on highs with limited source rock potential, where instead pressurized basinal fluids migrated through the chalk when seal integrity was compromised.

The expulsion events predate thermal maturity of the main prolific source rock (e.g. Bo Member of the Farsund Formation), and therefore thermogenic sources consisted of Lower-Middle Jurassic mudstones and coals, and lower parts of the Farsund Formation. Only biogenic gas was generated from the upper parts of the Farsund Formation. The areas where these features occur show large overlap

with present-day hydrocarbon accumulations (with expulsion from the Bo Member), and therefore indicate that fluid migration pathways have been re-used and were long-lived.

The insights from this study have important applications in exploration and production of hydrocarbons, and for future well planning. Firstly, the occurrence of syn-depositional fluid expulsion features overlap with present-day hydrocarbon accumulations, and thus directly reflect both long-lived source rock maturity, and fluid migration pathways. Depending on the basin maturity history and emplacement of an integer seal, gas venting features point to areas that potentially hold hydrocarbon accumulations. Secondly, understanding the lithological variability within a pockmarked hydrocarbon reservoir is of key importance for increasing sweep and recovery, by optimizing reservoir models, and for planning future well trajectories.

In conclusion, integrated seismic geomorphology is a powerful tool that aims at understanding seismic reflectors as a result of a stack of buried seafloors, rather than a pure geophysical signal. It provides a spatial framework to other types of data, and helps to more intuitively establish geological models for seismic-scale heterogeneities. The methodology integrates seismic data, petrography, and geochemistry, and has led to the first recognition of giant and mega pockmarks, seep carbonates, and importantly, also seismic-scale diagenesis in the Chalk Group.

We have shown that the basin-wide spatial distribution of syn-depositional and post-depositional processes occurring in the Chalk Group, to a large extent, is controlled by the tectonic evolution, basin morphology, and source rock maturity. These insights have thus important implications for other chalk reservoirs in the North Sea, and could lead to re-evaluation of established exploration ideas and reservoir models.

Dansk resumé

Integreret seismisk geomorfologisk analyse af Øvre Kridt og Nederste Palæocæn Kridtgruppe i den danske Central Graben har ført til vigtig ny viden om heterogeneitet på seismisk skala af oprindelsen til enten synsedimentvæske-/gasmigration og/eller migrerende væske efter begravelse, der er forbundet med en bedre forståelse af den flerfasede væskemigrationshistorie. Afhandlingen består af en offentliggjort artikel, to indsendte manuskripter og et manuskript som forberedelse til indsendelse. Der er et resumé i synopsiskapitlet.

Integration er opnået både i form af skalaer og discipliner ved anvendelse af en kombination af seismisk geomorfologi, stratigrafi, petrofysik, petrografi samt geokemi (herunder klumpet isotopanalyse) på seismiske kridtfacies. Seismisk geomorfologi giver palæorekonstruktioner af havbunden ud fra seismiske 3D-data, som derefter fungerer som en rumlig kontekst for integration med borehulsdata. For første gang anvendes klumpet isotopanalyse på kridt fra Nordsøbassinet til at studere lukket og åben systemdiagenese i forhold til heterogeneitet på seismisk skala.

Formålet med metoden er at nå frem til en geologisk forståelse af særpræg på seismisk skala, der observeres på palæohavbundene. Ved at fortolke en "stak" af palæohavbundsrekonstruktioner kan der være en sammenhæng mellem geologiske særpræg, der belyser den geologiske udvikling inden for interesseområdet. Dette forbereder integration med andre tendenser på bassinskala, såsom den tektoniske evolution, forkastningsmønster og termiske modenhedsdata fra vigtige kildebjergarter. Vi kalder denne tilgang for integreret seismisk morfologi, og den er blevet anvendt på Kridtgruppen. Selvom den geografiske fortolkning af særprægene er baseret på geofysiske, petrofysiske, petrografiske og geofysiske data, udgør den kernen i metoden.

De vigtigste resultater af denne afhandling er (a) revisionen af det "seismiske kridtparadigme" med hensyn til arten og oprindelsen af den seismiske heterogeneitet, der observeres i kridtet, og (b) en langt bedre forståelse af den gradvise migration af

bassinvæsker og deres indvirkning på kridtaflejringerne.

Det seismiske kridtparadigme er underinddelt i to hovedkategorier: 1) syn-depositionelle særpræg og processer; 2) post-depositionelle særpræg og processer. De syn-depositionelle særpræg omfatter de tidligere kendte pelagiske kridt (1.A), nederste nuværende aktivitetssærpræg (1.B) og skråningsskred (1.C). Med denne undersøgelse tilføjer vi gasventilerende særpræg på seismisk skala, der dannes som følge af eksplosive udslip af gasbærende væsker (gigantiske og megastore kopar, 1.D1) og fra udsivning (udsivende karbonater, 1.D2). Disse særpræg er indgående beskrevet i *kapitel III og IV (artikel 2 og 3)*. Under de gasventilerende særpræg, som forekommer på toppen af omvendte Campanianstrukturer, der dannede de højeste dele af det Sene Kridtbassin, ligger omvendte, dybt rodfæstede Sene Juraforkastninger, der udligner store rækker af organisk rige slamsten. Disse særpræg afspejler således syn-depositionelle væskeuddrivningsepisoder under kridtaflejring og peger på sammenhængen mellem bassinmorfologi, forkastninger og kildebjergartens modenhed.

Post-depositionelle særpræg omfatter kendt, men raffineret forkastet/brudt kridt (2.A) og tilsætning af diagenetiske signaturer på seismisk skala (2.B). Disse særpræg er nærmere beskrevet i *kapitel II (artikel 1)*. En kombination af nyudviklede metoder til billedbehandling af seismiske data og sværminelligens gjorde det muligt at visualisere næsten sub-seismiske forkastninger og brudte zoner. Integrationen af petrografiske og geokemiske substitutter har for det andet betydet, at diagenetiske signaturer på seismisk skala for første gang er blevet genkendt i Kridtgruppen. Signaturernes omfang og 3D-arkitektur styres af kontraster i permeabilitet/porøsitet og afspejler forekomsten af bjergartstoppe og feeder-forkastningssystem. Den giver derfor vigtig ny viden om væskemigrationsveje gennem Kridtgruppen.

Klumpet isotopanalyse (*kapitel V, artikel 4*) viste, at det meste kridt har en positiv korrelation mellem nedbørstemperatur og væskeværdi $\delta^{18}\text{O}$ (stigende med temperaturen), hvilket afspejler den

præferentielle optagelse af den lettere ^{16}O i krystalgitteret i takt med stigende temperatur, mens den tungere ^{18}O forbliver i bjergartsvæsken. Den fortolkes således, at den afspejler diagenetisk adfærd i lukkede systemer (jf. Swart *et al.* 2016). Blotninger, der er unormalt varme og har negative $\delta^{18}\text{O}$ værdier, fortolkes, som om de afspejler diagenetisk adfærd i åbne systemer og forekommer i årer og i omgivende snævre zoner, der er begrænset til høj permeabilitet og porøsitet, såsom i områder beskadiget af forkastninger. Disse data, koblet til seismiske palæorekonstruktioner, giver vigtig viden om væskemigrationshistorikken og -diagenesen i Kridtgruppen. Det viser, at det meste af kridtet oplevede normal begravelsesdiagenese, selv i områder med migration af væsker uden for bjergarterne. I betragtning af kridts ekstremt lave matrixpermeabilitet er det ikke en stor overraskelse, at det meste af diagenesen sker i lukkede systemer, og at diagenesen i åbne systemer er begrænset til smalle zoner langs baner med høj permeabilitet og områder med højtryksgradienter.

Bortset fra den stratigrafiske variation er den geografiske variation i disse ventilationsepisoder udtryk også blevet dokumenteret. En prædiktiv model foreslås, der forklarer forekomsten eller fraværet af gasventilerende særpræg og diagenese på seismisk skala, baseret på potentialet og modenheten af kildebjergarten i hele bassinet. Gasventilerende særpræg forekommer i Sene Kridt-bassin-højder (dikteret af Campanian-inversion), hvor termogeniske og/biogene kilder til gasbærende væsker var til stede, samt inverterede Sene Jura-forkastninger. Diagenese på seismisk skala forekom i højder med begrænset kildebjergartspotentiale, hvor bassinvæsker under tryk i stedet migrerede gennem kridtet, når forseglingsintegritet blev kompromitteret.

Uddrivningsepisoderne går forud for den termiske modenhed af den væsentligst forekommende kildebjergart (f.eks. Bo Member i Farsund Formation), og derfor bestod termogeniske kilder af Nedre-Midt Jura slamsten og kul, og lavere dele af Farsund Formation. Der blev kun genereret biogen gas fra de øvre dele af Farsund Formation. De

områder, hvor disse særpræg forekommer, udviser store overlapninger med nuværende kulbrinteakkumuleringer (med uddrivning fra Bo Member), hvilket derfor tyder på, at væskemigrationsveje er blevet genbrugt og har holdt længe.

Viden fra denne undersøgelse har vigtige anvendelsesmuligheder inden for efterforskning og produktion af kulbrinter samt for planlægning af fremtidige borehuller. For det første overlapper forekomsten af syn-depositionelle særpræg nutidens kulbrinteakkumuleringer og afspejler dermed direkte både langlivede kildebjergarters modenhed og væskemigrationsveje. Afhængigt af bassinets modenhedshistorik og anbringelsen af en hel forsegling peger gasventilerende særpræg på områder, der kan indeholde kulbrinteakkumuleringer. For det andet er forståelse af den lithologiske variabilitet i et koparret kulbrintereservoir af afgørende betydning for at øge scanning og udvinding ved at optimere reservoirmodeller samt til planlægning af fremtidige borehulsbaner.

Afslutningsvis er integreret seismisk morfologi et stærkt værktøj, der har til formål at forstå seismiske reflektorer som følge af en stak af begravede havbunde og ikke som et rent geofysisk signal. Det giver en rumlig sammenhæng for andre typer data og hjælper til en mere intuitiv etablering af geologiske modeller for heterogeneitet på seismisk skala. Metoden forener seismiske data, petrografi og gemokemi på en stærk måde og har ført til den første genkendelse af gigantiske og megastore kopar, udsivende karbonater, og hvad der er vigtigt, desuden diagenese på seismisk skala i Kridtgruppen.

Vi har vist, at den rumlige fordeling af syn-depositionelle og post-depositionelle processer på tværs af bassinet, der forekommer i Kridtgruppen, sandsynligvis og i høj grad er styret af den tektoniske udvikling, bassinmorfologi og kildebjergartens modenhed. Denne viden har således vigtige konsekvenser for andre kridtreservoirs i Nordsøen og kan medføre en revurdering af etablerede efterforskningsideer og reservoirmodeller.

Publications in this thesis

Included manuscripts:

Paper 1 (Chapter II).

- **Smit, F. W. H.**, van Buchem, F. S. P., Holst, J. H., Lüthje, M., Anderskouv, K., Thibault, N., Welch, M., and L. Stemmerik (2018). Seismic geomorphology and origin of diagenetic geobodies in the Upper Cretaceous Chalk of the North Sea Basin (Danish Central Graben). Basin Research, published March 1st 2018, <https://doi.org/10.1111/bre.12285>

Paper 2 (Chapter III)

- **Smit, F.W.H.**, Stemmerik, L., Lüthje, M., Hertle, M., and F.S.P. van Buchem (submitted). Seismic expression of fluid and gas expulsion episodes in the Jurassic to Eocene of the Danish Central Graben. Submission to Journal of the Geological Society (London)

Paper 3 (Chapter IV)

- **Smit, F.W.H.**, van Buchem, F.S.P., Lüthje, M., Swart, P.K., Staudigel, P.T., and L. Stemmerik (submitted). Amalgamated pockmarks on the Danian seafloor caused by large-scale outbursts of gas-bearing fluids (Chalk Group, Greater Dan Region, Danish Central Graben). Submission to Marine and Petroleum Geology

Paper 4 (Chapter V)

- **Smit, F.W.H.**, Staudigel, P.T., Swart, P.K., van Buchem, F.S.P., and L. Stemmerik (in prep). Distinguishing syn- and post-depositional fluid migration in the Chalk Group using clumped isotope analysis and seismic geomorphology (Upper Cretaceous, Danish Central Graben and onshore United Kingdom).

Included abstracts

- **Smit, F.W.H.**, van Buchem, F.S.P., Schmidt, I., and L. Stemmerik (2017). Updated seismic geomorphological workflow applied to the Chalk Group. *In 2017 SEG International Exposition and Annual Meeting. Society of Exploration Geophysicists.*
- **Smit, F. W. H.**, van Buchem, F. S. P., Holst, J. H., Lüthje, M., Anderskouv, K., Thibault, N., Welch, M., and L. Stemmerik (2017). Basinal fluid flow through the Chalk Group in the southern Danish Central Graben as seen on 3D seismic data – ancient examples of large-scale fluid seepages. *GSA Cordilleran Section Meeting 2017, T12. Fluid Flow, Submarine Seeps, and Gas Hydrate Systems: Implications for the Global Carbon Cycle and Seafloor Stability, Honolulu, Hawaii, USA*
- **Smit, F.W.H.**, Stemmerik, L., Lüthje, M., Hertle, M., and F.S.P. van Buchem (2018). Mega pockmarks within the Upper Cretaceous Chalk Group in the Danish Central Graben: evidence for large-scale outburst of fluids. *Seismic Characterisation of Carbonate Platforms and Reservoirs, Geological Society of London Conference (October 2018)*

Contents



Please use PDF bookmarks or page numbers to navigate this document

Acknowledgements.....	6
English summary.....	7
Dansk resumé	9
Publications in this thesis.....	11
Chapter I. Synopsis	14
1. Introduction to the Chalk Group and study area	14
2. Background of study: an evolving seismic chalk paradigm (1960s – 2010s)	16
3. Statement of problem and scope of study	17
4. Research methods.....	19
4.1 Seismic data, interpretation techniques, and seismic attributes	19
4.2 Well data and microscopy	20
4.3 Geochemical analysis.....	21
4.4 Classification of features.....	21
5. Summary and relationship of publications.....	21
<i>Paper 1. Seismic geomorphology and origin of diagenetic geobodies in the Upper Cretaceous Chalk of the North Sea Basin (Danish Central Graben) – published in Basin Research (2018).....</i>	<i>21</i>
<i>Paper 2. Seismic expression of fluid and gas expulsion episodes in the Jurassic to Eocene of the Danish Central Graben – Submitted to Geological Society of London.....</i>	<i>23</i>
<i>Paper 3. Amalgamated pockmarks on the Danian seafloor caused by large-scale outbursts of gas-bearing fluids (Chalk Group, Greater Dan Region, Danish Central Graben).....</i>	<i>25</i>
<i>Paper 4. Distinguishing syn- and post-depositional fluid migration in the Chalk Group using clumped isotope analysis and seismic geomorphology (Upper Cretaceous, Danish Central Graben, onshore United Kingdom) – to be submitted to a journal (unpublished manuscript)</i>	<i>26</i>
Publication not included in this PhD.....	26
6. Contributions of this study: Updated seismic chalk paradigm.....	28
6.1 Syn-depositional features and processes	28
6.2 Post-depositional features and processes	30
6.3 Timing and integrated model	31
6.4 Implications for exploration and production.....	35
6.5 Conclusions.....	36
6.6 Outlook	38
References	38

Chapter II. Paper 1	41
Chapter III. Paper 2.....	72
Chapter IV. Paper 3.....	109
Chapter V. Paper 4.....	131
Supplements to papers	
From Chapter I - Synopsis: HQ version of Fig. 12 (Top Chalk morphology).....	151
From Chapter III – Paper 2: HQ version of Fig. 24 (Model mega pockmarks).....	152
From Chapter IV – Paper 3: HQ version of Fig. 14 (Model giant pockmarks).....	153
Appendices (conference abstracts)	
SEG 2017 Abstract.....	154
GSA Cordilleran Section Meeting 2017.....	160
Geological Society of London carbonate conference 2018.....	161

Chapter I. Synopsis

1. Introduction to the Chalk Group and study area

The Upper Cretaceous and lowermost Paleocene Chalk Group is found throughout northwestern Europe, and is known from impressive outcrops along the coasts of southern England, France, and Denmark. Chalk deposits are a mud-grade biogenic sediment, with very low permeability and fairly high porosity (Surlyk *et al.*, 2003), and host the most important hydrocarbon reservoirs in the Danish part of the North Sea (Megson, 1992; Vejrbæk *et al.*, 2005) and a significant part of the hydrocarbons in the Norwegian sector (Brewster & Dangerfield, 1984; D'Heur, 1984). Recognizing chalk facies, understanding their influence of reservoir quality, and being able to predict their spatial distribution are key in the Chalk Play. In the North Sea Basin, where the main hydrocarbon accumulations are found, the chalks are buried below Cenozoic sediments up to 3.5 km thick (Surlyk *et al.*, 2003). Therefore, characterization of the North Sea chalks relies heavily on penetrations of wells, and acquired (3D) seismic data, as outcrop analogues might only have limited compatibility (Frykman *et al.*, 2004).

The main Danish hydrocarbon accumulations are in chalks in the Danish Central Graben, which forms the southernmost branch of the North Sea Central Graben (Fig. 1). It comprises a complex set of half-grabens bounded to the south and east by the Ringkøbing-Fyn High, and to the west by the Mid North Sea High (Fig. 2). The half-grabens formed during two major tectonic rifting phases (Japsen *et al.*, 2003). During the Permo-Triassic, an E–W oriented stress regime led to N–S oriented half-grabens (Glennie *et al.*, 2003; Goldsmith *et al.*, 2003), whereas Late Jurassic rifting occurred in a NE–SW oriented stress regime, leading to generally NW–SE oriented half-grabens (Fraser *et al.*, 2002). Substantial creation

of accommodation space combined with high sedimentation rates led to deposition of thick Mesozoic siliciclastic successions (up to 4 km thick) below the Chalk Group.

The Upper Jurassic syn-rift succession is separated from the post-rift succession by the Base Cretaceous Unconformity (BCU), a basin-wide diachronous surface that is polygenetic in nature (Kyrkjebø *et al.*, 2004). Thermal subsidence prevailed throughout most of the Cretaceous, but was interrupted by a distinct compressional phase that reached its climax during the early Campanian inversion. This resulted in the major rearrangement of depocenters (Cartwright, 1989; Vejrbæk & Andersen, 2002; van Buchem *et al.*, 2018), and sediment remobilization along newly formed highs (e.g. Back *et al.*, 2011; Smit, 2014; van Buchem *et al.*, 2018).

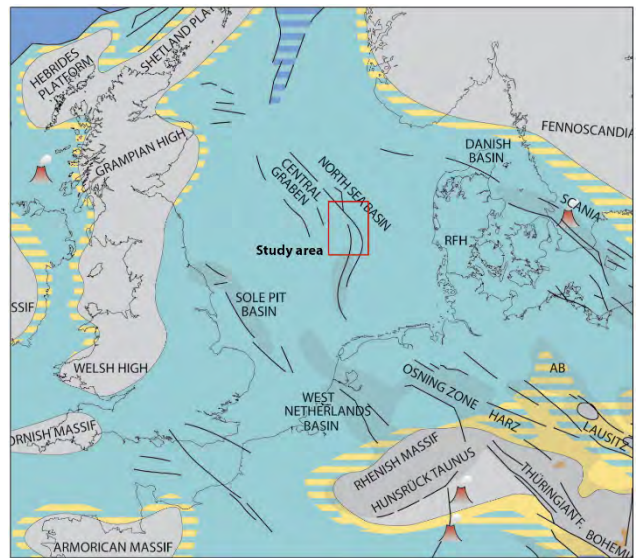
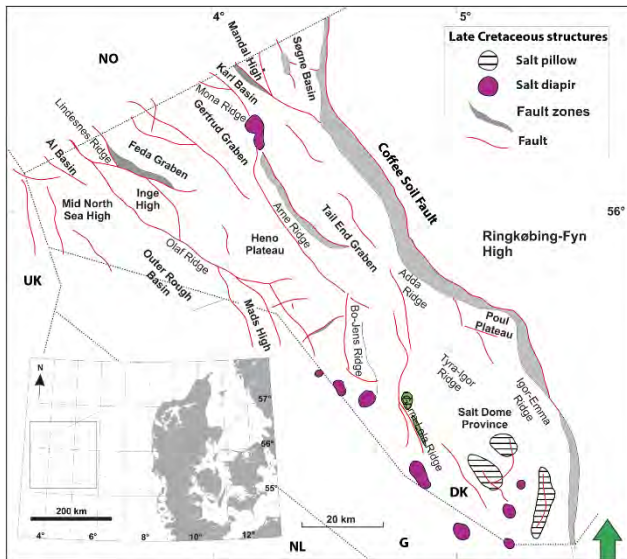


Figure 1. Palaeoreconstruction of the Late Cretaceous to Danian. Light grey: non-depositional area; yellow: deltaic to shallow marine clastic deposits; turquoise: carbonates, mainly shallow marine; blue: deep marine shales. Dark grey overlay: inverted in Cretaceous times. An epeiric sea existed within NW Europe as a result of high eustatic sea level and low topography. Danish Central Graben indicated in red. From Vejrbæk *et al.* (2010)



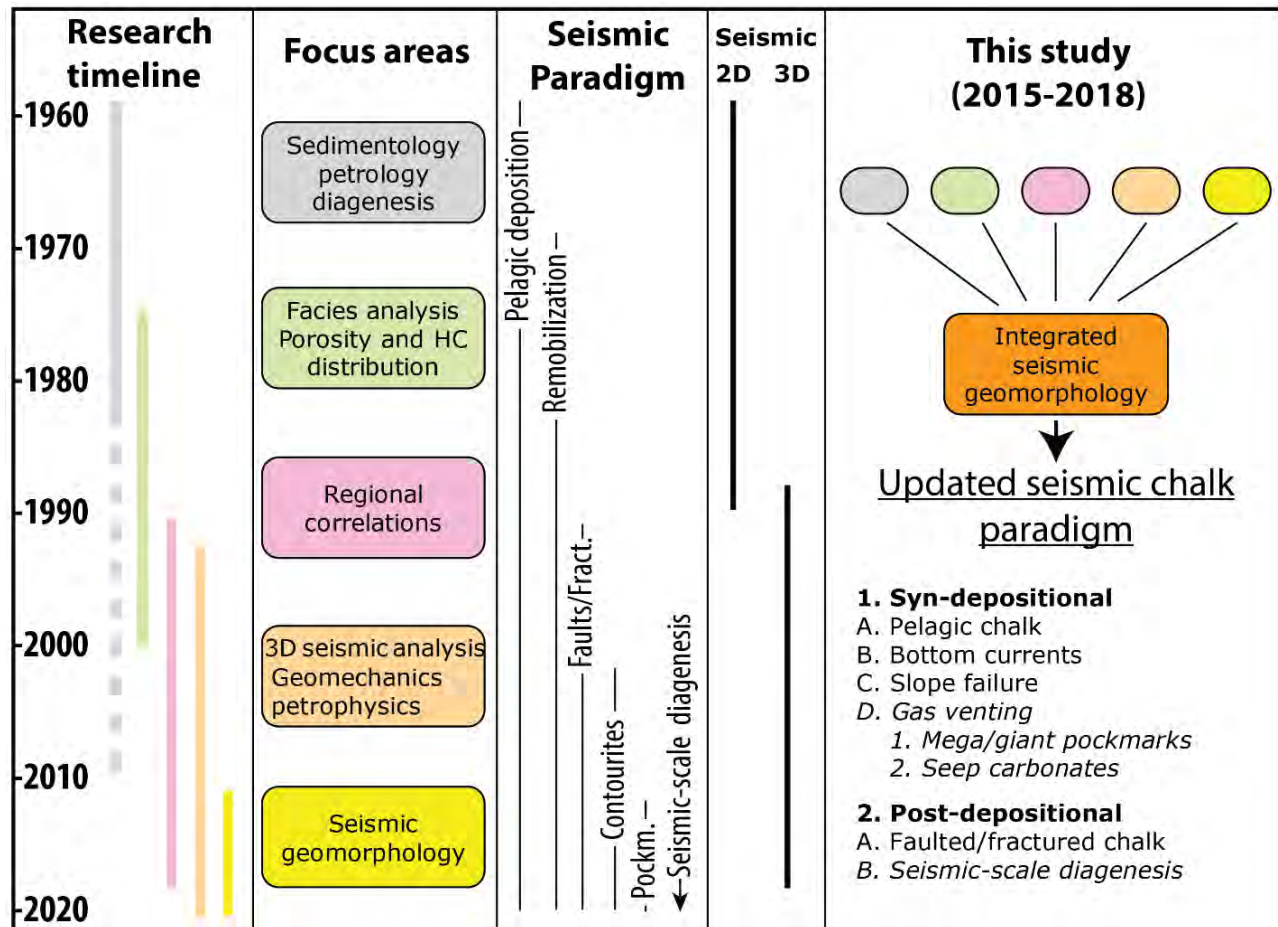


Figure 3. Generalized timeline for past research focus areas that have evolved as a result of availability of data, proposed geological models, and technological advances (e.g. 2D and 3D seismic data). Additions to the seismic chalk paradigm indicated using same timescale. Dominance of usage of 2D and 3D seismic data indicated. Lastly, the integrated seismic geomorphological workflow used in this study that led to an updated seismic chalk paradigm (additions in *italic*).

changing pore fluid pressures is indeed of great importance for chalk hydrocarbon fields, where production-induced compaction leads both to enhanced recovery, but at the cost of seafloor subsidence (Fabricius, 2014; Keszthelyi *et al.*, 2016). Fabricius (2007) provided a thorough overview of rock mechanical and rock physical research in chalk.

With the development of more powerful workstations, larger regional seismic datasets could be visualized, and 3D seismic geomorphology became slowly introduced into the Chalk Group (Arfai *et al.*, 2016; Back *et al.*, 2011; Gennaro *et al.*, 2013). Implementation of neural network technology in seismic interpretation software, made it possible to establish basin-wide correlations in a time-efficient way and to scan through the seismic data for ‘Funny

Looking Things’ (FLT) (c.f. Posamentier *et al.*, 2007; Smit, 2014). By using seismic stratigraphic principles, biostratigraphy data, and seismic geomorphology van Buchem *et al.* (2018) proposed the first formal stratigraphic subdivision of the Chalk Group. They showed that major basin rearrangement occurred as a result of tectonic inversion, which triggered large-scale remobilization along the newly formed basinal highs, while non-deposition and erosion occurred on top of the inverted structures.

The palaeoreconstructions of the seafloor, based on seismic geomorphology, are very suitable for integration with other kinds of data (petrographical and geochemical), which led to the idea of integrated seismic geomorphology that is utilized in this project.

3. Statement of problem and scope of study

The prediction of depositional and/or diagenetic facies in chalk is notoriously difficult, yet has a large impact on reservoir quality and sweep efficiency (Henriksen *et al.*, 2009; Nygaard *et al.*, 1983; Scholle, 1974). Acoustic properties in chalk are a function of porosity, grain-to-grain contact, as well as mineralogy, and therefore, seismic data are a great starting point to investigate spatial distribution of acoustic properties (Fabricius, 2007). These properties are a function of syn-depositional (e.g. depositional surfaces and early cementation) and post-depositional processes (e.g. burial diagenesis, establishment of overpressure, hydrocarbon entry, and fracturing/faulting). With so many variables influencing acoustic properties, it can be a challenge to establish geological models that predict reservoir quality based on seismic geometries. For this reason, most of the reservoir stratigraphy in the Chalk Group is based on porosity stratigraphy: separation of porous beds and non-porous beds. As many variables influence the final porosity in the chalk, such stratigraphy can cross important time lines, and makes formulation of predictive geological models difficult. Indeed, it takes integration with a variety of proxies and methodologies, to anatomize the geological content from the seismic signal.

Seismic geomorphology is an ultimate tool to move away from porosity stratigraphy, as it approaches seismic data as a stack of buried seafloors (e.g. geological layering) (Posamentier *et al.*, 2007). Careful construction of time-consistent stratigraphic horizon slices by integration with biostratigraphy provides a seismic stratigraphic framework that offers insights into shifting depocenters in the basin, forming the (tectonic) background information when studying buried seafloors (Smit *et al.*, 2017; Van Buchem *et al.*, 2018). By evaluating a large set of stratigraphy-consistent horizon slices through the Chalk Group with seismic attributes, morphological features are revealed that can reflect geological processes.

The seismic geomorphological seascapes provide a spatial framework to evaluate well data, which can consist of petrophysical logs, examination of rock chips under scanning electron microscope, as well as geochemical analysis. Indeed, such an integrated seismic geomorphological approach allows integration both in scale, as well as in disciplines, and forms the main scope of this study (Fig. 3). The purpose is to be able to provide geological explanations for ‘Funny Looking Things’ in the Chalk Group, so that prediction of facies, based on geological models, becomes possible. An important challenge with such approach is that the scales and resolution of each method is very different (Fig. 4), impeding a 1:1 correlation. Therefore, as seismic data form the basis of the observations, the large-scale trends within petrographical and geochemical data rather than individual samples form the basis for integration. Once a geological interpretation is established, the spatial distribution of certain features within the basin might be explained by juxtaposing other basin-wide data, such as the tectonic evolution, fault patterns, and source rock maturity. Such predictive analysis is indeed part of the scope of this study as well.

Based on previous reconnaissance (Smit, 2014), three case studies have been selected that reflect some common seismic expressions in the Chalk Group (Fig. 5 for locations). Case study 1 occurs in the southernmost part of the Danish Central Graben, on top of the Ryan Anticline, where steeply dipping ‘Stratigraphy Cross-cutting Reflectors’ occur that affect the stratigraphy over 500 m. Case study 2 occurs in the Roar Basin, in the central part of the Danish Central Graben, where kilometre-scale U-shape reflectors occur, previously studied by Back *et al.* (2011) and Esmerode *et al.* (2008). Case study 3 occurs within the Halfdan NE and Tyra Field, where the top of the chalk reflector shows highly irregular lens-shaped features. Lastly, a fourth case study was added, by coincidence, during a field trip in Flamborough Head (United Kingdom), where large calcite veins occur in heavily deformed chalk strata due to faulting and folding.

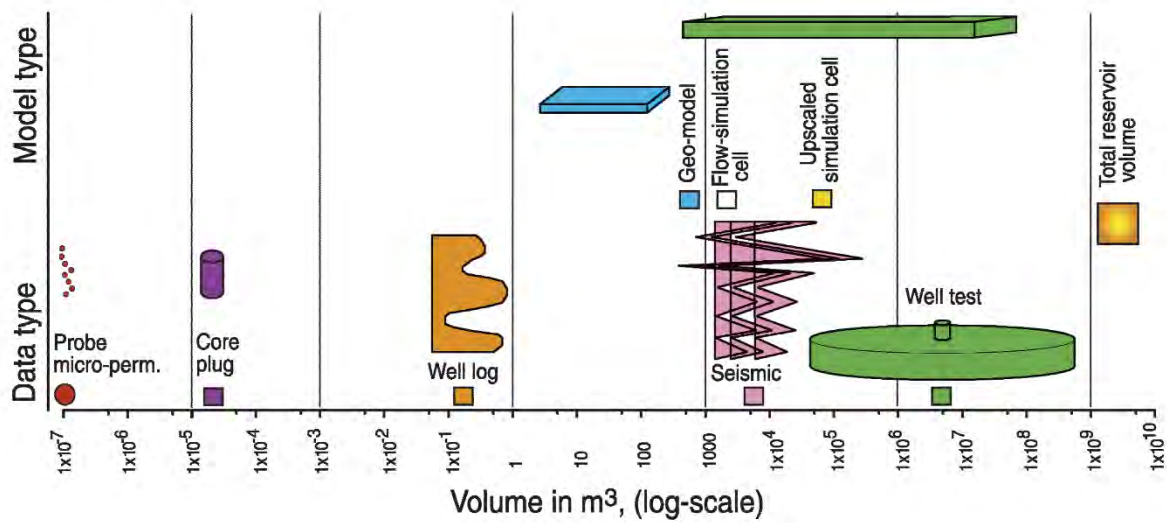


Figure 4. Integration between proxies is a challenge due to large discrepancies in studied scale and resolution. This study utilizes Scanning Electronic Microscope data (10^{-7} m^3), geochemical data (10^{-5} m^3), well log data (10^{-1} m^3), and seismic data (10^4 m^3). Rather than individual samples, it focus on large-scale trends observed within the data. From Frykman and Deutsch (2002)

4. Research methods

This study utilizes a large variety of research methods and data, in order to characterize features observed within the seismic data.

4.1 Seismic data, interpretation techniques, and seismic attributes

Seismic data

The seismic data consist of a Pre-Stack Depth Migrated (PSDM) regional megamerge covering almost the entire Central Graben (Fig. 5). The signal quality is excellent within the Chalk Group, while it deteriorates towards salt diapirs. The polarity follows North Sea convention, with a downward increase in acoustic impedance reflected by a trough (red). The dominant frequency in the Chalk Group averages around 30 Hz, average acoustic velocity averages around 3400 m/s, leading to an average vertical resolution of 28.3 m as a quarter of the wavelength of the dominant frequency (Sheriff, 1980). Petrel 2016 has been used as common integration platform for seismic and well data, PaleoScan™ horizon slices, spectral decomposition data, as well as image processing data.

Seismic interpretation with a neural network

A neural network methodology has been applied for seismic interpretation (PaleoScan™ 2016, c.f. Pauget *et al.*, 2009) in order to create, in a time-efficient manner, a large number of stratigraphy consistent horizon slices through the Chalk Group. This methodology creates a node network for every peak, trough, and zero-crossing. It then calculates the best correlation coefficients between two seismic traces, which results in minimization of the ‘cost’ of correlation (the distance needed to connect all points). The correlation can and must be modified by human constraints in order to provide geological input around complex structural zones, pinch-out (depositional) surfaces, and low signal/noise areas. When the user is satisfied with the generated correlation cube, it is followed by calculation of a 3D Relative Geological Time model (RGT). This is the intra- and extrapolated version of the correlation cube, which generates a continuous 3D model of the subsurface, and can be used to generate a large set of seismic stratigraphic consistent horizons. These horizons can then be used to scan through the seismic dataset for ‘Funny Looking Things’ with standard seismic attributes such as coherence, RMS amplitude, and instantaneous frequency (e.g. Posamentier *et al.*, 2007).

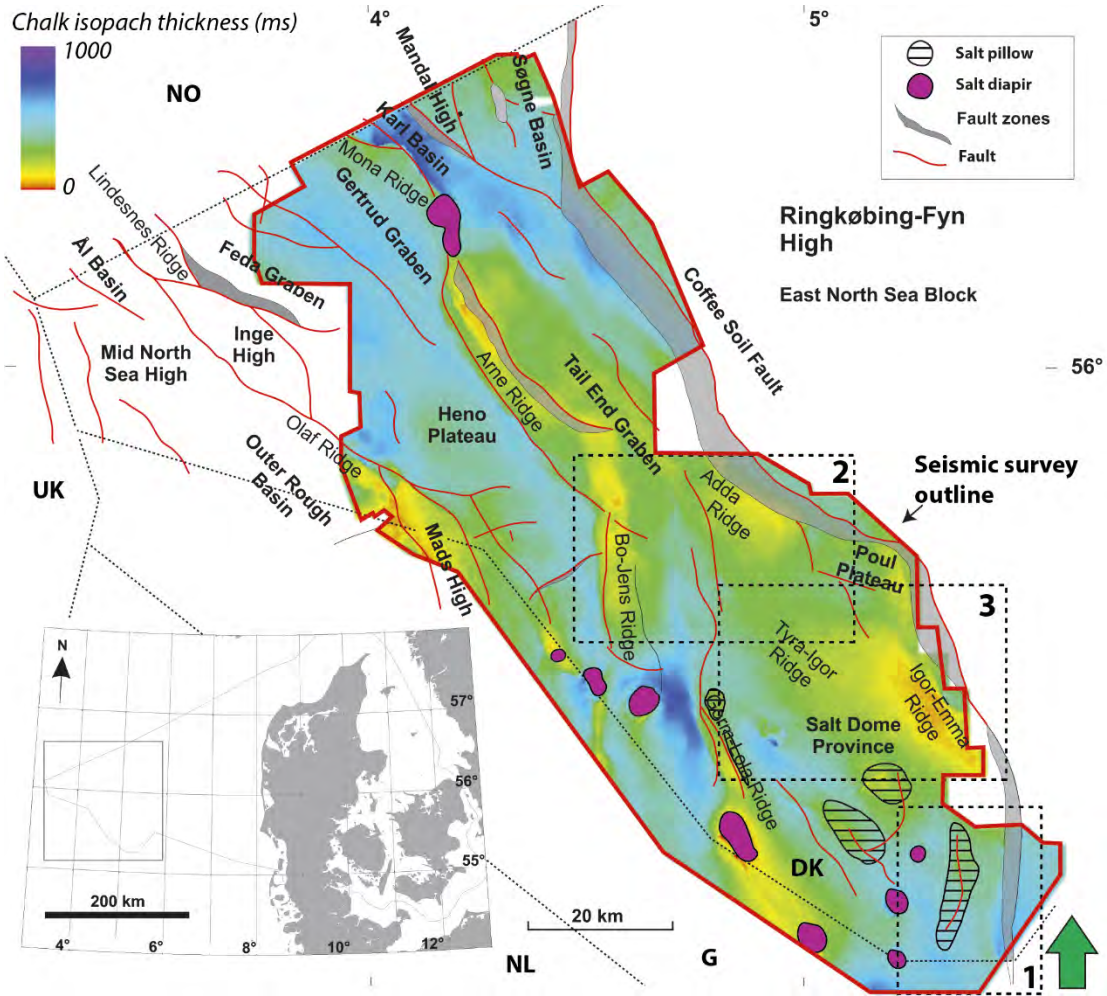


Figure 5. Danish Central Graben with Late Cretaceous structures. Outline of the seismic megamerge is indicated by red solid line. Case study areas indicated by dashed black line and associated number.

Spectral Decomposition

In order to extract more information from seismic amplitude data, spectral decomposition is used to ‘decompose’ the original seismic wavelet into its individual (low, mid, and high) frequency components (c.f. Partyka *et al.*, 1999). In this study we used GeoTeric 2016.2 (ffA) for obtaining spectral decomposition data. Three main methods are used in spectral decomposition, namely: 1) Short Time Fourier Transform (STFT) (e.g. Marfurt and Kirilin, 2001); 2) Continuous Wavelet Transform (CWT) (e.g. de Matos and Marfurt, 2011); and 3) Matching Pursuit (MP) (e.g. Liu and Marfurt, 2005; Mallat and Zhang, 1993).

STFT is also called *constant bandwidth* spectral decomposition as it uses the same bandwidth

of the synthetic wavelet throughout the designed spectrum. The amount of overlap between individual synthetic wavelets is therefore large, which leads to good frequency separation, but to poorer resolution due to broad bandwidth wavelets.

CWT is also called *constant Q* spectral decomposition, which keeps spectral energy constant instead of bandwidth. As wavelet energy decreases with increasing frequency, broader bandwidths (longer windows) are needed towards the higher frequencies, while shorter bandwidths are needed in the low frequency part. Combined, this gives a better resolution compared to STFT, at the cost of less frequency overlap leading to poorer decomposition.

MP is called *HD Frequency Decomposition (HDFD)* in GeoTeric, and is an spectral decomposition algorithm that decomposes the

original seismic wavelet into a sum of frequency-dependent Gabor wavelets from a wavelet dictionary that ‘match’ the signal structures found in the original wavelet (Cooke *et al.*, 2014; Mallat and Zhang, 1993). A trace can be reconstructed at any given frequency, which match the original seismic trace the best, and has as benefit the highest vertical resolution. In this study, we are mostly interested in coupling well data to seismic facies at the highest resolution, and therefore we have mainly used the MP algorithm.

Image processing of seismic data and ant-tracking

Seismic image processing is a relatively new method to extract heterogeneities from seismic data (eXchroma^{SG} Petrel plug-in, c.f. Laake, 2013). Rather than acting on the wavelet, it treats seismic data as a stack of images (time slices) with amplitude values. Default settings lead to three new cubes (Red, Green, and Blue) whereby each cube is time-shifted 1 sample with respect to the other. It then merges the individual time slices from the three cubes on top of one another, creating a colour at changing amplitudes between the adjacent slices (using a RGB cube model), which can be enhanced with image processing (e.g. setting contrast and saturation). The RGB model is then transformed to a Hue Saturation Value (HSV) model, of which the saturation component (0 to 1) indicates the intensity of change (e.g. the heterogeneity). An edge-detection procedure follows, so that the structural cube (S-cube) indicates heterogeneities and homogeneities. The original seismic data (time-shifted R, G, B cubes) are ‘sharpened’ by convolving it with the S-cube and are used for a ‘sRGB’ display.

These three cubes can be used in a colour blend (sRGB), similar to spectral decomposition data, to show heterogeneities. The main advantage over spectral decomposition methodology is that the resolution is much higher as it uses three adjacent time slices (1.5x 4 ms sampling rate, 6 ms) compared to a wavelet windowed interval (typically 20-30 ms). It therefore picks up heterogeneities that are close to seismic resolution. In addition, whereas spectral decomposition is merely a visualization tool for frequency dominance and not actual data of heterogeneities, S-cube data is in fact directly

reflecting heterogeneity. By using ‘swarm intelligence’ of artificial ants, heterogeneities in a certain range (e.g. dip azimuth) can be extracted with an ant-tracking procedure in Petrel (Pedersen *et al.*, 2002). It is therefore very suitable to further explore heterogeneities that are related to structural deformation, such as near sub-seismic faults and fracture swarms (Smit *et al.*, 2017).

4.2 Well data and microscopy

A large database of vertical exploration wells (150+), and horizontal production wells (150+) with full geophysical log suites is available. Wells that penetrate features of interest provided drill cutting material for scanning electron microscope (SEM) analysis, as well as geochemical analysis. Cuttings interval varied between 3 m and 10 m. SEM analysis on gold-coated rock chips and thin-sections was performed on a FEI Inspect S with tungsten filament, and FEI Quanta S200 with field emission gun, to provide observations on cementation and mineralogy of the samples.

4.3 Geochemical analysis

Stable carbon and oxygen isotope analysis

A deviation of the oxygen isotope ratio ($\delta^{18}\text{O}$) from Cretaceous seawater can indicate a certain degree of diagenesis, as with increasing temperature lighter oxygen isotopes will be taken up into the crystal lattice, although bulk values also depend on the fluid from which the cement precipitated (Craig, 1957). Carbon and oxygen isotopes were analysed at Iso-Analytical (UK) using continuous flow isotope ratio mass spectrometry (CF-IRMS), and values are reported as $\delta^{13}\text{C}$ and $\delta^{18}\text{O}$, deviations in parts per thousand relative to the V-PDB and V-SMOW standard. Standard deviations are reported to be better than 0.08‰ for $\delta^{13}\text{C}$ and 0.02‰ for $\delta^{18}\text{O}$.

Clumped isotope analysis

In order to constrain diagenesis further, this study has utilized, for the first time for chalks in the North Sea Basin, clumped isotope analysis of 70 samples to provide an absolute carbonate

palaeothermometer (Ghosh *et al.*, 2006; Schauble *et al.*, 2006; Swart, 2015). Samples were chosen based on their position with respect to features of interest, and previous results from carbon and oxygen isotope analysis. Sample preparation and $\Delta 47$ measurements were done in the Stable Isotope Laboratory at University of Miami and follow the procedures as outlined by Staudigel *et al.* (2018) and Swart *et al.* (2016).

This method measures the amounts of isotopologues of CO_2 (e.g. same molecule, different isotope configurations) in an adjusted mass spectrometer (Thermo-Fischer Scientific, MAT 253). There are six different isotopologues (44-49), the amount of isotopologue 47 ($\Delta 47$, $\text{C}^{13}\text{O}^{16}\text{O}^{18}$ is by far the most common) is a function of absolute precipitation temperature (Ghosh *et al.*, 2006). With increasing temperature, the amount of $\Delta 47$ will become smaller, and by comparison to reference materials that precipitated at known temperatures, the absolute temperature can be estimated. As bulk $\delta^{18}\text{O}$ is measured at the same time, two of the three unknowns in the classic palaeothermometer (equation 1, 2, c.f. Kim and O'Neill, 1997) are known (e.g. bulk $\delta^{18}\text{O}_{\text{calcite}}$ and temperature T), and the last unknown ($\delta^{18}\text{O}_{\text{fluid}}$) can be estimated:

$$1000 \ln \alpha(\text{calcite} - \text{H}_2\text{O}) = 18.03 \left(\frac{10^3}{T} \right) - 32.42 \quad (1)$$

$$\text{With } \alpha(\text{calcite} - \text{H}_2\text{O}) = \frac{1000 + \delta^{18}\text{O}_{\text{calcite}}}{1000 + \delta^{18}\text{O}_{\text{H}_2\text{O}}} \quad (2)$$

X-ray Fluorescent (XRF) analysis

Certain chemical components can be used to describe the type of diagenesis, such as Mn and Sr (open or closed-system c.f. Banner & Hansen, 1990), Mg (dolomitisation), and Si/Al (for the presence of silica phases). To characterize this throughout the stratigraphy, XRF analyses were carried out at ALS Minerals (Ireland) on drill cutting material.

4.4. Classification of features

Based on seismic geomorphological analysis, two classification schemes for seismic features are used: one for characterizing cross-cutting reflectors in Paper 1 found in seismic-scale diagenesis (Type 1-8, Table 1), and one for syn-depositional surfaces related to fluid migration/expulsion episodes found

in Papers 2 and 3 (Cat. 1-6, Table 2). The interpreted features are categorized according to their origin in the updated seismic chalk paradigm. (Table 3 and 4).

4.5 Basin model

The formation of several features in the Chalk Group are strongly linked to transportation of gas-bearing fluids along faults. In order to get a first order idea of possible sources of gas at the time of fluid expulsion, a 3D basin model was provided by M. Hertle (Total) that predicts source rock thermal maturity (expressed in vitrinite reflectance) in the region over time. In addition, paleo-temperature maps at BCU level provides insight in the likelihood of biogenic gas formation, with peak generation assumed to occur at c. 40°C and ceases at temperatures higher than 65/70°C (c.f. Schneider *et al.* 2016).

5. Summary and relationship of publications

Four papers are included in this thesis that aim at providing geological interpretation and formation mechanisms for ‘Funny Looking Things’ found within the chalk seismic package, with the use of an integrated seismic geomorphological workflow. One paper is published (Paper 1), two are in submission (Paper 2 and 3), and one paper is an unpublished manuscript (Paper 4). The following section contains a summary of the papers and indicates how the papers are interlinked.

Paper 1. *Seismic geomorphology and origin of diagenetic geobodies in the Upper Cretaceous Chalk of the North Sea Basin (Danish Central Graben) – published in Basin Research (2018)*

The first paper (Chapter II) deals with understanding ‘Stratigraphy Cross-cutting seismic Reflectors’ (SCRs) with various shapes (U, V, W, Table 1) that occur on top of a faulted, salt-cored anticline in the southernmost part of the Danish Central Graben (Fig. 6, see Fig. 5 for location). Such features have previously been described in the German sector as channel segments based on seismic geomorphological considerations (Arfai *et al.*, 2016).

Type		2D Seismic	Seismic porosity	HD Spectr. Decom	Orientation
1	U				Line parallel through axis of single large lobate diagenetic geobody
2	V				Line perpendicular through a single lobate diagenetic geobody
3	W				Line parallel to axis of multiple lobate diagenetic geobody
4	2W				Line perpendicular to axis of multiple lobate diagenetic geobody
5	\\ \\				Line perpendicular to major fault and fracture swarms, initiation of front creating "fingers"
6					Line perpendicular to axis of single lobate diagenetic geobody with deformation
7					Small anomaly. "nose" of the diagenetic geobody, furthest extent of the diagenetic form
8					Line parallel to axis of single diagenetic geobody that is not deeply affecting the chalk

Table 1. The seismic expression of the SCRs depends on the orientation of the seismic section in relation to the lobate shape of the feature. Horizontal scale bar is 500 m, vertical scale bar 400 m, peaks are blue (boundary to lower AI beds), troughs are red (boundary to higher AI beds), and porosity colour scale is from pink (10%), blue (20%), green (25%), yellow (30%) to red (45%). Eight different expressions (types) have been recognized, and some are related to one another as a result of a different orientation. For example, within the same SCR both U- and V-shapes can be found by changing the orientation parallel to the axis and perpendicular respectively. (2)W-shapes are the result of the merging of two V-shapes. Also, importantly, small seismic anomalies might represent the distal expressions of the lobate shapes (Type 7), showing the importance of 3D seismic data.

With the usage of spectral decomposition, the 3D architecture of these 1-3 km wide, 50-500 m deep geobodies is revealed (Fig. 6). It shows an upside-down Christmas tree spreading pattern that seemed to be controlled by porosity/permeability contrasts of stratigraphic origin, such as hardgrounds associated with formation tops, and feeder fault systems (revealed with ant-track S-cube data).

The geobodies represent high-density chalk nested within low-density chalk, which to a large extent could reflect porosity (e.g. low-porosity nested within high-porosity chalk). SEM analysis showed increased amounts of cementation within the SCR zone, and geochemical analysis revealed open-system diagenetic signature. The top of the Chalk Group is some 50-70 m lower than surrounding unaffected chalk, which must mean that significant

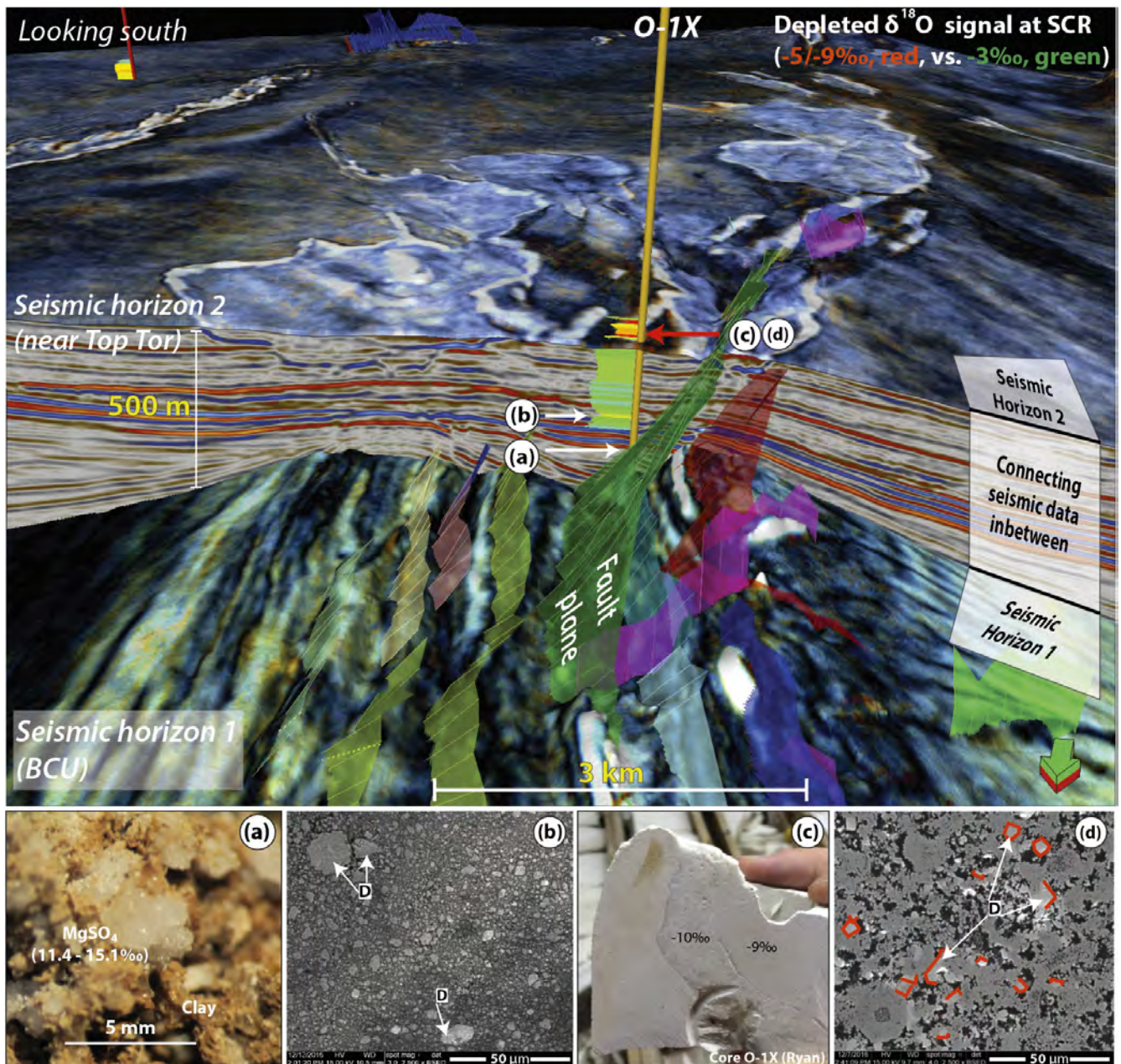


Figure 6. Integrated seismic geomorphology on top of the Ryan Anticline in a staircase diagram (see perspective description on right-hand side), showing SCRs within the chalk (blue peaks), and the spatial distribution with the use of a seismic horizon with spectral decomposition data near top Tor Formation level. The faults are very clear at BCU level (lower seismic horizon) and some are mapped out (coloured planes). Well O-1X displays the bulk $\delta^{18}O$ values from drill cutting material. (a) Sulphates are observed where the well penetrates the fault plane. (b) low-porous chalk is observed in the lower part of the chalk in thin section with scanning electron microscope (c) The core is located where the seismic anomaly appears (see light anomaly towards well) (d) Thin sections show increased amount of pore-filling cement, as well as dolomite ('D'). Modified from Smit *et al.* (2018), Paper 1.

mechanical compaction occurred. We interpret the SCRs as reflecting the first example of seismic-scale diagenetic geobodies within the chalk formed as a result fault-related escape of overpressure that led to compaction. At the same time, extra-formational fluids were able to migrate into the chalk to form the observed open-system diagenetic calcite cement (Fig. 6 b,c and d). SEM observations also showed indications that possibly dolomite had formed within

these diagenetic geobodies. This study thus provides new insights into the 3D relationship between fault systems, fluid migration and diagenesis in chinks, and has important applications for basin modelling (fluid migration), reservoir characterization (dense zones in chalk), and potentially a new play type where the SCRs form traps.

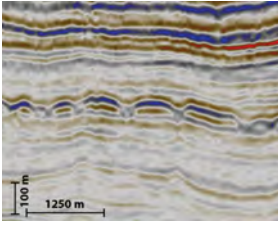
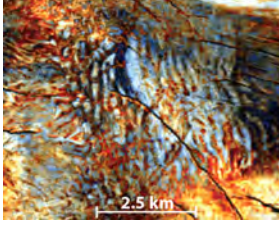
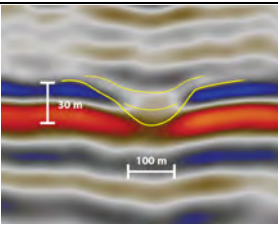
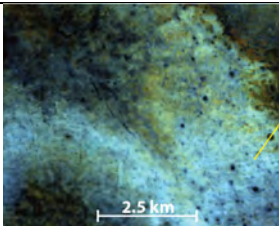
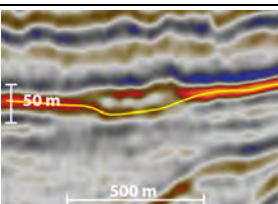
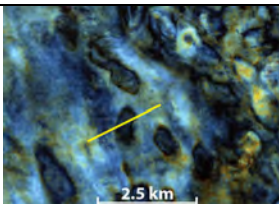
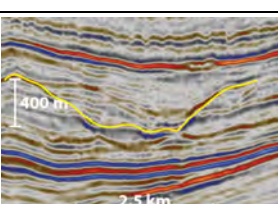
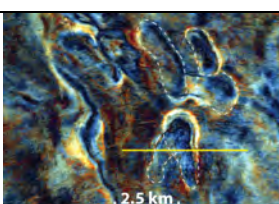
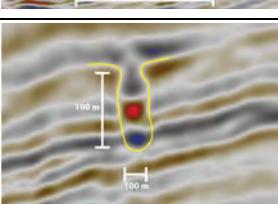
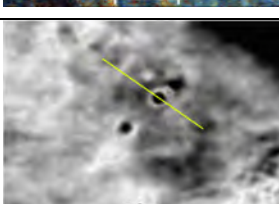
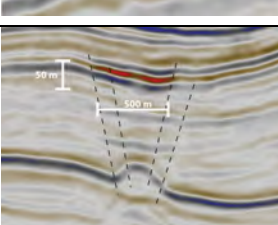
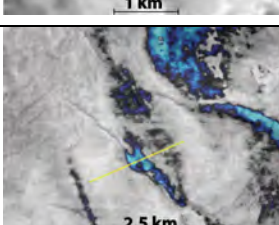
Cat.	2D seismic expression	Map view expression	Architecture	Dimensions	Stratigraphy	Interpretation
1			Hill and valley morphology Hills can be highly elongated and slightly sinusoidal, rectangular, squared, rounded or a complex combination. Valleys interrupt the hill topography, and depressions are elongated, or rounded. Doming underneath valley. Typically shows infilling younger packages	Hills: elongated (0.4 - 5 km by 0.1-0.4 km), rectangular (200-400 by 100 m), rounded (20-40 m), composite (50 - 300 m) Valleys: 20 m (rounded) to 3 km (elongated). Slopes are typically between 5-20°. Depth to valley floor (30 - 100 m).	Best expression at Base Cretaceous Unconformity reflector (BCU), where major Late Jurassic faults terminate (prior to Campanian inversion). Features are also found in Lower and earliest Upper Cretaceous strata.	Slumping and pockmark complex causing erosional depressions on basin floor. Driver of erosion is fluid expulsion following Late Jurassic faults and subsequent bottom current activity.
2			Small/medium depressions Mainly circular depressions with limited incisional depth. Infill thickest in depression centre, and wedges out to the side. Not necessarily clear link to fault systems, but found nested within larger depressions (e.g. cat. 3 and 4), hill and valley morphology (cat. 1), and within HARP's (cat. 6). Different from cat. 5 features due to gentle U-shape slopes (5-10°).	Depressions are between 10 to 200 m in radius, 10 - 40 m deep (e.g. 10 m is close to seismic detectability). Slopes are typically between 3-10°.	Occur throughout the Late Jurassic to Eocene strata.	Small to medium, round pockmarks due to fluid expulsion. Roundness indicates limited reworking by currents. Occurrence away from major fault systems indicate regional fluid expulsion from within the strata. Nested within larger depressions indicate smaller outbursts.
3			Giant depressions Circular, elliptical, and complex depressions with significant incisional depth. Often linked to fault systems and found above cat. 4 features. Ellipse and complex shapes likely due to amalgamation of single events.	Depressions are between 200 to 500 m wide (short axis), 200 - 1.5 km across (long axis), 20-60 m deep. Slopes are typically between 3-10°.	Occur within the Danian strata (Ekofisk Formation), incisions occur into the Maastrichtian Tor Formation.	Giant pockmarks with significant erosion into the underlying strata (up to 60 m). Occur on top of ridges where faults occur. The elongation is likely the result due to amalgamation of single pockmarks into more complex shapes, combined with possible bottom current reworking.
4			Mega depressions Round (rare) to elongated (common) large depressions, cutting deeply into strata causing several stratal terminations against surface. Seismic character of the infill comprise parallel reflectors onlapping onto surface, discontinuous to chaotic, and to transparent (low S/N) strata. Strong link to faults.	Depressions are between 0.5 to 4.0 km wide (short axis), 0.5 - 5.0 km across (long axis), 100 - 400 m deep. Slopes are typically between 5-15°.	Exclusively within Santonian - Campanian strata. Youngest incisional surface is Campanian in age (e.g. top 'intact' strata).	Mega pockmarks with very significant erosion into the underlying strata. Location strongly linked Late Jurassic faults underlying Roar Basin, and its position at the crest of the Mesozoic basin. Campanian inversion movement caused formation of these mega pockmarks.
5			Deep tube depressions Steeply dipping, round depressions, cutting deep into underlying strata causing stratal terminations. Widest at bottom, becoming narrower to the top (cone/tube shaped). High amplitude seismic reflectors occur within. Sometimes cross-cutting reflector can be observed above it. Strong link to faults.	Depressions are between 50 - 100 m wide at bottom, and become narrower at top (10-30 m). 20 - 100 m deep. Slopes are typically between 75-110° (near vertical to overhanging at top).	Observed within Hidra and Kraka Formations (Cenomanian to Santonian strata).	Interpretation 1: small pockmarks within semi-consolidated chalks. Interpretation 2: collapse structure due to hypogenic karst or fluidization of chalk. Interpretation 3: seep carbonate chimneys (favourite)
6			High amplitude reflector packages (HARP's) Strongly fault-bound hard beds within clays and chalks. Often in association with depressions, which occur above. Limestone material with highly negative $\delta^{13}C$ values (-1 to -40‰).	Reflectors show hardening between 0.1 - 5 km wide, 1 - 5 km in length. Well data shows individual beds are 1 - 7 meter thick.	Observed within Lower Cretaceous marls and chalks (Tuxen & Sola Formations), throughout Upper Cretaceous chalks, and within Paleogene and Neogene clays.	Hard beds reflect microbially mediated limestone precipitation from seeping methane to seafloor, utilized by sulphate-reducing bacteria just below seafloor. Pockmarks above may indicate short-lived explosive release of methane, causing erosion.

Table 2. Overview of the different morphological features related to syn-depositional fluid migration episodes.

Paper 2. *Seismic expression of fluid and gas expulsion episodes in the Jurassic to Eocene of the Danish Central Graben – Submitted to Geological Society of London*

The second paper (Chapter III) deals, amongst other types of features (Table 2), also with 'SCRs' (Cat. 4 features) that are found within the Roar Basin (see Fig. 5 for location). Seismic mapping revealed that these 1-2 km wide, 50-200 m deep features, unlike the diagenetic bodies in the south, are

U-shaped on all sides, and slopes are more gentle (1-15° vs 35-55° in the Ryan Area). The U-shape reflectors truncate many host rock reflectors, and the infill pattern differs from the host rock it cuts into. Seven individual bowl-shaped depressions (Cat. 4 features) are mapped out, aligning N-S within the Roar Basin, but occurred within different parts of the Campanian stratigraphy (Gorm Formation). RMS amplitude time slices within the depressions show the occurrence of a large field of round depressions (Cat. 2/5 features), which did not occur outside

(within the host rock), and are interpreted to reflect pockmarks or carbonate chimneys. Based on the internal and external architecture, and the truncation pattern, we concluded that these Cat.4 features must represent depositional profiles. The spatial distribution of these Cat. 4 features is special: 1) they occur within Campanian strata (syn-inversion strata); 2) above a deep Late Jurassic basin with deeply rooted normal faults that became inverted in the Campanian inversion event; and 3) within a zone of maximum inversion movements, above a significant Early Cretaceous four-way closure. Basin modelling data show thermal maturity of several source rocks at the time of chalk deposition, as well as the possibility for formation of biogenic gas from Upper Jurassic strata. Based on the above, we concluded that these U-shape reflectors represent mega pockmarks that formed as a result of catastrophic release of gas-bearing bearing fluids to the Campanian seafloor in reaction to tectonic uplift and fault reactivation. While initially steep, subsequent reworking by mass movements, bottom current activity, and renewed fluid expulsion activity led to gentle U-shape depositional profiles on the basin floor. They are bowl-shaped due to their formation mechanism (e.g. focussed erosion where fluid expulsion occurred above Late Jurassic faults).

This study provides an alternative interpretation for the U-shape reflectors that other workers proposed to have formed as a result of bottom scouring (e.g. Back *et al.*, 2011; Esmerode *et al.*, 2008). This was mainly possible due to availability of larger amount of data (well and geochemical data), recognition of several other fluid expulsion features (giant pockmarks, Cat. 3, and seep carbonates, Cat. 6), and juxtaposition of basin-wide data (tectonic evolution, faults, and thermal maturity maps). Importantly, it shows that hydrocarbon migration already occurred during chalk deposition, reveals fluid migration pathways, and it indicates that the main seal for the Chalk Play was leaking for a long time (e.g. at least until the Eocene).

Paper 3. *Amalgamated pockmarks on the Danian seafloor caused by large-scale outbursts of gas-bearing fluids (Chalk Group, Greater Dan Region, Danish Central Graben)*

While building forth on Paper 2 (Chapter III), Paper 3 (Chapter IV) is a study that in great detail

investigates giant depressions (Cat. 3) close to the top of the Chalk Group on top of the Igor-Emma Ridge, within the hydrocarbon-bearing Ekofisk Fm. in the Halfdan and Tyra Area (see Fig. 5 for location). This is possible due to several penetrations by horizontal production wells, which provide logging data and material for geochemical analysis from the depressions. The lens-shaped depressions disturb the top Chalk Group seismic reflector in 2D seismic sections. Seismic geomorphological analysis shows a highly complex morphology, where the depression wall has a high amplitude, low-frequency signal, and the depression infill a low-mid amplitude, high-frequency signal. A horizontal well with sidetracks that penetrates three adjacent depressions reveals a complex infill of Danian chinks, marls, cherts, and Paleocene marls and clays. These surfaces and lithologies seem to dictate the gas-water-contact. For the first time, we utilize clumped isotope analysis on chinks from the North Sea Basin, and couple this here to seismic geomorphology. The method reveals that both the chinks from the infill as well as the host rock experienced similar normal burial diagenesis in a closed system.

The giant depressions (Cat. 3) occur mainly on top of inverted Campanian structures that are underlain by a deep Late Jurassic depocenter with deeply rooted faults, while smaller Cat. 2 features occur along the flanks. Basin modelling data showed thermal maturity of several source rocks at the time of mid-Danian chalk deposition, as well as the possibility to form biogenic gas from Upper Jurassic source rocks. Based on the internal characterization of the features, their location on top of the highest parts of the Danian seafloor, and connection to thermogenic and biogenic sources of gas-bearing fluids, we interpret the Cat. 3 depressions as giant pockmarks. Their highly amalgamated morphology reflects the time-transgressive nature of fluid expulsions on the seafloor, as well as mass movements, and potential bottom-current activity.

The importance of this study is that it provides a geological model for a highly complex reservoir within large hydrocarbon accumulations. The prediction of facies and understanding the nature of the pockmark walls, which all influence gas-water-contacts, are of key importance for well planning, and should form a focus of future research. The giant pockmarks also directly show the

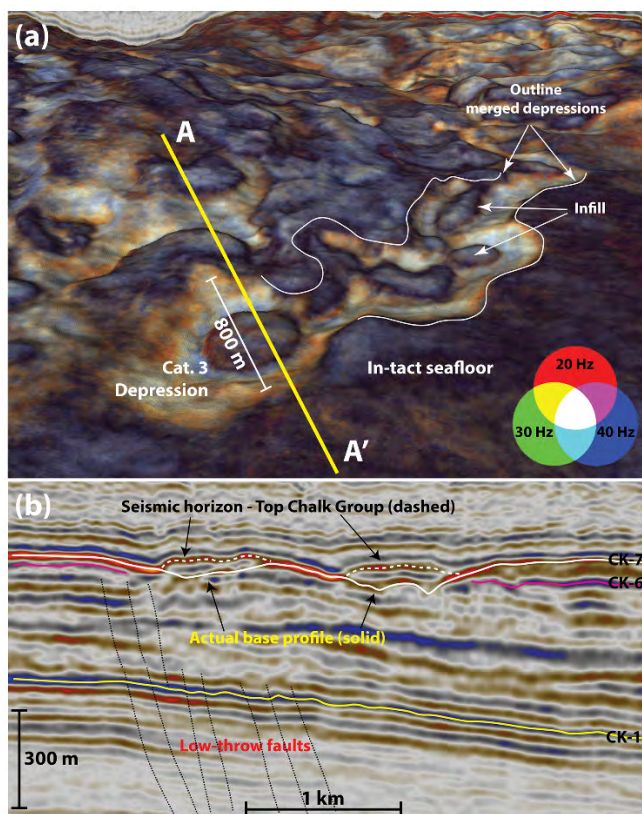


Figure 7. Category 3 features. (a) 3D mapview with RGB blend of spectral decomposition data on top Chalk seismic horizon (20, 30, 40 Hz). Category 3 features have circular (diameter 200-500 m), elliptical (200-500 m long axis, 200-300 short axis), highly elongated morphology (0.5-3 km in length), or complex shapes. The round ‘islands’ are actual top depression infill and not base of the category 3 depression, as highlighted in A-A’. (b) Section A-A’ runs perpendicular through a circular (diameter 800 m) and a highly elongated (long axis 3 km) category 3 feature, which are almost merged (see a). The U-shape depressions are up to 60 m deep, and truncate the CK-6 seismic marker, and have an undulating bottom profile (solid white line). Slopes are between 3-10 degrees to the horizontal. The infill has a general continuous, medium-amplitude character. Note the low-throw faults seen at the base of the Chalk Group (black dashed lines). From Paper 2.

relationship between source rock maturity, fluid migration pathways, and how the basin morphology plays a key role in funnelling gas-bearing fluids to the highest parts of the basin (e.g. small pockmarks along the flank, giant pockmarks on top).

Paper 4. *Distinguishing syn- and post-depositional fluid migration in the Chalk Group using clumped isotope analysis and seismic geomorphology (Upper Cretaceous, Danish Central Graben, onshore United Kingdom) – to be submitted to a journal (unpublished manuscript)*

Paper 4 is focussed on utilizing clumped isotope analysis (CIA) palaeothermometer in chalks

on case studies that have experienced syn- and post-depositional fluid migration, and builds forth on the outcome and interpretations of Paper 1, 2, and 3. The aim is to observe if one can distinguish diagenesis in closed-system and open-system in an absolute temperature vs. fluid $\delta^{18}\text{O}$ plot, and thereby provide model for recognition of extra-formation fluids that have been migrating through a rock. CIA provides an estimate of the bulk precipitation temperature of the rock (e.g. original coccoliths temp, and subsequent cement temperatures), which is independent of the fluid $\delta^{18}\text{O}$ value that is needed in classical palaeothermometers (e.g. Craig, 1965; Kim and O’Neil, 1997). The fluid $\delta^{18}\text{O}$ value can therefore be inferred from the absolute temperature estimate and the bulk $\delta^{18}\text{O}$ of the sample by using equation 1 and 2 (see paragraph Research Methods).

The sample points come from chalks associated with giant pockmarks (Paper 2, 3), fault-bound seismic-scale diagenesis (Paper 1), and calcite veins around heavily deformed and faulted chalks (Paper 4, Fig. 8). A strong positive correlation is observed between absolute precipitation temperature and fluid $\delta^{18}\text{O}$ values. This trend is interpreted to reflect normal burial diagenesis in a closed-system, whereby with increasing temperature lighter ^{16}O isotopes are preferentially taken up into the crystal lattice of the calcite cement, and the heavier ^{18}O remains within the formation fluid. Outliers occur within calcite veins and in chalk in direct vicinity of the veins, which show precipitation of fluids that are hot and have a negative fluid $\delta^{18}\text{O}$ value. These outliers are interpreted to reflect open-system diagenesis, whereby extra-formational fluids penetrated the chalk rock along fault planes (see Fig. 8 b and c). CIA, in combination with an integrated seismic geomorphology has therefore shown to provide great insights into closed- and open-system behaviour within chalk diagenesis. An interesting learning was that most of the chalk experienced closed-system diagenetic behaviour, and open-system diagenesis was only limited to narrow zones associated with faults.

Publication not included in this PhD

The following publication has been published with contribution by the author during the course of the PhD project but is not included in the thesis:

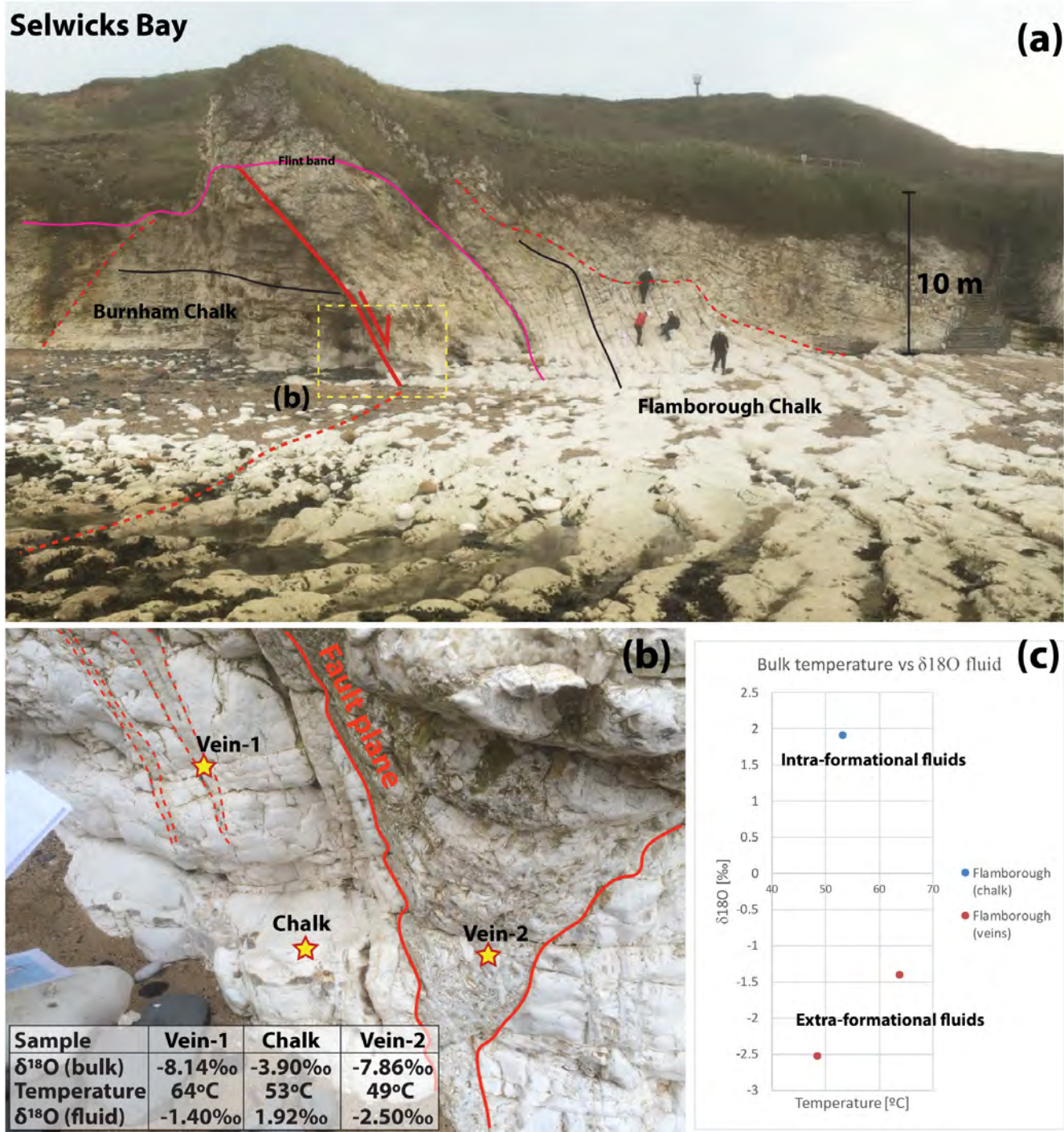


Figure 8. (a) Outcrop photo at Selwicks Bay showing the heavily deformed strata around the fault plane. (b) At the fault plane, large calcite veins occur that contain brittle chalk and translucent calcite crystals. Several smaller veins are splitting off the master vein. Sample locations are indicated with stars. Vein-1 contained very pure, coarse grained, translucent calcite crystals. Vein-2 also contained coarse grained calcite material, but was less pure (e.g. milkier). A chalk sample was taken directly adjacent to the major fault plane. (c) cross-plot of clumped isotope data show how closed-system and open-system diagenetic behaviour plot in different parts of the plot.

- van Buchem, F.S.P., Smit, F.W.H., Buijs, G.J.A., Trudgill, B., Larsen, P.H., 2018. Tectonostratigraphic framework and depositional history of the Cretaceous – Danian succession of the Danish Central Graben (North Sea) – new light on a mature

area, in: Bowman, M.B., Levell, B. (Eds.), Petroleum Geology of NW Europe: 50 Years of Learning - Proceedings of the 8th Petroleum Geology Conference. Geological Society of London, pp. 9–46

6. Contributions of this study: Updated seismic chalk paradigm

The integrated seismic geomorphological approach made it possible to document and interpret various features within the Chalk Group, and categorize them into five syn-depositional features (Table 3): 1.A. Pelagic deposition; 1.B. Bottom current activity; 1.C. Slope failure; 1.D1. Explosive gas venting features (pockmarks); 1.D2. Gas venting by seepage (seep carbonates); and two post-depositional features (Table 4): 2.A. Faulting and fracturing; 2.B. Seismic-scale diagenetic overprinting. The features will be addressed individually in the next two paragraphs, and reference is given to the individual chapters of this thesis where detailed documentation is provided. Based on an integration of the tectono-stratigraphic evolution during the Late Cretaceous (c.f. van Buchem *et al.* 2018), the underlying Jurassic depocenter locations, and source rock maturity, an integrated model is proposed for the formation of syn- and post-depositional fluid expulsion features. Lastly, the implications and applications for exploration and production of hydrocarbons is addressed.

6.1 Syn-depositional features and processes

Based on integration of core material (sedimentology), biostratigraphy, outcrop analogues, and seismic data, several syn-depositional features have been described in previous studies. Gennaro *et al.* (2013) summarized the observations in a table with 2D seismic examples. Here we build forth on the observations, but add 3D visualization with spectral decomposition data (Table 3). Importantly, we add two new types of features within the syn-depositional paradigm: explosive gas venting (1.D1) and seep-style gas venting (1.D2).

Known syn-depositional features

Pelagic deposition of chalk onto a rather flat basin floor, creates (semi-)parallel seismic reflectors (Table 3, 1.A). In 3D view, these chalks are rather featureless.

The recognition of moats and drifts within the Chalk Group by Lykke-Andersen and Surlyk

(2004) in the Danish Basin, led to documentation of several more examples within the North Sea Basin (Back *et al.*, 2011; Esmerode *et al.*, 2008, 2007; Esmerode and Surlyk, 2009; Gennaro and Wonham, 2014; Surlyk *et al.*, 2008). An example is shown from the Gulnare basin, where 100-500 m wide, 10-30 m deep moats occur, that show bifurcation towards the north (Table 3, 1.B).

Slope failure features have been recognized frequently within the Chalk Group, both in core (Anderskov and Surlyk, 2011), as well as on seismic data with chaos attributes on time slices (Back *et al.*, 2011; Bramwell *et al.*, 1999; Esmerode *et al.*, 2008; Gennaro *et al.*, 2013; van der Molen, 2004). By using stratigraphic horizons with spectral decomposition data as used in this study, it is even better possible to anatomize the seascape through a slope failure feature (Table 3, 1.C).

New syn-depositional features

Pockmarks have previously been recognized within the Chalk Group by Masoumi *et al.* (2014), who reported small (20-100 m diameter) pockmarks near the top of the chalk. Henriksen *et al.* (2009) recognized large depressions within the Halfdan NE gas field, and made the first interpretation as large pockmarks. However, further documentation on shape, spatial occurrence, and formation mechanism was not given. In this study, we have documented in detail giant pockmarks (100 to 800 m across, 20 to 80 m deep) and mega pockmarks (2 to 2.5 km wide, 100 – 250 m deep), and add these firmly to the seismic chalk paradigm as a subtype of gas venting features (explosive) (Table 2, 3, 1.D1).

Seep carbonates are a second subtype of gas venting features that are added to the paradigm (Table 1, 1.D2). Rather than explosive releases of gas-bearing fluids on the seafloor, slow seepage of methane from thermogenic and/or biogenic sources created colonies of sulphate reducing bacteria close to the seafloor that metabolized the gas (Teichert *et al.*, 2005). Cryptocrystalline calcite material was precipitated within the sediments, and are recognized as low-porous calcite that has a negative $\delta^{13}\text{C}$ values. At the seismic scale, these beds are recognized as high-amplitude troughs that are strongly coupled to the Late Jurassic faults.

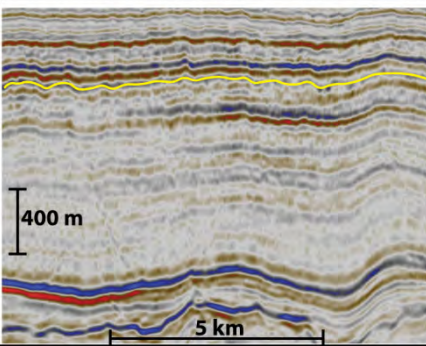
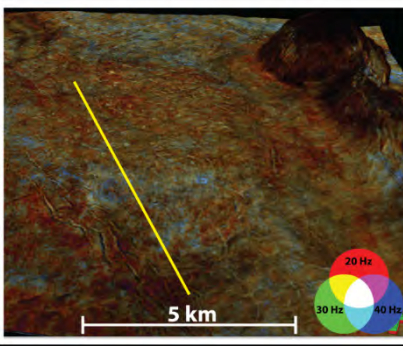
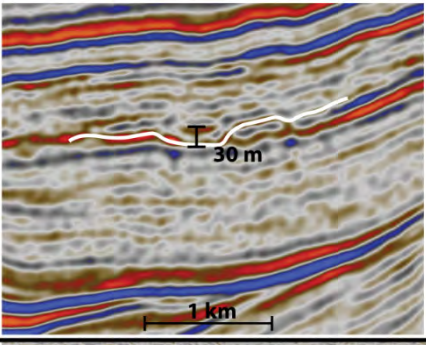
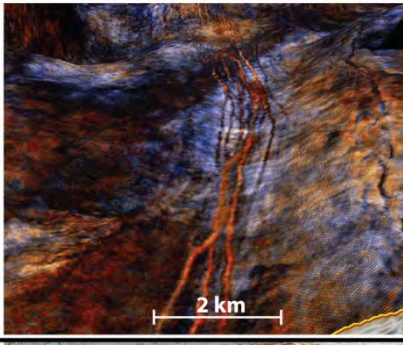
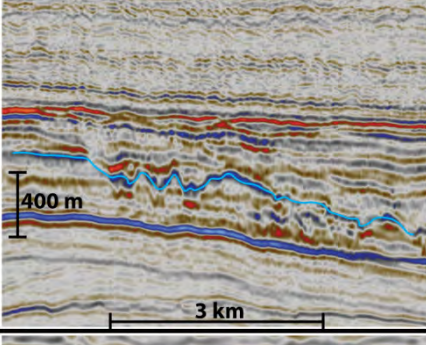
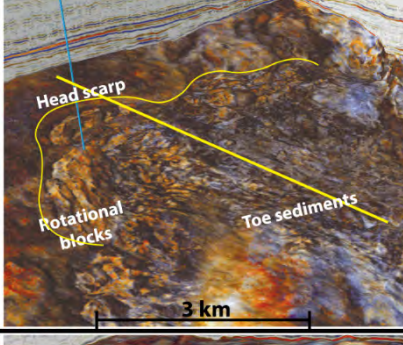
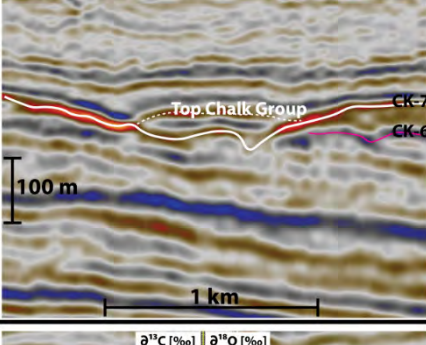
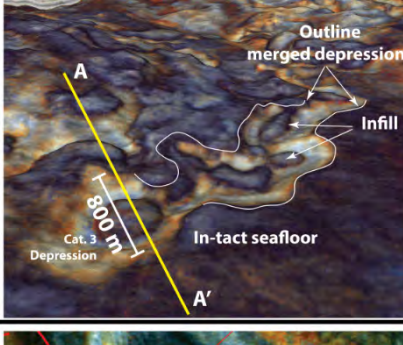
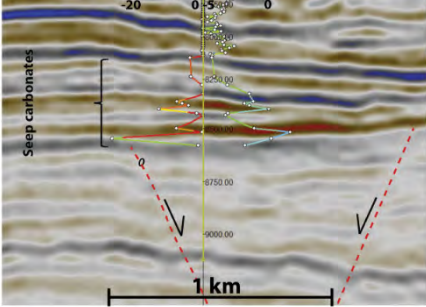
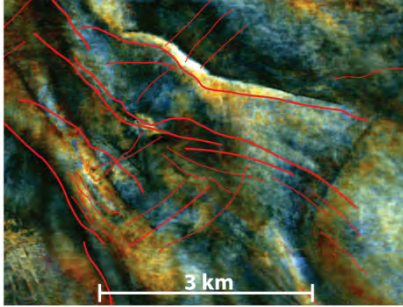
	Type	2D seismic example	3D seismic example
1. (syn-) depositional features	A. Pelagic deposition		
	B. Bottom current activity		
	C. Slope failure		
	D1. Gas venting (explosive)		
	D2. Gas venting (seepage)		

Table 3. Generalized overview of the different types of syn-depositional seismic facies in the Chalk Group. 1C from Smit *et al.* (2017).

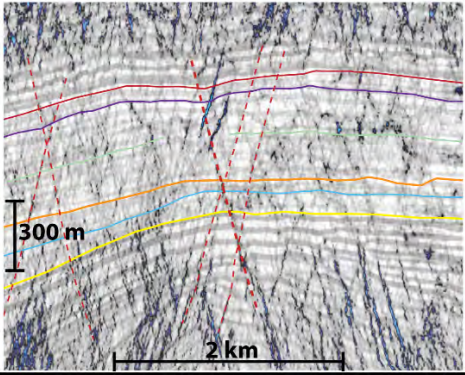
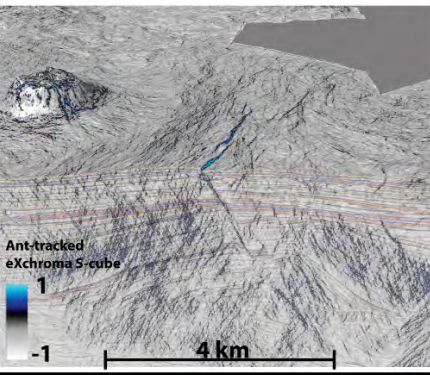
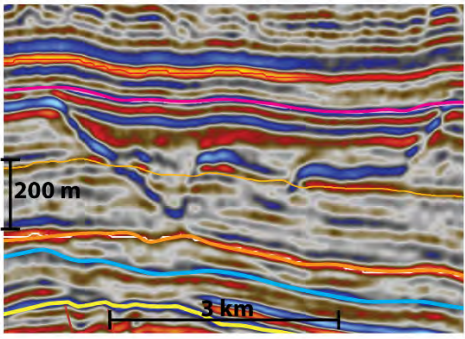
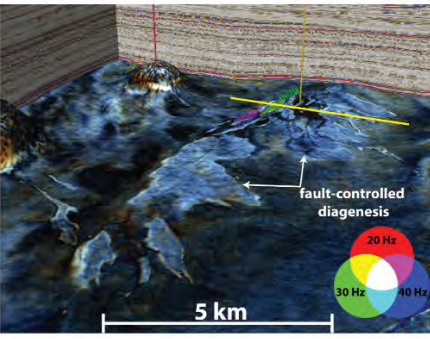
	Type	2D seismic example	3D seismic example
2. Post-depositional features	A. Structural deformation		
	B. Diagenetic overprint		

Table 4. Generalized overview of the different types of post-depositional seismic facies in the Chalk Group. 2B from Smit *et al.* (2018).

6.2 Post-depositional features and processes

Post-depositional features and processes represent deformation or alteration of the chalk rock after burial has occurred. With the updated seismic geomorphological approach, structurally controlled features (2.A) can be better defined, while seismic-scale diagenesis (2.B) has been added to the paradigm (Table 4).

Known post-depositional features

Tectonic forces acting on chalk coeval or after burial can lead to plastic or brittle deformation (Table 4, 2.A). Unless the offset between contrasting chalk packages is larger than the seismic resolution, it might be challenging to recognize structural features. Several previous studies have attempted to highlight faults and fractures within chalk with the use of seismic attributes on both 3D seismic amplitude data as well as 4D time-lapse data (Astratti *et al.*, 2012; Kuich, 1989; MacBeth *et al.*, 1999). These studies were using conventional wavelet-based seismic attributes that ‘smear’ the seismic signal over a relative large window (20-30 ms),

resulting in a seismic resolution possibly too low for certain structural features (e.g. low-throw faults and fracture swarms).

New post-depositional features

With a recently developed seismic image processing technique by Laake (2013), the ‘smearing’ of the signal is minimized (1.5x sample interval [4ms], 6ms). By ant-tracking the ‘structural-cube’ output, and eliminating low-dip signals, Smit *et al.* (2017) showed the possible occurrence of low-throw faults and fracture swarms within the chalk (Table 4, 2.A). A good correlation occurs between the attribute and seismic-scale faults on top of an anticline, which indicates that the attribute is highlighting structural features. In addition, it was shown that these features possibly relate to fracture corridors that could be observed as zones with increased fracture density in borehole images (Aabø *et al.*, 2017). Though architecture and dimensions appear similar to outcrops of fractured chinks in the UK (Starmer, 1995), further validation is needed to fully understand this seismic attribute.

Seismic-scale diagenetic overprint is another important addition to the seismic chalk paradigm (Table 4, 2B). ‘Stratigraphy Cross-cutting Reflectors’ occur on top of the Ryan Anticline in the southern Central Graben, where the ‘peaks’ (boundary to lower acoustic impedance chalks) outline bodies of high-density chalk (Smit *et al.*, 2018). Integrated seismic geomorphology has shown that these features are low-porous zones nested within high-porous chalks, and formed as a result of compaction and open-system diagenesis (Fig. 6). Understanding these features provided insights into the 3D relationship between fluid migration, diagenesis, and compaction, which seems to be controlled by the occurrence of formational tops, as well as feeder fault systems.

6.3 Timing and integrated model

Source rock depocenters

The occurrence of syn-depositional gas venting features within the Chalk Group indicates the presence of gas sources (thermogenic or biogenic) and fluid migration pathways (Fig. 7). In contrast, the absence of these features indicates that no source was present and/or fluid migration pathways. Based on seismic geomorphological mapping, the spatial distribution of gas venting features can be plotted on top of the isochore thicknesses of Lower-Middle Jurassic and Upper Jurassic successions, which hold potential source rocks for gases (Fig. 9a-b). The area with gas venting features is characterized by both thick Lower-Middle Jurassic (250 – 1000 ms) and Upper Jurassic strata (1500 – 3000 ms), and the occurrence of Late Jurassic normal faults. In addition, the features occur within the area of main Campanian inversion tectonics, which resulted in the formation inverted structures that formed the higher parts of the basin floor during chalk deposition (Fig 9c) (Van Buchem *et al.*, 2018). This can be seen in 2D seismic sections over the Igor-Emma Ridge, whereby post-inversion strata are onlapping the ridge (Fig. 10a).

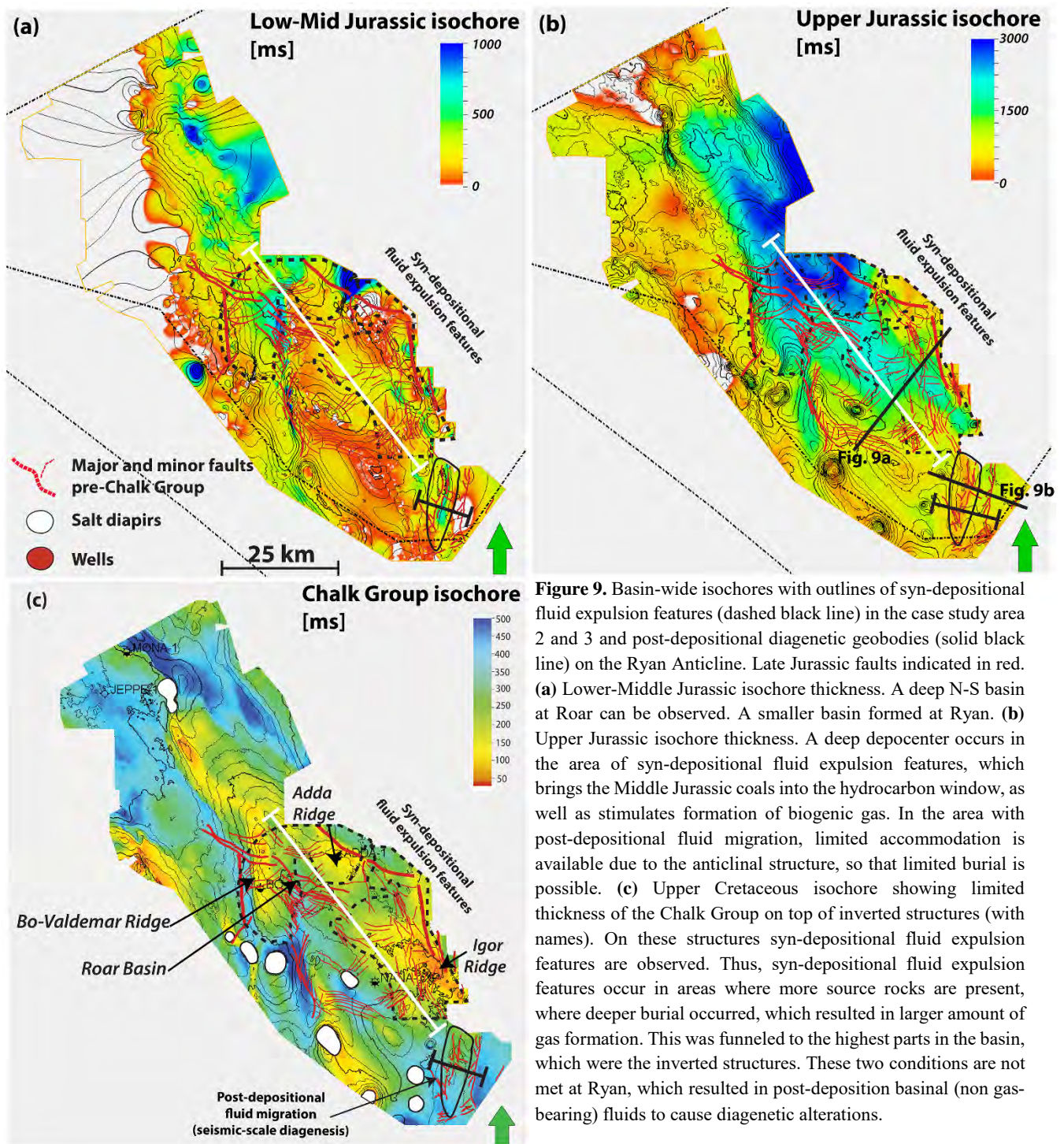
In contrast, seismic-scale diagenesis is observed outside the area with major Jurassic depocenters, but with Late Jurassic faults (Figs 9a-c, and 10b). The differences in thickness of the Jurassic successions between the two regions suggest that the possibility for large-scale gas-bearing fluid

accumulation was limited in the area with seismic-scale diagenesis (e.g. compare Jurassic thicknesses in Fig. 10a and b). In addition, the 2D seismic sections over the Ryan anticline show that the structure became buried during the Early Maastrichtian, and the isochore indeed shows that this area was more in a basinal setting compared to the area with syn-depositional fluid expulsion features.

Modelled thermal maturity juxtaposed on features

Modelled source rock maturity maps show that within the region where gas venting features occur within the Chalk Group, such as seep carbonates, giant pockmarks, and mega pockmarks, Middle Jurassic coals and lower parts of the organic-rich Upper Jurassic Farsund Formation were thermally mature (Fig. 11). The prolific Bo Member (‘hot shale’ c.f. Ineson *et al.*, 2003) was not yet thermally mature during Chalk deposition. However, palaeotemperature estimates of the Bo Member show that throughout large parts of the Chalk Group deposition, biogenic gas generation was possible (Fig. 12, e.g. temperatures below 50-60°C). Concluding, the gas venting features were likely sourced by both thermogenic and biogenic sources within Jurassic strata. In the area that experienced seismic-scale diagenesis, source rock thickness and maturity were low throughout chalk deposition, indicating limited sources of gas-bearing fluids (Fig. 11, yellow solid line). We therefore conclude that the occurrence of gas venting features occurs mainly in areas where source rock is present and mature, and seismic-scale diagenesis occurs outside of this zone (Fig. 13a-c).

Key in the formation of seismic-scale diagenesis is the episodic leaking of pressurized fluids out of the chalk due to the occurrence of a failing seal (Smit *et al.*, 2018). The increase in effective stress results in inelastic compaction, and cementation of pore-spaces (Fig. 13c). The occurrence of seep carbonates within the Paleogene and Neogene clays above present-day hydrocarbon accumulations in the syn-depositional expulsion features area, indicates that the top seal of the Chalk Play was leaking here as well. Possibly due to a steady supply of gas-bearing fluids from the underlying Jurassic depocenter, pore pressures could remain more constant, resulting in no or limited mechanical compaction when leaking occurred.



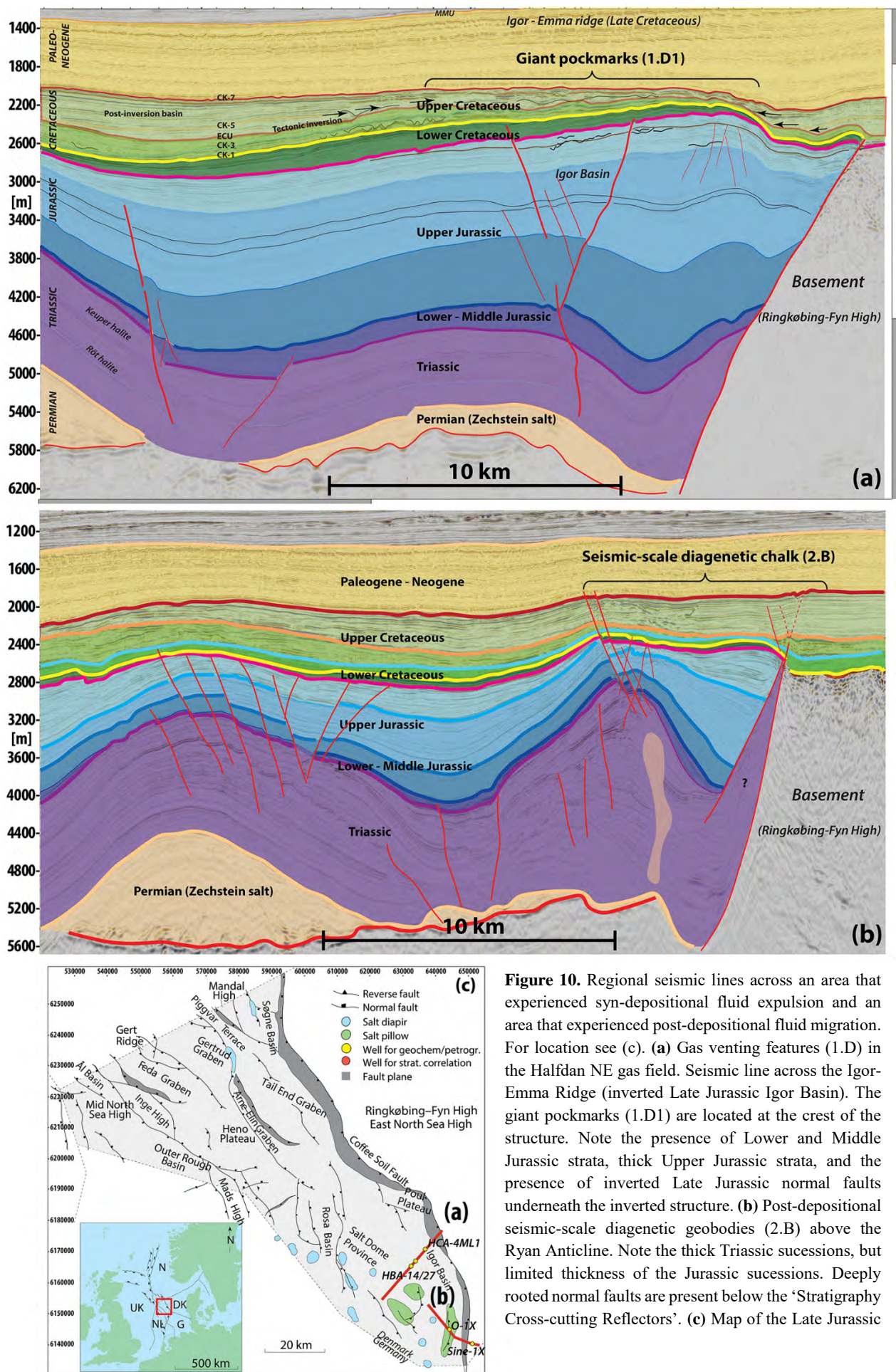


Figure 10. Regional seismic lines across an area that experienced syn-depositional fluid expulsion and an area that experienced post-depositional fluid migration. For location see (c). **(a)** Gas venting features (1.D) in the Halfdan NE gas field. Seismic line across the Igor-Emma Ridge (inverted Late Jurassic Igor Basin). The giant pockmarks (1.D1) are located at the crest of the structure. Note the presence of Lower and Middle Jurassic strata, thick Upper Jurassic strata, and the presence of inverted Late Jurassic normal faults underneath the inverted structure. **(b)** Post-depositional seismic-scale diagenetic geobodies (2.B) above the Ryan Anticline. Note the thick Triassic successions, but limited thickness of the Jurassic successions. Deeply rooted normal faults are present below the 'Stratigraphy Cross-cutting Reflectors'. **(c)** Map of the Late Jurassic

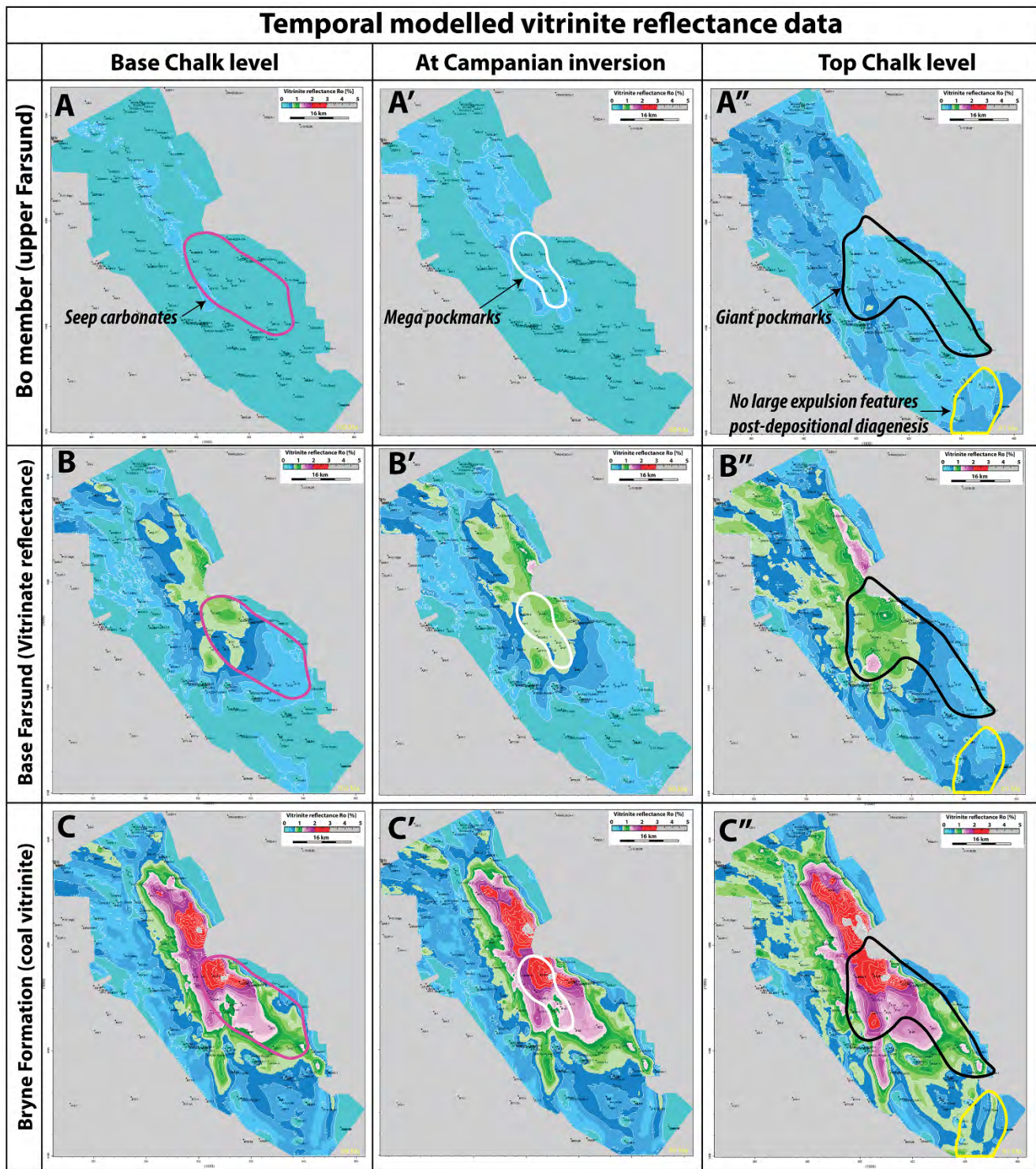


Figure 11. Modelled values of vitrinite reflectance (R_o in %) of three main source rocks in the Danish Central Graben at the base of the Chalk Group (100 Ma), start of the Campanian inversion (86 Ma), end of the Danian (top Chalk Group level, 61 Ma). Purple outlines represent seep carbonates close to the base of the Chalk Group, white outlines represent mega pockmarks within the Gorm Formation (**A-A'**) Bo Member of the Farsund Formation ('hot shale' c.f. Ineson *et al.* 2003); (**B-B''**) Base Farsund Formation; (**C-C''**) Middle Jurassic coals of the Bryne Formation. Candidates for providing thermogenic gas-bearing fluids for the formation of seep carbonates, mega pockmarks, and giant pockmarks are the Middle Jurassic coals of the Bryne Formation, and lower parts of the organic-rich Farsund Formation. The Bo member was immature at this time for providing thermogenically derived gas-bearing fluids.

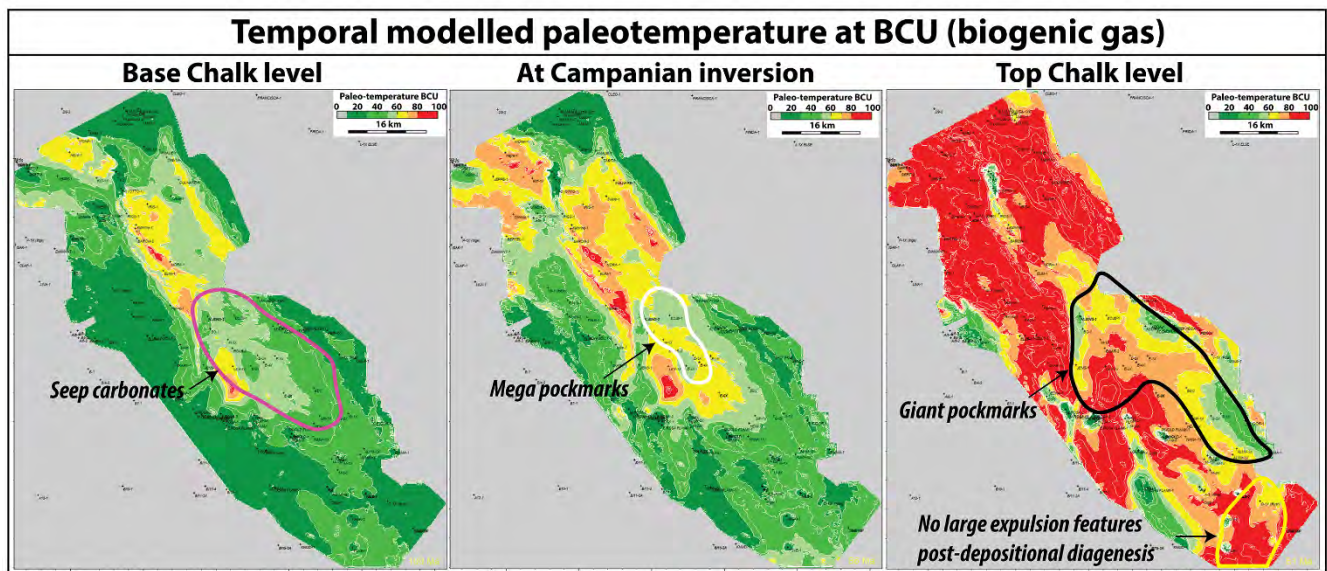


Figure 12. Modelled palaeotemperature of the BCU surface in the Danish Central Graben at (a) the start of the Cenomanian (base Chalk Group level, 100 Ma). Outline of the spatial occurrence of seep carbonates in purple; (b) the start of the Campanian inversion (82 Ma). Outline of the spatial distribution of mega pockmarks in white; (c) the end of the Danian (top Chalk Group level, 61 Ma). Outline of the spatial distribution of giant pockmarks in black (Chapter III, and IV), of post-depositional diagenesis in yellow (Chapter II). Biogenic gas generation is possible until 50–60°C, and therefore for all gas venting features, it is possible that an additional biogenic gas sources from Upper Jurassic organic-rich intervals added to the thermogenic gas-bearing fluids

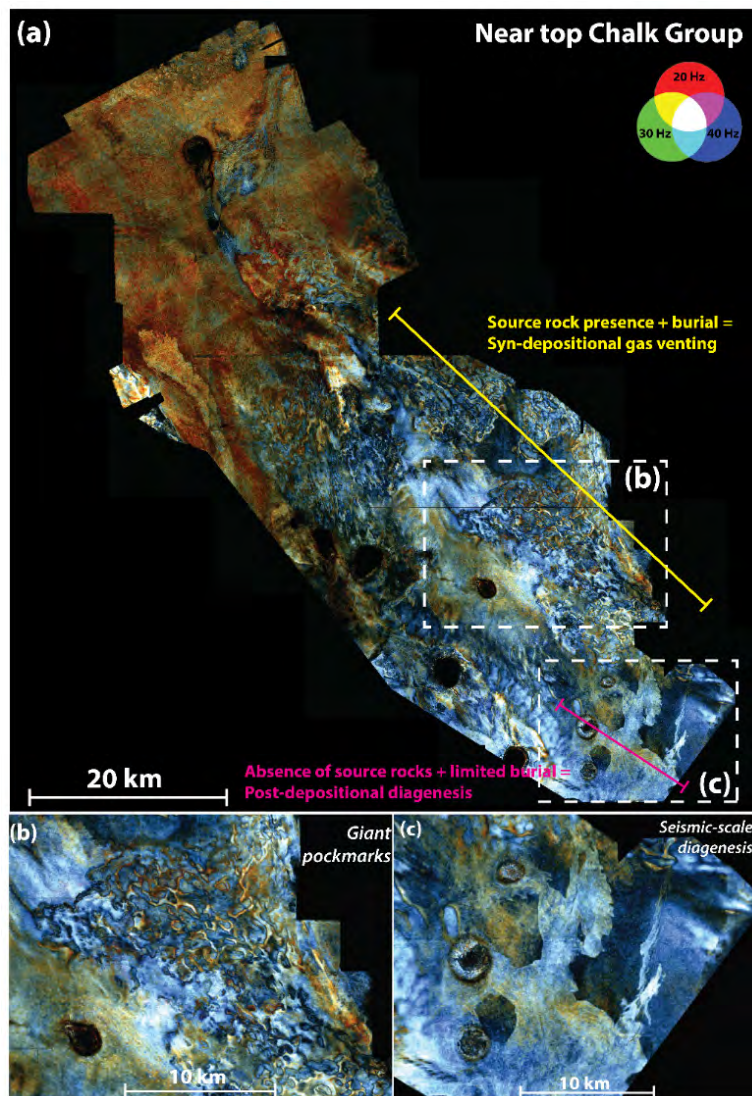


Figure 13. Seismic horizon at near Top Chalk Group with spectral decomposition data in RGB blend. It shows a clear zonation between syn-depositional fluid expulsion features in the central part of the Danish Central Graben and post-depositional seismic-scale diagenesis in the southernmost part of the Danish Central Graben. See Supplement 1 for a high-quality version.

6.4 Implications for production and exploration of hydrocarbons

The recognition and documentation of different types of seismic geomorphological features within the Chalk Group has important applications for production and exploration of hydrocarbons (Tables 3 and 4).

The internal seismic geometries within the Chalk Group are often complex, and it can be a challenge to provide a geological interpretation that can aid reservoir characterization workflows for production. Tables 3 and 4 provide an overview of well-documented end-members of different types of seismic facies where a geological interpretation has been given. In order to make prediction of rock properties possible, more work is needed to integrate such seascapes to cored intervals and observe changes in facies, porosity, and permeability. Such correlations might then provide a guideline for populating

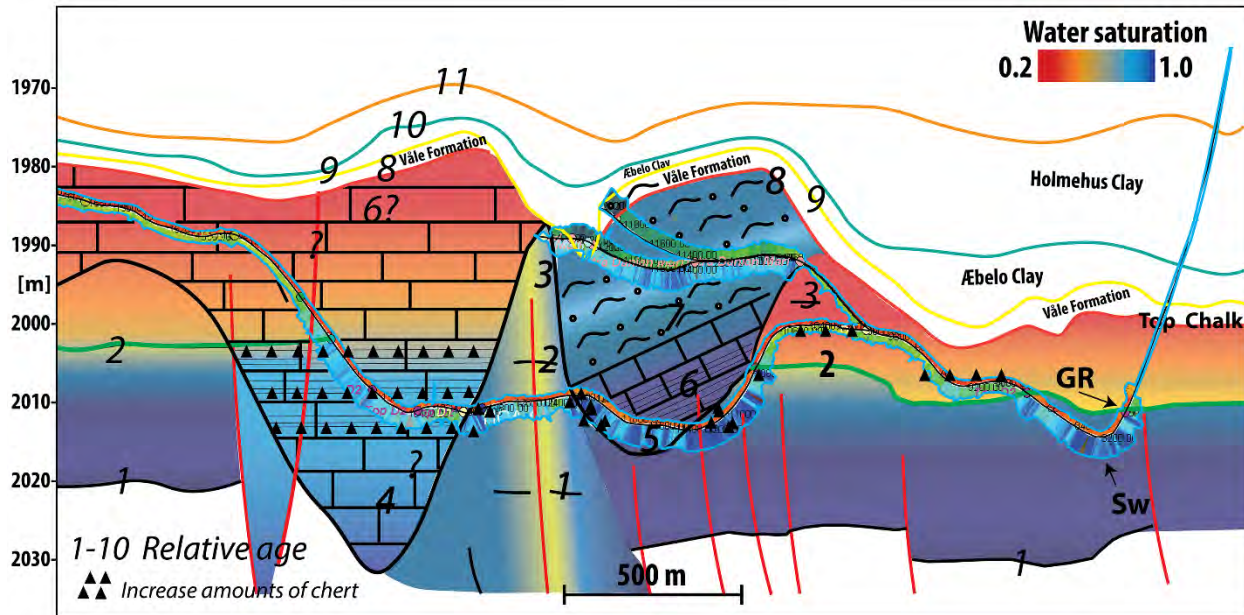


Figure 14. Sketch of predicted water saturation in the category 3 features based on the seismic geometries, and well data (GR and water saturation).

the reservoir with meaningful properties that could for example explain the position of gas-water-contact surfaces (Fig. 14). Another benefit of a seismic geomorphological approach within the Chalk Group is that the visualizations help to identify possible analogues from other parts of the basin, and/or see comparisons to present-day seafloor studies that observe similar features.

The recognition of gas venting features within the Chalk Group shows not only that source rocks were present and generated biogenic or thermogenic gases, it also provides evidence of fluid migration pathways. Therefore, these features form important blueprints of the plumbing system of the basin, which can help to identify overlooked areas for exploration. Gas venting features possible reflect long-term fluid migration, and once an effective seal formed on top of the chalk, the early hydrocarbon entry could keep pore spaces open due to retardation of calcite cementation (Fabricius, 2007; Scholle and Halley, 1985). It might therefore explain porosity anomalies within chinks that experienced early charge.

Lastly, the recognition of seismic-scale diagenetic geobodies can possibly open up a new Chalk Play type. The formation of high-density chinks as a result of compaction and cementation due

to episodic overpressure leakage will result on non-reservoir chalk. The low-porous chinks can act as intra-chalk seals, and can trap highly pressured basinal fluids (e.g. establish high overpressures), that will retard burial diagenesis and keep porosities high. If a source rock is present and becomes mature, and fluid pathways are not blocked by cement, high-porous zones underneath diagenetic geobodies could become hydrocarbon reservoirs (Fig. 15). Alternatively, the diagenetic geobody can divert ascending hydrocarbons away towards the higher parts of the basin, therefore forms an important fluid migration element (Fig. 15).

6.5 Conclusions

The aim for this PhD project was to better define seismic-scale heterogeneities within the Chalk Group, based on an integrated seismic geomorphological approach, in order to improve the prediction of facies for reservoir characterization purposes. Improved computation power and developments in seismic interpretation software made it possible to formulate an updated seismic geomorphological workflow that aims at anatomizing the geological content from the seismic signal by through integration with other petrographical and geochemical proxies.

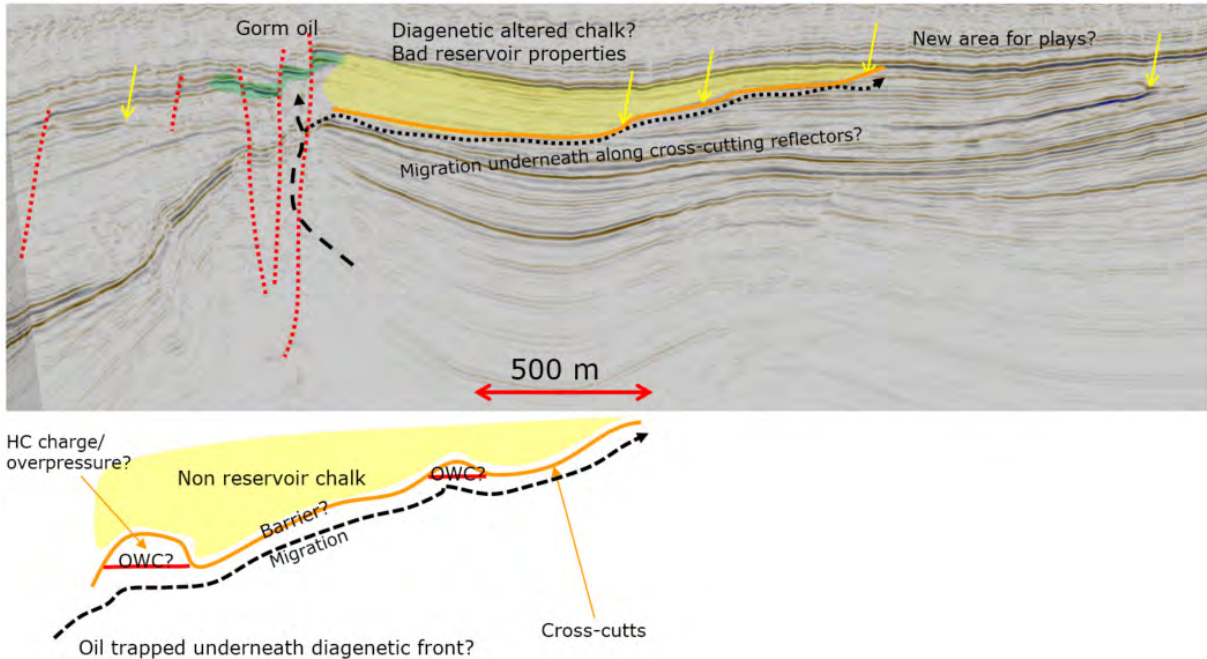


Figure 15. New Chalk Play type based on seismic-scale diagenetic geobodies (e.g. Smit *et al.* 2018).

The main result of this study has been to contribute significantly to our understanding of seismic reflectors within the Chalk Group that on first sight might be named ‘Funny Looking Things’, but now have proposed geological interpretation and formation mechanisms.

In the process of doing so, we have established an updated seismic-scale chalk paradigm that builds forth on work from previous four decades (see background paragraph). The new subdivision includes four syn-depositional seismic features (pelagic chalk, bottom current activity, slope failure, and gas venting features), and two post-depositional features (structurally deformed chalk and seismic-scale diagenesis). For the first time clumped isotope analysis has been performed on chalks from the North Sea Basin and combined with seismic geomorphology, resulting in the formulation of a geochemical model for recognition of closed-system diagenetic behaviour and open-system.

By investigating regional spatial patterns for the different seismic geomorphological features, and juxtaposing fault fabric maps, tectonic evolution from tectono-stratigraphy, as well as basin modelling data, we have been able to provide a predictive model for the occurrences of syn- and post-depositional

fluid migration features (e.g. gas venting features vs seismic-scale diagenesis). The main learning from these case studies is that already during chalk deposition, source rocks were generating thermogenic and biogenic gas within the Late Jurassic depocenters. Along major faults, these gas-bearing fluids were funnelled to the highest parts of the Late Cretaceous seafloor to form giant craters. Outside of the depocenter, only limited gas venting occurred, while basinal compaction fluids build up pressure within the Mesozoic basin and the Chalk Group. Faulting, possibly due to differential compaction, led to escape of these fluids that caused compaction and open-system diagenesis in the chalk.

Lastly, the updated seismic chalk paradigm provides opportunities for both exploration and production of hydrocarbons. The recognition of seismic-scale diagenesis, forming low-porosity chalks, could form a new Chalk Play (or any carbonate play), if a source rock is present and the underlying fault are not completely clogged up with calcite material. The recognition and geological interpretation of giant pockmarks within hydrocarbon-bearing strata provide an opportunity to explore the influences of surfaces and infills on the GWC, by combining all data available derived from horizontal wells, as well as seismic (3D and 4D) data.

6.6 Outlook

The formulation of the updated seismic chalk paradigm invites for recognition of similar features elsewhere in the North Sea Basin, to provide a larger range of examples, and possibly refine the paradigm further. While well penetrations in the Danish Central Graben are plenty, cored intervals nearly never cover the features of interest. Therefore, by recognizing such features elsewhere, chances increase that a well has directly penetrated the centre of the feature (such as with the seismic-scale diagenesis, or mega pockmark), and has core in that interval, which can lead to further characterization. Ultimately, it would be very beneficial for predicting reservoir quality, to have a large catalogue of case studies available that report on the impact of a certain feature on permeability, porosity, and mineralogy. Building such database asks for standardization of techniques and reporting styles, but this is possible.

With increasing availability of (3D and 4D) seismic data, (horizontal) wells, and real-time sensors, a ‘data explosion’ seems to be happening soon. In order to grasp the geological content from such data, machine-learning on seismic chalk facies might prove very beneficial for further data integration (Liu, 2017). Rather than trying out which variables correlate with one another (such as geochemical, porosity, and seismic facies), machine learning can help point out these relationships, which can form a starting point for further geological investigation.

Hancock’s statement in 1975 that “instead of a homogeneous rock that it first appears to be, various chalks show rhythmic bedding, lamination bedding, submarine erosion surfaces and current-piled banks” certainly hit the nail on the head. This mud-grade, biogenic, white rock known from impressive outcrops, holds many more secrets than one would imagine in the first place. Though care has been taken to avoid inconsistencies, there will possibly be some in this thesis, but, as Yuval Harari points out in his book *Sapiens*, they will only lead “*us to think, re-evaluate and criticize*”, which will only further our understanding of the (highly undersampled) subsurface.


References

- Anderskov, K., & Surlyk, F. (2011). Upper Cretaceous chalk facies and depositional history recorded in the Mona-1 core, Mona Ridge, Danish North Sea (Vol. 25). Geological Survey of Denmark and Greenland
- Arfai, J., Lutz, R., Franke, D., Gaedicke, C., & Kley, J. (2016). Mass-transport deposits and reservoir quality of Upper Cretaceous Chalk within the German Central Graben, North Sea. *International Journal of Earth Sciences*, 105(3), 797-818.
- Astratti, D., Aarre, V., Vejbæk, O. V., & White, G. (2015). Mapping and time-lapse analysis of South Arne Chalk fault network using new developments in seismic dip computation. Geological Society, London, Special Publications, 406(1), 331-358.
- Back, S., Van Gent, H., Reuning, L., Grötsch, J., Niederau, J., & Kukla, P. (2011). 3D seismic geomorphology and sedimentology of the Chalk Group, southern Danish North Sea. *Journal of the Geological Society*, 168(2), 393-406.
- Bramwell, N. P., Caillet, G., Meciani, L., Judge, N., Green, M., & Adam, P. (1999, January). Chalk exploration, the search for a subtle trap. In Geological Society, London, Petroleum Geology Conference series (Vol. 5, No. 1, pp. 911-937). Geological Society of London.
- Brewster, J., & Dangerfield, J. A. (1984). Chalk fields along the Lillesnes Ridge, Eldfisk. *Marine and Petroleum Geology*, 1(3), 239-278.
- Cooke, N., Szafian, P., Gruenwald, R., & Schuler, L. (2014). Forward modelling to understand colour responses in an HDFD RGB blend around a gas discovery. *First Break*, 32(3), 87-97.
- Craig, H. (1965). The measurement of oxygen isotope paleotemperatures. Stable isotopes in oceanographic studies and paleotemperatures: Consiglio Nazionale delle Ricerche, 161-182.
- D’Heur, M. (1984). Porosity and hydrocarbon distribution in the North Sea chalk reservoirs. *Marine and Petroleum Geology*, 1(3), 211-238.
- de Matos, M. C., & Marfurt, K. J. (2011, January). Inverse continuous wavelet transform “deconvolution”. In 2011 SEG Annual Meeting. Society of Exploration Geophysicists.
- Egeberg, P. K., & Aagaard, P. (1989). Origin and evolution of formation waters from oil fields on the Norwegian shelf. *Applied Geochemistry*, 4(2), 131-142.
- Esmerode, E. V., Lykke-Andersen, H., & Surlyk, F. (2008). Interaction between bottom currents and slope failure in the Late Cretaceous of the southern Danish Central Graben, North Sea. *Journal of the Geological Society*, 165(1), 55-72.

- Esmerode, E. V., Lykke-Andersen, H., & Surlyk, F. (2007). Ridge and valley systems in the Upper Cretaceous chalk of the Danish Basin: contourites in an epeiric sea. *Geological Society, London, Special Publications*, 276(1), 265-282.
- Esmerode, E. V., & Surlyk, F. (2009). Origin of channel systems in the Upper Cretaceous Chalk Group of the Paris Basin. *Marine and Petroleum Geology*, 26(8), 1338-1349.
- Fabricius, I. L. (2014). Burial stress and elastic strain of carbonate rocks. *Geophysical Prospecting*, 62(6), 1327-1336.
- Fabricius, I. L. (2007). Chalk: composition, diagenesis and physical properties. *Geological Society of Denmark. Bulletin*, 55, 97-128.
- Fabricius, I. L., Gommessen, L., Krogsbøll, A., & Olsen, D. (2008). Chalk porosity and sonic velocity versus burial depth: Influence of fluid pressure, hydrocarbons, and mineralogy. *AAPG bulletin*, 92(2), 201-223.
- Fritsen, A., Bailey, H., Gallagher, L., Hampton, M., Krabbe, H., Jones, B., Jutson, D., ... & Sawyer, D. (1999). Joint chalk research phase V: a joint chalk stratigraphic framework. *Norwegian Petroleum Directorate (NPD), Stavanger*.
- Frykman, P., Deutsch, C. V., 2002. Practical Application of Geostatistical Scaling Laws for Data Integration. *Petrophysics* 43 (3), 153–171.
- Frykman, P., Jacobsen, F., & Surlyk, F. (2004). The chalk at Stevns Klint—a reservoir chalk analogue. *Danmarks og Grønlands Geologiske Undersøgelse Rapport*, Copenhagen.
- Gennaro, M., & Wonham, J. P. (2014). Channel development in the chalk of the Tor Formation, North Sea. From Depositional Systems to Sedimentary Successions on the Norwegian Continental Margin, 551-586.
- Gennaro, M., Wonham, J. P., Gawthorpe, R., & Sælen, G. (2013). Seismic stratigraphy of the chalk group in the Norwegian Central Graben, North Sea. *Marine and Petroleum Geology*, 45, 236-266.
- Ghosh, P., Adkins, J., Affek, H., Balta, B., Guo, W., Schauble, E. A., ... & Eiler, J. M. (2006). 13C–18O bonds in carbonate minerals: a new kind of paleothermometer. *Geochimica et Cosmochimica Acta*, 70(6), 1439-1456.
- Hancock, J. M. (1975). The petrology of the Chalk. *Proceedings of the Geologists' Association*, 86(4), 499-535.
- Henriksen, K., Gommessen, L., Hansen, H. P., Kistrup, J. P., & Steekelenburg, C. (2009, January). Optimizing Chalk Reservoir Development Using Detailed Geophysical Characterization: The Halfdan Northeast Field, Danish North Sea. In *Offshore Europe*. Society of Petroleum Engineers.
- Ineson, J. R., Bojesen-Koefoed, J. A., Dybkjær, K., & Nielsen, L. H. (2003). Volgian–Ryazanian ‘hot shales’ of the Bo Member (Farsund Formation) in the Danish Central Graben, North Sea: stratigraphy, facies and geochemistry. *The Jurassic of Denmark and Greenland. Geological Survey of Denmark and Greenland Bulletin*, 1, 403-436.
- Japsen, P., Britze, P., & Andersen, C. (2003). Upper Jurassic–Lower Cretaceous of the Danish Central Graben: structural framework and nomenclature. *The Jurassic of Denmark and Greenland. Geological Survey of Denmark and Greenland Bulletin*, 1, 233-246.
- Jensenius, J., Buchardt, B., Jørgensen, N. O., & Pedersen, S. (1988). Carbon and oxygen isotopic studies of the chalk reservoir in the Skjold oilfield, Danish North Sea: implications for diagenesis. *Chemical Geology: Isotope Geoscience Section*, 73(2), 97-107.
- Jensenius, J., & Munksgaard, N. C. (1989). Large scale hot water migration systems around salt diapirs in the Danish central trough and their impact on diagenesis of chalk reservoirs. *Geochimica et Cosmochimica Acta*, 53(1), 79-87.
- Jensenius, J., & Munksgaard, N. C. (1989). Large scale hot water migration systems around salt diapirs in the Danish central trough and their impact on diagenesis of chalk reservoirs. *Geochimica et Cosmochimica Acta*, 53(1), 79-87.
- Keszhelyi, D., Dysthe, D. K., & Jamtveit, B. (2016). Compaction of North-sea chalk by pore-failure and pressure solution in a producing reservoir. *Frontiers in Physics*, 4, 4.
- Kim, S. T., & O'Neil, J. R. (1997). Equilibrium and nonequilibrium oxygen isotope effects in synthetic carbonates. *Geochimica et Cosmochimica Acta*, 61(16), 3461-3475.
- Kuich, N. (1990). Seismic Fracture Identification and Horizontal Drilling: Keys to Optimizing Productivity in a Fractured Reservoir, Giddings Field, Texas. *Gulf Coast Assoc. Geol. Soc. Trans.* 39, 153–158.
- Kyrkjebø, R., Gabrielsen, R. H., & Faleide, J. I. (2004). Unconformities related to the Jurassic–Cretaceous synrift–post-rift transition of the northern North Sea. *Journal of the Geological Society*, 161(1), 1-17.
- Liu, J., & Marfurt, K. J. (2005, January). Matching pursuit decomposition using Morlet wavelets. In *2005 SEG Annual Meeting*. Society of Exploration Geophysicists.
- Liu, Y., 2017. Applications of Machine Learning for Seismic Quantitative Interpretation, in: *GeoConvention*. Calgary, Canada, pp. 1–5
- Lykke-Andersen, H., & Surlyk, F. (2004). The Cretaceous–Palaeogene boundary at Stevns Klint, Denmark: inversion tectonics or sea-floor topography?. *Journal of the Geological Society*, 161(3), 343-352.
- Laake, A., 2013. Structural interpretation in color—A new RGB processing technique for extracting geological structures from seismic data, in: *SEG Technical Program Expanded Abstracts 2013*. Society of Exploration Geophysicists, pp. 1472–1476.

- MacBeth, C., Jakubowicz, H., Kirk, W., Li, K. Y., & Ohlsen, F. (1999). Fracture-related amplitude variations with offset and azimuth in marine seismic data. *First Break*, 17, 13-26.
- Mallat, S.G., Zhang, Z., 1993. Matching Pursuit With Time-Frequency Directories. *IEEE Trans. Signal Process.* 1–43.
- Marfurt, K. J., & Kirlin, R. L. (2001). Narrow-band spectral analysis and thin-bed tuning. *Geophysics*, 66(4), 1274-1283.
- Masoumi, S., Reuning, L., Back, S., Sandrin, A., & Kukla, P. A. (2014). Buried pockmarks on the Top Chalk surface of the Danish North Sea and their potential significance for interpreting palaeocirculation patterns. *International Journal of Earth Sciences*, 103(2), 563-578.
- Nygaard, E., Lieberkind, K., & Frykman, P. (1983). Sedimentology and reservoir parameters of the Chalk Group in the Danish Central Graben. In *Petroleum Geology of the Southeastern North Sea and the Adjacent Onshore Areas* (pp. 177-190). Springer, Dordrecht.
- Partyka, G., Gridley, J., & Lopez, J. (1999). Interpretational applications of spectral decomposition in reservoir characterization. *The leading edge*, 18(3), 353-360.
- Pedersen, S. I., Skov, T., Randen, T., & Sønneland, L. (2005). Automatic fault extraction using artificial ants. In *Mathematical Methods and Modelling in Hydrocarbon Exploration and Production* (pp. 107-116). Springer, Berlin, Heidelberg.
- Posamentier, H.W., Davies, R.J., Cartwright, J. a., Wood, L.J., 2007. Seismic geomorphology - an overview. *Journal of the Geological Society, Special Publication 277*, 1–14.
- Schauble, E. A., Ghosh, P., & Eiler, J. M. (2006). Preferential formation of ^{13}C – ^{18}O bonds in carbonate minerals, estimated using first-principles lattice dynamics. *Geochimica et Cosmochimica Acta*, 70(10), 2510-2529.
- Schneider, F., Dubille, M., Montadert, L. (2016) Modeling of microbial gas generation: application to the eastern Mediterranean “Biogenic Play”. *Geologica Acta*, 14, issue 4, 403-417
- Scholle, P. A. (1974). Diagenesis of Upper Cretaceous chalks from England, Northern Ireland and the North Sea. *Pelagic Sediments: on Land and under the Sea*, 177-210.
- Scholle, P.A., Halley, R.B., 1985. Burial diagenesis: Out of sight, out of mind!, in: *Carbonate Sedimentology and Petrology*. American Geophysical Union, Washington, D. C., pp. 135–160.
- Smit, F.W.H., 2014. Seismic stratigraphy, basin evolution and seismic geomorphology of the Late Cretaceous and earliest Paleocene Chalk Group in the Danish Central Graben. Aarhus Univ. Aarhus University.
- Starmer, I. C. (1995). Deformation of the Upper Cretaceous Chalk at Selwicks Bay, Flamborough Head, Yorkshire: its significance in the structural evolution of north-east England and the North Sea Basin. *Proceedings of the Yorkshire Geological Society*, 50(3), 213-228.
- Staudigel, P. T., Murray, S., Dunham, D. P., Frank, T. D., Fielding, C. R., & Swart, P. K. (2018). Cryogenic Brines as Diagenetic Fluids: Reconstructing the Diagenetic History of the Victoria Land Basin using Clumped Isotopes. *Geochimica et Cosmochimica Acta*.
- Surlyk, F., Dons, T., Clausen, C.K., Higham, J., 2003. Upper Cretaceous, in: *The Millennium Atlas: Petroleum Geology of the Central and Northern North Sea*. pp. 213–233.
- Surlyk, F., Jensen, S. K., & Engkilde, M. (2008). Deep channels in the Cenomanian–Danian Chalk Group of the German North Sea sector: Evidence of strong constructional and erosional bottom currents and effect on reservoir quality distribution. *AAPG bulletin*, 92(11), 1565-1586.
- Swart, P. K. (2015). The geochemistry of carbonate diagenesis: The past, present and future. *Sedimentology*, 62(5), 1233-1304.
- Swart, P. K., Cantrell, D. L., Arienzo, M. M., & Murray, S. T. (2016). Evidence for high temperature and ^{18}O -enriched fluids in the Arab-D of the Ghawar Field, Saudi Arabia. *Sedimentology*, 63(6), 1739-1752.
- Teichert, B. M., Bohrmann, G., & Suess, E. (2005). Chemoherms on Hydrate Ridge—Unique microbially-mediated carbonate build-ups growing into the water column. *Palaeogeography, Palaeoclimatology, Palaeoecology*, 227(1), 67-85.
- van Buchem, F.S.P., Smit, F.W.H., Buijs, G.J.A., Trudgill, B., Larsen, P.H., (2018). Tectonostratigraphic framework and depositional history of the Cretaceous – Danian succession of the Danish Central Graben (North Sea) – new light on a mature area, in: Bowman, M.B., Levell, B. (Eds.), *Petroleum Geology of NW Europe: 50 Years of Learning - Proceedings of the 8th Petroleum Geology Conference*. Geological Society of London, pp. 9–46.
- Van Der Molen, A. S. (2004). Sedimentary development, seismic stratigraphy and burial compaction of the Chalk Group in the Netherlands North Sea area. PhD dissertation, Department of Earth Sciences. University of Utrecht
- Vejbæk, O.V., Andersen, C., Dusa, M., Herngeen, W., Krabbe, H., Leszczynski, K., Lott, G.K., Mutterlose, J., van der molen, A.S., 2010. Cretaceous, in: *Petroleum Geological Atlas of the Southern Permian Basin Area*. pp. 195–209.
- Aabø, T. M., Dramsch, J. S., Welch, M. J., & Lüthje, M. (2017, June). Correlation of Fractures From Core, Borehole Images and Seismic Data in a Chalk Reservoir in the Danish North Sea. In *79th EAGE Conference and Exhibition 2017*.

Seismic geomorphology and origin of diagenetic geobodies in the Upper Cretaceous Chalk of the North Sea Basin (Danish Central Graben)

F. W. H. Smit¹  | F. S. P. van Buchem² | J. C. Holst¹ | M. Lühje¹ | K. Anderskov³ | N. Thibault³ | G. J. A. Buijs² | M. J. Welch¹ | L. Stemmerik⁴

¹Danish Hydrocarbon Research and Technology Centre, Technical University of Denmark, Lyngby, Denmark

²Maersk Oil and Gas, Copenhagen, Denmark

³Department of Geoscience and Natural Resource Management, University of Copenhagen, Copenhagen, Denmark

⁴University of Copenhagen, Natural History Museum of Denmark, Copenhagen, Denmark

Correspondence

Florian W. H. Smit, Technical University of Denmark, Danish Hydrocarbon Research and Technology Centre, Lyngby, Denmark.

Email: fsm@dtu.dk

Present address

F. S. P. van Buchem, Halliburton-Landmark, 97 Jubilee Avenue, Milton Park, Abingdon OX14 4RW, UK

Abstract

Kilometre-scale geobodies of diagenetic origin have been documented for the first time in a high-resolution 3D seismic survey of the Upper Cretaceous chalks of the Danish Central Graben, North Sea Basin. Based on detailed geochemical, petrographic and petrophysical analyses, it is demonstrated that the geobodies are of an open-system diagenetic origin caused by ascending basin fluids guided by faults and stratigraphic heterogeneities. Increased amounts of porosity-occluding cementation, contact cement and/or high-density/high-velocity minerals caused an impedance contrast that can be mapped in seismic data, and represent a hitherto unrecognized, third type of heterogeneity in the chalk deposits in addition to the well-known sedimentological and structural features. The distribution of the diagenetic geobodies is controlled by porosity/permeability contrasts of stratigraphic origin, such as hardgrounds associated with formation tops, and the feeder fault systems. One of these, the Top Campanian Unconformity at the top of the Gorm Formation, is particularly effective and created a basin-wide barrier separating low-porosity chalk below from high-porosity chalk above (a Regional Porosity Marker, RPM). It is in particular in this upper high-porosity unit (Tor and Ekofisk Formations) that the diagenetic geobodies occur, delineated by “Stratigraphy Cross-cutting Reflectors” (SCRs) of which eight different types have been distinguished. The geobodies have been interpreted as the result of: (i) escaping pore fluids due to top seal failure, followed by local mechanical compaction of high-porous chalks, paired with (ii) ascension of basinal diagenetic fluids along fault systems that locally triggered cementation of calcite and dolomite within the chalk, causing increased contact cements and/or reducing porosity. The migration pathway of the fluids is marked by the SCRs, which are the outlines of high-density bodies of chalk nested in highly porous chalks. This study, thus, provides new insights into the 3D relationship between fault systems, fluid migration and diagenesis in chalks and has important applications for basin modelling and reservoir characterization.

1 | INTRODUCTION

Heterogeneities controlled by initial depositional facies, post-depositional deformation and diagenetic overprinting greatly influence recovery factor and production rates of oil and gas-bearing limestones. Yet, they are notoriously difficult to predict from seismic data and require integration with other data sets and disciplines. Seismic geomorphology has helped during the last decade to better understand large-scale depositional systems, notably in the deep marine siliciclastic environment (e.g. Posamentier, Davies, Cartwright, & Wood, 2007). More recently, seismic data have also been instrumental in developing a more dynamic depositional paradigm with large moats and drifts formed by contourite currents, and large-scale slope remobilization features, in the extensive pelagic Upper Cretaceous chalk deposits of NW Europe (Esmerode, Lykke-Andersen, & Surlyk, 2008; Gennaro & Wonham, 2014; Lykke-Andersen & Surlyk, 2004; van der Molen, 2004).

The chalk deposits are a mud-grade biogenic sediment, with very low permeability and fairly high porosity (Surlyk, Dons, Clausen, & Higham, 2003), and host the most important hydrocarbon reservoirs in the Danish part of the North Sea (Megson, 1992; Vejrbæk, Frykman, Bech, & Nielsen, 2005) and a significant part of the hydrocarbons in the Norwegian sector (Brewster & Dangerfield, 1984; D'Heur, 1984). It is a fairly homogenous sedimentary rock, composed mainly of remnants of eukaryotic phytoplankton (coccolithophorids) (e.g. Fabricius, 2007; Hancock, 1975; Scholle & Halley, 1985), though some chalks in the Norwegian section of the North Sea can be rather argillaceous or cherty (e.g. Gennaro et al., 2013). The acoustic impedance (density multiplied by velocity) in chalk is dependent on three main parameters: porosity and pore fluid, matrix mineralogy and amount of contact cement (El Husseiny & Vanorio, 2015; Fabricius, 2003; Gommessen, Fabricius, Mukerji, Mavko, & Pedersen, 2007; Regnet et al., 2015). Because of its general purity in the Danish Central Graben (90%–100% CaCO_3), and well-constraint fluid content, seismic reflections in the chalk are often interpreted as porosity variations, which can be quantified through (deterministic) seismic inversion (Cherret, Escobar, & Hansen, 2011; Japsen et al., 2005). However, it is possible that other minerals than calcite occur within the chalk, which could potentially offset the porosity estimation from such seismic inversion. Also, contact cement can increase the velocity without increasing the density of the rock significantly, and therefore cause a seismic signal (Fabricius, 2003). Geochemical and petrographical analyses from wells can potentially provide some insights into these effects.

Here, we present a case study of seismic-scale heterogeneities within the Chalk Group in the Danish North Sea

which we believe to be diagenetic in origin (Figure 1 for location). We apply a seismic geomorphological workflow, which provides insights into the 3D architecture of large-scale heterogeneities and also serves as a spatial framework for combining other datasets at different scales (seismic to nanoscale) and from different disciplines (geophysics, geology and geochemistry). We combine methods that have previously been used to investigate diagenetic induced heterogeneity at outcrop- (e.g. Iran, Sharp et al., 2010; southern Spain, Martín-Martín et al., 2015), core and plug- (e.g. Fabricius, 2007; Scholle & Halley, 1985), and micro-scale (e.g. Faÿ-Gomord et al., 2016) to characterize these heterogeneities further, and thereby better predict properties in undrilled areas. Improving ability to predict reservoir properties away from wells is indeed important for exploration (reservoir quality) and production purposes (understanding sweep efficiency).

First, the stratigraphic units from Triassic to seafloor have been mapped using advanced seismic interpretation to provide the broad 3D geological model (stratigraphic units and fault fabric). Second, seismic attributes (e.g. spectral decomposition) have been displayed upon stratigraphic horizons below and within the chalk, to further highlight seismic heterogeneities, and reveal possible relationships with the underlying fault fabric (c.f. Smit, Van Buchem, Schmidt, & Stemmerik, 2017). Finally, by closely matching petrophysical, petrographical and geochemical information from two wells located within the heterogeneities, we are able to associate the heterogeneities with extra-formational fluids.

A likely candidate for introduction of these external fluids is the underlying fault systems that offset a thick succession of Mesozoic rocks. Therefore, this study not only demonstrates a combination of seismic geomorphology and well data, it also provides (i) new insights in the 3D relationship between fault systems, fluid migration and diagenesis in limestones in general based on seismic data; (ii) an alternative to published interpretations of similar features elsewhere in the North Sea Basin.

2 | GEOLOGICAL SETTING

The Danish Central Graben forms the southernmost branch of the North Sea Central Graben (Figure 1). It comprises a complex set of half-grabens bounded to the south and east by the Ringkøbing-Fyn High and to the west by the Mid North Sea High. The half-grabens formed during two major tectonic rifting phases (Japsen, Britze, & Andersen, 2003; Figure 2 for an overview of lithostratigraphic units and major tectonic events). During the Permo-Triassic, an E-W-oriented stress regime led to N-S-oriented half-grabens

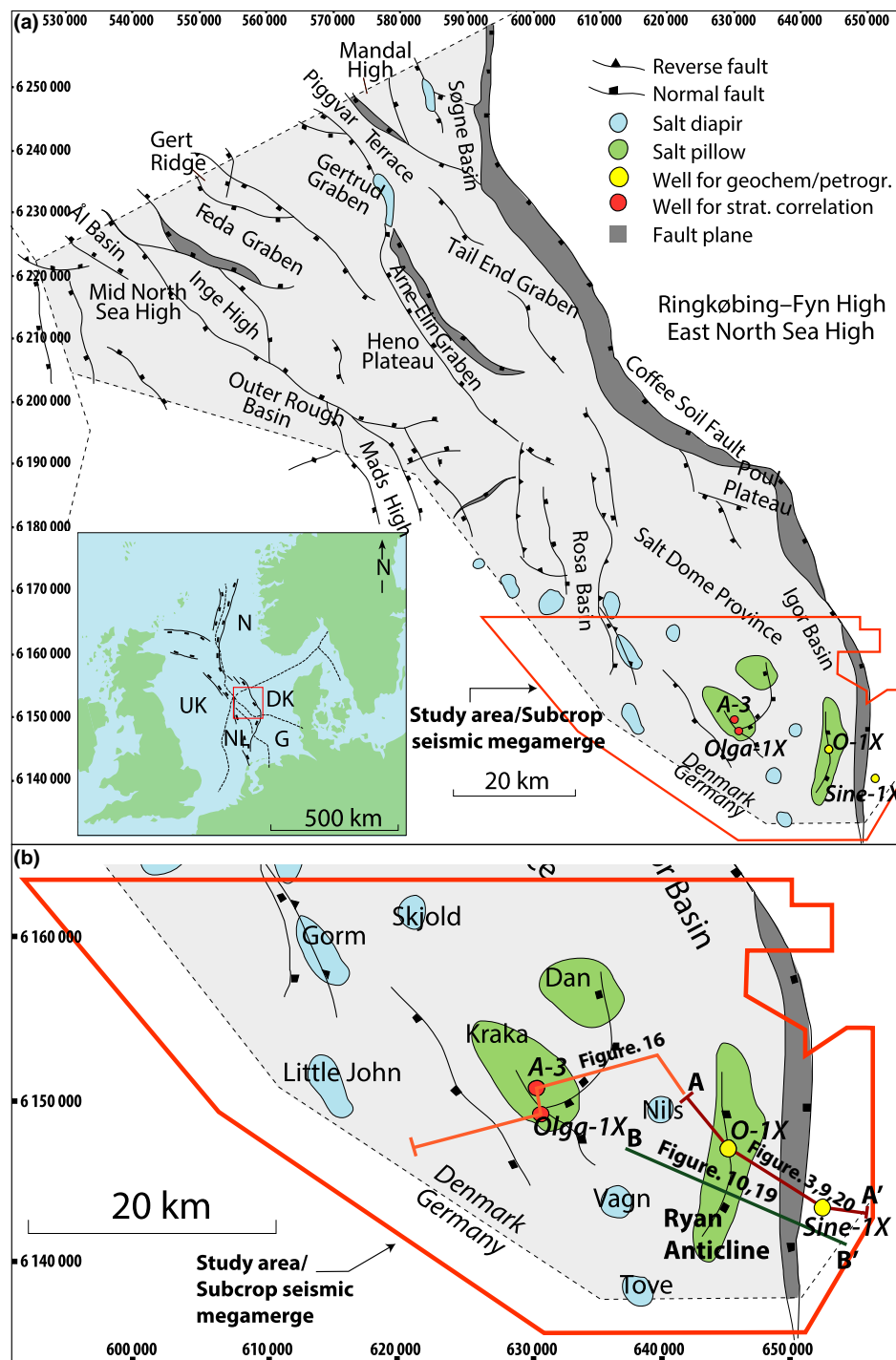


FIGURE 1 (a) Location map with Late Jurassic structural elements and its location within the North Sea Basin (inset), where UK = United Kingdom; NL = The Netherlands; G = Germany; DK = Denmark; N = Norway. The Coffee Soil Fault forms the dark grey rim around the Danish Central Graben. The seismic subcrop used in this study is outlined in red. (b) Study area, which shows the wells used in this study in bold, as well as the orientation of the seismic sections used in Figures 3, 9, 10, 16, 19 and 20

Modified and reprinted from Møller and Rasmussen (2003)

(Glennie, Higham, & Stemmerik, 2003; Goldsmith, Hudson, & Van Veen, 2003), whereas Late Jurassic rifting occurred in a NE-SW-oriented stress regime, leading to generally NW-SE-oriented half-grabens (Fraser et al.,

2002). Substantial creation of accommodation space combined with high sedimentation rates led to deposition of thick Mesozoic siliciclastic successions (up to 4 km thick) below the Chalk Group.

Extensional faulting and rapid sediment loading led to multiple phases of Permian salt remobilization, thereby influencing semi-regional sedimentation patterns due to the formation of diapirs and salt pillows (Karlo, van Buchem, Moen, & Milroy, 2014; Michelsen, Nielsen, Johannesen, Andsbjerg, & Surlyk, 2003). In addition, salt movements initiated large radial fault systems that remained active

throughout Mesozoic and Cenozoic times (e.g. Harding & Huuse, 2015).

The Upper Jurassic syn-rift succession is separated from the post-rift succession by the Base Cretaceous Unconformity (BCU), a basin-wide diachronous surface that is polygenetic in nature (Kyrkjebø, Gabrielsen, & Faleide, 2004). Thermal subsidence prevailed throughout most of the

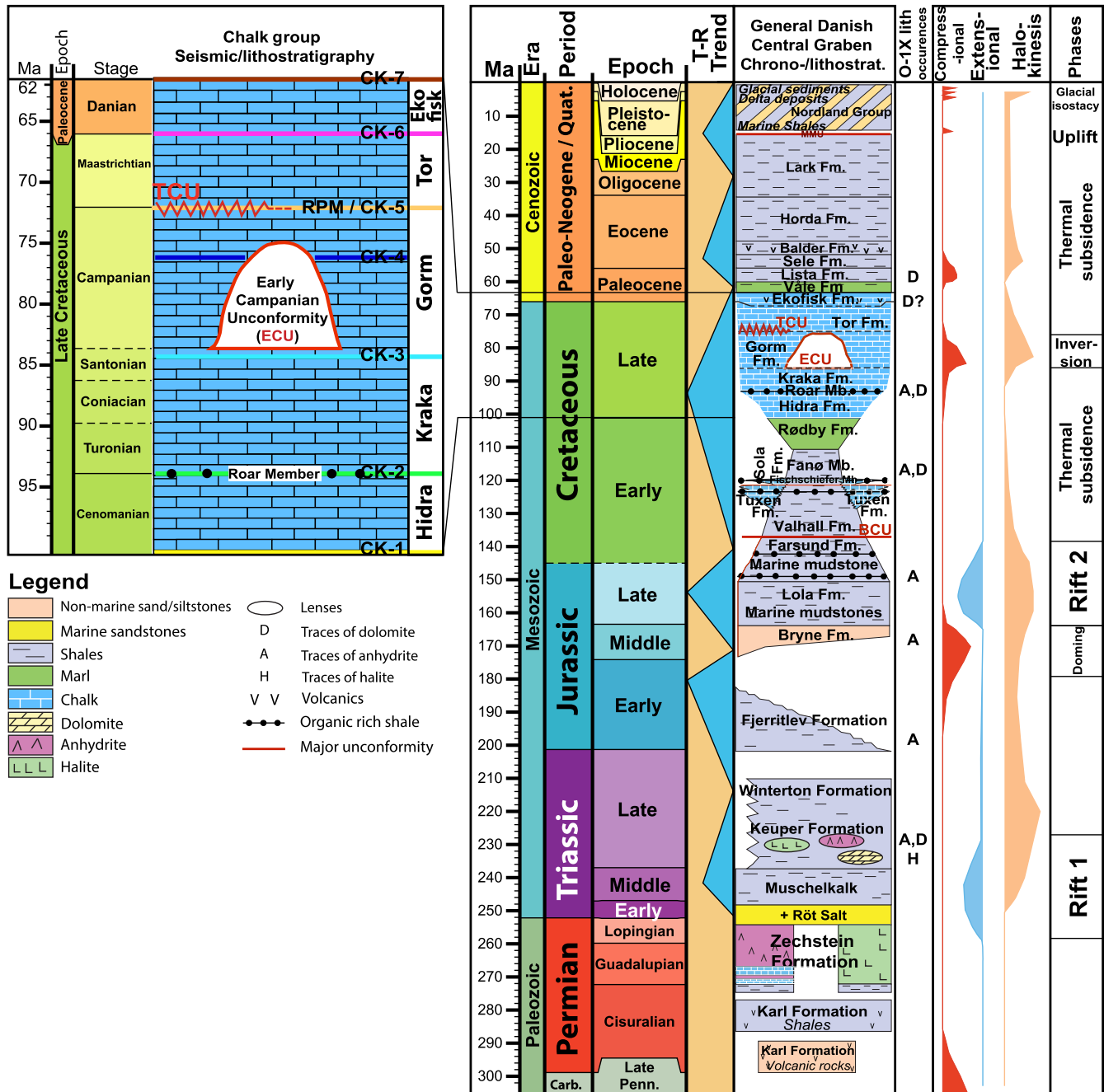


FIGURE 2 Chrono-/lithostratigraphic subdivision of the Danish North Sea. Stratigraphic units and tectono-sedimentary phases based on a literature synthesis. Coward, Dewwey, Hempton, Holroyd, and Mange (2003) for Permian–Middle Jurassic, Møller and Rasmussen (2003) for the Middle Jurassic–Lower Cretaceous, Michelsen et al. (2003) for Jurassic, Japsen et al. (2003) for Late Jurassic and Lower Cretaceous, Ineson, Bojesen-Koefoed, Dybkjær, and Nielsen (2003) for Late Jurassic, and van Buchem, Smit, Buijs, Trudgill, & Larsen (2018) for the Lower and Upper Cretaceous, Schjøler et al., 2007; for Early Cenozoic, and Rasmussen, Dybkjær and Piasecki (2010) for Late Cenozoic. Tectonic phases are simplified and serve as broad tectonic framework for this study. Time scale generated with Geological Time Scale Creator, conforming with Ogg, Ogg, and Gradstein (2016)

Cretaceous, but was interrupted by a distinct compressional phase that reached its climax during the early Campanian inversion. This resulted in major rearrangement of depocenters (van Buchem et al., 2018; Cartwright, 1989; Vejbæk & Andersen, 2002) and sediment remobilization along newly formed highs (e.g. Back et al., 2011; van Buchem et al., 2018; Smit, 2014; figs 17, 18 therein).

Palaeocene inversion movements likely resulted from intra-plate compressional stresses related to the Alpine collision and possibly ridge-push forces (Vejbæk & Andersen, 2002) and could have reactivated fault systems present underneath the chalk rock. Rapid sediment loading, differential compaction of the Mesozoic sediments and halokinesis continued to play an important role for fault reactivation during the Cenozoic, and glacial loading and unloading during the Quaternary may have impacted the stability of the salt structures and associated fault systems (Harding & Huuse, 2015; Rasmussen, 2013).

Until recently, the official stratigraphic nomenclature for the chalk in the Danish North Sea was a subdivision into informal “units” (e.g. Lieberkind, Bang, Mikkelsen, & Nygaard, 1982), but a more pragmatic subdivision borrowed from the Norwegian and UK sectors was commonly used (e.g. Surlyk et al., 2003). van Buchem et al. (2018) proposed the first formal lithostratigraphic subdivision for the Chalk Group in the Danish Central Graben (Figure 2). Formations are based on a combination of seismic markers (CK-1/7), biostratigraphy and log markers (see Appendix in van Buchem et al., 2018). The Early Campanian Unconformity (ECU) reflects a shift in basin morphology due to inversion tectonics and separates the lower Hydra and Kraka formations (pre-inversion succession) from the upper Gorm, Tor and Ekofisk formations (syn- and post-inversion successions).

3 | DATA AND METHODS

3.1 | Seismic (inversion) data and interpretation methods

3.1.1 | Seismic data

A 2,000-km² subcrop of a recently re-processed regional seismic data set (prestack depth migrated) was available (Figure 1). The quality of the data is in general very good, though it deteriorates around salt diapirs. The polarity follows North Sea convention, with a downward increase in acoustic impedance represented by a trough (shown in red). The dominant frequency in the Chalk Group is approximately 30 Hz, and average acoustic velocity is around 3,400 m/s, leading to an average vertical resolution of 28.3 m as a quarter of the wavelength of the dominant frequency (Sheriff, 1980).

3.1.2 | Seismic inversion porosity

Seismic inversion porosity data are available over most of the study area. It was obtained from a deterministic inversion workflow (c.f. Cherret et al., 2011), using the Sine-1X and Olga-1X wells (Figure 1) to derive the empirical relationships between seismic interval velocity from seismic data, and corresponding P-impedance and porosity from well data (Wagner, 2014). Standard deviation of the porosity was estimated from a detrended cross-plot of porosity over $\ln(I_p)$ and amounts to 0.2 $\ln(I_p)$ or 20% I_p , which corresponds to 10 porosity units. Importantly, the Olga-1X and Sine-1X wells did not penetrate the high AI chalks that are the focus of this study, and therefore, factors other than porosity are ignored (e.g. possible heavier minerals and occurrence of near porosity-neutral contact cement) and could form a source of error. If significant amounts of minerals other than calcite (density 2.71 g/cm³) occur within the rock, such as chert (2.3% lighter), dolomite (7% heavier) or sulphates ($x\text{SO}_4 \cdot x\text{H}_2\text{O}$, 11% heavier), the inversion-based porosity can be inaccurate. To evaluate such factors, mineralogical and petrographical analyses throughout the stratigraphy are important.

3.1.3 | Seismic interpretation methods and post-processing techniques

A neural network methodology has been applied for seismic interpretation (PaleoScanTM, c.f. Pauget, Lacaze, & Valding, 2009) in order to create, in a time-efficient manner, the large number of stratigraphy consistent horizon slices needed to investigate the limestone heterogeneities in detail. To increase the information extracted from the stratal horizons, spectral decomposition data revealed information in the frequency domain. Based on a dominant frequency of 30 Hz, three spectral frequency cubes (20, 30, 40 Hz) were calculated using a matching pursue algorithm in GeoTeric 2016.2 (c.f. Morozov et al., 2013). Similar in aim but different in workings, seismic image processing was used to reveal high-resolution structural information using the eXchroma^{SG} plug-in for Petrel (c.f. Laake, 2013). Vertical linear features (which can represent faults or fracture swarms) are emphasized through “swarm intelligence” of artificial ants (c.f. Pedersen, Randen, Sonneland, & Steen, 2003). Petrel E&P 2016 software (Schlumberger) has been applied to bring together data in a 3D visualization environment.

3.2 | Wireline logs

Well O-1X only has gamma ray and deep resistivity logs, whereas Sine-1X has a full log suite, including sonic velocity, density and neutron-porosity, so Sine-1X was used for

the seismic-well tie. In order to compute porosity in O-1X, the deep resistivity log of O-1X can be used in conjunction with core porosity data and Archie's Law (Archie, 1942). With known average porosity (0.253), water saturation (1) and deep resistivity ($0.5236 \Omega\text{m}$, true resistivity), a mud resistivity of $0.0335 \Omega\text{m}$ is calculated, in line with the brine saturated system during logging (final well report). Now the porosity can be re-written as a function of resistivity, water saturation (assuming no hydrocarbons) and previous calculated mud resistivity:

$$S_w = \sqrt{\frac{1}{\Phi^2} * \frac{R_w}{R_t}}, \text{ becomes } \Phi = \sqrt{\frac{0.0335}{R_t}}$$

3.3 | Drill cutting analyses

More direct characterization from the rocks was obtained using a 10-m core from O-1X and drill cuttings (9-m intervals for O-1X and 3-m intervals for Sine-1X). For petrographical characterization, rock chips and 12 thin sections were investigated under SEM. Nomenclature of Faÿ-Gomord et al. (2016) is loosely followed to classify the diagenetic overprint of the samples. From each well, 50 nanofossil slides were prepared and analysed quantitatively (c.f. Thibault & Gardin, 2006) in order to establish a time framework, following the subdivision of Fritsen et al. (1999) modified by Boussaha, Thibault, and Stemmerik (2016). Sample spacing is 9 m in O-1X and 18 m Sine-1X, with closer spacing around the RPM (3 m).

Geochemical analyses include carbon, oxygen and sulphur isotope geochemistry, and X-ray fluorescence (XRF). A deviation of the oxygen isotope ratio ($\delta^{18}\text{O}$) from Cretaceous seawater can indicate a certain degree of diagenesis, as with increasing temperature lighter oxygen isotopes will be taken up into the crystal lattice, although bulk values also depend on the fluid from which the cement precipitated (Craig, 1957; Egeberg, & Saigal, 1991). Carbon and oxygen isotopes were analysed at Iso-Analytical (UK) using continuous flow isotope ratio mass spectrometry (CF-IRMS), and values are reported as $\delta^{13}\text{C}$ and $\delta^{18}\text{O}$, deviations in parts per thousand relative to the V-PDB and V-SMOW standard. Analyses were performed on every drill cutting sample from the entire Chalk Group, giving a resolution of 9 m (O-1X) and 3 m (Sine-1X). Standard deviations are reported to be better than 0.08‰ for $\delta^{13}\text{C}$ and 0.02‰ for $\delta^{18}\text{O}$. Sulphur isotope ratios in anhydrite from O-1X were obtained at Isotope Tracer Technologies Inc. (Canada) and reported as $\delta^{34}\text{S}$ showing deviation in parts per thousand relative to the Vienna-Canyon Diablo Troilite (VCDT) standard. Standard deviation from repeated samples is reported to be 0.2‰ .

Certain chemical components can be used to describe the type of diagenesis, such as Mn and Sr (open or closed system c.f. Banner & Hanson, 1990), Mg (dolomitization)

and Si/Al (for the presence of silica phases). To characterize this throughout the stratigraphy, XRF analyses were carried out at ALS Minerals (Ireland) of drill cutting material with a vertical spacing of 9 m in O-1X, 6 m for the upper 305 m of Sine-1X and 46 m for the remaining of the Chalk Group. Accuracy is reported to be within the limits of the reference samples.

4 | RESULTS

4.1 | Unconformities at the crest of the Ryan structure

A seismic section between wells O-1X and Sine-1X shows the different positions of the two wells within the basin: O-1X on top of the Ryan Anticline, Sine-1X on the Rinkøbing-Fyn High (Figure 3a). Biostratigraphic data from well O-1X show that the lowermost chalks between CK-1 and 3 (65 m thick) are highly condensed, of Santonian–earliest Campanian age, and overlie Barremian shales (Lower Cretaceous), thus reflecting a major hiatus (maximum of 45 Myr). Onlapping onto the Ryan structure is observed within the thin CK-1 to CK-3 strata in the seismic section and truncation is observed at the CK-3 marker (Figure 3a, black arrows, “T”). In Sine-1X, a thin package of Albian shales (Lower Cretaceous) overlies the Precambrian basement rocks. The oldest chalks are of Coniacian–Santonian age (160 m thick) and are separated from the shales by a major hiatus.

Onlapping onto the CK-3 marker occurs at the transition from the eastern basement high to the Mesozoic basin (i.e. where the Coffee Soil Fault offsets the lowermost chalk; Figure 3a, white arrows) and onto the Ryan Anticline, as well as truncated reflectors (Figure 3a, T's and black arrows). Biostratigraphic data from O-1X show that the chalks between CK-3 to CK-5 are condensed (37 m thick) and of Early/Mid Campanian age, while the upper Campanian is missing (Figure 4). A thicker and complete Campanian succession occurs at Sine-1X (240 m), and thus a correlative conformity is observed at Top Campanian (Figure 4, “C.C.”). The CK-3 marker reflects the separation of the pre-inversion basin (Cenomanian–Earliest Campanian, CK-1 to CK-3, Figure 2) from the post-inversion basin (Early Campanian–Danian, CK-4 to CK-7, Figure 2) (c.f. van Buchem et al., 2018). The seismic section and biostratigraphic data, thus, show that the CK-3 marker forms an unconformity due to tectonic inversion, and that sedimentation rates at the Ryan Anticline remained low during Campanian times, while at Sine-1X sedimentation was continuous.

The seismic section shows strata on top of the CK-5 marker onlapping towards the Ryan Anticline (yellow arrows in Figure 3a), and the surface itself shows erosional truncation

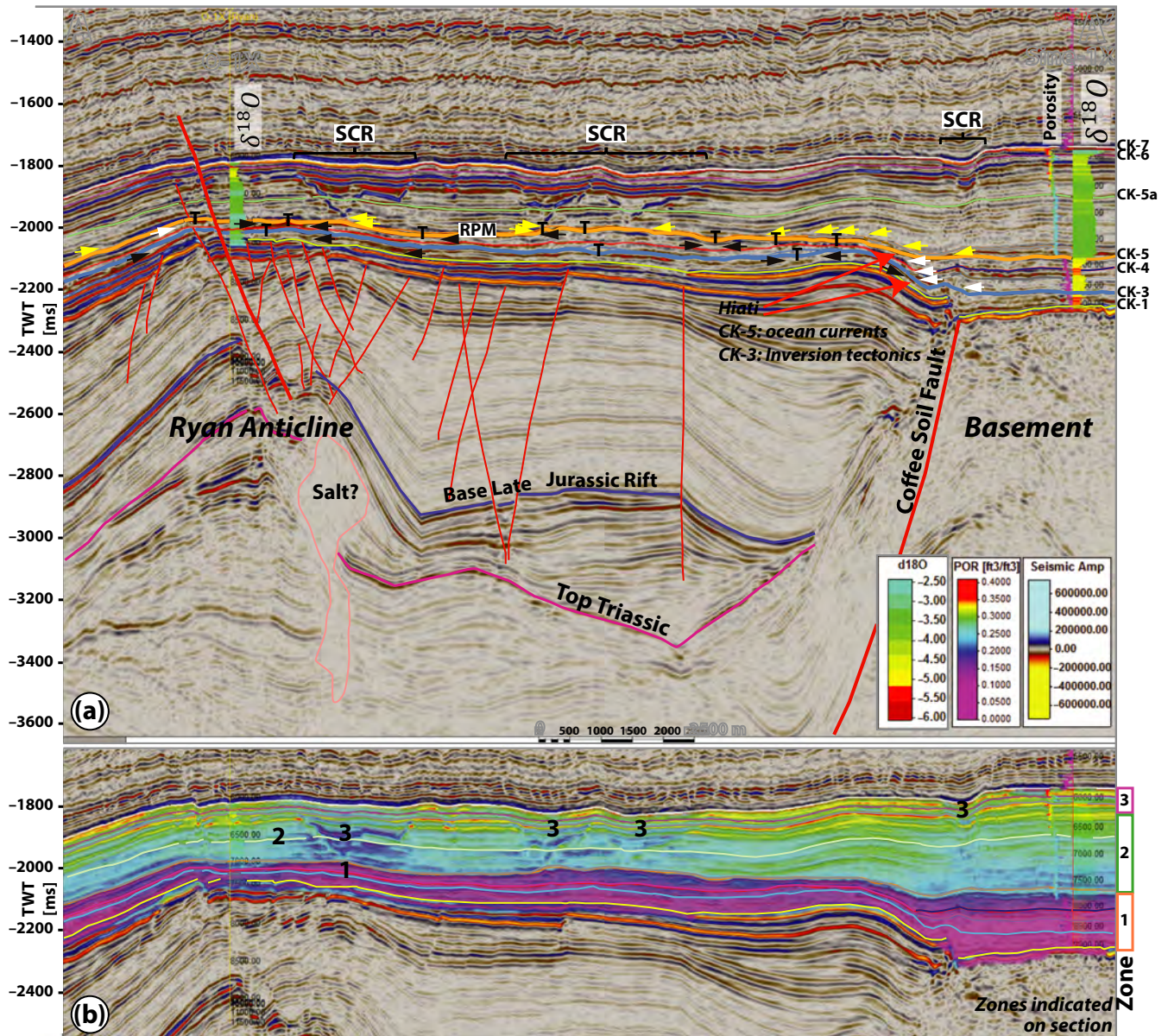


FIGURE 3 Seismic amplitude section (a) and seismic inversion derived porosity data (b). See Figure 1 for location of seismic line. Seismic markers within the chalk (CK-1 to 7) according to Van Buchem et al. (2017). Zones 1–3 according to subdivision in the text. See Figure S1 for an uninterpreted section. In (a), the RPM (Regional Porosity Marker) can be observed as a low-wavelength high-amplitude trough (red) within the lower part of the Chalk Group. Truncations indicated by “T” and black arrows, onlaps onto CK-3 by white arrows, onlaps onto CK-5 by yellow arrows. These markers are interpreted to represent unconformities: CK-3 tectonically controlled, CK-5 by ocean current activity. The SCRs can be recognized by high-angle (30–55°), high-amplitude peak reflectors (blue), cutting through the seismic stratigraphy. Porosity estimates in (b), where the RPM separates high-porosity chalk (Zone 2) and low-porosity chalk (Zone 1). The SCRs outline bodies of low-porosity chalk (Zone 3) nested within high-porosity chalk (Zone 2). The location of the SCRs seems to be an extension of the underlying fault fabric

of underlying Campanian strata (T's and black arrows in Figure 3a). The CK-5 marker forms a major hiatus within the biostratigraphy of O-1X (where the Upper Campanian missing), whereas in Sine-1X continuous sedimentation occurred creating onlapping onto the Ryan anticline (Figures 3a and 4). The biostratigraphy and seismic stratigraphy indicate that the Ryan Anticline remained a basinal high during latest Campanian to earliest Maastrichtian times with

low sedimentation rates and erosion, and it became buried during the UC-16 S3 subzone (Figures 3a and 4).

The CK-5 marker is a high-amplitude and low-frequency trough reflecting significant increase in acoustic impedance at the interface (Figures 3a,b). Both neutron-derived porosity and seismic inversion porosity data show that it divides the chalk regionally into an upper high-porosity unit with 20%–40% porosity, and a lower low-porosity unit with

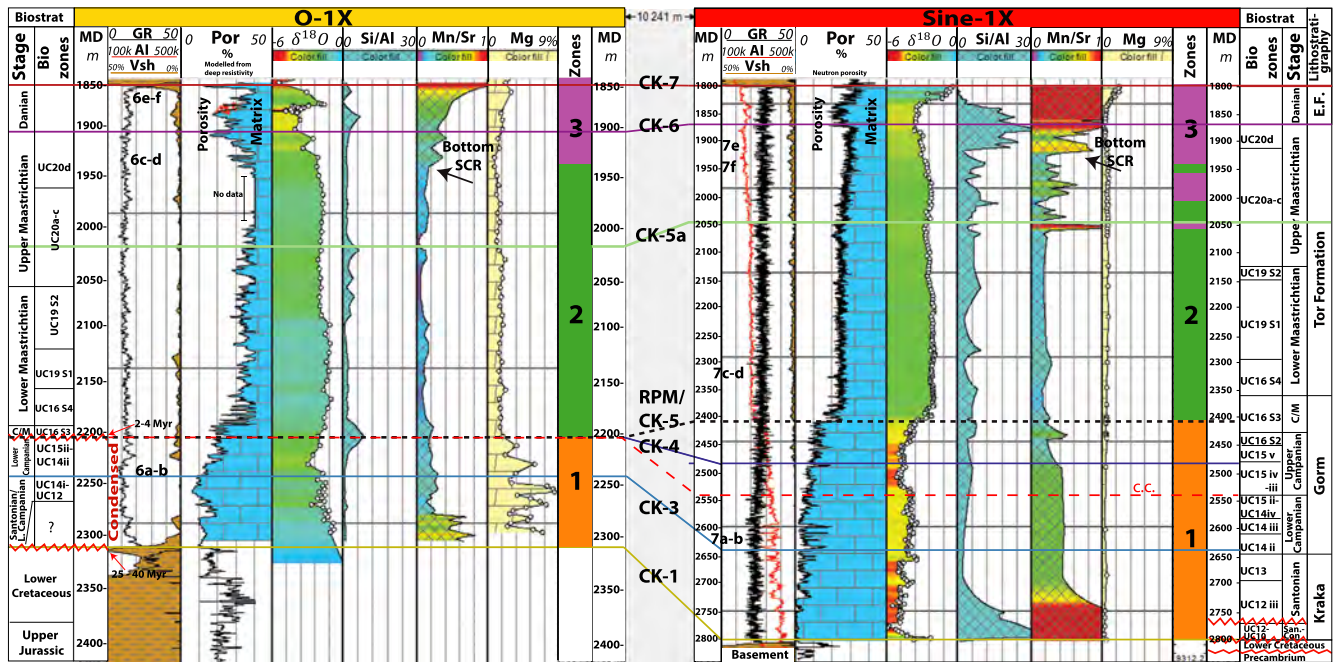


FIGURE 4 Well section with relevant geophysical (AI), petrophysical (GR, Porosity), geochemical data (oxygen isotopes, Si/Al ratio, Mn/Sr ratio, magnesium content) and biostratigraphy data (according to Fritsen et al. (1999) and Boussaha et al. (2016)). Scales between wells differ, see depth scale. On the Ryan Anticline (O-1X), a 25–40 Myr hiatus occurs at the base of the Chalk Group (red serrated line), and a second occurs at the position of the RPM in O-1X, at near top Campanian. Very condensed sections occur in between the hiatuses (2–5 m/Myr sedimentation), reflecting low accommodation space, nondeposition and/or erosion. In Sine-1X, Lower Cretaceous shales overly Precambrian basement, and first chalks occur in between two hiatuses, and are of Coniacian–Santonian age. The near top Campanian hiatus and condensed sections beneath are not observed in time-equivalent packages, indicating continuous deposition compared with the O-1X location, and thus a correlative conformity is observed (C.C.). The three zones have a distinct combination of porosity (high/low), $\delta^{18}\text{O}$, and Mn/Sr ratio. See text for a description of the different zones. Note that the lowermost parts of the Chalk Group show large Mn/Sr ratios within Zone 1 and could potentially be called Zone 3 as well. High magnesium content in Zone 1 in O-1X could well indicate the presence of dolomite and magnesium sulphates as seen in drill cuttings and under SEM. SEM locations of Figures 6 and 7 are shown in the first column

overall porosity between 0% and 10% and some thinner intervals with up to 20% porosity (Figures 3b and 4). We, therefore, suggest using the more informative name “Regional Porosity Marker” (RPM) for the CK-5 surface. The neutron-derived porosity log in Sine-1X shows a stepwise downward transition from high to low porosity within a 20-m interval corresponding to the RPM (Figure 5). In O-1X, modelled porosities show slightly higher values below the RPM, between 8% and 20%, though the GR-calculated shale volumes might mean that the modelled (resistivity) porosity underestimates true porosity (Figures 3b and 4).

4.1.1 | Petrography and geochemistry

The chalk beneath the RPM is generally well-cemented. Nano- and microfossils (fragments) are recrystallized with large overgrowths, and grain-to-grain contacts have coalesced (Figures 6a,b and 7a,b). The main differences between the two wells are the large amounts of crystalline dolomite in O-1X (Figure 6b) and the presence of

stylolites in Sine-1X (Figure 7b). The dolomite crystals are 10–100 micron in size, replacing a large amount of the chalk. In contrast, the chalk above the RPM is less cemented with better preservation of coccolith material, less calcite overgrowth, and less contact cement (Figures 6c and 7c, Zone 2). It shows generally good preservation of porosity and limited amounts of larger dolomite crystals (Figures 6d and 7d).

The chalk below the RPM shows a bulk shift towards more negative $\delta^{18}\text{O}$ values, from -3.5‰ ($\Phi = 25\%$) to -6‰ ($\Phi = 1.5\%$) in Sine-1X (Figure 5a), though some intervals have slightly more positive values (e.g. 2,525–2,650 m). The shift is less dramatic in O-1X, from -2.9‰ ($\Phi = 22\%$) to -3.7‰ ($\Phi = 7\%$), and values increase again towards the base of the chalk (Figures 4 and 5). The neutron-porosity correlates positively with the $\delta^{18}\text{O}$: with decreasing porosity, the $\delta^{18}\text{O}$ values also become more negative (Figure 5b). Cross-plotting $\delta^{13}\text{C}$ and $\delta^{18}\text{O}$ values shows a clear distinction between the low-porosity chalk below the RPM with high $\delta^{13}\text{C}$ and low $\delta^{18}\text{O}$ values (yellow) and high-porosity chalk above the RPM characterized

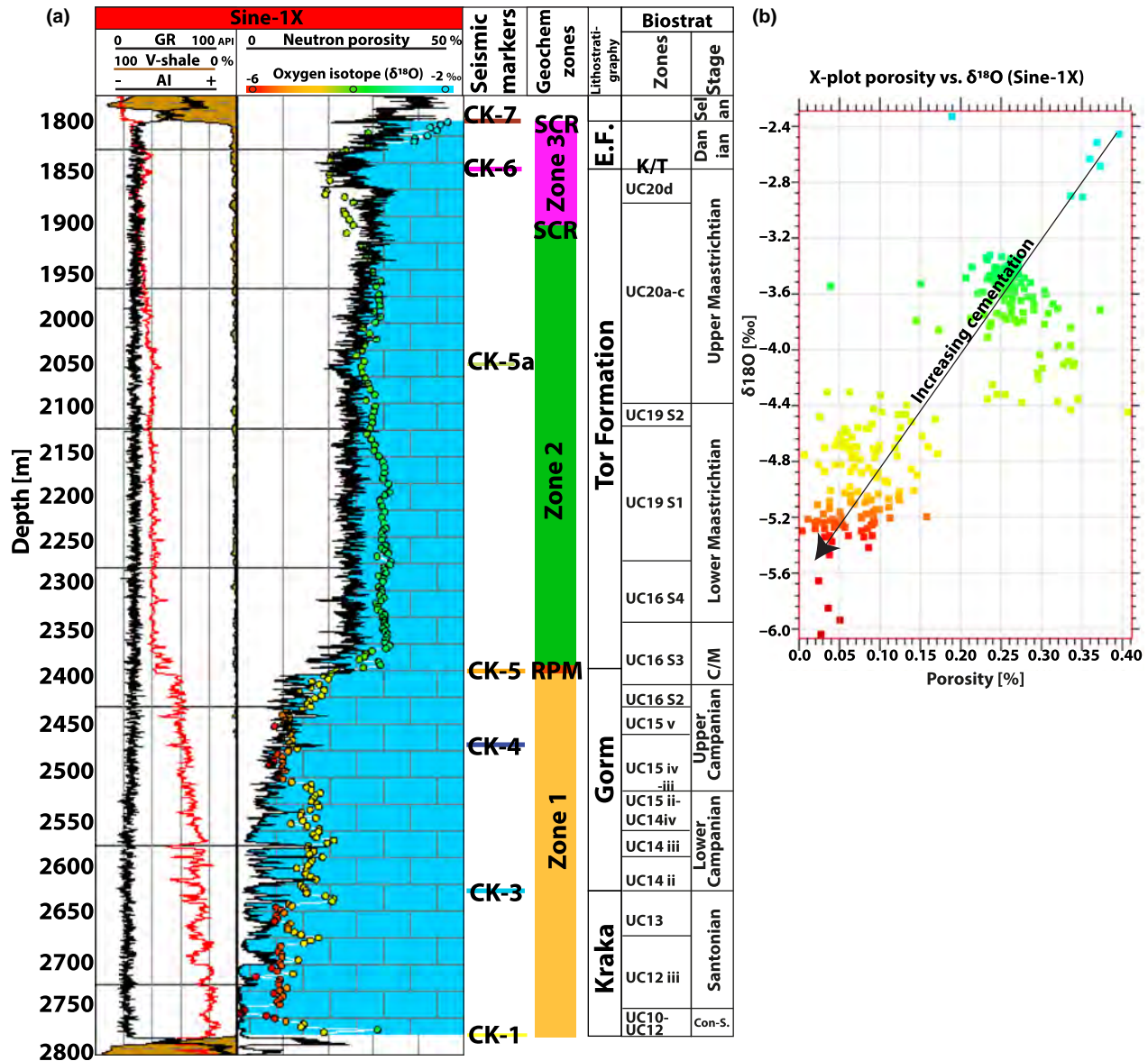


FIGURE 5 (a) Porosity log of Sine-1X with $\delta^{18}\text{O}$ in colour, and biozones according to Fritsen et al. (1999) and Boussaha et al. (2016). The geochemical zones are defined based on porosity trend, $\delta^{18}\text{O}$ and Mn/Sr ratios. Different porosity-reducing trends can be seen, where the break from 28% to 10% within 20 m at the RPM interface is the most significant. The bulk shift in porosity is accompanied with a decrease in $\delta^{18}\text{O}$ values from -3.5‰ to -5.5‰ , which must mean that more cement with a depleted $\delta^{18}\text{O}$ signature is present. (b) cross-plot of porosity vs. $\delta^{18}\text{O}$ based on Sine-1X data. There is a clear positive relationship between decreasing porosity and decreasing $\delta^{18}\text{O}$ values, indicating that the porosity-reducing mechanism causes a geochemical signal

by high $\delta^{13}\text{C}$ and high $\delta^{18}\text{O}$ values (green) (Figure 8a). In O-1X, higher porous zones below RPM form outliers with higher $\delta^{18}\text{O}$ values.

The Mn/Sr ratio is highest at the base and top of the Chalk Group in both wells. The high-porosity chalk immediately above the RPM is characterized by the lowest overall Mn/Sr ratios, and in both wells, the Mn/Sr ratio increases immediately beneath the RPM (Figures 4 and 8b). The Si/Al ratio shows rather low values below the RPM in Sine-1X, increasing rapidly towards the base of the Chalk Group, coinciding with higher Mn/Sr ratios

(Figure 4, and see red dots in Figure 8c). In O-1X, an increase in Si/Al is found at the RPM. The low Mn/Sr ratios in the high-porosity chalk (Zone 2) indicate that diagenesis likely occurred in a closed system (Banner & Hanson, 1990) (Figure 8b). The increased Mn/Sr ratios in chalk beneath the RPM, in both wells, suggest larger water:rock interaction and thus more open-system diagenesis. The high Mn/Sr ratios at the base of the Chalk Group suggest that more open-system diagenesis has occurred here. The magnesium content of the chalk below the RPM is relatively high and fluctuates by a large amount in O-1X

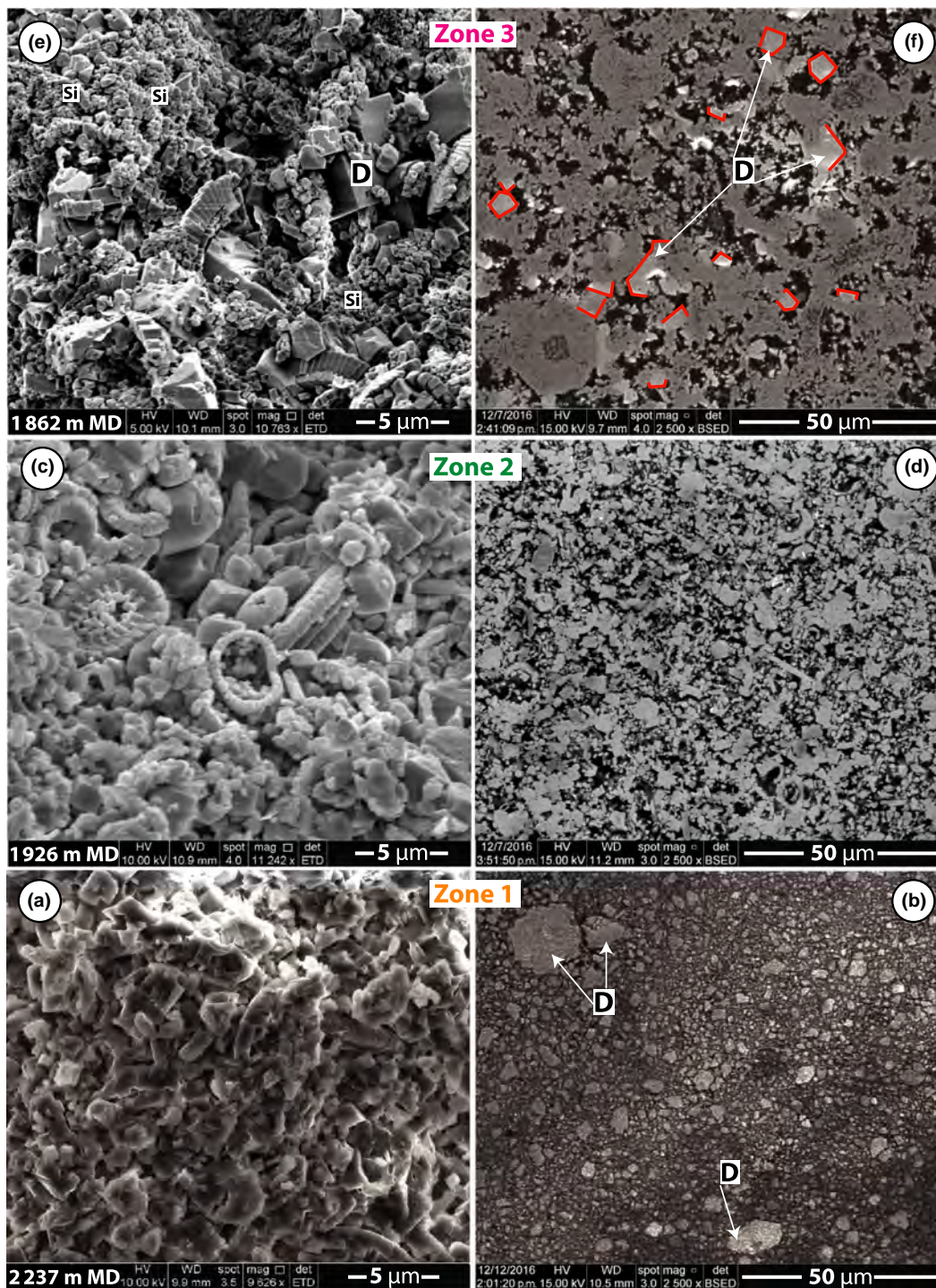


FIGURE 6 Scanning electron microscope of chips (secondary electrons, left column) and thin sections (backscattered electrons, right column) from chalk drill cuttings in O-IX. Oldest stratigraphy at bottom. For location within stratigraphy, see Figure 4. (a–b) Zone 1 shows a highly cemented chalk, with poor preserved coccoliths ($\Phi = 10\%$, $\pm 5\%$). The thin section shows low porosity with highly coalesced grain contacts, and occurrence of large dolomite crystals (D) that seem to replace (micro)fossil fragments. (c–d) Zone 2 shows a chalk with better preserved coccoliths and porosity ($\Phi = 25\%$, $\pm 5\%$). (e–f) Zone 3 shows a chalk ($\Phi = 20\%$, $\pm 5\%$) with good preservation of coccoliths, but contrasts with Zone 2 by having 5–25 micron-sized dolomite crystals (D). Sharp edges of the dolomites are highlighted in red. A larger amount of contact cement can be observed compared to Zone 2. In addition, submicron-sized quartz lepispheres are covering coccoliths (Si)

(up to 8 weight per cent, Figure 4), which could partly reflect the presence of the dolomite. Within the Lower Cretaceous, and at the fault plane, increased amounts of

sulphates occur with $\delta^{34}\text{S}$ values of 11‰ – 15‰ , which is similar to Triassic/Permian anhydrites in the adjacent Nils-1 well (Figure 1).

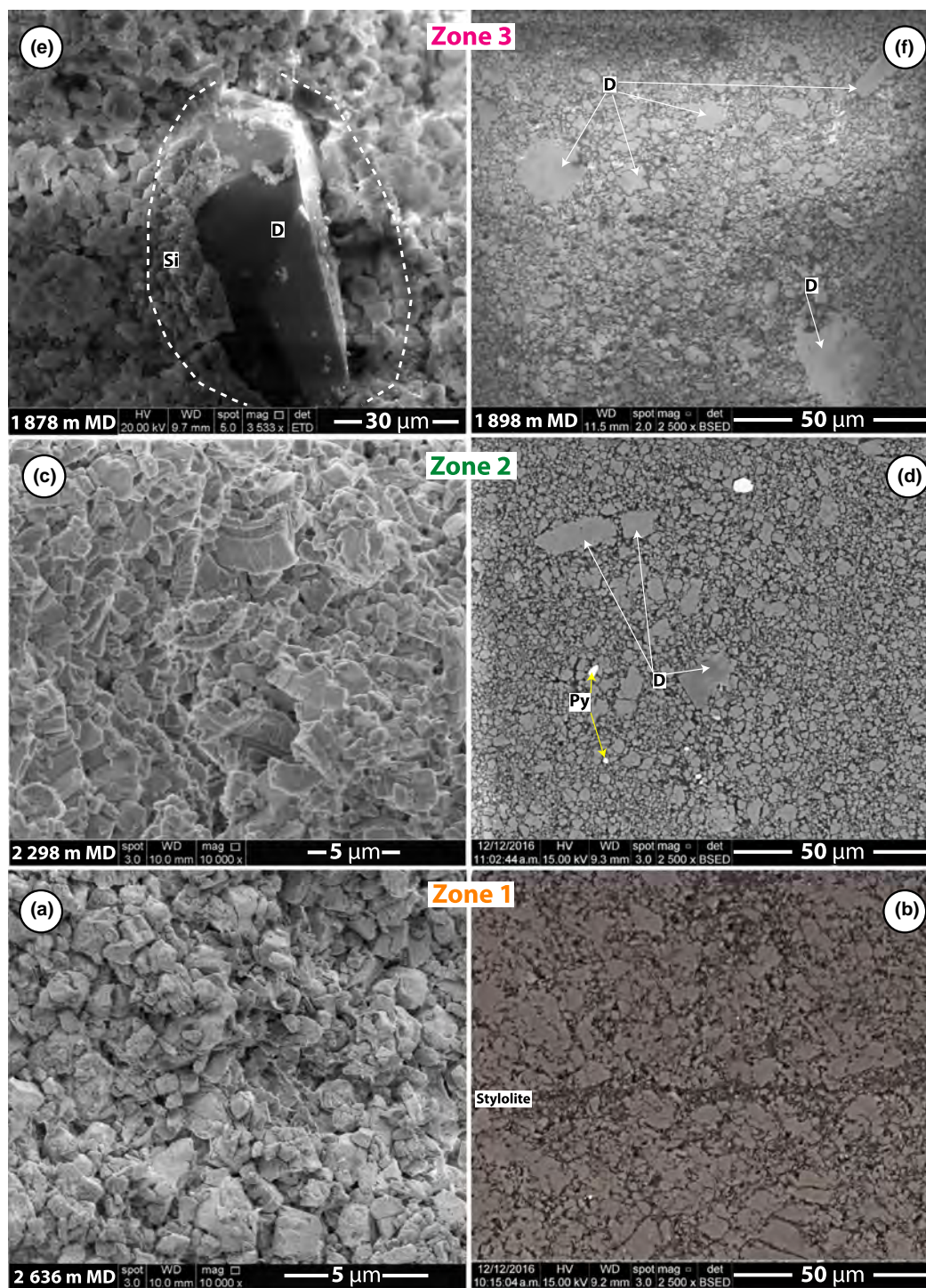


FIGURE 7 Scanning electron microscope of chips (secondary electrons, left column) and thin sections (backscattered electrons, right column) in Sine-1X. Oldest stratigraphy at bottom. For location within stratigraphy, see Figure 4. (a–b) Chalk from Zone 1 shows poor coccoliths and fossil preservation (a), likely due to recrystallization and cementation as seen in thin section (b). The occurrence of many stylolites from these samples shows that some chemical compaction has occurred in these chalks, which could have provided a source for calcite cement. (c–d) Zone 2 shows in a highly recrystallized chalk ($\Phi = 25\%$), but with better preserved porosity than Zone 1. Coccolithic plates can still be recognized. Several dolomite crystals (D) can be observed, as well as pyrite, as confirmed by EDS analysis. (e–f) Zone 3 shows a cemented chalk, with recrystallization of microfossils and contact cement between grains ($\Phi = 20\%$). Large dolomite crystals (D) occur within microfossils (forams, dashed white line), which also can be observed in thin section (f). Note different scale between (e) and (a)

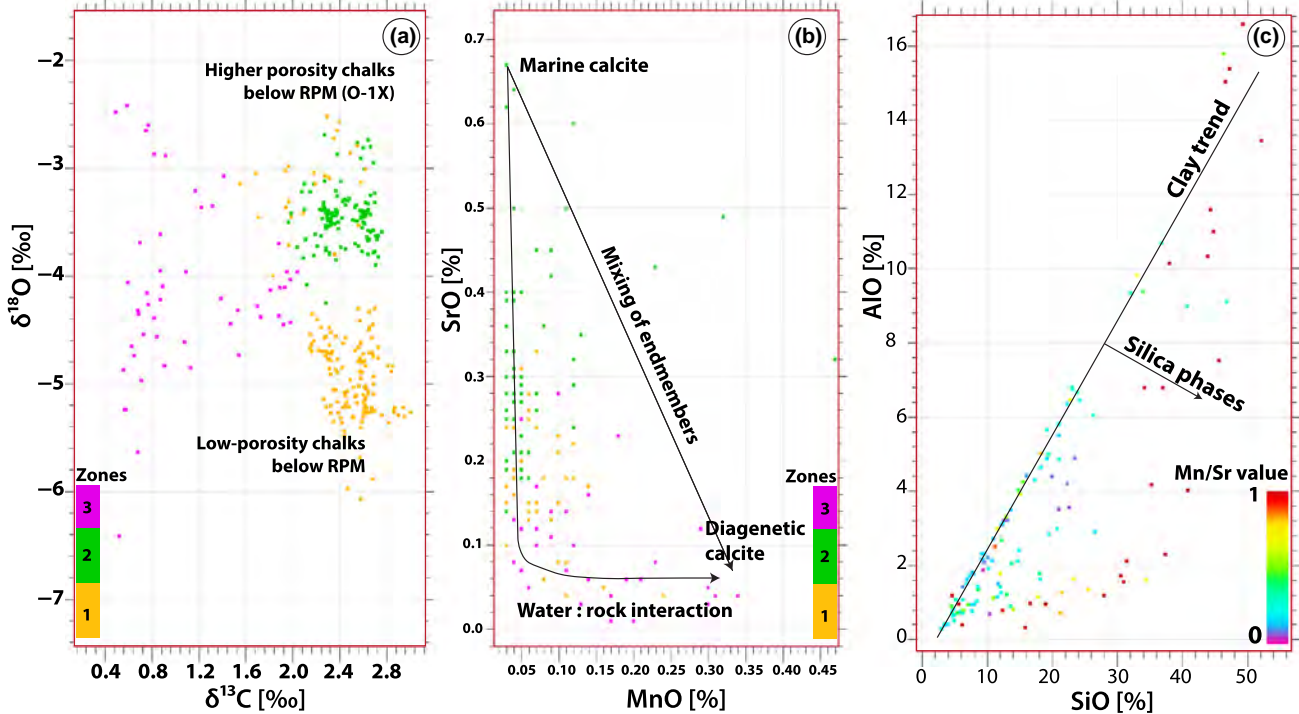


FIGURE 8 Cross-plots of geochemical data of wells O-1X and Sine-1X. (a) Correlation between oxygen and carbon isotope values, coloured by zone according to Figure 4. A distinct pattern can be seen between the different zones: Zone 1, high $\delta^{13}\text{C}$ values and low $\delta^{18}\text{O}$ values (less negative more porous chalks in O-1X). Zone 2, high $\delta^{13}\text{C}$ values and least negative $\delta^{18}\text{O}$ values. Zone 3, low $\delta^{13}\text{C}$ values and general low $\delta^{18}\text{O}$ values, although rather scattered due to rough zonation. (b) Cross-plot MnO and SrO in %, similar to Banner and Hanson (1990), with endmembers upper left and lower right, with endmember mixing line. J-trend shows how an increased water:rock interaction lowers the Sr content and increases Mn. Low Mn/Sr ratio in Zone 2, increasing in Zone 1, and large ratios in Zone 3, reflecting increasing water:rock interaction from Zone 2 (least), to Zone 1, to Zone 3 (most). (c) SiO and AlO correlation; a clay trend can be seen as a linear relationship. Offsets to higher SiO represent silica phases (arrow). Silica phases might have a correlation with higher Mn/Sr values

4.2 | Stratigraphy cross-cutting reflectors

4.2.1 | 2D architecture

Several high-angle ($30\text{--}55^\circ$) reflectors with anomalously high amplitudes cross-cut the seismic stratigraphic framework defined by van Buchem et al. (2018) (Figure 9). They are accordingly named Stratigraphy Cross-cutting seismic Reflectors (SCRs). The SCRs are characterized by continuous to semi-continuous, low-frequency, high-amplitude peak reflectors (i.e. bounding lower AI rocks), which cut through the seismic stratigraphic horizons at variable angles ($30\text{--}55^\circ$ relative to horizontal) (Figure 9). The cross-cutting creates apparent erosional truncation of the reflectors outside the boundaries and apparent onlapping patterns within the SCRs. In many sections, these reflectors can be traced across and within the area of the SCRs (CK-5a in Figure 9).

The SCRs architecture is characterized by: (i) an anomalously high-amplitude trough (i.e. bounding high AI rocks) at the top of the features at Top Chalk; (ii) steeply dipping ($30\text{--}55^\circ$) conjugate and downward-converging anomalously

high-amplitude peak reflectors (i.e. bounding rocks with lower AI), which create various shapes depending on transect orientation; (iii) anomalously high-amplitude, high-frequency reflectors inside the V-shape; (iv) a vertical anomalous high-amplitude peak/trough couplet at the base, “cutting” through a continuous horizontal reflector (Figure 9, Table 1). The height of the SCR-defined V-shapes is typically 20–200 ms two-way-time (TWT) (i.e. 34–340 m, with a velocity of 3,400 m/s). The lower part of the V-shape is 50 m wide, and it widens to 5 km in the upper part.

Table 1 summarizes the observed types of SCR, which are illustrated with 2D and plan view images. Three main groups are distinguished: (i) simple U- or V-shapes (Types 1, 2), (ii) single or double W-shapes (Types 3, 4) and (iii) more diverse patterns (Types 5, 6, 7 and 8). The 2D-architecture is highly dependent on orientation of the seismic section relative to the main axis. The U-shape is seen in sections subparallel to the main axis, the V-shape in sections is perpendicular to a single feature, whereas the (double) W-shapes seem to be the result of merging of adjacent V-shapes. Where faults offset the chalk, “dashed” anomalies can be seen (Table 1, type 5) in combination with V-

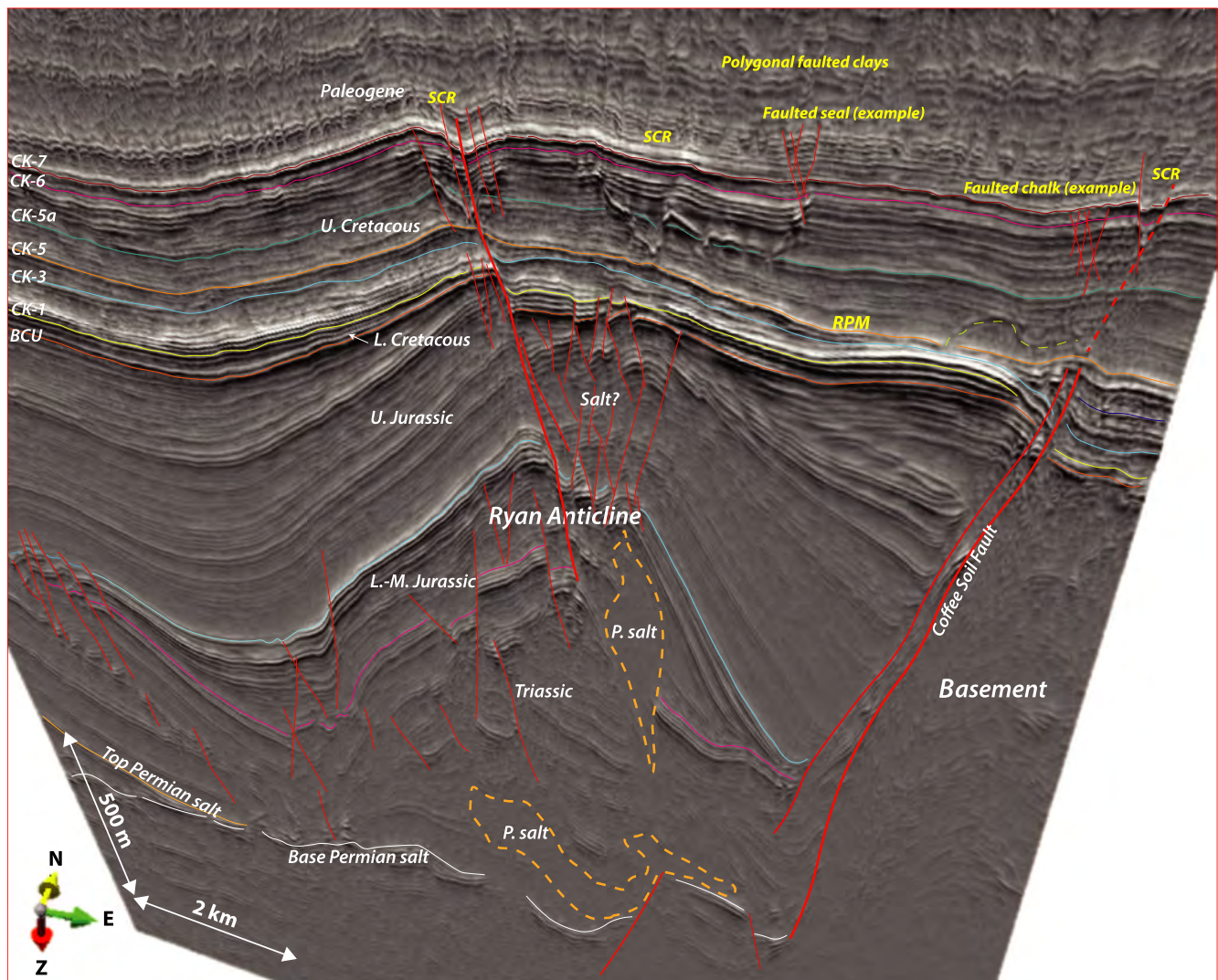


FIGURE 9 2D seismic section with Pseudo-Relief attribute (tecVA attribute, see Bulhões and de Amorim, 2005 for explanation). High amplitudes (black/white) reflect high AI “hard” beds that “stand out,” low amplitudes (grey) reflect low AI “soft” beds. Two deeply rooted faults can be observed that offset the Chalk Group (Ryan anticline, Coffee Soil Fault), as well as several smaller normal faults at the crest of the Ryan Anticline that terminate in the lower parts of the Chalk Group. In the extension of these faults, Stratigraphy Cross-cutting Reflectors occur (SCRs). Some salt remnants (low S/N packages) can be recognized within the Triassic and Jurassic successions, which is heavily faulted due to halokinesis and subsequent tectonic events

and (double) W-shapes (Type 6). Subtle amplitude anomalies can indicate a distal position relative to the features (Type 7, see Figure 3a at O-1X location).

Subtle linear “pseudo-reflectors,” with conjugate architecture (45–55°), can be seen throughout the chalk (Figure 10a and insets therein). These linear amplitude variations are emphasized on ant-tracked structural data from eXchroma^{SG} (Figure 10b). They correlate well with underlying fault fabric and extend far into the Palaeocene–Eocene mudstones. They seem to be the precursor of the better developed V/W-shaped SCRs. The latter resemble gentle horst and graben structures, where the chalk inside the SCRs is analogous to the grabens and the chalk outside is analogous to the horsts. The

topography is 10–50 ms TWT (i.e. 17–85 m, with an average velocity of 3,400 m/s).

4.2.2 | Lateral architecture

In map view, the SCRs are lobate to elliptic and typically have “fingers” at one side of the lobe (Figure 11a,b). The lobes/ellipses are typically 1–5 km long and 0.2–3 km wide, and occur: (i) at the crest of the Ryan Anticline, most clearly where the master normal fault is linking up with the NW-SE-oriented fault (compare with Figure 12a); (ii) along the Coffee Soil Fault, where en-echelon faults can also be seen; (iii) along radial faults of salt diapirs. The lobes are

TABLE 1 The seismic expression of the SCRs depends on the orientation of the seismic section in relation to the lobate shape of the feature

Type		Seismic	Porosity	HD Spectr. Dec.	Orientation
1	U				Line parallel through axis of single large lobate diagenetic geobody
2	V				Line perpendicular through a single lobate diagenetic geobody
3	W				Line parallel to axis of multiple lobate diagenetic geobody
4	2W				Line perpendicular to axis of multiple lobate diagenetic geobody
5	\\ \\ \\				Line perpendicular to major fault and fracture swarms, initiation of front creating 'fingers'
6					Line perpendicular to axis of single lobate diagenetic geobody with deformation
7					Small anomaly, 'nose' of the diagenetic geobody, furthest extent of the diagenetic front
8					Line parallel to axis of single diagenetic geobody that is not deeply affecting the chalk

Horizontal scale bar is 500 m, vertical scale bar 400 m, peaks are blue (boundary to lower AI beds), troughs are red (boundary to higher AI beds), and porosity colour scale is the same as Figure 3b. Eight different expressions (types) have been recognized, and some are related to one another as a result of a different orientation. For example, within the same SCR both U- and V-shapes can be found by changing the orientation parallel to the axis and perpendicular, respectively. 2W-shapes are the result of the merging of two V-shapes. Also, importantly, small seismic anomalies might represent the distal expressions of the lobate shapes (Type 7), showing the importance of 3D seismic data.

often surrounded by “halos” with dimmer seismic expression, because of the lower seismic amplitude. Cross-cutting relationships between individual lobes/ellipses are common and at least four “generations” can be distinguished, where the most recent lobes are the brightest (have the highest seismic amplitudes) (Figure 11b). The merging of lobes leads to the W-shapes in 2D section.

4.2.3 | 3D stratigraphic architecture

Stratal slicing shows that the 3D stratigraphic architecture outlined by the SCRs follows a system of vertical conduits, which connect to the underlying fault system, coincide with the subtle linear features seen on 2D section and spread laterally over time in a zigzagging pattern (Figure 12). At the

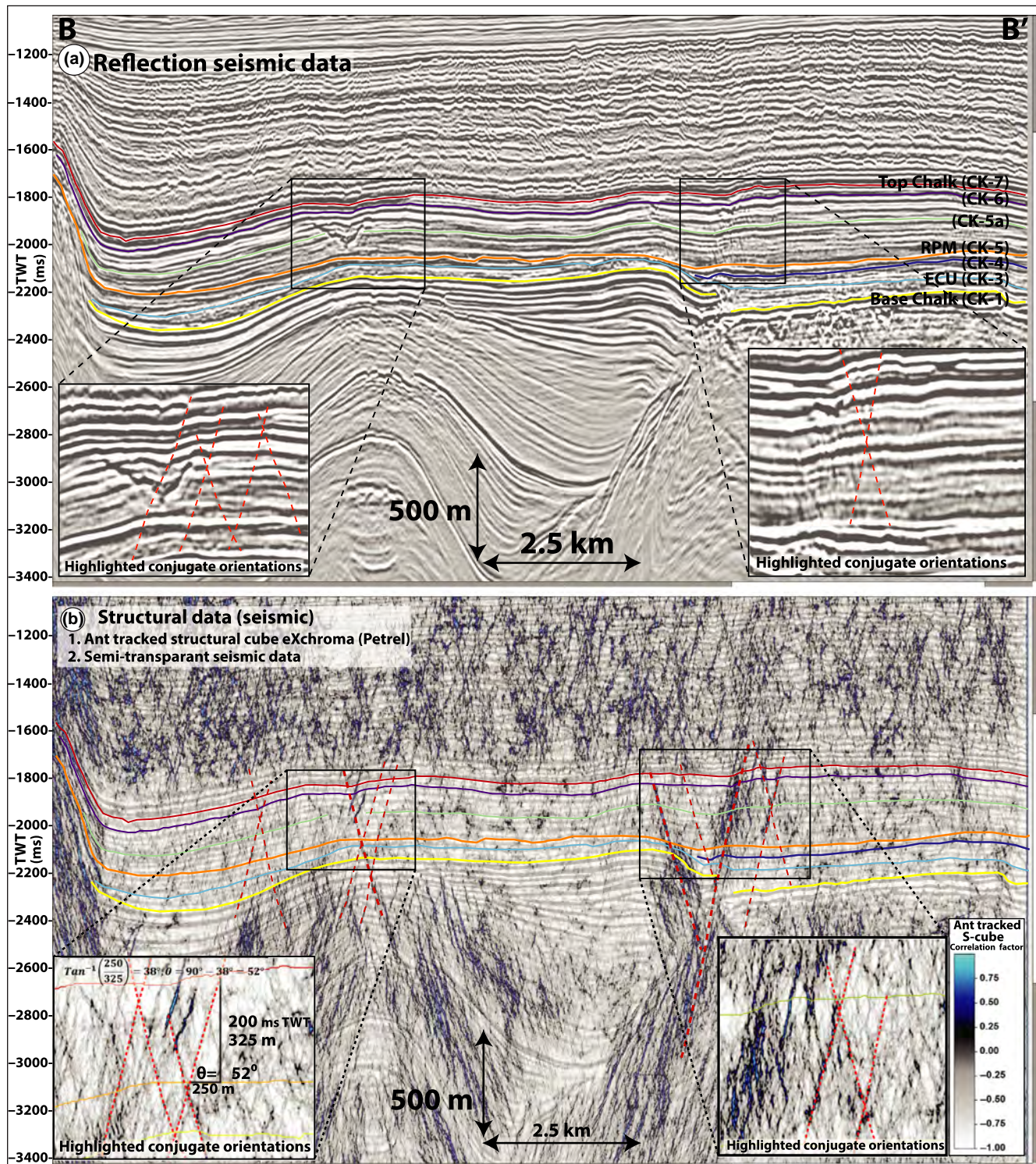


FIGURE 10 Subtle linear features within the chalk that likely reflect conjugate faults. For location, see Figure 1. See Figure S2 for an uninterpreted section. (a) Reflection seismic data show very subtle dimming of amplitudes within the chalk which are difficult to see. (b) By ant-tracking (Petrel structural algorithm) eXchroma's structural data cube, these conjugate lineations become much more apparent, and are an extension of the underlying fault fabric (high-angle, 45–55° to the normal). They may represent low-throw conjugate faults, known from chalk outcrops in England (Starmer, 1995). The SCRs have similar orientations and seem to form by merging of these conjugate faults, giving them lower angles (30–55° to the normal)

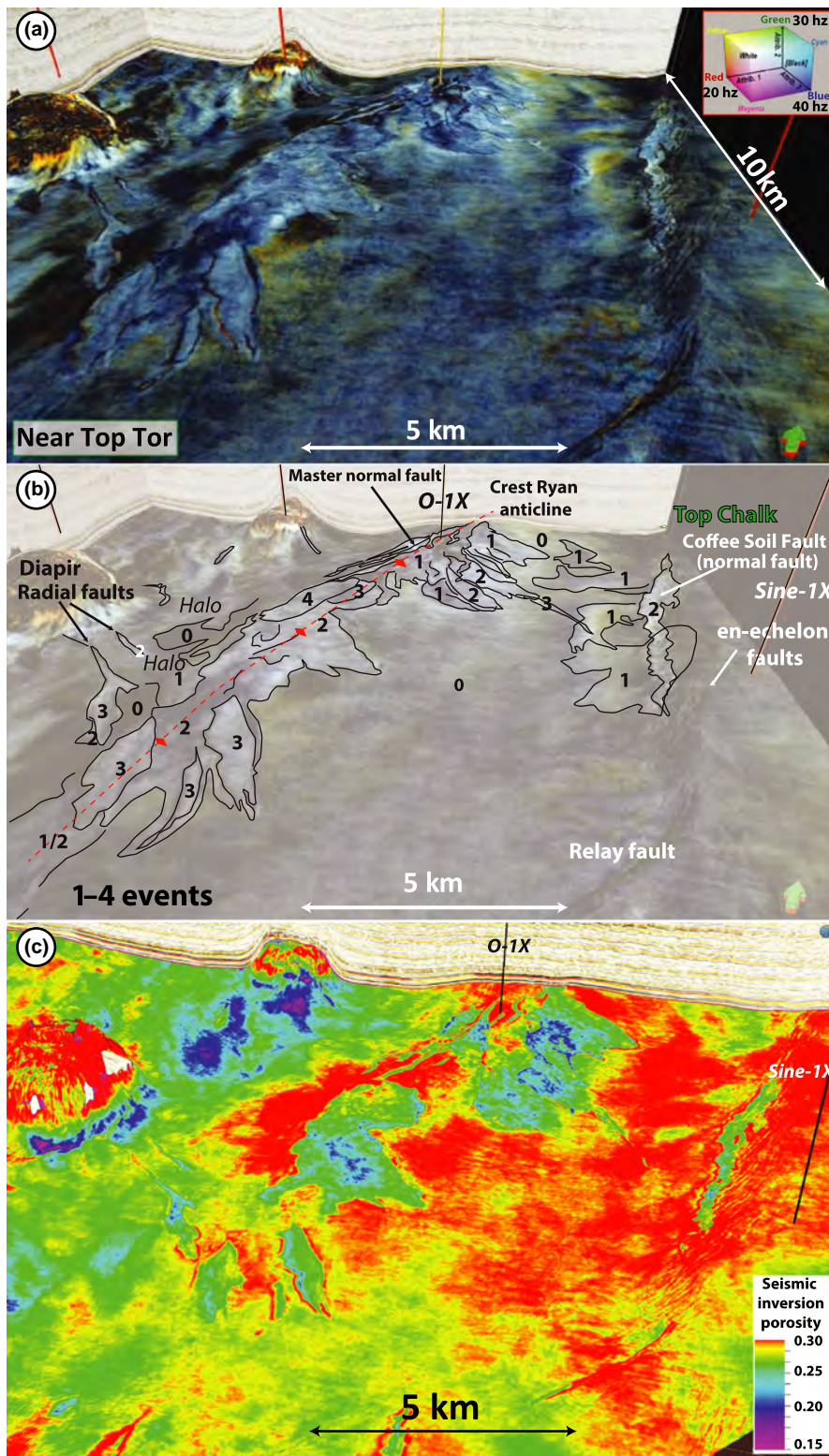


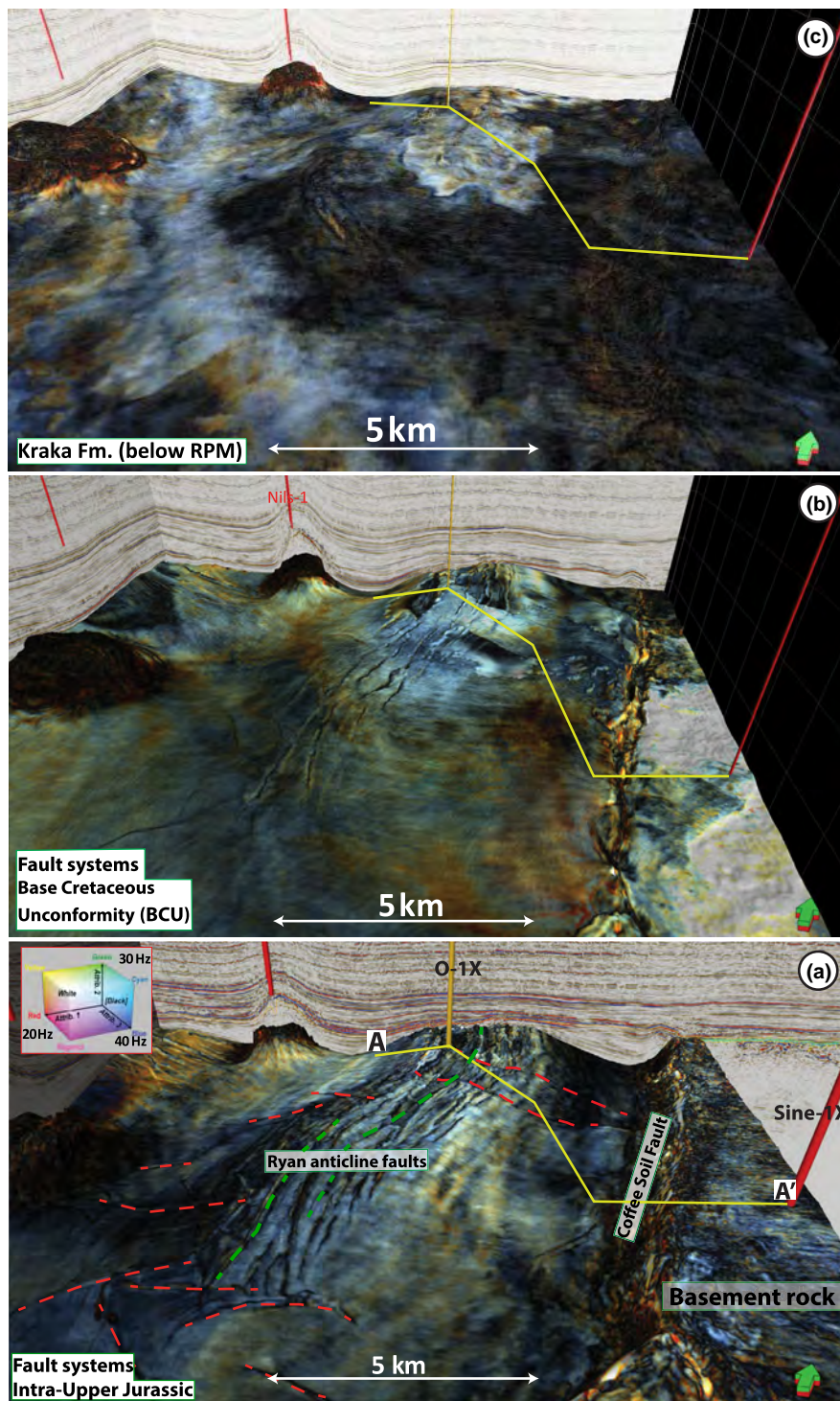
FIGURE 11 Spectral decomposition and porosity at the near top Tor Formation stratigraphic horizon. (a) RGB display that shows in map view the extent of the SCRs at this level, which is mainly at the crest of the Ryan Anticline, along the Coffee Soil Fault, and along radial faults. Lobate to elliptical shapes are observed, and "fingers" are found on one side. (b) Cross-cutting relationships can be seen (up to four generations, 1-4), where "younger" lobes cross-cut older lobes. The result is a brighter seismic expression (higher acoustic impedance). (c) The SCRs outline low-porosity bodies of chalk nested within high-porosity chalk based on seismic inversion data, but this can underestimate porosity due to occurrence of larger amounts of contact cements and dense/fast minerals (dolomite, magnesium sulphates). Note that the multi-generation cross-cuts can be recognized in the porosity data: the more generations, the brighter the expression, and the lower the porosity

deepest stratigraphic level (Figure 12a, Intra-Jurassic), the Jurassic fault structures at the top of the Ryan crest are clearly seen as N-S striking lineations, corresponding to the normal faults seen in 2D section (Figure 9). The Coffee Soil Fault is represented as a westward dipping fault plane,

and the Upper Jurassic growth package can be seen on the seismic section in the back (Figure 12a).

The N-S striking normal faults can still be observed at the Base Cretaceous Unconformity (BCU) level (Figure 12b), showing that they remained active until at least

FIGURE 12 Stratigraphic slicing with spectral decomposition attribute in colour (20 Hz (red), 30 Hz (green), 40 Hz (blue), from oldest (a, lower left) to youngest (f, upper right). Location of Figure 3 is given by the yellow line. (a) Intra-Upper Jurassic level, observing 5- to 10-km-long N-S lineations (green lines) that correspond to the normal faults seen in Figures 8 and 14. The Coffee Soil Fault stands out as a complex deformed zone. Note that also a NW-SE trend can be seen (red lines). (b) Base Cretaceous Unconformity level (BCU). These normal faults can still be observed and occur close to the base of the Chalk Group. (c) Intra-Kraka Formation level, underneath the RPM. A bright 5 by 5 km zone can be distinguished south of O-1X, corresponding to an increased acoustic impedance. (d) Base Tor Formation, above the RPM. Sharp elliptical outlines are observed (yellow arrows), with high-amplitude, low-frequency rims, corresponding to the bases of the SCRs. These features represent vertical corridors. (e) Near top Tor Formation, lobate shapes with a high-frequency content can be distinguished in a much larger area (15 by 5 km) on the crest of the Ryan Anticline, along the Coffee Soil Fault, and the radial faults of the diapirs. (f) Top Ekofisk level, maximum extent of the seismic anomaly. The bright expression corresponds to the chalk outlined by the SCR, the dim expression by the chalk outside the SCR



the Early Cretaceous. The crestal zone of the Ryan Anticline shows a dominance of blue colours, indicating a large contribution of high-frequency wavelets to the seismic traces representing thin beds or sharp lithology changes (c.f. Partyka, Gridley, & Lopez, 1999). It is also clear that the O-1X well penetrates a first-order normal fault at 2,335 m, and cuttings from this interval contain a large amount of sulphates with typical Permian/Triassic sulphur isotope values between 11.4‰ and 15.1‰ (Figure 13a).

The lower part of the Chalk Group immediately below the RPM (Figure 12c) shows that there is a distinct high-frequency zone in the seismic signal in the area over the Ryan crest. This distinct zone diminishes 50 ms upwards and the spectral signal becomes more homogenous at the RPM. High magnesium contents (4–8 wt%) and dolomite are common in this interval (Figures 5 and 13b).

The sharp NW-SE-oriented lobate shapes above the RPM (Figure 12d) correspond to the base of the V-shapes

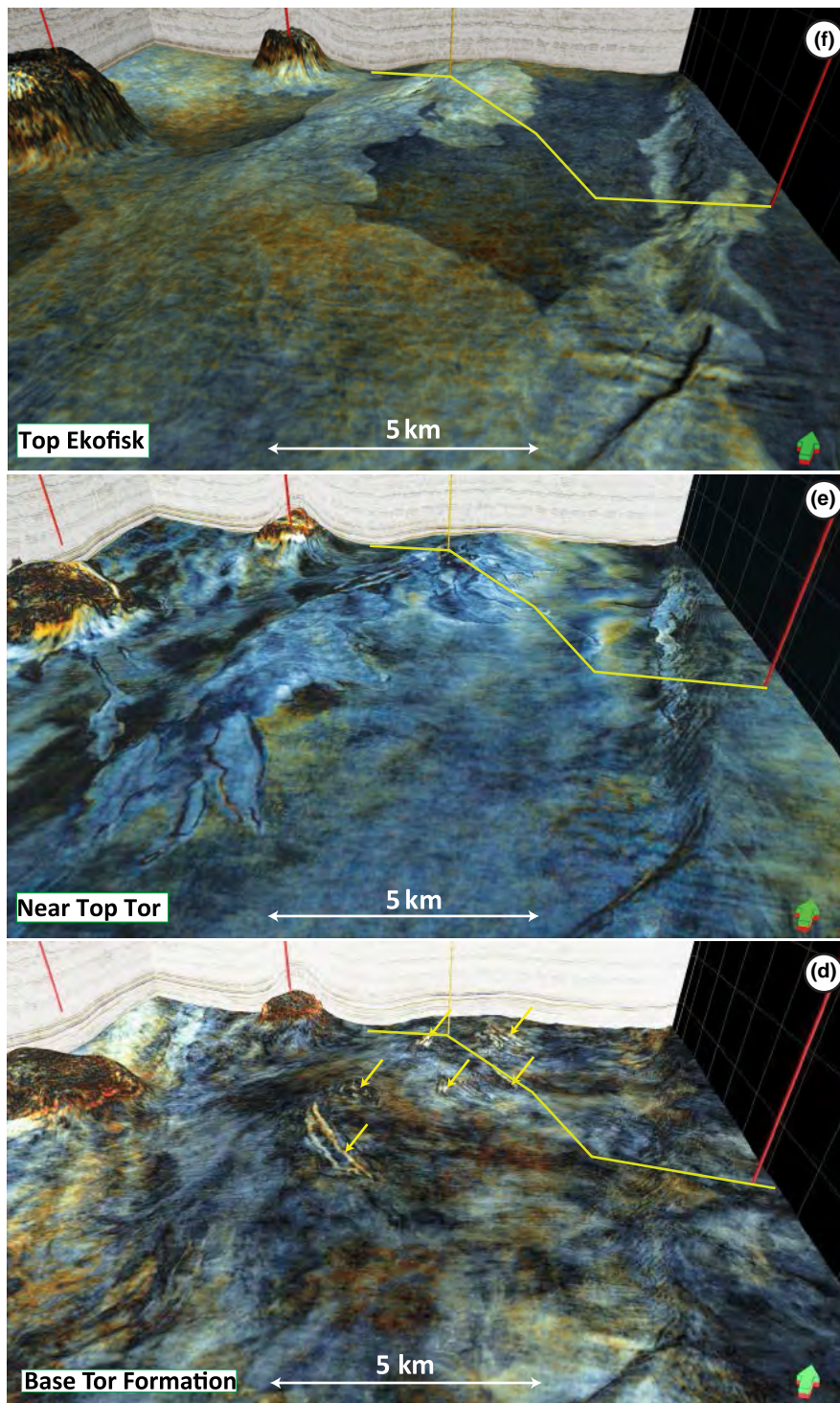


FIGURE 12 Continued.

and (double) W-shapes. They are 50–500 m wide, and 1–3 km long, and occur between the O-1X and Sine-1X wells.

Near the top of the Tor Formation, the anomaly outlined by the SCRs extends further laterally (5 km by 10 km) (Figure 12e), corresponding to the widened V-shapes seen in cross-section, and the contribution of high-frequency wavelets is more dominant. It is also evident that W and

2W shapes are the result of the merging of V-shapes, as the rims of the individual V's sometimes are still visible and correspond to the subtle conjugate lineations (see Figure 10b). Along the Coffee Soil Fault, NE-SW en-echelon faults running oblique to the main N-S faults are over-printed by the seismic anomaly (Figures 10b and 12e). In addition, lobate shapes are observed along the radial faults of the diapirs.

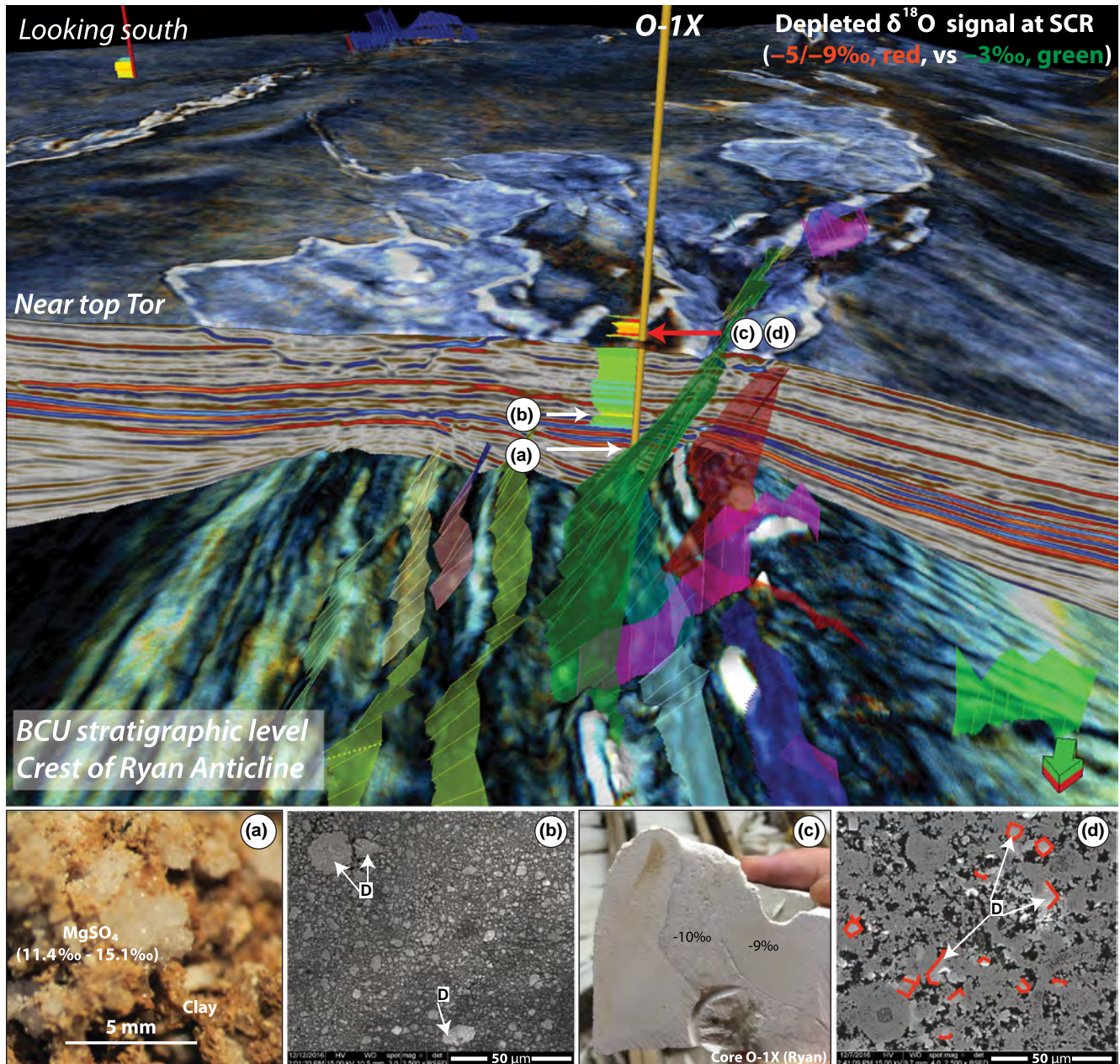


FIGURE 13 Staircase diagram with 3D visualization of the integration methodology and samples from selected intervals (a–d). Shown are two stratigraphic levels (BCU and near top Tor Formation) with spectral decomposition, mapped fault planes, and $\delta^{18}\text{O}$ log for the Chalk Group in O-1X, where O-1X penetrates the first-order normal fault plane, sulphates with Permian/Triassic $\delta^{24}\text{S}$ are found in drill cuttings (2,335 m, inset a). The chalk below the RPM shows larger amounts of dolomite crystals (“D,” in inset b), coincident with higher Mg content (Figure 5). Where the bright anomaly reaches O-1X, the most negative $\delta^{18}\text{O}$ values are observed in calcite-filled fractures and surrounding chalk (inset c, 1,925 m, red arrow). In addition, more dolomite cement occurs in the chawks above the anomaly

At the Top Chalk surface (Figure 12f), the anomaly covers the largest area (20 km by 45 km) and occurs at: (i) the crest of the Ryan Anticline; (ii) along the flanks of the Nils, Vagn and Tove salt diapirs; and (iii) the Coffee Soil Fault. The outline is sharply defined, with a transition zone of only 20–30 m into unaffected low acoustic impedance chalk. Sine-1X penetrates the rocks characterized by this

higher acoustic impedance signal (up to $6\times$ background value).

4.2.4 | Seismic inversion and petrophysics

Seismic inversion data (Figures 3b, 10c, and Table 1) show that the chalk within the SCRs (Zone 3, Figure 4) has

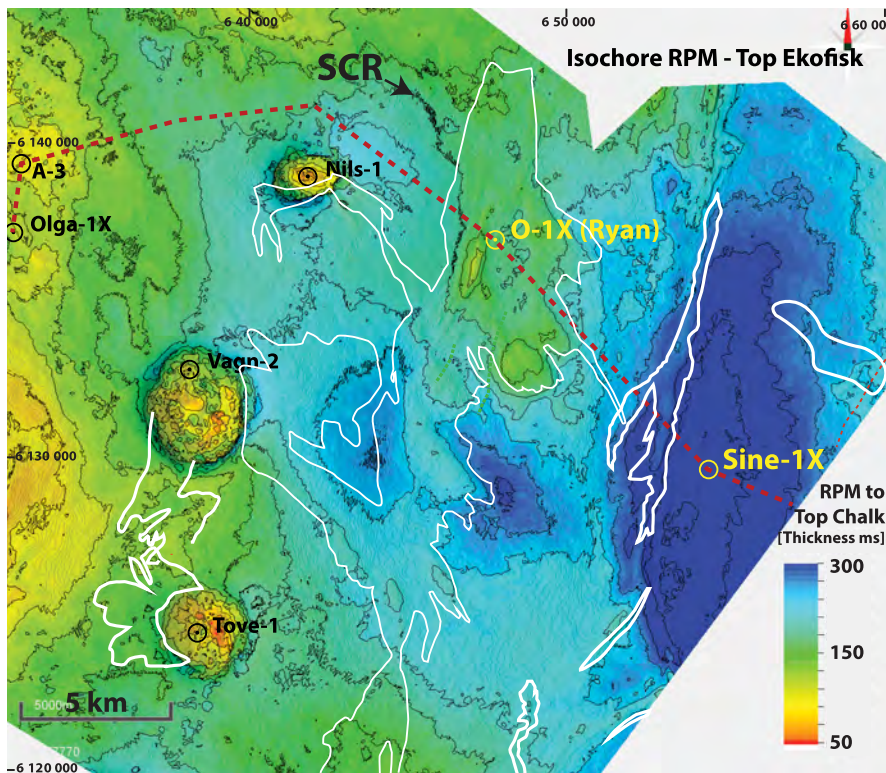


FIGURE 14 Time thickness (isochore) between the RPM and top Ekofisk. The SCR outlines are shown in solid white, seismic section of Figure 3 in dashed red line. Although there is some thinning because of the topography of the Ryan Anticline (see onlapping pattern in Figures 3 and 14), a local deviation occurs where the SCRs are present. In these areas, the chalk interval between the cross-cuts shows a maximum thickness change of 70 ms (150 ms vs. 220 ms, 22% volume change). Using a seismic velocity of 3,400 m/s for the chalk within the SCRs and 3,000 m/s for the background chalk, this represents a thickness change of 75 m. This corresponds to the horst and graben topography seen at the top of the Chalk Group at the SCRs in Figure 3. Longitude and latitude shown in ED50 UTM 31N Projected Coordinate System, also in Figures 17 and 19

10%–20% percentage points lower porosity than the chalk at the same stratigraphic level outside of the features. A sharp transition from 30% to less than 15% porosity occurs over less than 20–30 m laterally. The highest amplitudes are the brightest expressions in spectral decomposition attribute and reflect the lowest porosity bodies (Figure 11). The most recent generation of cross-cuts, thus, shows the lowest porosity. This pattern continues upwards in the Ekofisk Formation where the areas with lower porosity widen up (Figure 12f). Areas with the lowest porosity in the Tor Formation also correspond to the areas the lowest porosity in the Ekofisk Formation.

O-1X penetrates a rod-shaped seismic anomaly at 1,925 m (Type 5), which persists upward and represents a (modelled) porosity reduction from 35% to 28% (Figures 13 and 5). Similarly, in Sine-1X at 1,829–1,872 m (Figures 4 and 5), a reduction in neutron-derived porosity from 34% to 20% coincides with an increase in AI. The interval between the RPM and the SCRs (Zone 2) is characterized by chalk with porosity of 25%–30%.

The time isochore between the RPM (base SCRs, CK-5) and Top Chalk (Top SCRs, CK-7) is on average 150 ms TWT thick (255 m, with average velocity 3,400 m/s) within the SCRs and 220 ms TWT thick (330 m, with average velocity 3,000 m/s) outside the SCRs (Figure 14, see Figure 9 for markers). This is roughly equivalent to a 20% volume reduction inside the SCRs and gives rise to the horst and graben topography seen in 2D sections (Figure 3a).

4.2.5 | Petrography and geochemistry

The O-1X core (1,873–1,882 m, Figure 4, Danian, 77% recovery) is potentially located within a SCR alteration (Figure 3a,b). The chalk has 20%–30% porosity (final well report) although it is fairly silicified, contains multiple 1–10 cm thick clay seams in the lower part (1,873–1,876 m, Figure 4), cleans upward and contains several 1–10 cm thick chert lenses. In addition, several mm-wide and centimetre to decimetre long calcite veins, containing coarse-grained (mm-sized) translucent calcite crystals, are present (Figure 13c). Unfortunately, no data are available from a fully developed SCR, so the data from O-1X are used to predict the properties of the rocks in the SCRs (e.g. the “rod,” Type 5 as seen in Figure 13).

SEM data from the chalk in Zone 3 show large calcite overgrowths on the coccoliths, which fill the pore spaces and create coalescent grain-to-grain contacts. It also shows recrystallized nano- and micro-fossil (fragments), as well as 5–100 micron dolomite crystals. Large amounts of micron-sized quartz aggregates are also seen to cover the coccoliths (“Si” in Figure 6e). Thin sections show higher degree of recrystallization of nano-fossils compared with Zone 2, and dolomite cements are reflected by lighter, sharp-edged crystals, 5–100 micron in size (“D” in Figures 6e,f and 7e,f).

The $\delta^{18}\text{O}$ values of the chalk inside the SCRs (Zone 3) range from -6 to -9‰ , with the most negative values representing calcite-filled fractures and the immediately adjacent chalk (Figures 4 and 13c). This is similar to the

values found by Egeberg and Saigal (1990) in fractured chalks. Less porous intervals show more negative $\delta^{18}\text{O}$ values, suggesting a correlation between oxygen isotopes and porosity (Figure 5b). It likely reflects that the pore-filling cement and dolomite, as observed in the SEM (e.g. Figures 6e,f, and 7e,f), have negative $\delta^{18}\text{O}$ values.

The Mn/Sr ratio of chalk within the SCRs is up to 1.10 in O-1X (11 \times baseline) and 26.6 in Sine-1X (13.3 \times baseline) (Figure 4). Zone 3 chalk has on average the largest ratio of Mn relative to Sr and falls furthest along the water:rock interaction trend (Figure 8b). A continuous increase in water:rock interaction can be interpreted from the Mn/Sr ratios from Zone 2 (the least) to Zone 1 and Zone 3 (the most).

The magnesium content increases towards the top of the chalk in both O-1X and Sine-1X (Figure 4). This could reflect the occurrence of dolomite crystals, as observed in SEM (Figures 6e,f and 7e,f).

Si/Al ratios are much higher in Zone 3 in both wells (1,844 m in Sine-1X and 1,908 m in O-1X), possible due to the presence of quartz aggregates as seen with SEM (Figures 4, 6e,f, and 7e,f). It seems to correlate with an increase in Mn/Sr ratios (Figure 4), which on cross-plots deviate from the clay trend at higher Mn/Sr ratios (Figure 8c).

4.3 | Pre- and post-chalk observations

The superposition of the SCRs and the underlying fault fabric points towards a correlation (Figure 15). In the study area, thickness variations are influenced by the two rifting phases, a doming phase, and salt (re-) mobilization (Figures 2 and 16, T-1 to T-3, and J-1 to J-3).

The Ryan Anticline is cored by a 2.5-km-thick Triassic growth wedge (T-1 to T-3), reflecting the Triassic rifting phase. These deposits comprise continental sandstones, mudstones and evaporites of the Triassic Keuper Group. Seismic packages with low signal/noise ratio, within the Triassic and Lower–Middle Jurassic sediments (J-1), may represent remobilized Triassic/Permian evaporites (“P” in Figures 9 and 16).

The Upper Jurassic (J2–3) is represented by a 1.5-km-thick growth wedge along the N-S trending Coffee Soil Fault, where mainly marine mudstones accumulated. Over the crest of the Ryan Anticline the packages rapidly thin to 500 m, indicating less accumulation space, which could have been the result of Mid-Jurassic doming (Michelsen et al., 2003).

The multiple tectonic events have generated a multi-oriented, complex fault fabric underneath the chalk (Figure 17). The most pronounced orientations are as follows: (i) N-S to NNE-SSW, reflecting Permo-Triassic extensional faults and the faults at the crest of the Ryan Anticline (e.g. Glennie et al., 2003; Goldsmith et al., 2003); (ii) NW-SE, reflecting Late Jurassic extensional faults (Michelsen et al.,

2003); and (iii) radial faults around the salt diapirs. Where a higher intensity of faults is present underneath the chalk, more pronounced SCRs are observed. The overall NE-SW trending SCRs are at critical places offset towards a NW-SE orientation, which coincides with the occurrence of underlying Late Jurassic faults.

A seismic velocity geosection over the Ryan Anticline shows three major elements (Figure 18): (i) low-velocity clays on top of the chalk (2,000 m/s); (ii) the chalk, comprising a low-velocity upper layer (2,800–3,400 m/s) and a high-velocity lower layer (3,400–5,000 m/s), divided by the RPM; (iii) low-velocity Jurassic-Triassic strata, forming a “wing” of low velocity just below the Chalk Group (2,300–2,600 m/s).

Anhydrite has been reported at three stratigraphic levels in O-1X (Final Well Report O-1X). The sulphates occur at 2,335 m, where the well penetrates the master fault, and in the overlying Lower Cretaceous and lowermost Chalk Group from 2,240 to 2,317 m (Figure 13a). Sulphur isotope analysis of mm-sized translucent sulphate crystals, forming up to 20% of the cuttings, gave $\delta^{34}\text{S}$ values of 11.4‰ (2,289 m), 12.1‰ (2,313 m), 14.1‰ (2,316) and 11.8‰ (2,320 m). For comparison, Triassic Keuper anhydrite in O-1X has $\delta^{34}\text{S}$ values between 14.3‰ and 15.5‰, and in the Permian anhydrite in Nils-1 $\delta^{34}\text{S}$ ranges from 12.3‰ to 13.1‰. Since samples were taken from unwashed material, it could reflect precipitation of salt from drill filtrate. However, its occurrence specifically at the fault plane and in Zone 1, and the similar isotope signatures, suggests that it is natural.

A spectral decomposition slice at the top of the Våle Formation (post-chalk, Figure 19) shows several discontinuities parallel to the Ryan Anticline, the Coffee Soil Fault and the Nils diapir. They correspond in 2D sections to places where the Våle marker is slightly offset by underlying faults. It will be argued that this is where the main top seal of the chalk failed and overpressure could leak out of the system, forming the SCRs.

5 | DISCUSSION

5.1 | Chalk below the regional porosity marker (RPM)

5.1.1 | Erosion and condensation forming early intra-chalk seals

Esmerode, Lykke-Andersen, and Surlyk (2007) observed an erosional unconformity at the top of the Campanian in the Danish basin. They interpreted this surface as reflecting increased ocean bottom current activity that winnowed chalk from basinal highs and deposited it as drifts in other parts. Similar observations were made by van der Molen

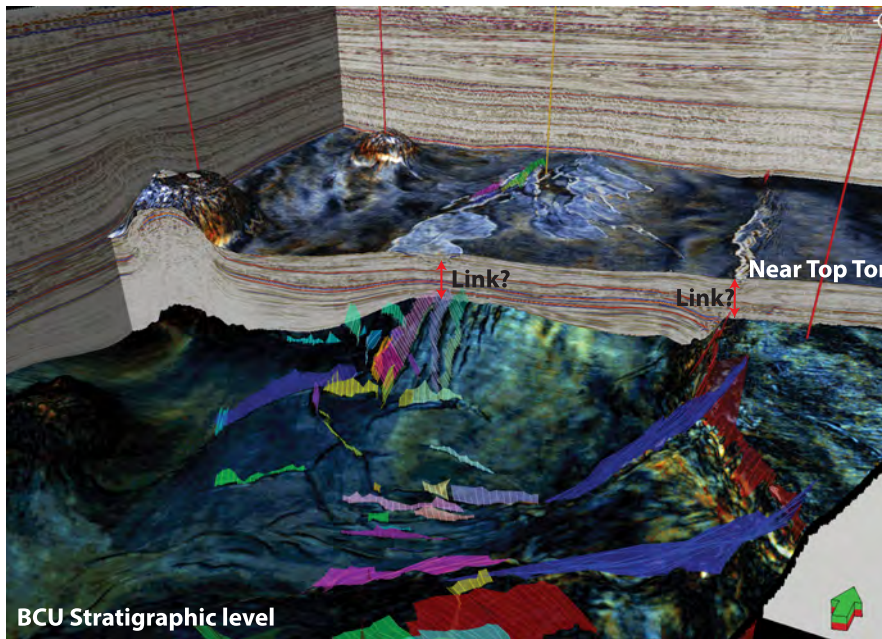


FIGURE 15 Staircase diagram showing the regional correlation with the underlying fault fabric. The juxtaposition of SCRs and faults seems to point towards a genetic relation. See Figure 17 for a 1:1 map view comparison

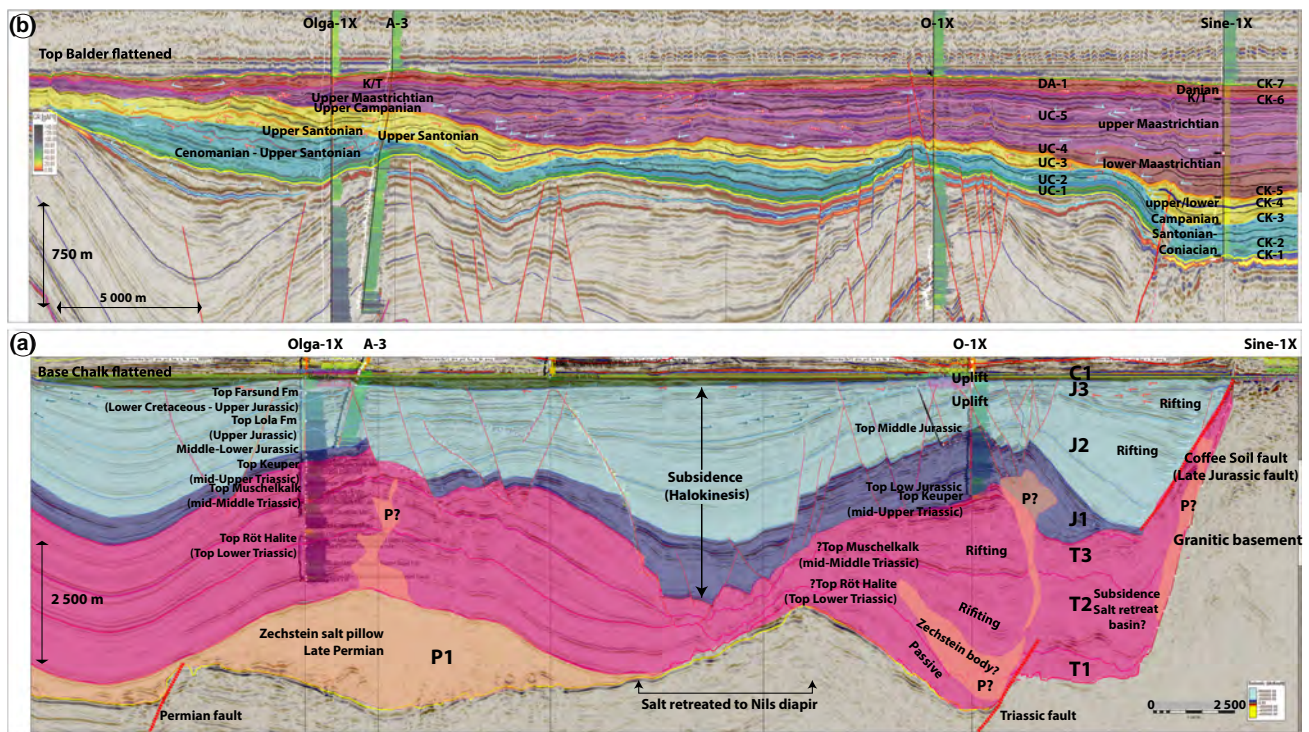


FIGURE 16 Structural and seismic stratigraphic interpretation of prechalk strata (a, lower) and Chalk Group (b, upper). See Figure S3 for an uninterpreted section. (a) Permian evaporites (P1) can be found underneath the Kraka salt pillow and potentially within the Ryan Anticline as low signal/noise packages (P?) and along the Coffee Soil Fault. Triassic packages (T-1 to T-3), Jurassic packages (J-1 to J-3) and Lower Cretaceous (C1) show large thickness variations along the transect, which are to a large extent controlled by the tectonic history. See text for further explanation. (b) The thickness of the pre- and syn-inversion strata (UC-1 to 3) closely follows the underlying Jurassic basin morphology, in contrast with the post-inversion package (UC-4,5 and DA-1). This shows that large basement re-arrangements took place during the Campanian inversion event, which could have reactivated some of the older faults. In addition, the normal faults offsetting the top of the chalk show that post-chalk deformation took place

(2004), who recognized erosion and nondeposition of the CK-7 sequence (Upper Campanian). Gennaro (2011) also recognized increased erosion at the Top Magne reflector

(top Campanian). This is in agreement with a global increase in ocean circulation as described by Jung, Voigt, Friedrich, Koch, and Frank (2013). In the study area, a

FIGURE 17 Juxtaposition of major fault systems (Triassic (NNE-SSW); Jurassic (NW-SE)) at BCU stratigraphic level (dark lineations from ant-tracked eXchroma structural data cube), and the occurrence and extent of the SCR (spectral decomposition attribute at near top Tor Formation stratigraphic horizon). The spatial distribution of SCR seems to be controlled or influenced by the N-S and NW-SE faults on the Ryan anticline, the Coffee Soil Fault, and the radial faults around the diapirs

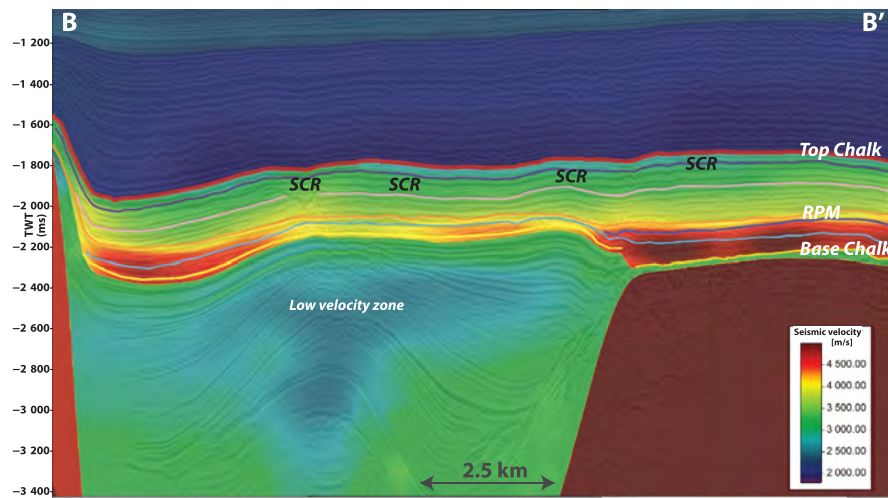
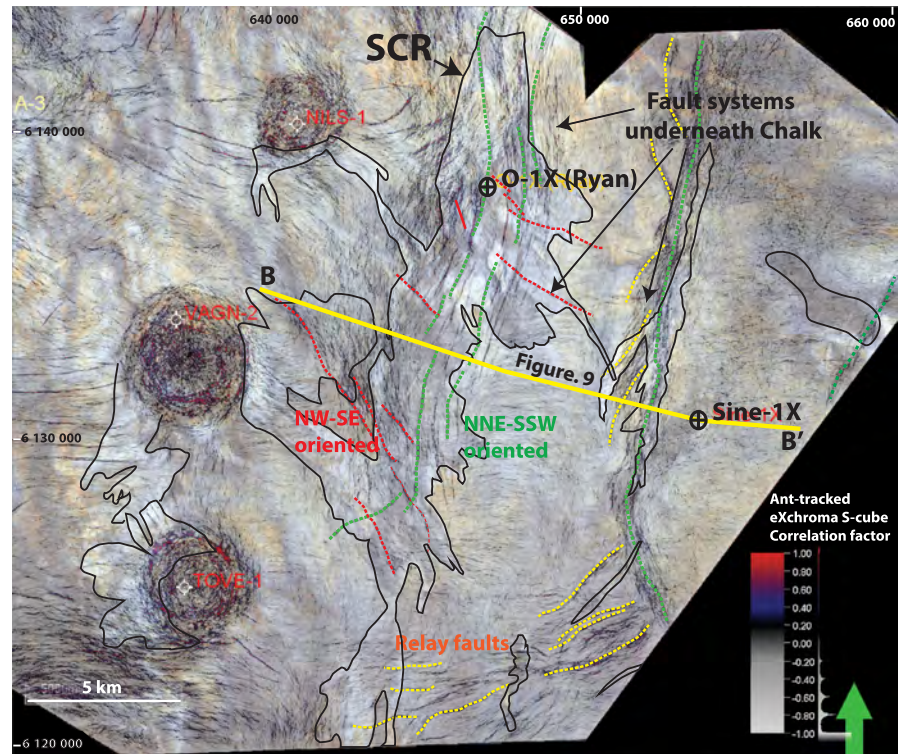


FIGURE 18 Seismic velocities along same transect as Figure 10, see Figure 17 for location of the line. The RPM stands out as a high-velocity package within the chalk (red colours, 4,500 + m/s). The lower velocities on the crest of the Ryan Anticline illustrate the higher porosities found underneath the RPM in O-1X (e.g. 20%–10%) compared with Sine-1X (e.g. 10%–0%). The SCR is seen as slightly higher velocities (3,400–4,000 m/s) compared with the lower velocity chalk it is embedded in (2,500–3,200 m/s), which could indicate lower porosity and/or occurrence of faster minerals (anhydrite, dolomite, etc.). Note the “wings” of a low-velocity zone in the Triassic–Jurassic package, which can represent overpressured zones on top of the crest of the Ryan structure and surrounding “bumps” below the Chalk Group where fluids accumulated. These could be formed by dehydration of the thick clayey packages and/or compaction-driven release of pore fluids

similar unconformity is observed at the top of the Campanian (i.e. the RPM), which is expressed as a hiatus at the Ryan Anticline (four subzones missing), while deposition continued at the more basinal Sine-1X location (Figure 3a). During times of low sedimentation rates, early cementation can occur at some distance below the seafloor under the

influence of organic degradation and internal bioclastic carbonate redistribution (Molenaar & Zijlstra, 1997). The long-term position of O-1X on a structural high resulted in condensation of most of the pre-Maastrichtian section. It is, therefore, possible that early diagenesis could explain the combination of low porosity and $\delta^{18}\text{O}$ values that are less

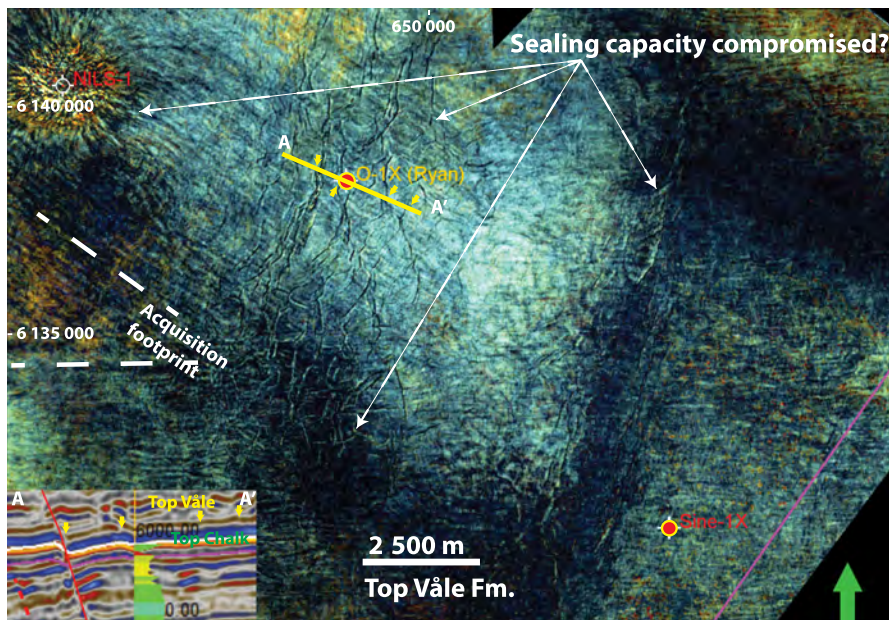


FIGURE 19 High-definition spectral decomposition on Top Våle Formation (first continuous reflector on top of Chalk Group, see inset with yellow arrows). Several discontinuities (“cracks,” yellow arrows inset) can be observed parallel to the Ryan structure, Coffee Soil Fault and Nils salt diapir, which are interpreted as locations where the overlying seal failed and overpressure could escape. The close correlation with the underlying SCRs (see Figure 12f) are interpreted as reflecting a causal relationship, in which the SCRs formed where overpressured fluids could drain from the chalk

negative than at Sine-1X (e.g. closer to Cretaceous seawater, Figure 5b). Subsequent burial compaction might have further reduced the porosity to form a very dense chalk rock at the top of the Ryan structure, which served as an important intra-chalk barrier for later fluid migration. The slightly increased Mn/Sr ratios immediately beneath the RPM in O-1X indicate that little rock:water interaction was possible in this zone and might reflect this sealing character. The higher Mn/Sr ratios within the lowermost chinks could reflect stagnating basinal fluids beneath this intra-chalk seal. The more negative $\delta^{18}\text{O}$ values and higher Mn/Sr ratios at Sine-1X beneath the RPM could indicate less early cementation and more burial diagenetic cement.

The highly fluctuating Mg content observed in O-1X below the RPM is likely to reflect the occurrence of dolomite, which is observed as “aggressive” crystals under SEM (Figures 6 and 7). As the chalk is a relative low-Mg calcite, small amounts of dolomite could originate from recrystallization of high-Mg or aragonite bioclasts (Moleenaar & Zijlstra, 1997). However, the large amounts of dolomite (with crystals up to 100 microns) suggest that it is more likely that the Mg was introduced by an extra-formational fluid. This is supported by the occurrence of magnesium sulphates on the fault plane, in the Lower Cretaceous strata, and in the lowermost part of the chalk. Evaporites within the chalk are not common and only present where salt diapirs have pinched the formation. A similar origin is argued here, as the major fault is deeply rooted into the Triassic and Permian salt that forms the anticline (Figures 9 and 16). In addition, the sulphur isotopic values are comparable to those of the sulphate salts obtained from the Nils diapir, where most of the salt

retreated to. The RPM, thus, represents the top of an early cemented/compacted zone in the chalk formed as a result of seafloor bathymetry and increased bottom currents. It formed an important intra-formational seal for later fluid migration. We argue that basinal fluids accumulated at the highest points underneath the chalk beneath the RPM (high Mn/Sr ratios), and ultimately found a way through the RPM into the overlying high-porous chinks along fairways that evolved into the SCRs.

5.2 | Stratigraphy cross-cutting reflectors (SCR)

5.2.1 | Diagenetic geobodies

The SCRs outline irregular seismic-scale bodies of high-density chalk that dip steeply and cross-cut the stratigraphy (Figure 3a, Table 1). Seismic inversion data suggest that the chalk within the SCRs is low-porosity chalk nested within high-porosity chalk (e.g. 15% porosity within the SCRs vs. 30% outside). Without data from within these features, it is difficult to assess whether the increase in acoustic impedance is entirely controlled by porosity or whether localized mineralogy (dolomite/sulphates) and/or contact cement contributed as well. The cored interval in O-1X represents the closest proxy of the SCRs, as it falls within the seismic anomaly. In this core, the chalk is heavily silicified, and larger amounts of contact cement are observed (compare Figure 6f with d). It also contains fractures that are filled with calcite characterized by the most negative $\delta^{18}\text{O}$ values, and surrounded by zones of chalk with pore-filling cement (which also has very negative

$\delta^{18}\text{O}$). The low porosity, high amounts of contact cement and possible dolomite will give these rocks a high acoustic impedance compared with the high-porosity chalk within which they are nested and will generate the peak reflector that outlines these geobodies (c.f. Fabricius, 2003).

At the SCRs, the later two-way travel time of top Chalk Group and the time isochore showing a volume reduction of 10%–20% suggest that some mechanical compaction and/or dissolution must have occurred. Stylolites have not been observed in the core but dissolution cannot be ruled out, as no direct data are available from within the SCRs. Mechanical compaction can be quite dramatic in high-porosity chalks due to the large strain accumulated in such rocks (Fabricius, 2014). If some of the overpressured fluid could escape due to seal failure, this would result in significant inelastic deformation due to increasing effective stress, similar to that observed in depleting chalk gas reservoirs (e.g. Keszthelyi, Dysthe, & Jamtveit, 2016). This combination of cementation and compaction could, therefore, create high-density geobodies of diagenetic origin.

5.2.2 | Model

We propose the following scenario for the formation of diagenetic geobodies delineated by SCRs: (i) accumulation of basinal fluids below the Chalk Group (Figure 18); (ii) differential compaction of the Triassic-Jurassic basin fill resulting in fault reactivation and failure of major seals (e.g. lowermost Chalk Group, RPM and base Palaeocene clays, Figures 12d and 19). Subsequently, trapped fluids started to escape from the Chalk Group through a system of fault/fracture swarms and permeable beds and were temporarily trapped locally below intra-chalk seals. Reduced pore pressure resulted in mechanical compaction. (iii) This was followed by cementation of high Mn-calcite/dolomite/magnesium sulphates from the extra-formational fluids. The pathway of the fluids is reflected by the 3D geometry of the SCRs, which follows a zigzagging and widening upward pattern starting from the RPM (Figure 12).

Step 1: accumulation of basinal fluids

SCRs occur at locations in the basin where thick sedimentary basins underlie the Chalk Group (Figure 16) and where pronounced fault systems occur (Figures 12, 14 and 17). In the absence of hydrocarbon emplacement, the occurrence of high-porosity chalk above the RPM is likely the result of early establishment of overpressure, which originates from nonequilibrium compaction of the chalk, and from a transference component (c.f. Japsen, 1998). Compaction of the 4-km thick Triassic-Jurassic succession and dehydration of the marine mudstones may have generated a large amount of fluid, which remained contained beneath major seals within the Jurassic basin, generating

overpressure. Because of the multiple orientations and interlinkage of the fault systems and zones (Figure 17), large basinal drainage areas were established and funnelled basinal fluids towards the base of the chalk at the crest of the Ryan Anticline and along the Coffee Soil Fault, where “winged” low-velocity zones occur that may reflect these fluids (Figures 18 and 20, Step 1).

Steps 2–4: Location of the SCRs dictated by the underlying fault system

During reactivation of the faults, or when critical pore pressure levels were reached, these seals failed and fluids migrated along permeable zones such as fault planes into the lowermost parts of the chalk (Figure 20, Steps 2–4). These fluids could generally be contained below the early cemented chalk underneath the RPM, though raised Mn/Sr ratios indicate that some fluid penetrated upward (Figures 5 and 12c).

Differential compaction would be a feasible driving force for seal failure (Figure 20 Step 2), and movement is most pronounced at the crest of the Ryan Anticline (transition from salt pillow to Mesozoic basin), Ringkøbing-Fyn High (transition from Mesozoic basin to basement), and on top of salt diapirs (halokinesis). The increase in shear stress generated by differential compaction exceeded the failure envelope, leading to brittle deformation within the chalk, as indicated by the upward propagation of the underlying faults into the chalk, visible as high-angle (30–55° to the normal) subtle linear contrasts in acoustic impedance (Figures 10, 12e,f, 20, Steps 3 and 4). Comparison of these geometries with chalk outcrops from Selwicks Bay (UK) suggests that these lineations could represent low-throw faults and fracture swarms, which can act as fluid conduits (cf. Starmer, 1995). The spatial correlation between the SCRs and underlying fault fabric points to this genetic relationship (Figures 13, 15 and 17). Continued differential compaction may, thus, have generated many episodes of fault reactivation, which eventually also offset the sealing low-porosity chalk beneath the RPM and the sealing clays on top of the chalk at the crest of O-1X (see Figures 9, 13, 19 and 20, Step 5).

Steps 5 and 6: Overpressure leak-off and intra-chalk spreading pattern

A significant offset of the sealing clays on top of the chalk might have compromised their sealing capacity (Figures 19 and 20, Step 5). The overlying polygonally faulted clays probably did not form a seal either (see Cartwright, 2007 for a discussion), so it is possible that the overpressured and newly transferred fluids could start to escape the chalk on a large scale. Draining of overpressure from this “valve” initiated mechanical compaction of the chalk, which in turn induced further displacement on the surrounding faults

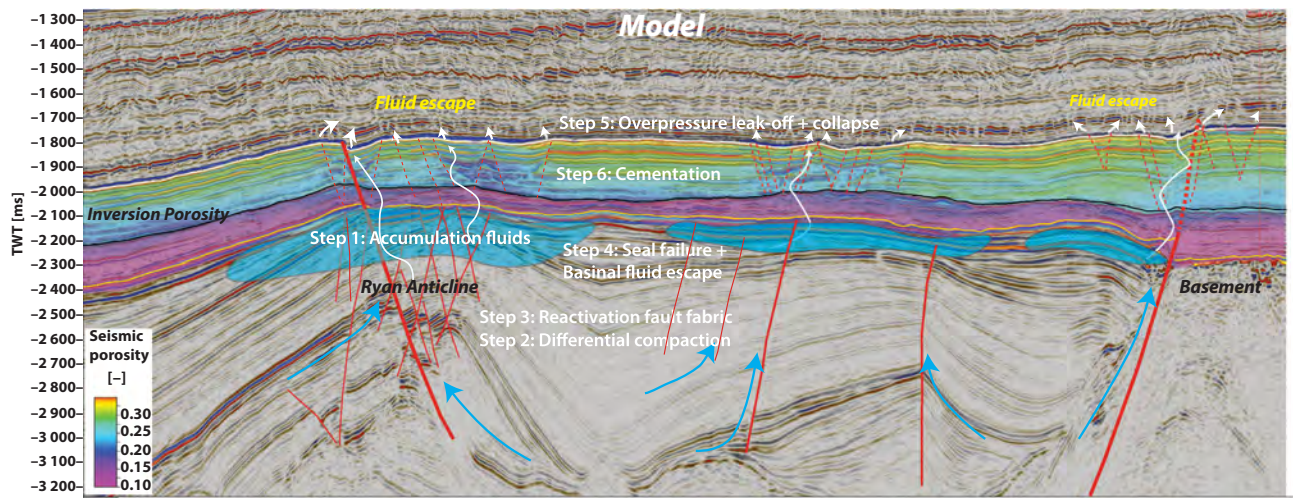


FIGURE 20 Proposed model for the formation of the SCR. Compaction and dehydration of Mesozoic marine shales led to fluid flow up towards the crest of the Ryan anticline (still observed as a low-velocity zone below the chalk, see Figure 18, Step 1). Low sedimentation rates at the crest of Ryan anticline likely led to early cementation in the chalk, forming an early intra-chalk seal. Ascending fluids would get trapped underneath the RPM, bringing in sulphates from the underlying evaporites as well as Mn/Mg fluids into Early Cretaceous and earliest Late Cretaceous strata. Differential compaction of the Mesozoic basin led to differential movement, fault reactivation and structural deformation of the chalk (Steps 2–4). The offset of the top seal likely compromised sealing capacity, making it possible to release some overpressure, leading to compaction (Step 5). At the same time, the trapped Mn/Mg-rich basinal fluids could now ascend into the high-porosity chalk along the weak zones thus formed, leading to precipitation of cement (calcite/dolomite) with high Mn/Sr ratios (Step 6). This chalk became denser than the surrounding high-porosity chalk, and therefore, the SCRs form the outer boundaries of this high-density chalk. The high density may reflect lower porosity due to compaction, a larger amount of contact cement, and might also reflect larger amounts of fracture filled calcite (as seen in outcrops in Flamborough Head, UK), dolomite and/or sulphates

and further offset the seal on top of the chalk (Figure 20, Step 5).

In this scenario, compaction would be followed by precipitation of very negative $\delta^{18}\text{O}$ pore-filling cement from ascending basinal fluids, rich in Mg/Mn minerals (e.g. extra-formational fluids) (c.f. Jensenius & Munksgaard, 1989; Egeberg & Saigal, 1991) (Figure 20, Step 6). The fluids ascended into the chalk following existing structural weaknesses and/or induced hydraulic fracturing (Sachau, Bons, & Gomez-Rivas, 2015; Figures 10 and 12). The strong correlation between the orientation of the faults and the SCRs (Figure 17) suggests that highly permeable zones were established where the N-S- and NW-SE-oriented faults crossed. Fault brecciation is common at these (Caine, Evans, & Forster, 1996).

The fluids spread laterally mainly at four stratigraphic levels which are associated with condensed sections/hiatitudes, and which possibly contain early cemented horizons: (i) below the Early Campanian Unconformity (ECU, Top Kraka Formation, CK-3); (ii) Top Campanian Unconformity (RPM, Top Gorm Formation, CK-5, Figure 12c); (iii) near the top of the Tor Formation (CK-6, Figure 12e); and (iv) at the top of the Ekofisk Formation (CK-7, Figure 12f). The fluids initiated precipitation of manganese-rich calcite cement (high Mn/Sr ratios) at the base of the

chalk and likely within the SCRs (inferred from Zone 3 and seismic anomaly, Figures 5 and 12), indicating large water:rock interaction (Figure 8b). The sulphates found at the fault plane, with Triassic-Permian sulphur signature, might also be sourced this way (Figure 13a).

5.3 | Analogues

The zigzagging geometry of the SCRs strikingly resembles geometries of seismic-scale dolostones formed by infiltration of Mg-rich fluids into limestone host rocks (Martín-Martín et al., 2015; Sharp et al., 2010). Migration of the Mg-rich fluids was largely controlled by faults, fractures and fissures, in addition to porous beds and stylolites, which together lead to a large-scale zigzagging geometry. The structural texture was controlled by tectonic stresses acting on the rocks and the pore fluid pressure (Bons, Elburg, & Gomez-Rivas, 2012). When fluid pressure increases, tensile stresses can become large enough for the rock to undergo brittle failure and form extensional fractures. These can provide both fluid pathways and space for crystallization of minerals. A similar pattern is recognized in the Ryan Anticline as Mg/Mn-rich fluids entered the Chalk Group, precipitating cements rich in those elements. Since the chalk generally has high purity,

then if the change in the porosity, the amount of minerals other than calcite, and/or contact cement is large enough, the resulting structures might be within seismic resolution, the pathways will be visible on 3D seismic data. The methodology and insights, however, are not limited only to chalk and can be used to understand fluid migration elsewhere.

5.4 | Concepts in the seismic chalk paradigm

There are three key processes that generate heterogeneity in chalk: (i) (re-)depositional processes (e.g. bottom currents and mass-waste deposits); (ii) tectonic deformation (e.g. fractures and faults); and (iii) diagenetic overprinting. Diagenesis is demonstrated here to have large impact on regional and local seismic patterns. This interpretation, therefore, adds an important concept to the seismic chalk paradigm, which until now was dominated by sedimentary and structural seismic heterogeneities. In order to distinguish between the different processes forming heterogeneity, it is key to use an integrated methodology as presented in our study.

The recognition of seismic-scale diagenesis in the Chalk Group has implications for hydrocarbon exploration, reservoir characterization and production. Similar features cross-cutting stratigraphy have been recognized in other parts of the basin that contain producing oil fields, for example, around diapirs (Skjold, Gorm, Nils), in the Roar Gas Field (c.f. Back et al., 2011; Esmerode et al., 2008), and in the German North Sea Sector (Arfai, Lutz, Franke, Gaedicke, & Kley, 2015). Investigating these SCRs with the same methodology will provide further insights into the fluid migration history and potential fault-bound diagenesis within the chalk, but with hydrocarbon emplacement as an additional complicating factor. Production at the Tyra (DK) Valhall, Elgin, and Ekofisk fields (NO) has already led to significant compaction of the reservoir and seafloor subsidence (metre to decametre scale), and this is expected to increase with further production (Keszthelyi et al., 2016). The Ryan Anticline SCRs could provide a natural analogue to these fields, but where reservoir compaction is a result of overpressure loss because of top seal failure.

Finally, the timing of the formation of the SCRs is crucial. If the fluid leak-off occurs after the main phase of hydrocarbon generation, the SCRs could represent breached reservoirs. At present, we are unable to determine this since, in the case of open-system diagenesis, fluid constraints are needed in order to arrive at a meaningful absolute precipitation temperature with the use of classical oxygen isotope palaeo-temperature functions (Craig, 1957). In order to circumvent this problem, future work will focus on clumped isotope palaeo-temperature measurements as described in Swart (2015).

6 | CONCLUSIONS

- By using a combination of geophysical, petrophysical, petrological and geochemical data presented in a 3D geological context, seismic-scale diagenesis in the Chalk Group has been recognized. The methodology and insights presented here can potentially be applied elsewhere and improve our general understanding of fluid migration, seal failure and diagenesis.
- The study focused on two specific types of seismic markers identified in the Chalk Group:
 1. A regionally continuous seismic marker, the Regional Porosity Marker (RPM), which represents a locally erosive, stratigraphic surface that separates high-porous chalks above from low-porous chalks below. It is dated as Top Campanian, represents a hiatus and condensation zone, shows early cementation and is interpreted to have formed as a result of erosion and/or nondeposition due to increased ocean bottom currents. This interval formed an important intra-chalk seal, trapping large amounts of ascending fluids until seal breach led to fluid escape into the overlying high-porous chalks.
 2. Local Stratigraphy Cross-cutting Reflectors (SCRs), which have a variety of expressions (V-, W- and 2-W-shapes) in 2D section, and develop a zigzagging geometry through the stratigraphy, delineate fault-bound high-density chalk geobodies nested inside high-porosity chalk. Their stratigraphic distribution is limited to the chalk above the RPM marker (i.e. the Tor and Ekofisk formations). The geographical distribution of the SCRs is closely related to the underlying fault fabric.
- The similarity between the geochemical character of the chalk beneath the RPM and within the SCR-delineated geobodies (increased Mn/Sr ratios), and the fact that the SCRs never cut through the RPM suggest that pore-filling cementation first occurred in low-porosity chalk below the RPM (characterized by a large amount of early cementation and some late cement), and later within the SCR-delineated chalk bodies (characterized by large amount of late cement). The chalk beneath the RPM would, thus, have formed an important seal where the Mesozoic fluids stagnated.
- SCR formation was likely initiated by differential subsidence of the Triassic/Jurassic sedimentary basin, leading to reactivation of the faults and their propagation up through the Chalk Group, followed by failure of seals throughout the Cretaceous and lower Palaeocene succession. This rupturing of pressure compartments resulted

in draining of overpressure followed by mechanical compaction and caused large fluxes of basinal fluids to pass through the Chalk Group.

- The width of the diagenetic geobodies delineated by the SCRs increases upward from the RPM (Top Gorm Formation), to the top of the Tor Formation and to the top of the Ekofisk Formation. This is interpreted to reflect the (temporary) sealing capacity of the Formation tops and associated cement precipitation.
- The concept of seismic-scale diagenesis, its implications for hitherto unrecognized heterogeneities, and its potential for fluid migration pathways may provide new insights for hydrocarbon exploration and production in the chalks of the North Sea Basin.

ACKNOWLEDGEMENTS

The authors kindly acknowledge the Danish Underground Consortium (Shell, Chevron, Maersk Oil and Nordsøfonden) for providing seismic and well data and the permission to publish the results. Frederic Armour and Solomon Seyum (DTU) are kindly thanked for technical discussions. Schlumberger is acknowledged for providing Petrel E&P and eXchroma^{SG} chromatic geology plug-in, Eliis for PaleoScanTM and fFA GeoTeriC for providing GeoTeriC software suits. Wolfgang Weinzierl (Schlumberger) is kindly thanked for sharing his extensive knowledge of Petrel. Ingelise Schmidt (Maersk Oil) is kindly thanked for providing access to the core facilities and the usage of the SEM. Reviewers Ida Fabricius, Thilo Wrona and Matteo Gennaro are kindly thanked for providing corrections and comments that helped to improve an earlier version of the manuscript. Edward Harris and Ellen Keerd are thanked for checking for spelling errors.

CONFLICT OF INTEREST

There is no conflict of interest for any of the authors.

ORCID

F. W. H. Smit  <http://orcid.org/0000-0001-8438-386X>

REFERENCES

- Archie, G. E. (1942). The electrical resistivity log as an aid in determining some reservoir characteristics. *Transactions of the AIME*, 146, 54–62. <https://doi.org/10.2118/942054-G>
- Arfai, J., Lutz, R., Franke, D., Gaedicke, C., & Kley, J. (2015). Mass-transport deposits and reservoir quality of upper cretaceous chalk within the German Central Graben, North Sea. *International Journal of Earth Sciences*, 105, 797–818.
- Back, S., Van Gent, H., Reuning, L., Grottsch, J., Niederau, J., & Kukla, P. (2011). 3d seismic geomorphology and sedimentology of the chalk group, Southern Danish North Sea. *Journal of the Geological Society, London*, 168, 393–405. <https://doi.org/10.1144/0016-76492010-047>
- Banner, J. L., & Hanson, G. N. (1990). Calculation of simultaneous isotopic and trace element variations during water-rock interaction with applications to carbonate diagnosis. *Geochimica et Cosmochimica Acta*, 54, 3123–3137. [https://doi.org/10.1016/0016-7037\(90\)90128-8](https://doi.org/10.1016/0016-7037(90)90128-8)
- Bons, P. D., Elburg, M. A., & Gomez-Rivas, E. (2012). A review of the formation of tectonic veins and their microstructures. *Journal of Structural Geology*, 43, 33–62. <https://doi.org/10.1016/j.jsg.2012.07.005>
- Boussaha, M., Thibault, N., & Stemmerik, L. (2016). Integrated stratigraphy of the late Campanian & – Maastrichtian in the Danish Basin: Revision of the Boreal Calcareous Nannofossil Zonation. *Newsletters on Stratigraphy*, 49, 337–360. <https://doi.org/10.1127/nos/2016/0075>
- Brewster, J., & Dangerfield, J. A. (1984). Chalk fields along the Lindessness Ridge, Eldfisk. *Marine and Petroleum Geology*, 1, 239–278. [https://doi.org/10.1016/0264-8172\(84\)90148-X](https://doi.org/10.1016/0264-8172(84)90148-X)
- van Buchem, F. S. P., Smit, F. W. H., Buijs, G. J. A., Trudgill, B., & Larsen, P. H. (2018). Tectonostratigraphic framework and depositional history of the cretaceous–Danian succession of the Danish Central Graben (North Sea) – New light on a mature area. In M. Bowman & B. Levell (Eds.), *Petroleum geology of NW Europe: 50 years of learning – Proceedings of the 8th Petroleum Geology Conference* (pp. 9–46). London, UK: Geological Society of London.
- Bulhões, E.M., & Nogueira de Amorim, W. (2005). Princípio de SismoCamada Elementar e sua aplicação à Técnica Volume de Amplitudes (TecVA). *Sociedade Brasileira de Geofísica, 9th International Congress of the Brazilian Geophysical Society*, 1382–1387.
- Caine, J. S., Evans, J. P., & Forster, C. B. (1996). Fault zone architecture and permeability structure. *Geology*, 24, 1025–1028. [https://doi.org/10.1130/0091-7613\(1996\)024<1025:FZAA>2.3.CO;2](https://doi.org/10.1130/0091-7613(1996)024<1025:FZAA>2.3.CO;2)
- Cartwright, J. (1989). The kinematics of inversion in the Danish Central Graben. *Geological Society, London, Special Publications*, 44, 153–175. <https://doi.org/10.1144/GSL.SP.1989.044.01.10>
- Cartwright, J. (2007). The impact of 3D seismic data on understanding compaction, fluid flow, and diagenesis in sedimentary basins. *Geological Society, London*, 164, 881–893. <https://doi.org/10.1144/0016-76492006-143>
- Cherret, A. J., Escobar, I., & Hansen, H. P. (2011). Fast deterministic geostatistical inversion. In *73rd EAGE Conference and Exhibition Incorporating SPE EUROPEC 2011*.
- Coward, M. P., Dewwey, J. R., Hempton, M., Holroyd, J., & Mange, M. A. (2003). Chapter 2: Tectonic evolution. In D. Evans, C. Graham, A. Armour, & P. Bathurst (Eds.), *The millennium Atlas: Petroleum geology of the Central and Northern North Sea* (Vol. 1, pp. 157–189). London, UK: The Geological Society of London.
- Craig, H. (1957). Isotopic standards for carbon and oxygen and correction factors for mass-spectrometric analysis of carbon dioxide. *Geochimica et Cosmochimica Acta*, 12, 133–149. [https://doi.org/10.1016/0016-7037\(57\)90024-8](https://doi.org/10.1016/0016-7037(57)90024-8)

- D'Heur, M. (1984). Porosity and hydrocarbon distribution in the North Sea Chalk reservoirs. *Marine and Petroleum Geology*, 1, 223–238.
- Egeberg, P. K., & Saigal, G. C. (1991). North Sea chalk diagenesis: Cementation of chalks and healing of fractures. *Chemical Geology*, 92, 339–354. [https://doi.org/10.1016/0009-2541\(91\)90078-6](https://doi.org/10.1016/0009-2541(91)90078-6)
- El Husseiny, A., & Vanorio, T. (2015). The effect of micrite content on the acoustic velocity of carbonate rocks. *Geophysics*, 80, L45–L55. <https://doi.org/10.1190/geo2014-0599.1>
- Esmerode, E. V., Lykke-Andersen, H., & Surlyk, F. (2007). Ridge and valley systems in the Upper Cretaceous chalk of the Danish Basin: Contourites in an epeiric sea. *Geological Society, London, Special Publications*, 276(1), 265–282. <https://doi.org/10.1144/GSL.SP.2007.276.01.13>
- Esmerode, E. V., Lykke-Andersen, H., & Surlyk, F. (2008). Interaction between Bottom currents and slope failure in the late cretaceous of the Southern Danish Central Graben, North Sea. *Journal of the Geological Society*, 165, 55–72. <https://doi.org/10.1144/0016-76492006-138>
- Fabricius, I. L. (2003). How burial diagenesis of chalk sediments controls sonic velocity and porosity. *AAPG Bulletin*, 87, 1755–1778. <https://doi.org/10.1306/06230301113>
- Fabricius, I. L. (2007). Chalk: Composition, diagenesis and physical properties. *Bulletin of the Geological Society of Denmark*, 55, 97–128.
- Fabricius, I. L. (2014). Burial stress and elastic strain of carbonate rocks. *Geophysical Prospecting*, 62, 1327–1336. <https://doi.org/10.1111/1365-2478.12184>
- Faj-Gomord, O., Soete, J., Katika, K., Galaup, S., Caline, B., Descamps, F., ... Vandycke, S. (2016). New insight into the microtexture of chalks from NMR analysis. *Marine and Petroleum Geology*, 75, 252–271. <https://doi.org/10.1016/j.marpetgeo.2016.04.019>
- Fraser, S. I., Robinson, A. M., Johnson, H. D., Underhill, J. R., Kadolsky, D. G. A., Connell, R., ... Ravnäs, R. (2002). Upper jurassic. In D. Evans, C. Graham, A. Armour, & P. Bathurst (Eds.), *The Millennium Atlas: Petroleum Geology of the Central and Northern North Sea* (Vol. 1, pp. 157–189). London, UK: The Geological Society of London.
- Fritsen, A., Bailey, H., Gallagher, L. T., Hampton, M. J., Krabbe, H., Jones, B., ... Riis, F. (1999). A joint chalk stratigraphic framework. In A. Fritsen, (Ed.), *Joint chalk research program topic V. Stavanger* (206 pp). Norway: Norwegian Petroleum Directorate.
- Gennaro, M. (2011). *3D seismic stratigraphy and reservoir characterization of the Chalk Group in the Norwegian Central Graben, North Sea*. PhD dissertation, University of Bergen, Norway.
- Gennaro, M., & Wonham, J. P. (2014). *Channel development in the chalk of the tor formation, North Sea* (pp. 551–586). Chichester, UK: John Wiley & Sons, Ltd. <https://doi.org/10.1002/9781118920435>
- Gennaro, M., Wonham, J. P., Sælen, G., Walgenwitz, F., Caline, B., & Fay-Gomord, O. (2013). Characterization of dense zones within the Danian chalks of the Ekofisk Field. *Norwegian North Sea, Petroleum Geoscience*, 19, 39–64. <https://doi.org/10.1144/petgeo2012-013>
- Glennie, K. W., Higham, J., & Stemmerik, L. (2003). Permian. In D. Evans, C. Graham, A. Armour, & P. Bathurst (Eds.), *The Millennium Atlas: Petroleum Geology of the Central and Northern North Sea* (pp. 91–103). London, UK: The Geological Society of London.
- Goldsmith, P. J., Hudson, G., & Van Veen, P. (2003). Triassic. In D. Evans, C. Graham, A. Armour, & P. Bathurst (Eds.), *The Millennium Atlas: Petroleum Geology of the Central and Northern North Sea* (Vol. 1, pp. 105–127). London, UK: The Geological Society of London.
- Gommessen, L., Fabricius, I. L., Mukerji, T., Mavko, G., & Pedersen, J. M. (2007). Elastic behaviour of North Sea chalk: A well-log study. *Geophysical Prospecting*, 55, 307–322. <https://doi.org/10.1111/j.1365-2478.2007.00622.x>
- Hancock, J. M. (1975). The petrology of the chalk. *Proceedings of the Geologists' Association*, 86, 499–535. [https://doi.org/10.1016/S0016-7878\(75\)80061-7](https://doi.org/10.1016/S0016-7878(75)80061-7)
- Harding, R., & Huuse, M. (2015). Salt on the move: Multi stage evolution of salt diapirs in the Netherlands North Sea. *Marine and Petroleum Geology*, 61, 39–55. <https://doi.org/10.1016/j.marpetgeo.2014.12.003>
- Ineson, J. R., Bojesen-Koefoed, J. A., Dybkjær, K., & Nielsen, L. H. (2003). Volghian-Ryazanian 'hot shales' of the Bo Member (Far-sund Formation) in the Danish Central Graben. *Geological Survey of Denmark and Greenland Bulletin*, 1, 403–436.
- Japsen, P. (1998). Regional velocity-depth anomalies, north sea chalk: A record of overpressure and neogene uplift and erosion. *AAPG Bulletin*, 82, 2031–2074.
- Japsen, P., Britze, P., & Andersen, C. (2003). Upper jurassic – Lower cretaceous of the Danish Central Graben: Structural framework and nomenclature. *Geological Survey of Denmark and Greenland Bulletin*, 1, 233–246.
- Japsen, P., Mavko, G., Gommessen, L., Fabricius, I. L., Jacobsen, F., Vejrbæk, O. V., ... Schjøtt, C. R. (2005). *Chalk background velocity: Influence of effective stress and texture*. 67th EAGE Conference & Exhibition, European Association of Geoscientists & Engineers Publications B.V. (EAGE).
- Jensenius, J., & Munksgaard, N. C. (1989). Large scale hot water migration systems around salt diapirs in the Danish Central trough and their impact on diagenesis of chalk reservoirs. *Geochimica et Cosmochimica Acta*, 53, 79–87. [https://doi.org/10.1016/0016-7037\(89\)90274-3](https://doi.org/10.1016/0016-7037(89)90274-3)
- Jung, C., Voigt, S., Friedrich, O., Koch, M. C., & Frank, M. (2013). Campanian-Maastrichtian ocean circulation in the tropical Pacific. *Paleoceanography*, 28, 562–573. <https://doi.org/10.1002/palo.20051>
- Karlo, J. F., van Buchem, F. S. P., Moen, J., & Milroy, K. (2014). Triassic-age salt tectonics of the Central North Sea. *Interpretation*, 2, SM19–SM28. <https://doi.org/10.1190/INT-2014-0032.1>
- Keszthelyi, D., Dysthe, D. K., & Jamtveit, B. (2016). Compaction of North-Sea chalk by pore-failure and pressure solution in a producing reservoir. *Frontiers in Physics*, 4, 4.
- Kyrkjebø, R., Gabrielsen, R., & Faleide, J. (2004). Unconformities related to the Jurassic-Cretaceous synrift-postrift transition of the northern North Sea. *Journal of the Geological Society*, 161, 1–17. <https://doi.org/10.1144/0016-764903-051>
- Laake, A. (2013). *Structural interpretation in color—A new Rgb processing technique for extracting geological structures from seismic data*. SEG Technical Program Expanded Abstracts 2013, Society of Exploration Geophysicists.
- Lieberkind, K., Bang, I., Mikkelsen, N., & Nygaard, E. (1982). Late cretaceous and Danian limestone. In O. Michelsen (Ed.), *Geology of the Danish Central Grben, Geological Survey of Denmark, Series B*, 8, 49–62.

- Lykke-Andersen, H., & Surlyk, F. (2004). The cretaceous-palaeogene boundary at Stevns Klint, Denmark: Inversion tectonics or sea-floor topography? *Journal of the Geological Society*, 161, 343–352. <https://doi.org/10.1144/0016-764903-021>
- Martín-Martín, J. D., Travé, A., Gomez-Rivas, E., Salas, R., Sizun, J.-P., Vergés, J., ... Alfonso, P. (2015). Fault-controlled and stratabound dolostones in the Late Aptian–earliest Albian Benassal Formation (Maestrat Basin, E Spain): petrology and geochemistry constrains. *Marine and Petroleum Geology*, 65, 83–102.
- Megson, J. B. (1992). The North Sea chalk play: Examples from the Danish Central Graben. *Geological Society, London, Special Publications*, 67, 247–282. <https://doi.org/10.1144/GSL.SP.1992.067.01.10>
- Michelsen, O., Nielsen, L. H., Johannesen, P. N., Andsbjerg, J., & Surlyk, F. (2003). Jurassic lithostratigraphy and stratigraphic development onshore and offshore Denmark. *Geological Survey of Denmark and Greenland Bulletin*, 1, 147–216.
- van der Molen, A. (2004). *Sedimentary development, seismic stratigraphy and burial compaction of the CHalk Group in the Netherlands*. PhD dissertation, Utrecht University.
- Møller, J. J., & Rasmussen, E. S. (2003). Middle Jurassic–Early Cretaceous rifting of the Danish Central Graben. The Jurassic of Denmark and Greenland. *Geological Survey of Denmark and Greenland Bulletin*, 1, 247–264.
- Molenaar, N., & Zijlstra, J. J. P. (1997). Differential early diagenetic low-Mg calcite cementation and rhythmic hardground development in Campanian – Maastrichtian chalk. *EAGE Sedimentary Geology*, 109, 261–281. [https://doi.org/10.1016/S0037-0738\(96\)00064-4](https://doi.org/10.1016/S0037-0738(96)00064-4)
- Morozov, P., Paton, G., Milyushkin, A. M., Kiselev, V. V., Llc, S., Myasoedov, D. N., & Llc, L. (2013). Application of high definition frequency decomposition techniques on Western Siberia reservoirs. *EAGE Tyumen*, 2013, 2013.
- Ogg, J. G., Ogg, G., & Gradstein, F. M. (2016). *A concise geological time scale*. Amsterdam: Elsevier.
- Partyka, G., Gridley, J., & Lopez, J. (1999). Interpretational applications of spectral decomposition in reservoir characterization. *The Leading Edge*, 18, 353–360. <https://doi.org/10.1190/1.1438295>
- Pauget, F., Lacaze, S., & Valding, T. (2009). *A global approach in seismic interpretation based on cost function minimization*, Society of Exploration Geophysicists.
- Pedersen, S. I., Randen, T., Sonneland, L., & Steen, Ø. (2003). Automatic fault extraction using artificial ants. In A. Iske, & T. Randen (Eds.), *Mathematical methods and modelling in hydrocarbon exploration and production* (pp. 107–116). Berlin, Germany: Springer Science & Business Media.
- Posamentier, H. W., Davies, R. J., Cartwright, J. A., & Wood, L. (2007). Seismic geomorphology – An overview. *Geological Society, London, Special Publications*, 277, 1–14. <https://doi.org/10.1144/GSL.SP.2007.277.01.01>
- Rasmussen, E. S. (2013). cenozoic structures in the eastern north sea basin – A case for salt tectonics: Discussion. *Tectonophysics*, 601, 226–233. <https://doi.org/10.1016/j.tecto.2012.10.038>
- Rasmussen, E. S., Dybkjær, K., & Piasecki, S. (2010). Lithostratigraphy of the upper Oligocene-Miocene succession of Denmark. *Geological Survey of Denmark and Greenland Bulletin*, 22, 92.
- Regnet, J. B., Robion, P., David, C., Fortin, J., Brigaud, B., & Yven, B. (2015). Acoustic and reservoir properties of microporous carbonate rocks: Implication of micrite particle size and morphology. *Journal of Geophysical Research: Solid Earth*, 120, 790–811.
- Sachau, T., Bons, P. D., & Gomez-Rivas, E. (2015). Transport efficiency and dynamics of hydraulic fracture networks. *Frontiers in Physics*, 3, 63.
- Schiøler, P., Andsbjerg, J., Clausen, O. R., Dam, G., Dybkjær, K., Hamberg, L., ... Rasmussen, J. A. (2007). Lithostratigraphy of the palaeogene – Lower neogene succession of the Danish North Sea. *Geological Survey of Denmark and Greenland Bulletin*, 12, 1–77.
- Scholle, P. A., & Halley, R. B. (1985). Burial diagenesis: Out of sight, out of mind!. In P. A. Scholle, N. P. James, & J. F. Read (Eds.), *Carbonate sedimentology and petrology* (Vol. 36, pp. 135–160). Washington, DC: American Geophysical Union.
- Sharp, I., Gillespie, P., Morsalnezhad, D., Taberner, C., Karpuz, R., Vergés, J., ... Hunt, D. (2010). Stratigraphic architecture and fracture-controlled dolomitization of the cretaceous Khamsi and Bangestan groups: An outcrop case study, Zagros Mountains, Iran. *Geological Society, London, Special Publications*, 329, 343–396. <https://doi.org/10.1144/SP329.14>
- Sheriff, R. E. (1980). Nomogram for Fresnel-zone calculation. *Geophysics*, 45, 968–972.
- Smit, F. W. H. (2014). *Seismic stratigraphy, basin evolution, and seismic geomorphology of the late cretaceous and earliest paleocene chalk group in the Danish Central Graben*. MSc thesis, Aarhus University.
- Smit, F. W. H., Van Buchem, F. S. P., Schmidt, I., & Stemmerik, L. (2017). Updated seismic geomorphological workflow applied to the Chalk Group. *Society of Exploration Geophysicists, SEG Technical Program Expanded Abstracts*, 2017, 1976–1981.
- Starmer, I. C. (1995). Deformation of the upper cretaceous chalk at Selwicks Bay, Flamborough Head, Yorkshire: Its significance in the structural evolution of North-East England and the North Sea Basin. *Proceedings of the Yorkshire Geological Society*, 50, 213–228. <https://doi.org/10.1144/pygs.50.3.213>
- Surlyk, F., Dons, T., Clausen, C. K., & Higham, J. (2003). Upper cretaceous. In D. Evans, C. Graham, A. Armour, & P. Bathurst (Eds.), *The Millennium Atlas: Petroleum Geology of the Central and Northern North Sea* (Vol. 1, pp. 213–233). London, UK: The Geological Society of London.
- Swart, P. K. (2015). The geochemistry of carbonate diagenesis: The past, present and future. *Sedimentology*, 62, 1233–1304. <https://doi.org/10.1111/sed.12205>
- Thibault, N., & Gardin, S. (2006). Maastrichtian calcareous nannofossil biostratigraphy and paleoecology in the Equatorial Atlantic (Demerara Rise, ODP Leg 207 Hole 1258A). *Revue de Micropaléontologie*, 49, 199–214. <https://doi.org/10.1016/j.revmic.2006.08.002>
- Vejbæk, O. V., & Andersen, C. (2002). Post mid-cretaceous inversion tectonics in the Danish Central Graben – Regionally synchronous tectonic events? *Bulletin of the Geological Society of Denmark*, 49, 139–144.
- Vejbæk, O. V., Frykman, P., Bech, N., & Nielsen, C. M. (2005). *The history of hydrocarbon filling of Danish chalk fields* (Vol. 12, pp.

1331–1345). London, UK: Geological Society of London.

Wagner, H. (2014). Tove acoustic inversion. *Maersk Oil in-house report GST QI Geophysics*.

SUPPORTING INFORMATION

Additional Supporting Information may be found online in the supporting information tab for this article.

How to cite this article: Smit FWH, van Buchem FSP, Holst JC, et al. Seismic geomorphology and origin of diagenetic geobodies in the Upper Cretaceous Chalk of the North Sea Basin (Danish Central Graben). *Basin Res.* 2018;00:1–31.

<https://doi.org/10.1111/bre.12285>

Chapter III, Paper 2;

Seismic expression of fluid and gas expulsion episodes in the Jurassic to Eocene of the Danish Central Graben

F.W.H. Smit^{1*}, L. Stemmerik², M. Lüthje¹, M. Hertle³, F.S.P. van Buchem^{3**}

Submission to Geological Society of London

1. Technical University of Denmark, Danish Hydrocarbon Research and Technology Centre, Elektrovej Building 375, 2800 Kongens Lyngby
2. University of Copenhagen, Natural History Museum of Denmark, Øster Voldgade 5-7, 1350 Copenhagen K
3. Total Denmark, Amerikaplads 29, 2100, Copenhagen

* Corresponding author: fsmitt@dtu.dk

** Now at Halliburton-Landmark, 97 Jubilee Avenue, Milton Park, Abingdon, OX14 4RW, UK.

Abstract

Direct fluid migration indicators in the Danish Central Graben from strata covering the latest Jurassic to Neogene reveal early, often overlooked, fluid expulsion events that contributed to syn-depositional processes that shaped the seafloor for more than 100 million years by creating (giant and mega) pockmarks and seep carbonates. Modelled vitrinite reflectance data show that these events predate thermal maturity of the most prolific source rock, the Bo Member of the Farsund Formation. The data rather suggests that gas-bearing fluids were sourced from biogenic degradation of Upper Jurassic organic mudstones, and from thermogenic expulsion from Lower Jurassic organic-rich mudstones, coal facies within Middle Jurassic strata, and organic-rich mudstones from the lower parts of the Farsund Formation. A fluid migration history can be distilled from the direct fluid migration indicators based on their spatial and stratigraphic occurrence. Large accumulations of gas likely resided within the Upper Jurassic strata, and only small amounts could seep along Late Jurassic normal faults, resulting in formation of small pockmarks, furrows, and seep carbonates in the Lower Cretaceous and pre-inversion chalk strata. Major tectonic inversion during the Campanian led to fault reactivation and uplift, causing rapid expansion of gas accumulation and rupturing of seals within the Late Jurassic to Early Cretaceous strata. This was followed by catastrophic fluid outbursts that left gigantic craters (mega pockmarks, 0.75-4 km across, 100-250 m deep) on the chalk seafloor, which subsequently became reworked by mass wasting and current scouring into U-shapes. The inverted faults formed important pathways for subsequent fluid migration into the Chalk Group as illustrated by smaller reactivation pockmarks within the mega pockmarks and within younger strata. The smaller dimensions likely indicate waning tectonic activity and diminishing outbursts. Giant pockmarks within the Danian Ekofisk Formation formed on top of the inverted structures, and were filled in with chinks, marls, and clays. Following burial of the Chalk Group by clays, syn-depositional polygonal faulting created a leaking seal, so that stable streams of methane could migrate towards the seafloor where they locally formed pockmarks and seep carbonates within the Paleogene and Neogene strata. This study thus provides a comprehensive overview of direct fluid expulsion indicators through time and space, as well as insights in fluid migration pathways.

Keywords: Pockmarks, fluid migration pathways, seismic geomorphology, seep carbonates, methanogenesis

Introduction

The timing of fluid migration and reservoir charge is an important element of play fairway analysis, yet, often obtained rather indirectly through basin modelling. Direct fluid expulsion indicators, such as pagoda structures, pockmarks, furrows, and gas chimneys, represent events where spontaneous leakage or venting of excess fluid pressure occurs for a limited amount of time (Strozyk *et al.*, 2018). In addition, the occurrence of seep carbonates often indicates venting of a steady stream of methane towards the seafloor, as they form by oxidation of methane by sulphate reducing bacteria (Teichert *et al.*, 2005). They can be sourced from either biogenic gas (Judd and Hovland, 2007), or thermogenic hydrocarbons from maturing source rocks (Andresen *et al.*, 2008; Heggland, 1997). Having overview over such features in space and time in a petroleum basin provides very valuable control points for assessing both maturation of source rocks, fluid pathways, potential seals, and reservoirs.

Pockmarks form a specific group of direct fluid expulsion indicators, and most knowledge about their architecture and formation mechanisms comes from present-day seafloor observations using a combination of sonar, UAV's, shallow geophysical methods, and shallow cores (Betzler *et al.*, 2011; Hovland and Judd, 1988; Judd and Hovland, 2007). They can be grouped into small/medium pockmarks (1-10's meters across, 1-10's meters deep), large/giant pockmarks (100-100's meters across, 10's of meters deep), and mega pockmarks (1-4 km's across, 50-100's meters deep) (Andresen *et al.*, 2008; Betzler *et al.*, 2011; Cole *et al.*, 2000; Sun *et al.*, 2011). The initial architecture is V-W shaped with steep walls (angle of repose) but subsequent reworking by mass-movements and bottom currents generally create wider U-shape depressions (Betzler *et al.*, 2011). In addition, reactivation pockmarks are common contributing to continuous re-shaping.

In this study we present seismic examples of fluid expulsion events within the Upper Jurassic to

Eocene strata in the Danish Central Graben. The focus is on the hydrocarbon-bearing Upper Cretaceous to Paleocene Chalk Group where most of the features occur, including km-scale U-shape reflectors. In a recent study Smit *et al.*, (2018) investigated V-W-shaped reflectors in the southern Danish Central Graben, and concluded a post-depositional diagenetic origin based on integration of seismic geomorphology with petrography and geochemistry. We will show how the features described in this paper differ from those, and reflect seismic expressions of syn-depositional fluid expulsion episodes during basin history. By studying the features within the detailed tectonostratigraphic framework established by van Buchem *et al.* (2018), we are able to propose correlation between Campanian inversion and formation of large U-shape reflectors within the Chalk Group.

The aim of this paper is to provide a spatial and stratigraphic overview of fluid expulsion events that influenced seafloor deposition from Late Jurassic to Eocene times, evaluate possible sources of (gas-bearing) fluids, and to link it the tectonic evolution of the basin. The younger, post-Paleocene fluid expulsion history has been described in detail by Andresen *et al.* (2008), and is only briefly touched upon in this paper. However, we will show that the HC in present accumulations migrated along long-lived pathways from source to reservoir, which were already present during earlier phases of gas venting to the seafloor.

Geological setting

The study area of the inverted Roar Basin is located in the central section of the Danish Central Graben between the Bo-Valdemar Ridge and the Adda Ridge (Figs 1b-c). The structure is a great example of Campanian inversion as the previous basin became uplifted several 100s of meters to form a basinal high (Fig. 1c and d). This was achieved by initial fault reactivation followed by bulk uplift (van Buchem *et al.*, 2018).

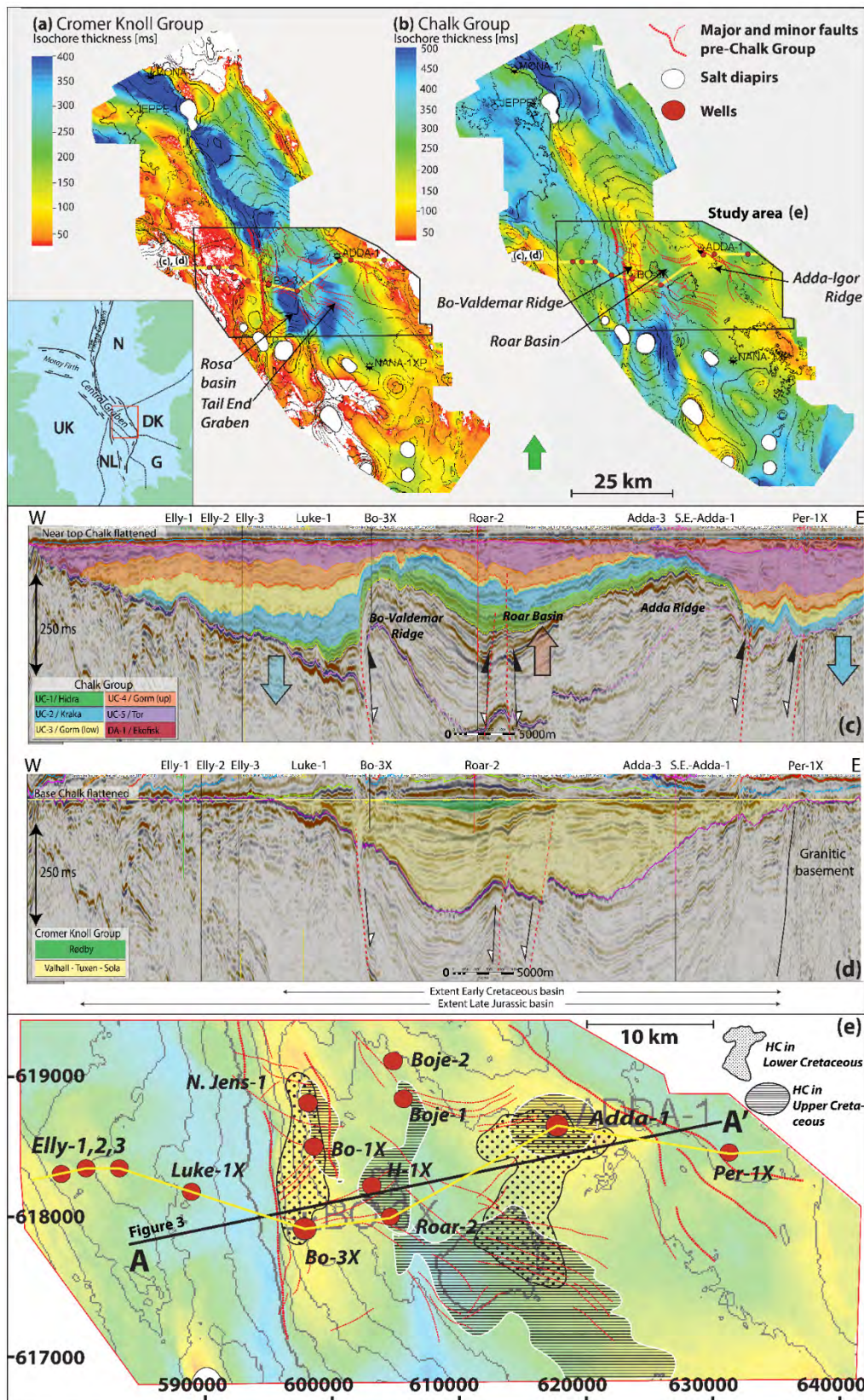


Figure 1 (a) and (b) Cromer Knoll Group isochore (Lower Cretaceous) and Chalk Group isochore (Late Cretaceous – Paleocene) and its location within the North Sea Basin (inset) where **UK** = United Kingdom; **NL** = Netherlands; **G** = Germany; **DK** = Denmark; **N** = Norway. Note the switching of depocenters between Lower and Upper Cretaceous strata, as a result of high eustatic sealevels and tectonic inversion. The impact of tectonic inversion is illustrated in (c) and (d) whereby former basins became basinal highs and vice versa. (e) Close-up of the study area showing major fault systems in the pre-chalk strata. Relevant wells are displayed as well as orientation of seismic transects. Hydrocarbons in Lower Cretaceous chinks as black outlines with dots, in Upper Cretaceous chinks as white outlines with stripes. (a-d) from van Buchem *et al.* 2018

Tectonostratigraphic evolution

The Danish Central Graben forms the southernmost branch of the North Sea Central Graben (Fig. 1a, inset). It comprises a complex set of half-grabens bounded to the south and east by the Ringkøbing-Fyn High, and to the west by the Mid North Sea High. The half-grabens formed during two major tectonic rifting phases, (Japsen *et al.* 2003; Fig. 2 for an overview of lithostratigraphic units and major tectonic events). During the first rifting phase in the Permian-Triassic, an E–W oriented stress regime led to N–S oriented half-grabens (Glennie *et al.*, 2003; Goldsmith *et al.*, 2003), whereas Late Jurassic a second rifting phase occurred in a NE–SW oriented stress regime, lead to generally NW–SE oriented half-grabens (Fraser *et al.*, 2002). Substantial creation of accommodation space combined with high sedimentation rates led to deposition of thick Upper Jurassic siliciclastic successions (up to 4 km thick) below the Chalk Group.

The Base Cretaceous Unconformity (BCU) is a basin-wide diachronous surface that marks the end of active rifting and start of thermal subsidence, which prevailed throughout most of the Cretaceous period (Kyrkjebø *et al.*, 2004; Vidalie *et al.*, 2014). It was interrupted by a distinct compressional phase in the Late Cretaceous, beginning with early inversion during Coniacian times, and reaching a climax during the early Campanian. This resulted in reactivation and movements along older faults and facilitated a major re-arrangement of depocenters and sediment remobilization along newly formed highs (Cartwright, 1989; Smit, 2014; Van Buchem *et al.*, 2018; Vejrbæk and Andersen, 2002). From the late Campanian thermal subsidence prevailed, and chalk sedimentation continued into the Maastrichtian within the new basin configuration, only influenced locally by tectonic activity associated with halokinesis, and some smaller inversion movements (Vejrbæk and Andersen, 2002)

Chalk deposition came to an end in the mid-Danian and was replaced by marine shale deposition, which continued until Mid-Miocene times. These

Paleogene – Neogene strata are heavily affected by polygonal features throughout, which are likely created by a combination of soft sediment deformation, density inversion, and syneresis, making their sealing capacity uncertain (Cartwright *et al.*, 2003; Lonergan *et al.*, 1998). Rapid sediment loading of the basin started during the Late Miocene and initiated fault reactivation due to differential compaction and halokinesis, thereby facilitating expulsion of methane to the seafloor that caused pockmark formation (Andresen *et al.*, 2008).

Stratigraphy

Open-marine mudstones of the Lower Jurassic Fjerritslev Formation are separated by a hiatus from paralic and non-marine sandstones, siltstones, mudstones and coal of the Middle Jurassic Bryne Formation (Fig. 2) (Møller and Rasmussen, 2003). The coal seams form important source rocks for the hydrocarbon accumulations in the Lulita oil field and Harald gas field north of the Roar Basin (Petersen *et al.*, 2000). The lack of well data from this interval in the study area prevents firm identification of the coals but the occurrences of bright reflectors and gas chimneys just below the base Callovian reflector are believed to reflect their presence (Fehmers *et al.*, 2012) (Fig. 3).

The Upper Jurassic syn-rift strata comprise open-marine mudstones and siltstones of the Lola Formation (Oxfordian – Kimmeridgian) and Farsund Formation (Kimmeridgian – Volghian) (Møller and Rasmussen, 2003). The organic-rich facies of the Farsund Formation (including the Bo Member) form important source rocks for present-day hydrocarbon accumulations (Ineson *et al.*, 2003).

The Lower Cretaceous post-rift strata comprise grey calcareous claystones of the Valhall Formation (Hauterivian – Barremian), hydrocarbon bearing chalk of the Tuxen Formation (Barremian – Aptian), marls of the Sola Formation (Aptian – Albian), and marls and marly chinks of the Rødby Formation (van Buchem *et al.* 2018). Two black organic-rich shales occur within these strata, the Munk Marl member of the Valhall Formation, and the Fischschiefer Member of the Sola Formation.

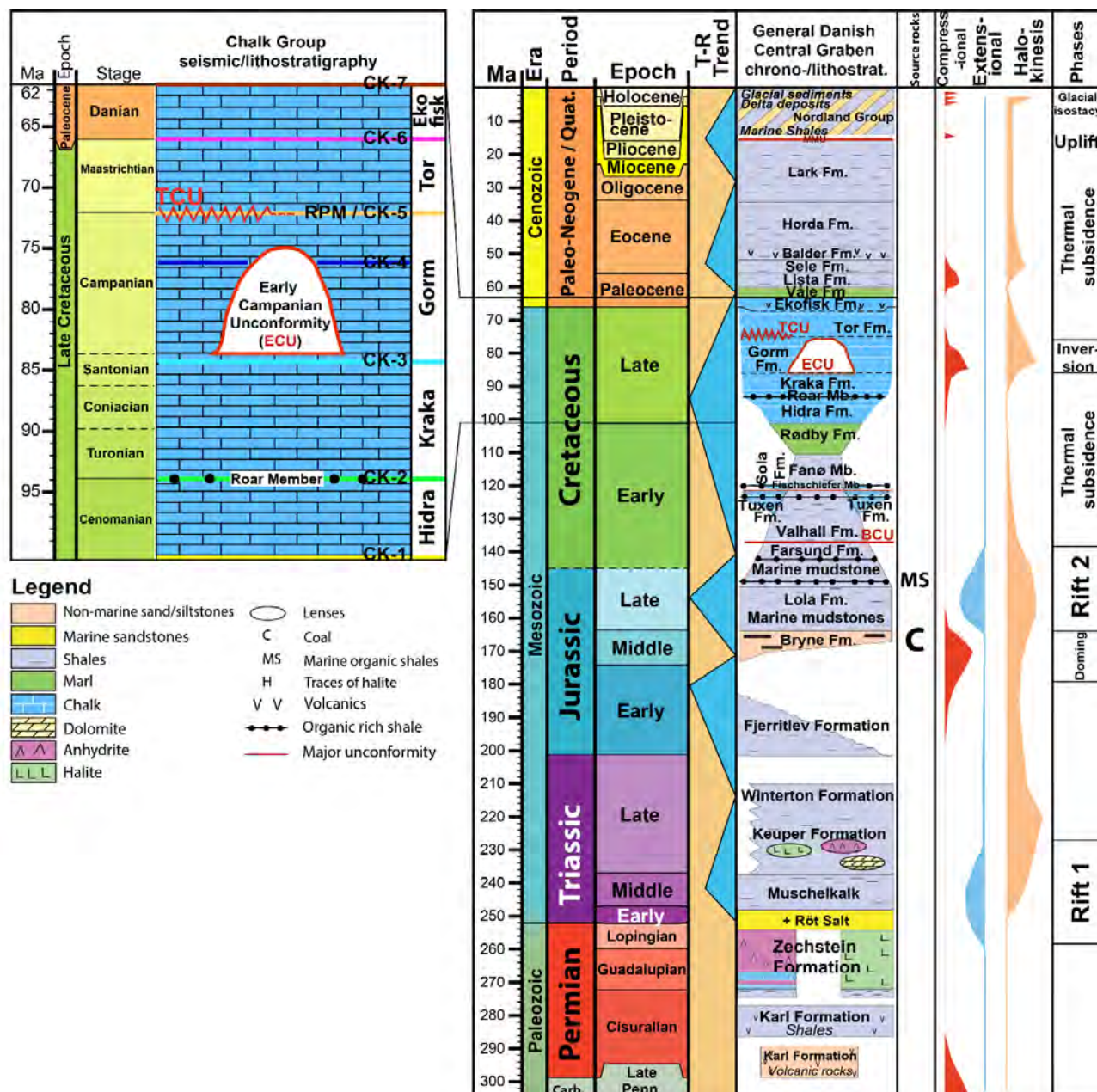


Figure 2. Chrono-/lithostratigraphic subdivision of the Danish North Sea. Stratigraphic units and tectono-sedimentary phases based on a literature synthesis. Coward *et al.* (2003) for Permian – Middle Jurassic, Rasmussen and Møller (2003) for the Middle Jurassic – Lower Cretaceous, Michelsen *et al.* (2003) for Jurassic, Japsen *et al.* (2003) for Late Jurassic and Lower Cretaceous, Ineson *et al.* (2003) for Late Jurassic, and Van Buchem *et al.* (2018) for the Lower and Upper Cretaceous, Schiøler *et al.* 2008 for Early Cenozoic, and Rasmussen *et al.* (2010) for Late Cenozoic. Tectonic phases are simplified and serve as broad tectonic framework for this study. Time scale generated with Geological Time Scale Creator, conform Ogg *et al.* (2016).

Chalk is a biogenic limestone composed of mainly coccoliths with minor additions of foraminifera and spiculites (Hancock, 1975), and forms the main hydrocarbon reservoir in the Danish North Sea. The stratigraphic nomenclature for the Chalk Group follows the tectono-stratigraphic framework of van Buchem *et al.* (2018), which

separates pre-inversion formations from post-inversion formations based on the occurrence of a 5-10 Myr hiatus (Early Campanian Unconformity, ECU, see Fig. 11 in van Buchem *et al.*, 2018). Pre-inversion strata consist of white to light-grey chalk of the Hydra (Cenomanian) and Kraka (Turonian – Santonian) Formations. The Kraka Formation is

hydrocarbon bearing at the Adda Ridge (Figs 1 and 3). The syn-inversion strata of the Gorm Formation (Campanian) show a distinctly different depocenter distribution and frequent occurrence of slumped deposits illustrating the impact of the basin inversion (van Buchem *et al.*, 2018). The post-inversion strata comprise the hydrocarbon-bearing Tor (Maastrichtian) and Ekofisk (Danian) Formations.

The Chalk Group is overlain by Upper Paleocene marlstones of the Våle Formation and hemipelagic mudstones of the Lista Formation (Schiøler *et al.*, 2008). The Eocene strata comprise restricted marine mudstones of the Sele Formation, mudstones with volcanic tuffs of the Balder Formation, and open-marine mudstones of the Hordaland Formation. The Upper Eocene – Middle Miocene mudstones of the Lark Formation were deposited in a neritic ocean setting. All strata between the top of the Chalk Group and the Lark Formation are heavily polygonal faulted and several possible (syn-depositional) formation mechanisms have been proposed (Cartwright *et al.*, 2003).

Source rocks

The commercial hydrocarbon accumulations within the Lower and Upper Cretaceous discoveries are mainly thermogenic in origin, and sourced from organic-rich facies of the Farsund Formation, with the ‘hot’ shales of the Bo Member being the most prolific (Ineson *et al.*, 2003; van Buchem *et al.*, 2018). Basin modelling indicates that oil was expelled from this source rock as early as the Late Eocene (Kubala *et al.*, 2003). Andresen *et al.* (2008) showed that pockmarks in the Oligocene – Upper Miocene section are located above gas-mature Jurassic source rocks, and concluded they have a thermogenic origin, and rapid loading of the basin during the Late Miocene caused reactivation of faults and bleeding of gas through the polygonal faulted shales (Rasmussen *et al.*, 2005). This event of hydrocarbon migration evidently post-dates deposition of the pre-Eocene succession forming the topic of this study, and fluid expulsion indicators recognized in this older part of the succession thus record earlier, hitherto unrecognized expulsion events, which possibly influenced reservoir architecture and kept porosities high during initial burial.

Organic-rich rocks that could have entered the hydrocarbon window prior to the Cretaceous include Middle Jurassic coals in the Bryne Formation which are shown to be oil and gas prone in the northern Lulita and Harald fields (Petersen *et al.*, 2000), and possibly supplied gas to the adjacent Tyra Field (Fehmers *et al.*, 2012). At even deeper stratigraphic levels, Carboniferous coals form an important source rock in the southern Permian Basin and are documented to have source potential on the Mid North Sea High (Petersen and Nytoft, 2007). This stratigraphic level is however eroded away over large areas of the Danish Central Graben or deeply buried, beyond seismic penetration depth, and therefore not considered any further.

Data and methods

Seismic data and interpretation techniques

A 1500 km² sub-crop of a recently re-processed regional seismic data set (pre-stack depth migrated) was used (Fig. 1e). The quality of the data is in general very good within the Late Jurassic basin, but deteriorates towards the margins (basement) and at salt influenced zones (Fig. 3). The polarity follows North Sea convention, with a downward increase in acoustic impedance reflected by a trough (red, white). The dominant frequency in the Chalk Group is approximately 30 Hz, average acoustic velocity is around 3400 m/s, leading to an average vertical resolution of 28.3 m as a quarter of the wavelength of the dominant frequency (Sheriff, 1980).

A neural network methodology has been applied for seismic interpretation (PaleoScan™, c.f. Pauget *et al.*, 2009) in order to create, in a time-efficient manner, the large number of stratigraphy consistent horizon slice needed to investigate the evolution of the Upper Jurassic – Eocene seafloor in detail. To increase the information extracted from the stratal horizons, spectral decomposition data revealed information in the frequency domain. Based on a dominant frequency of 30 Hz, three spectral frequency cubes (20, 30, 40 Hz) were calculated using a matching pursue algorithm in GeoTeric 2016.2 (c.f. Morozov *et al.*, 2013).

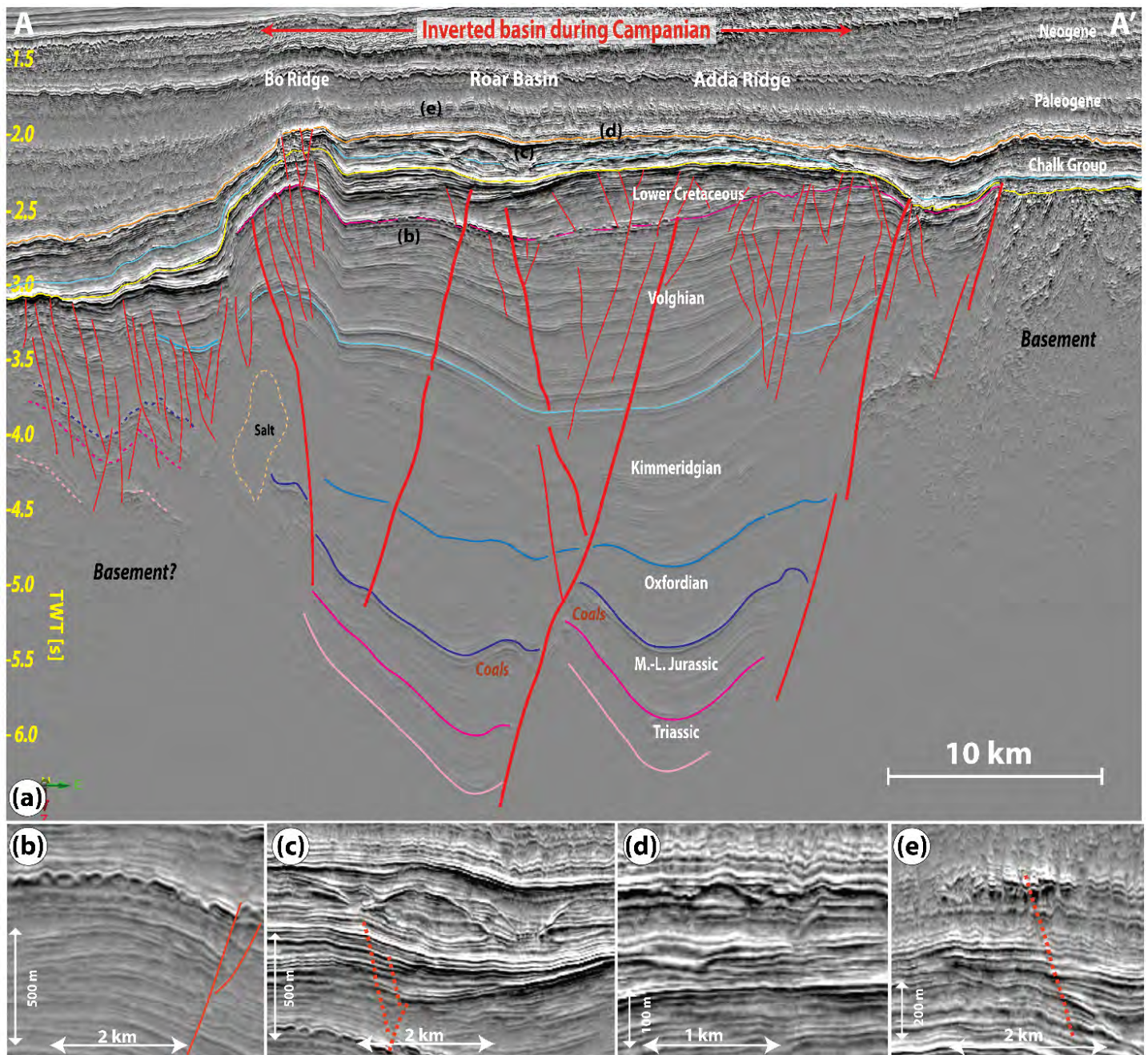


Figure 3 (a) Seismic line A-A' through the southern Roar Basin (see Fig. 1e for location) with TecVa attribute (c.f. Bulhões and Amorim, 2005). The section shows an inverted Late Jurassic to earliest Late Cretaceous basin as a pop-up structure, with deeply rooted faults into Middle to Late Jurassic strata. The inversion movement took mainly part during the Campanian (van Buchem *et al.* 2018), and the structure might have been altered by later halokinesis and differential compaction. Inline 8420. (b) 'Doubling' of the BCU reflector (c) Large U-shaped reflectors within the Chalk Group. (d) Disturbances of the stratigraphy near the top of the Chalk Group. (e) Hard beds within the overlying Paleogene clays of the Lista Formation.

Well data

Wireline logs are available from 10 vertical wells in the study area and have been used to integrate petrophysical information to seismic horizons (Fig. 1e). Drill cutting material was used for geochemical analysis in H-1X, Roar-2, Boje-1/2A, Per-1X in order to recognize possible seep carbonates within the strata. For H-1X, carbonates were manually picked from the clay material, while in all other wells the seep carbonates occur within chalk and could not be separated. This inherently results in dampening of the signal from these wells due to mixing of seep carbonates with highly negative $\delta^{13}\text{C}$ values ($<-20\text{‰}$) with chalk having positive $\delta^{13}\text{C}$ values. Carbonates were analysed for stable isotopes of carbon and oxygen at Iso-Analytical (UK) using continuous flow isotope ratio mass spectrometry (CF-IRMS). Values are reported as $\delta^{13}\text{C}$ and $\delta^{18}\text{O}$, deviations in parts per thousand relative to the V-PDB and V-SMOW standard. Analyses were performed on every drill cutting sample from the entire Chalk Group, giving a resolution of 3 m. Standard deviations are reported to be better than 0.08‰ for $\delta^{13}\text{C}$ and 0.02‰ for $\delta^{18}\text{O}$.

Basin modelling

This study investigates direct fluid migration indicators, and in order to link the features to source rock maturity, we utilize spatially modelled vitrinite reflectance data through geological time. This data is constrained by the extrapolation of the occurrences and thickness of the source rock from well data, present-day vitrinite reflectance measurements, the thermal history, and burial history of the basin based on back-stripping. Three different source rock intervals are considered: 1) Middle Jurassic Bryne Formation, coals; 2) lower organic-rich facies of the Late Jurassic Farsund Formation; 3) Bo Member of the Farsund Formation (e.g. ‘hot shale’ c.f. Ineson *et al.*, 2003). In addition, to evaluate the likelihood of biogenic gas expulsion, paleo-temperature maps at BCU level are provided. Biodegradation of organic matter, forming biogenic methane, peaks at 40°C and ceases at temperatures higher than 65/70°C (c.f. Schneider *et al.*, 2016).

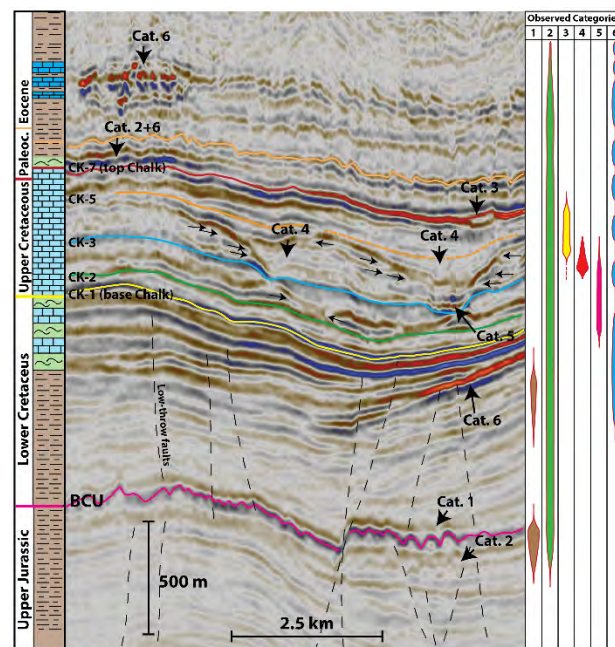


Figure 4. Overview features within stratigraphy. Column on the right indicating dominance of features. The ellipses in Category 6 indicate isolated events within the stratigraphy, whereas a continuous bulb shape indicate continuous occurrence.

Seismic morphologies in the Upper Jurassic to Eocene succession – description and distribution

Seismic geomorphological features with a large range of dimensions and architecture have been observed in the Roar-Tyra study area (Fig. 1e). They are assigned to six categories based on size and other geomorphological characteristic as summarized in Table 1. The stratigraphic and spatial distribution of the six types of geomorphological features have been mapped based on analyses of stratigraphic horizon slices from the BCU to the Eocene and recognition of the features in 2D section. A summary of their stratigraphic distribution is provided in Fig. 4.

Category 1 features

Category 1 features define a hill and valley morphology of 0.1-2.5 km long slightly sinuous, elongated pairs of hills and valleys (Fig. 5a). The hills correspond to a peak, trough, and peak triplet, and are rounded (20-40 m), rectangular (40-600 m), or have a composite shape (Fig. 5b-d). The valleys comprise 1 or 2 peaks, their 2D geometry is U, V, or

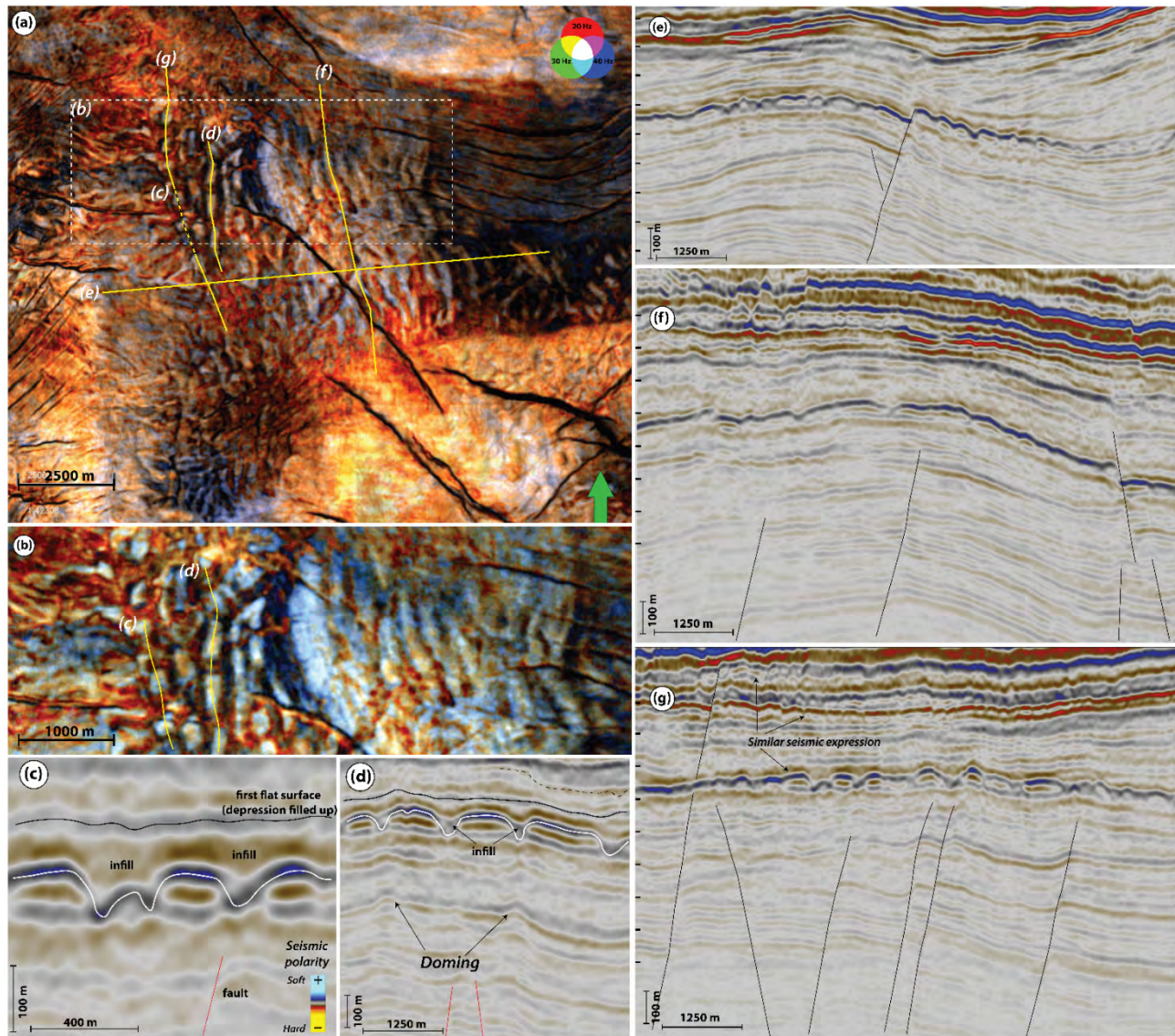


Figure 5. Category 1 features, in mapview and 2D seismic section. The vertical exaggeration is three times the horizontal, in all following seismic sections. **(a)** 2D mapview of seismic horizon at Base Cretaceous Unconformity with spectral decomposition RGB blend (20, 30, 40 Hz). The surface shows continuous to discontinuous hill and valley morphology, which can have elongated (0.4 – 5.0 km by 0.1-0.4 km), rectangular (200-400 m by 100 m), rounded (diameter 20-40 m), and composite shapes (50 – 300 m). The hills show dominantly high-frequency content (blue color), while the valleys are dominated by low frequency (red color). **(b)** Close-up of (a), to highlight the different shapes and dimensions of category 1. 2D sections (c-d) are also highlighted in yellow. **(c)** Tangential seismic section (subsection of g) through discontinuous rounded hills and valleys, which shows a topography of some 100 m from hill to valley bottom (white line). Slopes are between 5 – 20 degrees to the horizontal. Hills show a triplet (peak, trough, and peak), while the valley shows only a peak. The valleys are U, V, or W-shaped, and the isopach reflector shows they are buried early (black line). **(d)** Tangential section through rectangular hills. Valleys are mainly V-shaped and depth to bottom is 50-100 m. Depressions become isopach at same level as (c) (black line). Below the valleys, some doming can be observed. **(e)** Seismic section normal to the hill and valley shapes. Dimensions of the hills vary over the section, between 100 – 750 m, while valleys are between 20- 50 m deep. **(f)** Tangential line over more continuous hills (up to 1250 m). **(g)** Tangential section through mainly rounded hills. Note in all sections the occurrences of fault systems underneath the valleys.

W-shaped with slopes between 5-20°, and they are round to highly elongate in map view. The depth from top of the hill to valley floor is between 30-100 m (Fig. 5e, f). The valleys are often underlain by faults (Fig. 5d), and occasionally the reflectors below

bend upwards (e.g. doming in Fig 5f). The immediately overlying younger strata are thicker within the valleys, and the topography is buried within 1-2 reflectors (Fig 5c shows a good example).

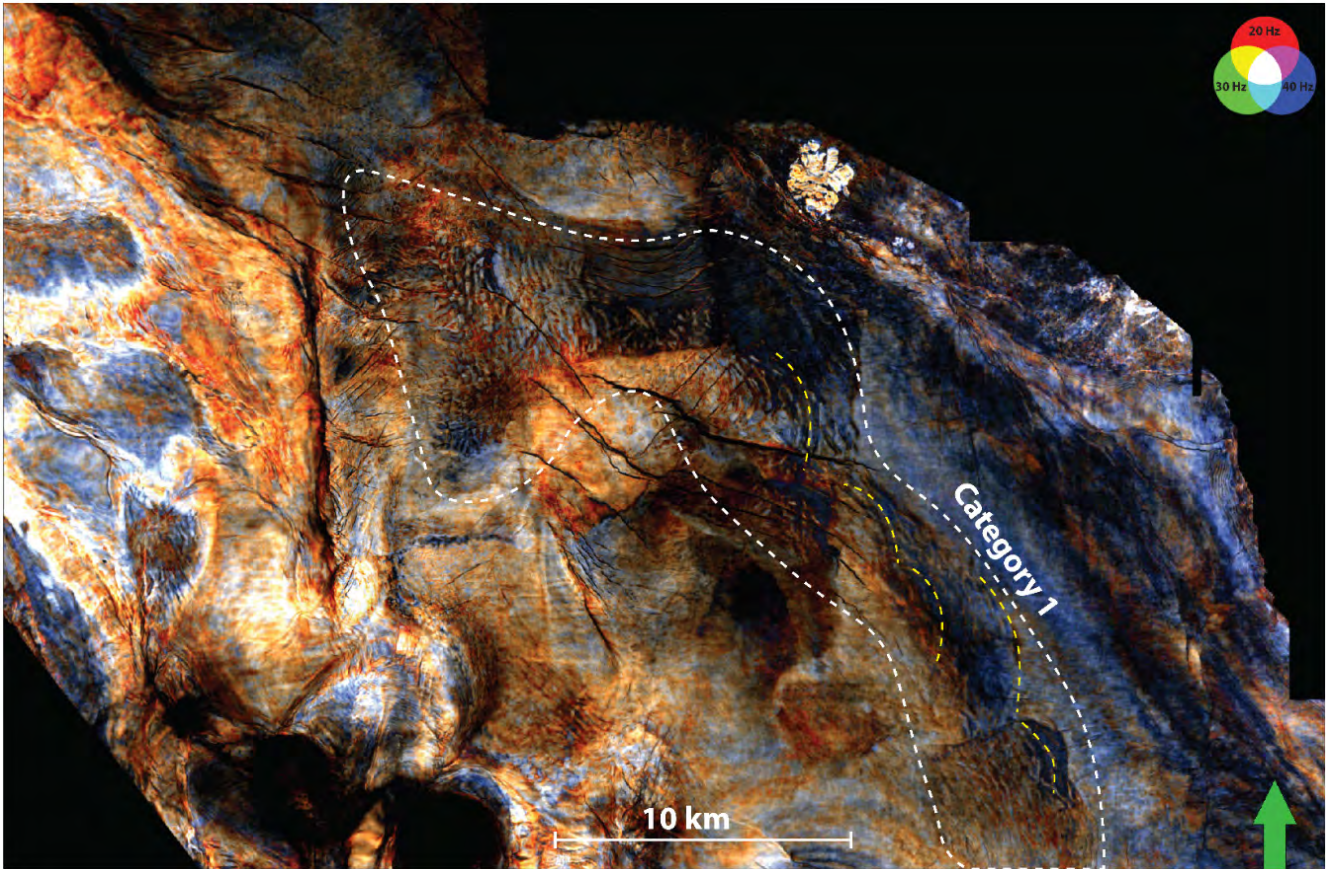


Figure 6. Category 1 spatial distribution. BCU stratigraphic horizon with spectral decomposition RGB blend (20, 30, 40 Hz). The features are recognized within the white dashed zone, and resemble hill and valley morphology. Cusate shapes can be recognized (dashed yellow lines).

Category 1 features are the best expressed at the Base Cretaceous Unconformity (BCU), where they are easily recognized as reflector ‘doubling’, showing typically hill and valley morphology (Fig 4). They are mainly occurring in the Upper Jurassic to lowermost Cretaceous strata beneath the BCU, but similar seismic expressions are also seen in middle and uppermost Lower Cretaceous strata (see Fig. 5g)

Features belonging to this category are spatially constrained to the Early Cretaceous basin (see horizon slice and isochore in Figs 6, 7a and b). Cusate shapes are common in the southern parts, whereas in the north more elongated and isolated hills occur. Due to post-depositional tectonic inversion and differential compaction, the basin morphology has changed significantly, and in order to investigate the spatial distribution of the Category 1 features in the corresponding Late Jurassic to Early Cretaceous basin morphology (Fig. 7c-e), flattening

on CK-2 (a maximum flooding surface) is applied. The flattened sections show that they developed both on sloping basin floor, along the basin margins and on basinal highs.

Category 2 features

Category 2 features comprise small/medium circular to slightly elliptical depressions, 10-200 m in diameter (10 m is close to seismic detectability) and 10-40 m deep (Fig. 8). In cross-section, they are V- and U-shaped with slopes typically between 3-10° (Fig. 8b, c). The surface does not cause a seismic reflector, but rather lowers the amplitudes of the reflectors, thereby creating the V- and U-shape depressions. The overlying strata are thicker within the centre of the depressions, and seem to wedge out towards the sides (Fig. 8c). Within one overburden reflector the packages become isopach, showing that the depression was filled at that time.

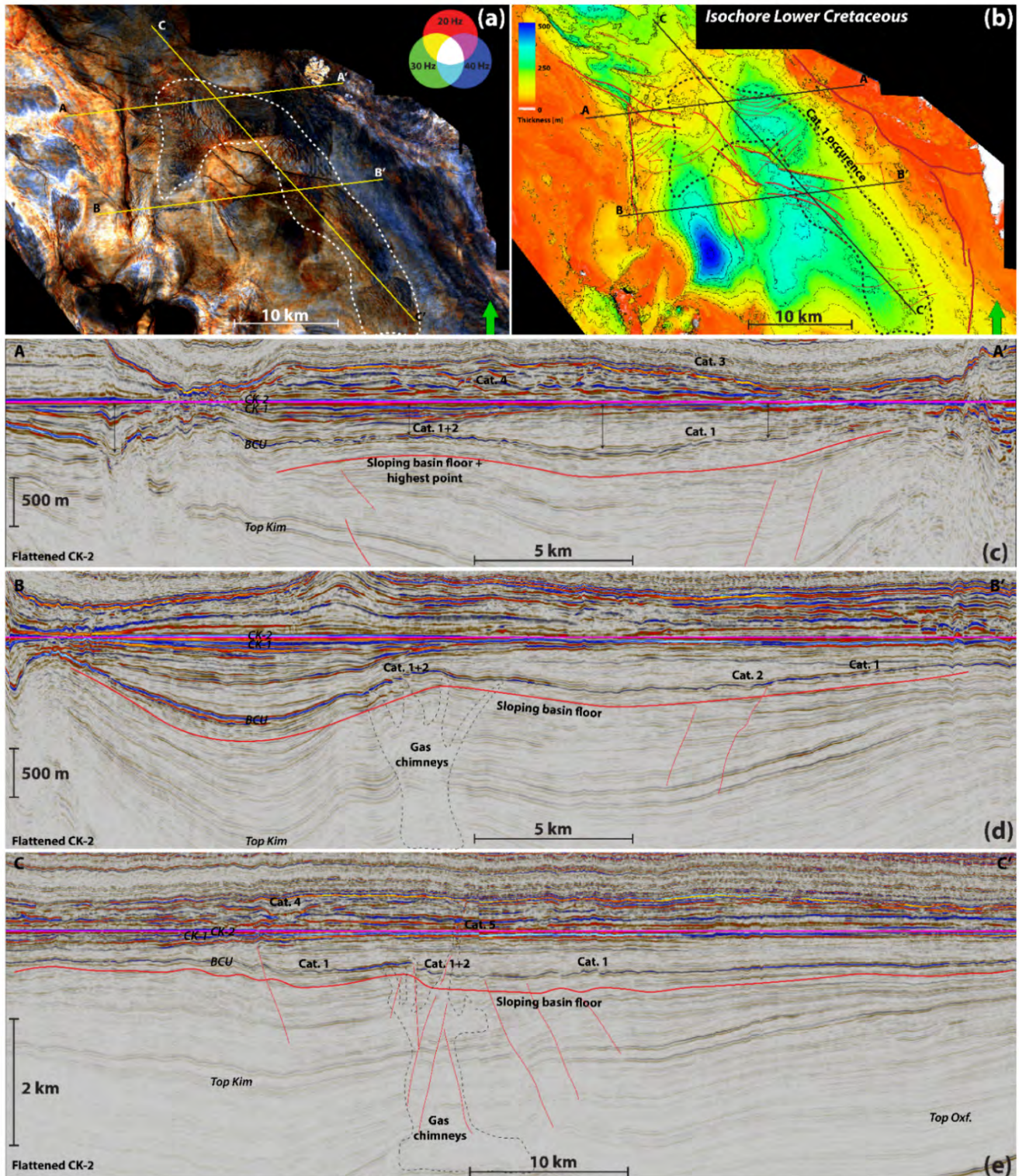


Figure 7. Category 1 spatial distribution. (a) BCU stratigraphic horizon with spectral decomposition RGB blend (20, 30, 40 Hz). The features are recognized within the white dashed zone. Seismic sections indicated as yellow lines. (b) Lower Cretaceous isochore with zone of Category 1 features, reflecting the basin morphology (c.f. van Buchem *et al.* 2018). Interpreted faults are indicated with red lines. Occurrence of Cat. 1 features along flank of the basin, as well as basinal high, which can also be seen in flattened seismic cross-sections A-A' (c), B-B' (d), and tangential C-C' (e). These sections show that basin morphology (sloping seafloor) controlled position of Cat. 1 features. Category 2 features can also be observed where faults are underlying category 1 features, as well as low signal to noise zones interpreted as gas chimneys (c.f. Fehmers *et al.* 2012)

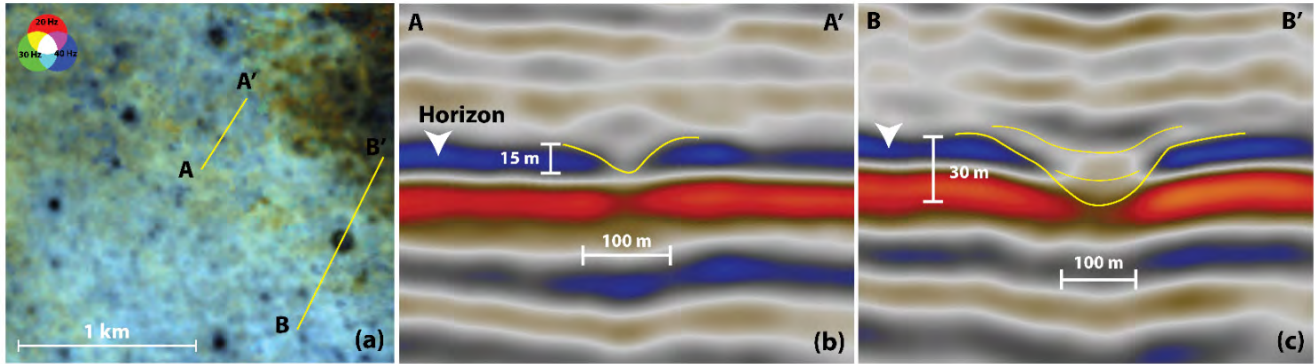


Figure 8. Category 2 features. (a) 2D mapview with RGB blend of spectral decomposition data on top Chalk seismic horizon (20, 30, 40 Hz). Category 2 features have circular morphology, range in diameter between 10-200 m, and are black in spectral decomposition data (e.g. low-amplitudes). (b) Section A-A' shows an example of a small black circular feature, which represents a 100 m wide and 15 m deep depression, and has transparent infill. (c) Section B-B' shows a larger black circular feature, which represents a 200 m wide and 30 m deep depression, and its infill shows a wedging out pattern to the sides. Slopes are between 3 to 10 degrees to the horizontal.

The circular depressions of Category 2 occur throughout the Upper Jurassic to Eocene succession (e.g. BCU, Lower and Upper Cretaceous, and Paleogene) (Fig. 4). The depressions can occur isolated, but are often nested within all other categories. Where underlain by deeply rooted faults and often low signal/noise packages, Category 2 features are observed within Category 1 features (e.g. central part of the sections) (Fig. 5c-d). They are well expressed at the top of the Chalk Group (Fig. 9a), and occur both with and without presence of underlying faults (e.g. see Fig. 8 for examples without clear fault).

Category 3 features

Category 3 features comprise large/giant circular, highly elongated, or complex-shaped depressions outlined by low- to high-amplitude trough reflectors (Fig. 10). They are 200-500 m wide (short axis), 0.2 – 1.5 km across (long axis), and 20-60 m deep. The floors of the depression are often to

undulating, while valley slopes typically dip 3-10°. The bottom reflector is a trough, and the infill often consists of 2 reflectors, a lower low-amplitude peak followed by a medium to high-amplitude trough at the top. In the upper part of the succession this reflector marks the top of the Chalk, and the auto-tracked Top Chalk (CK-7) trough horizon therefore highlights the top of the infill, surrounded by depression walls (Fig. 10b-c, dashed white line). Previous investigations of similar features in the Halfdan NE gas field by Henriksen *et al.* (2009) showed that the infill consists of Danian chinks, marls and clays.

The larger circular to highly sinuous depressions of Category 3 dominate mainly strata at CK-3 (latest Coniacian, c.f. van Buchem *et al.* 2018), and between CK-6 and CK-7 (Danian Ekofisk Formation) (Fig. 4). They mainly occur on top of the Bo-Valdemar Ridge as well as the Adda Ridge (Fig. 9a), and are often sitting over deeper faults (Fig. 10).

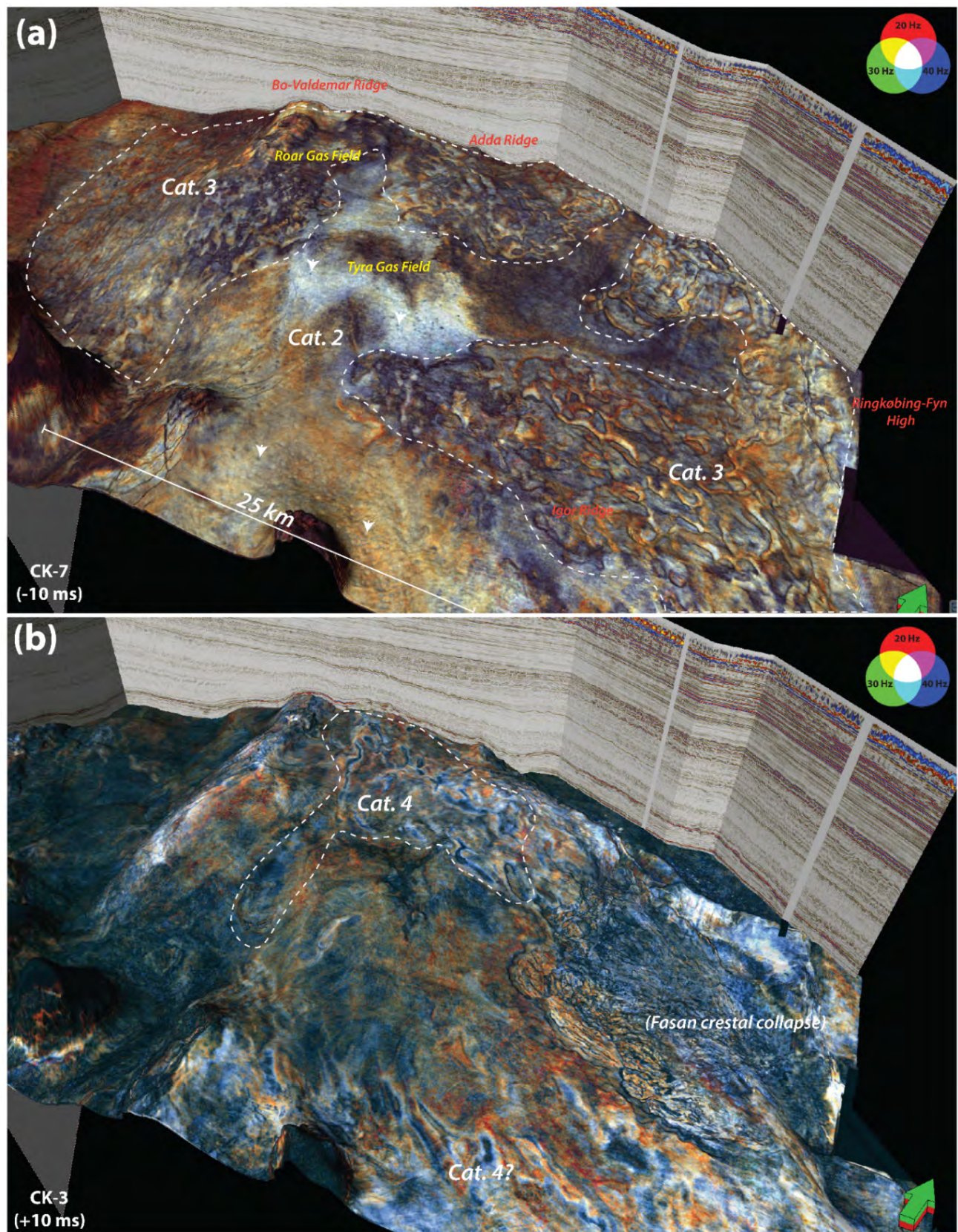


Figure 9. Spatial distribution of Category 2, 3, and 4 features. **(a)** Seismic horizon CK-7 (time shifted -10 ms) with spectral decomposition data in RGB blend to highlight geomorphological features. Category 2 features, circular depressions 50-130 m in diameter, can be observed within the central part of the inverted Bo-Adda-Igor ridges. Category 3 features are observed at this level on top and eastern flank of the Bo-Valdemar Ridge, on top of the Adda Ridge, the Igor Ridge, and along the flank of the Ringkøbing-Fyn High. **(b)** Seismic horizon CK-3 (time shifted +10 ms) to highlight spatial distribution of Category 4 features. This horizon cuts through the depressions and therefore are recognized by the dark-blueish elongated features. These mainly occur within the Roar basin area (white dashed lines), though potentially some are observed in the southern end of the Igor Ridge. The Fasan crestal collapse has been described in van Buchem *et al.* (2018).

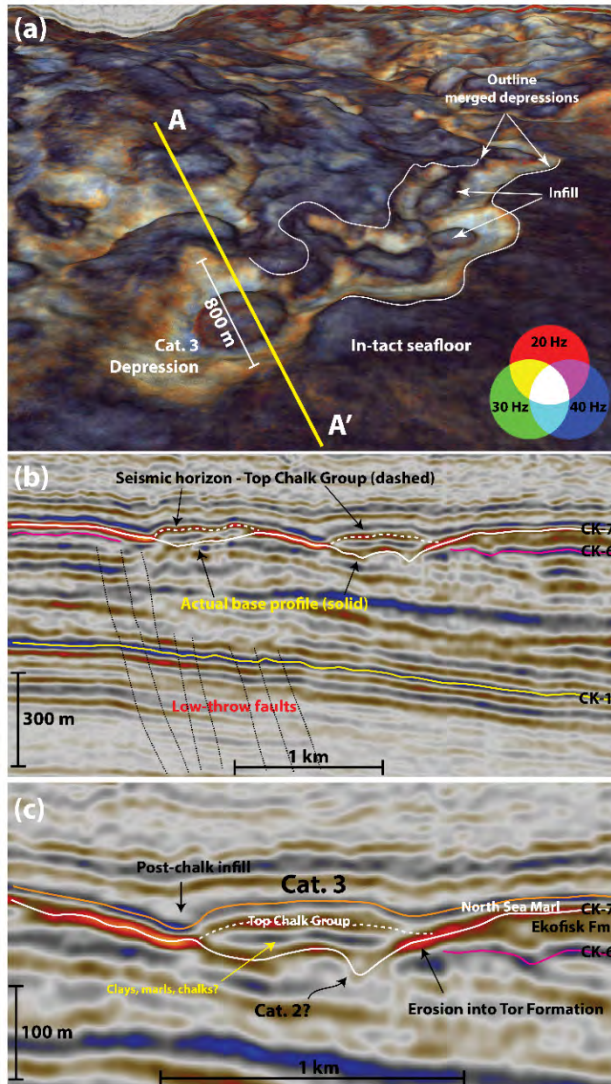


Figure 10. Category 3 features. (a) 3D mapview with RGB blend of spectral decomposition data on top Chalk seismic horizon (20, 30, 40 Hz). Category 3 features have circular (diameter 200-500 m), elliptical (200-500 m long axis, 200-300 short axis), highly elongated morphology (0.5-3 km in length), or complex shapes. The round ‘islands’ are actual top depression infill and not base of the category 3 depression, as highlighted in A-A’. (b) Section A-A’ runs perpendicular through a circular (diameter 800 m) and a highly elongated (long axis 3 km) category 3 feature, which are almost merged (see a). The U-shape depressions are up to 60 m deep, and truncate the CK-6 seismic marker, and have an undulating bottom profile (solid white line). Slopes are between 3-10 degrees to the horizontal. The infill has a general continuous, medium-amplitude character. Note the low-thrust faults seen at the base of the Chalk Group (black dashed lines). (c) Close-up of the round depression as seen in (a). The seismic horizon (dashed white line) actually follows the Top Chalk trough instead of the base of the Category 3 depression (solid white line), and therefore the top of the fill is seen within the merged depression as outlined in (a).

Category 4 features

Category 4 features comprise the largest depressions found in the study area, and are classified as mega depressions outlined by high-amplitude U-shaped trough reflectors (Fig. 11). They are mainly elongated, 0.5-2.5 km wide (short axis), 0.5-5.0 km across (long axis), 100-250 m deep, and cutting deeply into the underlying strata causing many stratal terminations (Fig. 11b-d red arrows). Multiple depressions with slightly different orientation can be found nested within larger features (Fig. 11c). Valley walls shallow up in all directions with slopes between 1-15° (Fig. 11b, c). In total, seven individual mega-depressions have been documented between marker CK-3 and CK-5 (Santonian – Campanian strata), each with a slightly different morphology, though all having in common that the walls shallow in all directions (e.g. are cup-shaped) (Fig. 12). The axial section through the depressions (G-G’) illustrates how strata below CK-3 have a dominantly parallel bedding orientation, while post-CK-3 marker Cat. 4 depressions occur, closely associated with a highly complex fault fabric (Fig. 12h). Indeed, Cat. 4 depressions closely align with deeply rooted faults that are well expressed at the BCU level (Fig 13).

The strata infilling the depressions are continuous (mid- to high-amplitude), discontinuous (low- to mid-amplitude), chaotic (mid- and high-amplitude), or transparent (low-amplitude) in character. (Figs 11 and 12). A depth slice with RMS amplitude at the base of depression 4 shows the large-scale occurrence of circular, high-amplitude depressions (Fig 14). Dimensions are similar to category 2 features, but the high-amplitude character differs from the low amplitudes common in category 2. They therefore fall in category 5.

Category 4 features occur mainly in the Roar Basin, a Cenomanian – Santonian basinal low between the Bo-Valdemar Ridge and Adda Ridge that was inverted into a high during the Campanian inversion (see isochores UC-1 to 3 in van Buchem *et al.*, 2018) (Figs 3 and 9b). A zone on top of the Igor-Emma Ridge potentially also shows Cat. 4 features (Fig. 9b, ‘Cat. 4?’).

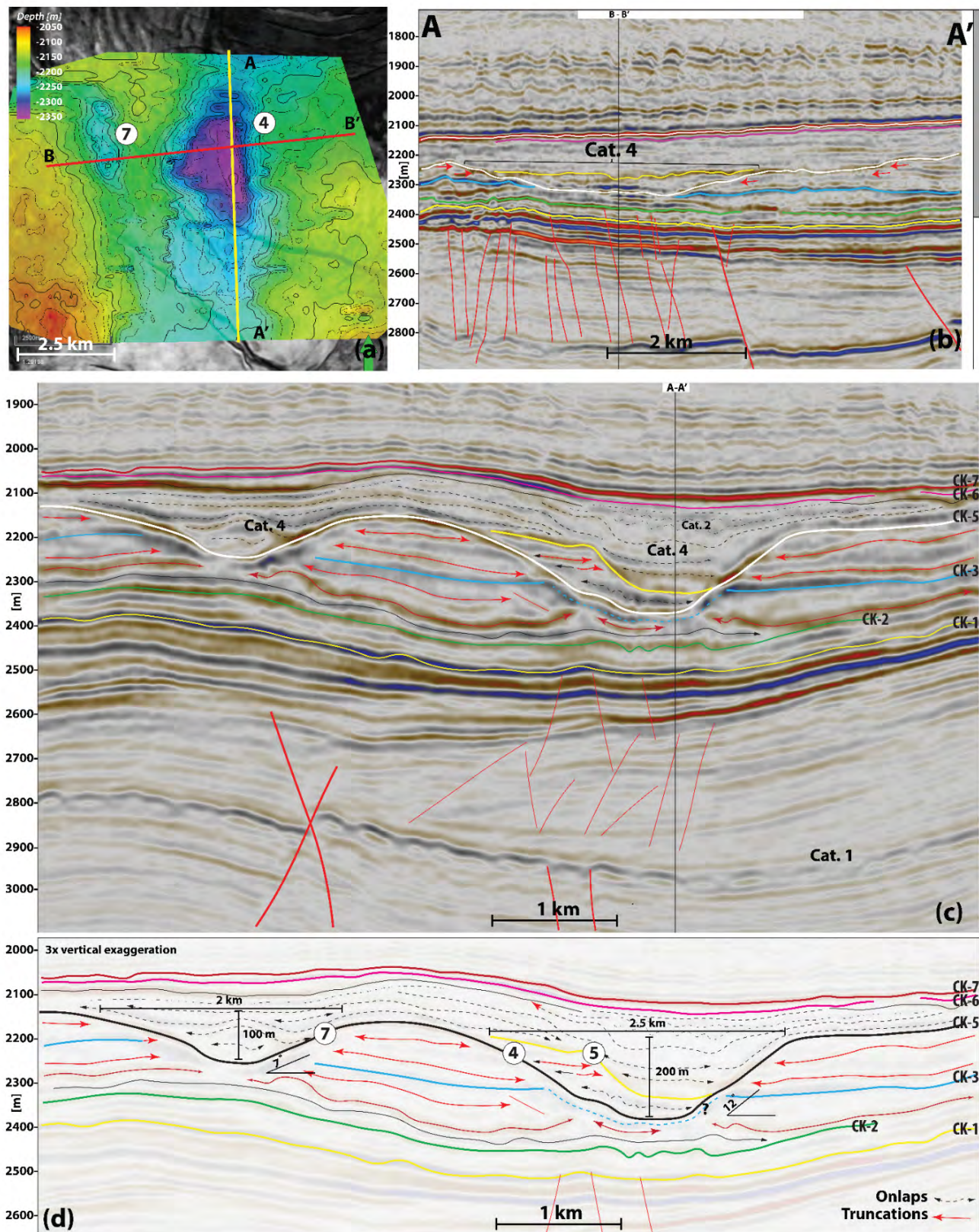


Figure 11. Category 4 features. (a) Seismic interpretation of depression 4 (see Fig. 8 for an overview of all segments), overlaying an RMS amplitude horizon slice at BCU level that shows lineations representing faults. The shown depressions are slightly elongated, and shallow up towards all sides. Dimensions are 2-2.5 km wide (short axis), 2-3 km long (long axis), and 100 – 250 m deep (measured from adjacent plateau). (b) Tangential section through depression axis shows shallowing up towards the north and south, and truncation into underlying strata. (c-d) cross-section through deeply incised U-shape depressions (white and yellow lines). Many truncations of strata can be observed (red arrows) as well as onlapping strata (black arrows) within the depressions. Slopes measured are between 1 to 15 degrees to the normal (note 3x vertical exaggeration). There are multiple category 4 features nested within one another (e.g. 4 and 5), as well as category 2 features within the infill.

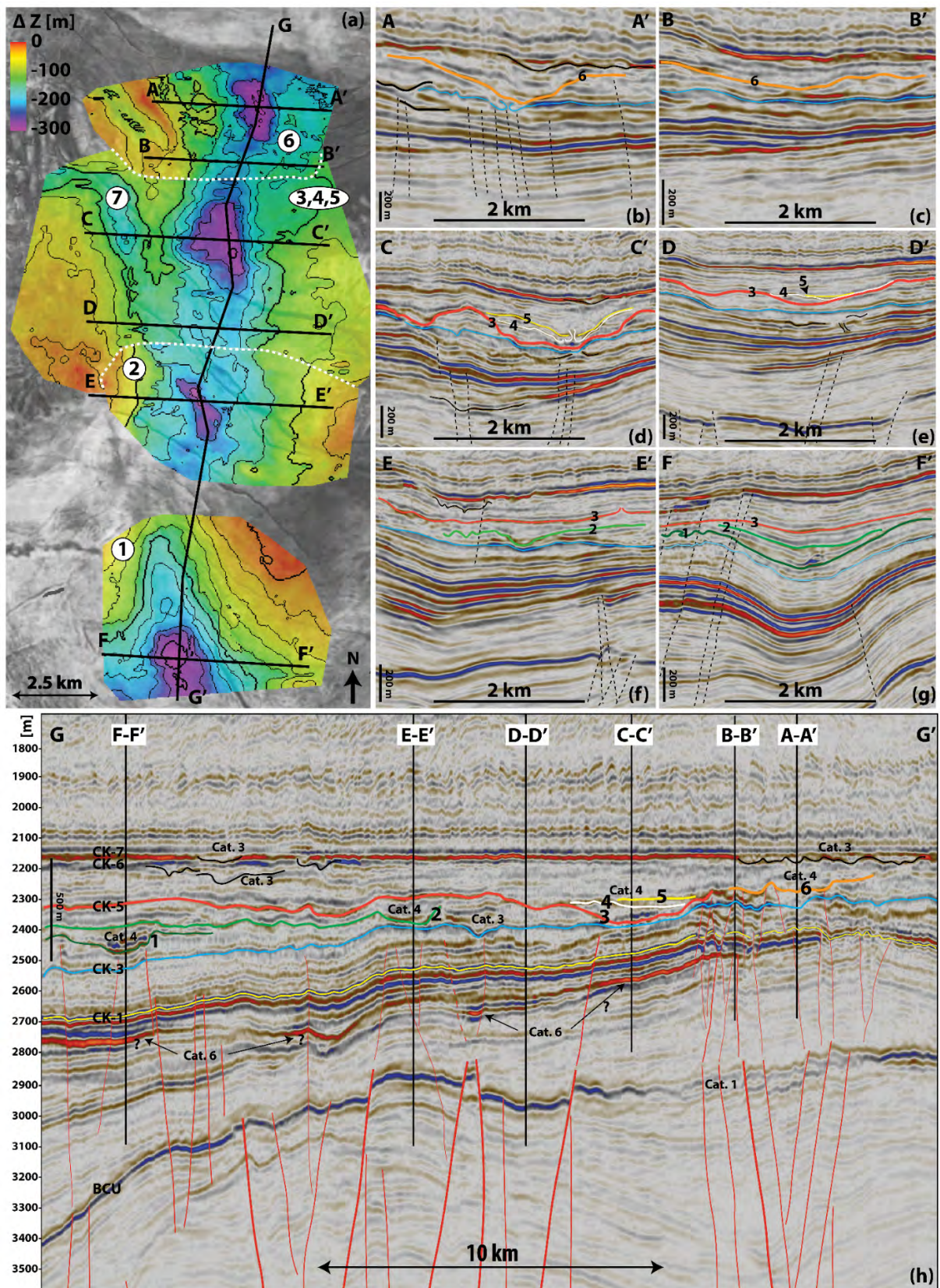


Figure 12. (a) Overview of the different category 4 depressions. At least 7 individual segments have been identified based on strata terminations. The depressions occur within different levels of the stratigraphy, and therefore a general difference in height is used (e.g. ΔZ in m's). (b-g) Cross-sections show that the depressions are mainly (a)symmetrically U-shaped (A-F), and short axis are between 0.5-2.0 km wide, long axis between 1.5 – 3.0 km long, and depths between 100 – 250 m. (h) Axial line shows that six category 4 features can be observed between CK-3 and CK-5. It also reveals the complex fault fabric that is present below the features. Some category 6 features might be observed associated with the faults, as well as some category 3 features at the CK-3 level (Top Kraka Formation, between E-E' and D-D') and at the top of the Chalk Group.

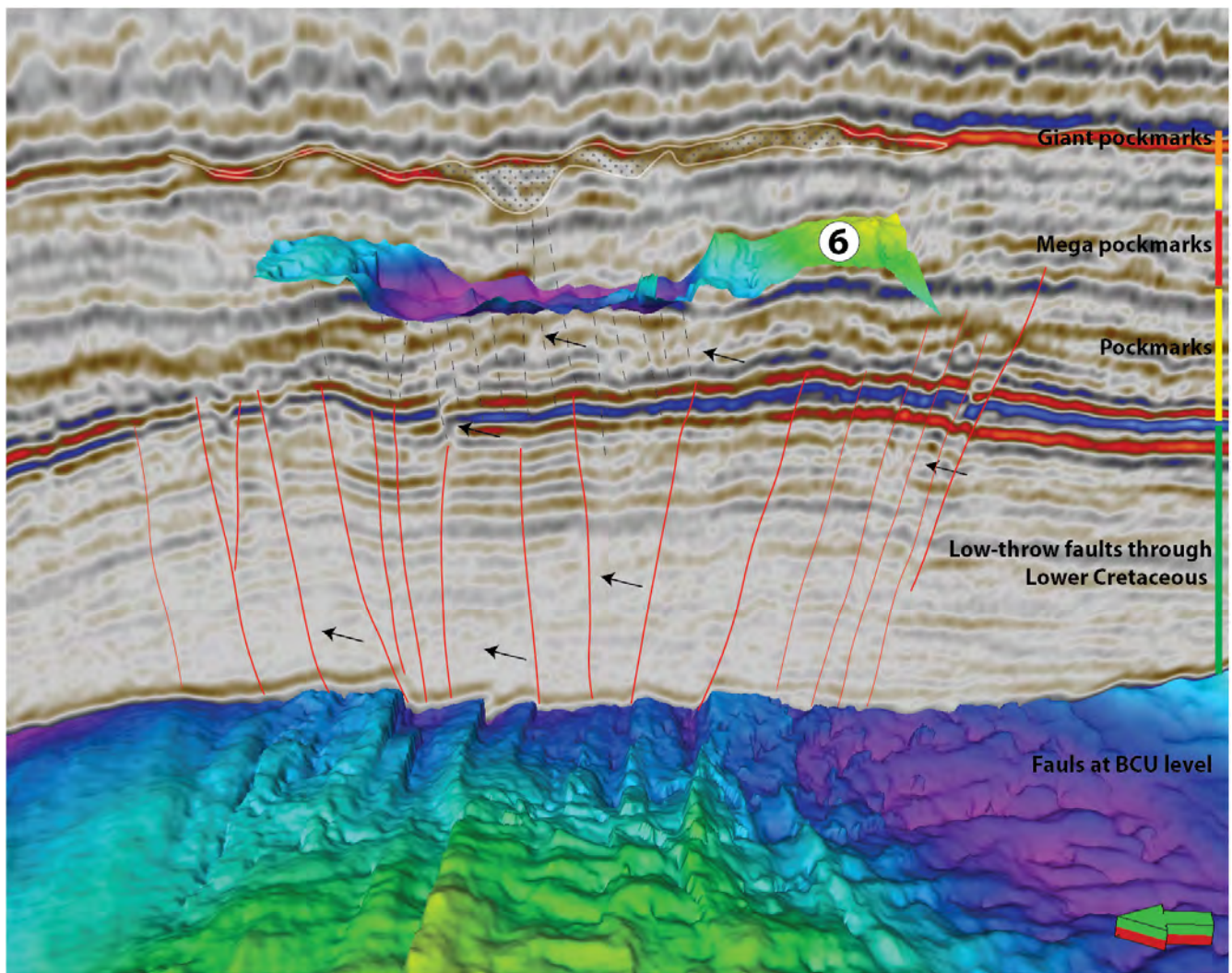


Figure 13. Relationship between occurrence of Category 4 and 3 and underlying fault system. Deeply rooted, inverted Late Jurassic-aged normal faults underlie the mega-pockmarks. Smaller low-throw faults provide a connection through the Early Cretaceous clays and marls into the Chalk Group, and systematic amplitude dimming within the chalk is interpreted to represent similar low-throw faults (black dashed lines). Near the top of the Chalk Group, smaller, though still giant, pockmarks occur.

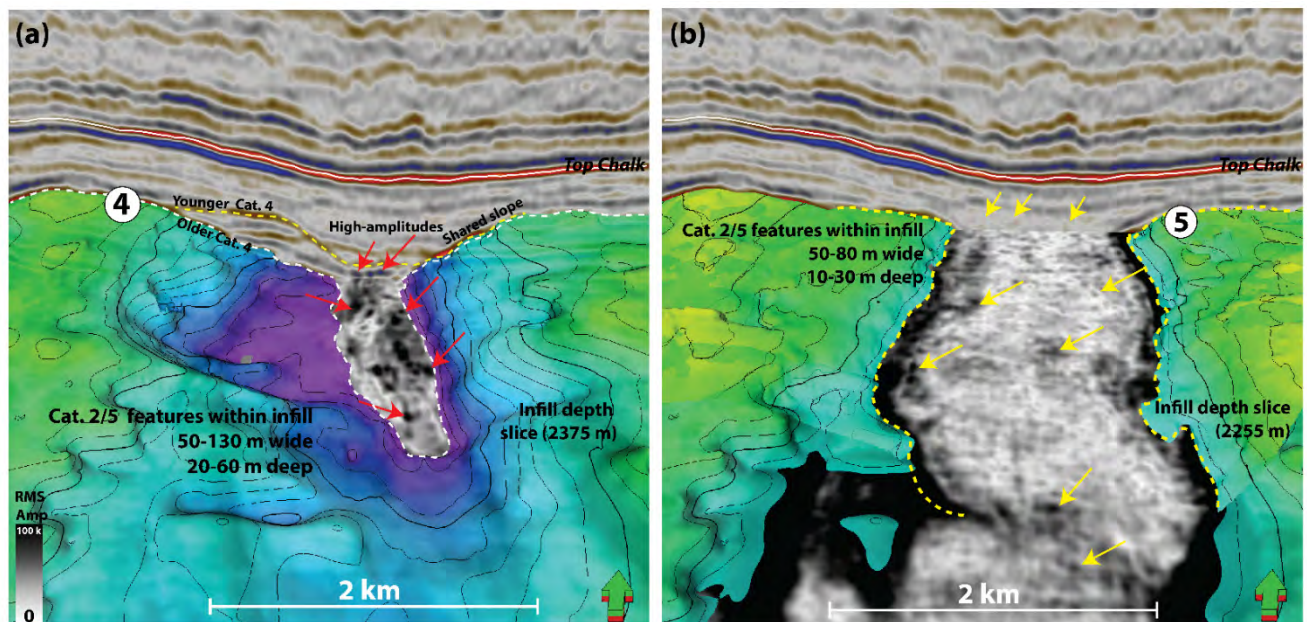


Figure 14. RMS amplitude on depth slices within infill of the category 4 features. (a) Outline of depression 4 with depth slice (2375 m), showing high-amplitude (black) circular depressions, 50-130 m in diameter, 20-60 m deep. These features correspond in 2D seismic section as localized round high-amplitude seismic packages and therefore differ from their low-amplitude category 2 feature counterparts, and make up category 5. (b) Outline of depression 5 with depth slice (2255 m) higher in the stratigraphy. Similar but smaller circular medium- to high-amplitude depressions (black) can be observed within the infill of depression 5.

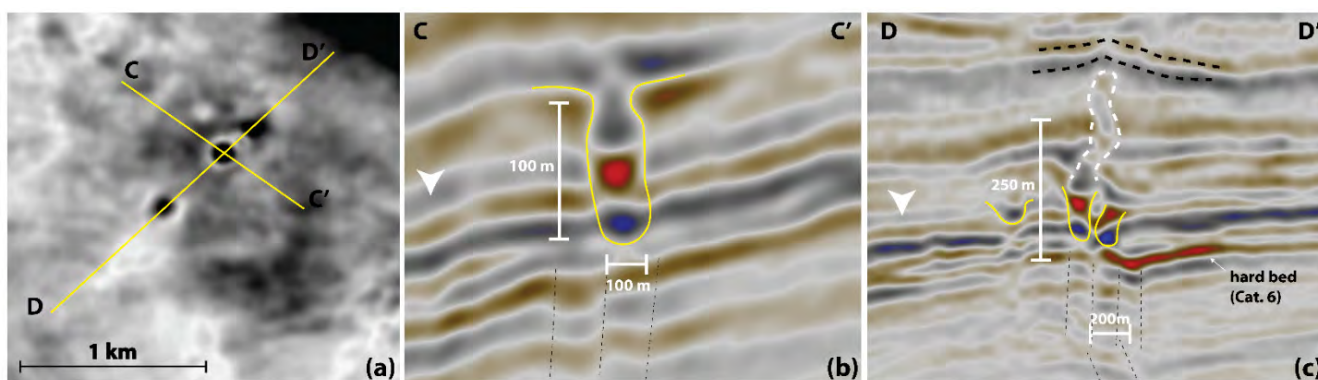


Figure 15. Category 5 features. (a) RMS amplitude data on horizon slice (location shown in b). High-amplitude circular features can be observed (black), 50 – 120 m in diameter. (b) Cross-section through circular features shows location of RMS depth slice (white arrow). These features are characterized by localized high-amplitude round packages, occurring as triplet (top-down: med-amplitude peak, high-amplitude trough, and high-amplitude peak) within a steeply dipping U-shaped ‘tube’, up to 100 m in depth. In the particular example, even some overhang can be observed at the top of the feature. Measured slopes are between 75-90 degrees on the wall, to 110 degrees in the overhang. Beneath, the small offsets in the strata represent some low-throw normal faults (dashed lines). (c) Tangential section through three category 5 features show how the stratigraphy is disturbed by the features, with polarity reversals (peak replaces trough and vice-versa, dashed white outline) and altered orientation of seismic reflectors (dashed black outline). Beneath the Category 5 features low-throw faults are observed as well as a high-amplitude trough, which represents a hard bed (Category 6 feature).

Category 5 features

Category 5 features comprise high-amplitude circular tubes, 50-130 m in diameter and up to 250 m deep (Fig. 15a). They are sharply outlined by polarity reversals and high-amplitudes, and their internal architecture comprises a seismic triplet with a mid-amplitude peak, high-amplitude trough, and high-amplitude peak (Fig. 15b, c). Wall slopes are dipping 75-90 degrees and wall overhangs are observed, corresponding to 110 degrees to the horizontal. Strata overlaying the tube show slightly concave bending (Fig. 15c, black dashed lines). Low-throw faults are often observed beneath category 5 features, as well as high acoustic impedance beds (category 6 features) (Fig. 15). These features are different from category 2 features as they are steeply dipping, and deeply affecting the strata.

Category 5 features are rare, and found in some places in uppermost Lower Cretaceous strata, and more commonly in Chalk Group deposits (Figs 4 and 16). Spatially they occur below the Tyra Gas Field and within the Category 4 features (Fig. 14), where they are strongly linked to fault systems and/or gas chimneys.

Category 6 features

Category 6 features consist of high-acoustic impedance beds, represented by high-amplitude

troughs in seismic sections (Fig. 16b). They are from 0.1-1 km across, 1-5 km long, and are often delineated by faults (e.g. see Fig. 12 G-G’), as well as presence of category 2-4 features (Fig. 17b). Well data show that pure sections consist of 1-7 m thick beds of low-porous, amorphous, grey, cryptocrystalline calcite. The influenced zone can be up to 20-50 m as seen in the Boje-1 well (Fig. 17a). Carbon and oxygen isotope analyses of drill cutting material gave $\delta^{13}\text{C}$ values from -40 to -1‰, and $\delta^{18}\text{O}$ values between -12 to +3‰ (Fig. 18). In comparison, pure chalk strata have more $\delta^{13}\text{C}$ values between 0 to 4‰, and $\delta^{18}\text{O}$ values between -4 to 0‰ (Fig. 18, ‘chalk’)

The high acoustic impedance beds of Category 6 are present in Lower Cretaceous strata, the Upper Cretaceous Chalk Group, and in Paleogene shale (Figs 16a). Their spatial distribution in the Lower Cretaceous strata is closely following faults offsetting the Base Cretaceous Unconformity (Fig. 16b). In the Chalk Group, they occur in the vicinity of Category 2-5 features (Fig 18, ‘Boje-2’), and in the polygonal faulted Paleogene strata they are limited to areas above the highest points of Top Chalk Group (see also Vejbaek, 2002) (Fig. 19 shows the example above the Roar Gas Field).

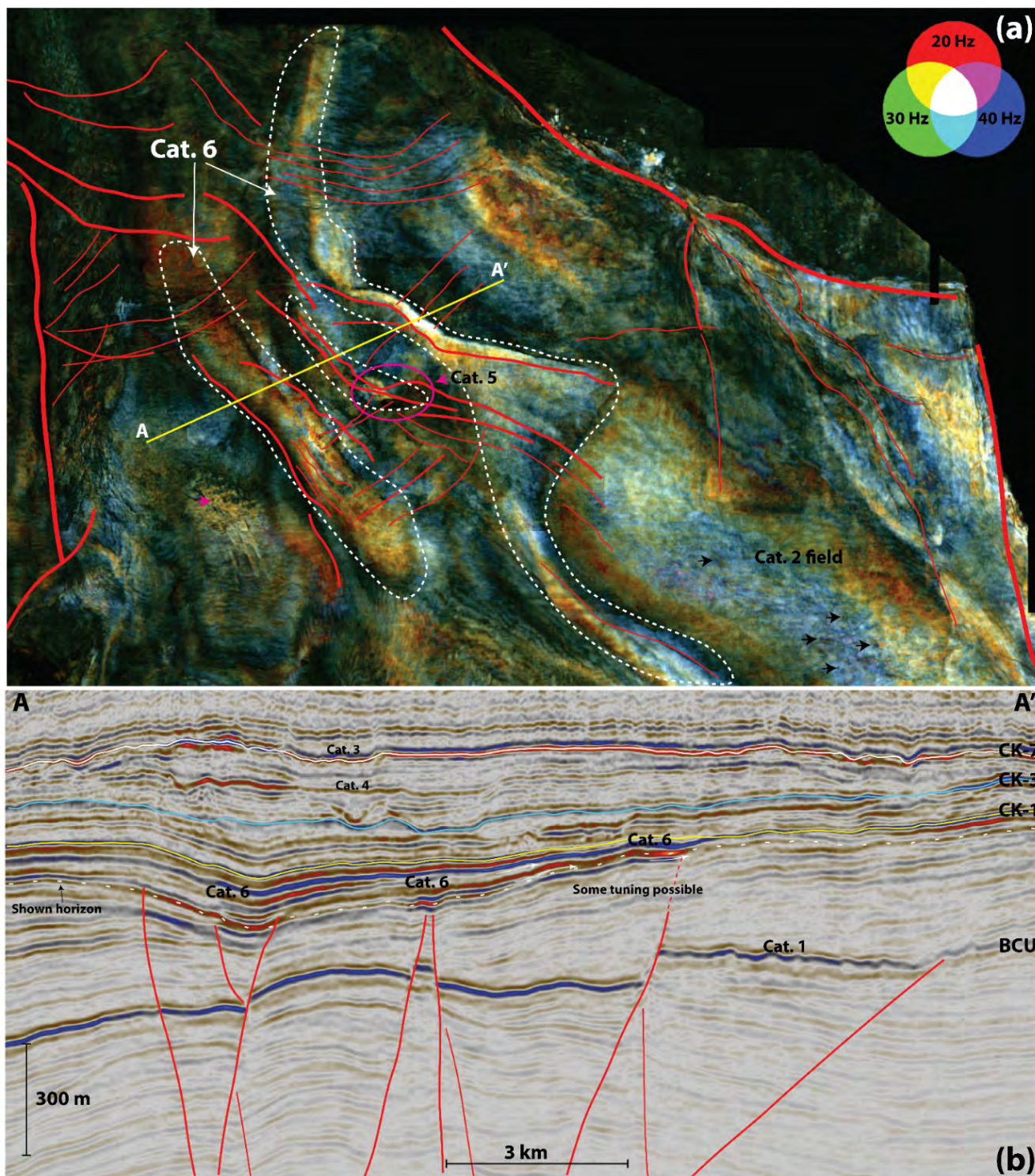


Figure 16. Spatial distribution of Category 5 and 6 features. **(a)** Intra-Tuxen Formation horizon slice with spectral decomposition RGB blend. Category 6 features are shown in white dashed outlines, and are recognized by light colors (high-amplitudes). Category 5 features are shown in magenta outline. A field of Cat. 2 features is observed in the southwestern part. Fault geometries from BCU level are projected upon this surface, and are slightly shifted due to the projection. **(b)** Seismic section A-A' that shows how the high-amplitude packages are strongly linked to the presence of faults. It is possible that part of the higher amplitude is due to tuning effects as a result of a sediment wedge.

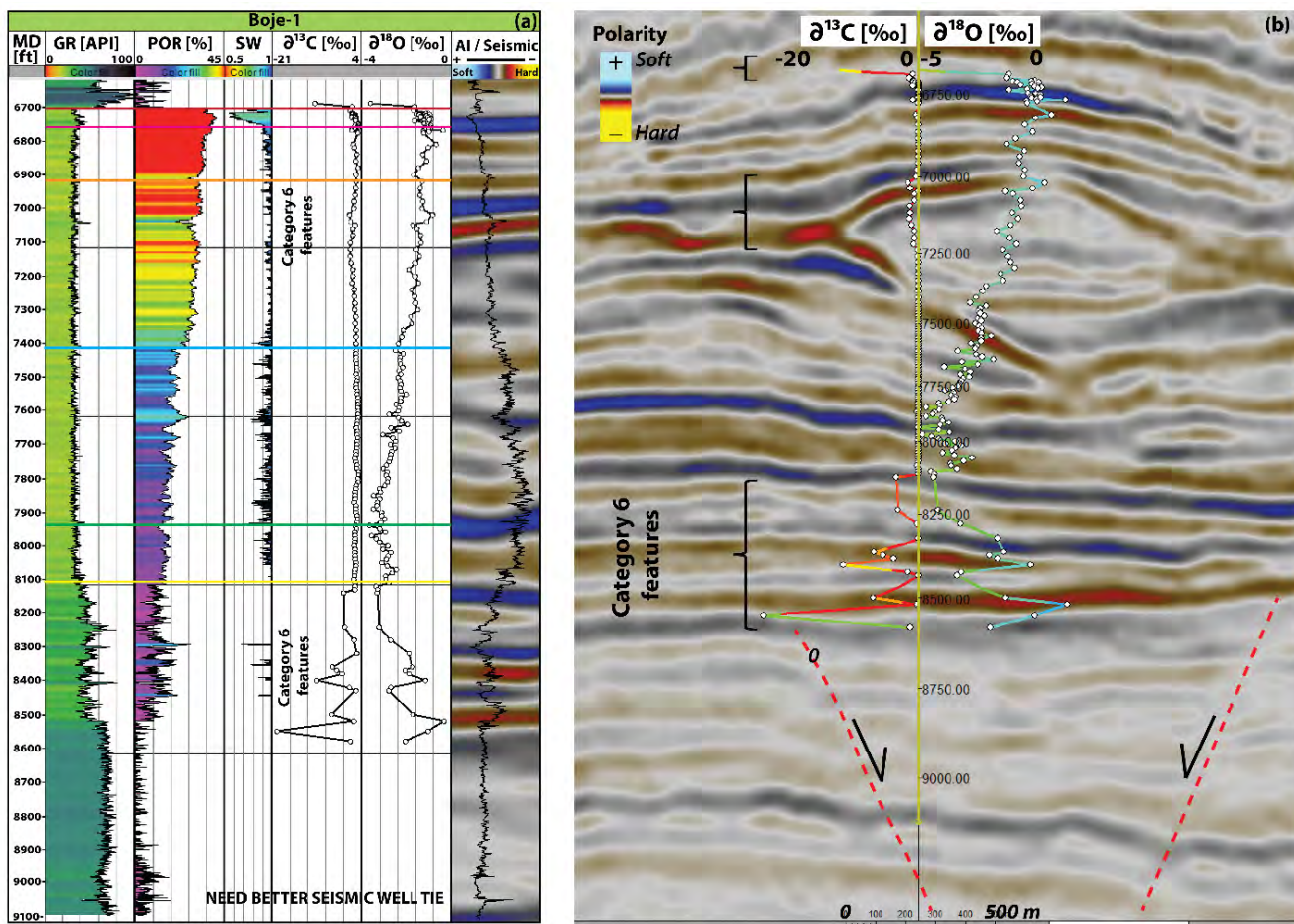


Figure 17. Category 6 features penetrated by Boje-1 well. The features are observed as high-amplitude troughs (red) within the stratigraphy, reflecting they represent higher acoustic impedance strata than surroundings (see seismic section). Widths range from 50 m to 1 km and the occurrences seem to be highly influenced by fault systems, and occur around Cat. 4 features.. Density-derived porosity logs show that the category 6 features are low-porosity beds. The category 6 strata are unique from other low-porosity beds as $\delta^{13}\text{C}$ values are negative within these strata and range from -1 to -21‰. The most negative $\delta^{13}\text{C}$ values represent the most pure beds, and these can be between 50 cm to 5 m (H-1X), whereas mixed with other strata they occur over several 10s of meters (see Boje-1).

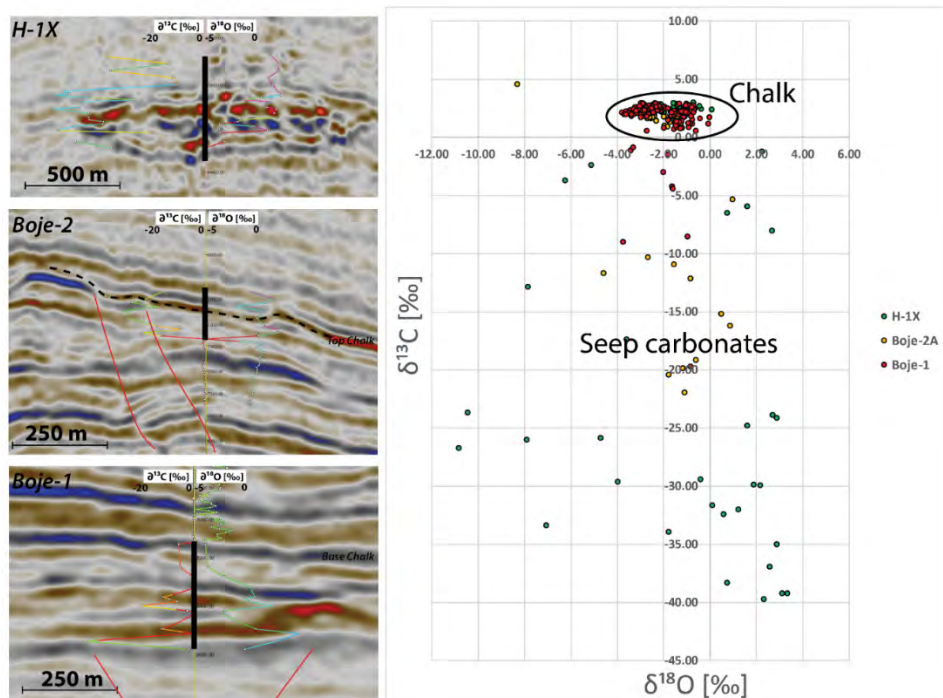


Figure 18. Stable carbon and oxygen isotopes of three wells containing negative $\delta^{13}\text{C}$ values (thick black lines along well path): H-1X (Eocene), Boje-1 (Lower Cretaceous), Boje-2 (Tor and Ekofisk Formation). There can be distinguished a clear zonation between the narrow range found within unaffected chalk lithology ($\delta^{13}\text{C}$ between 0 and 4‰, $\delta^{18}\text{O}$ between -4 to 0‰) and wide range found within Category 6 features, reflecting a source with negative $\delta^{13}\text{C}$ (e.g. methane), and bacterial kinetics or diagenesis for $\delta^{18}\text{O}$.

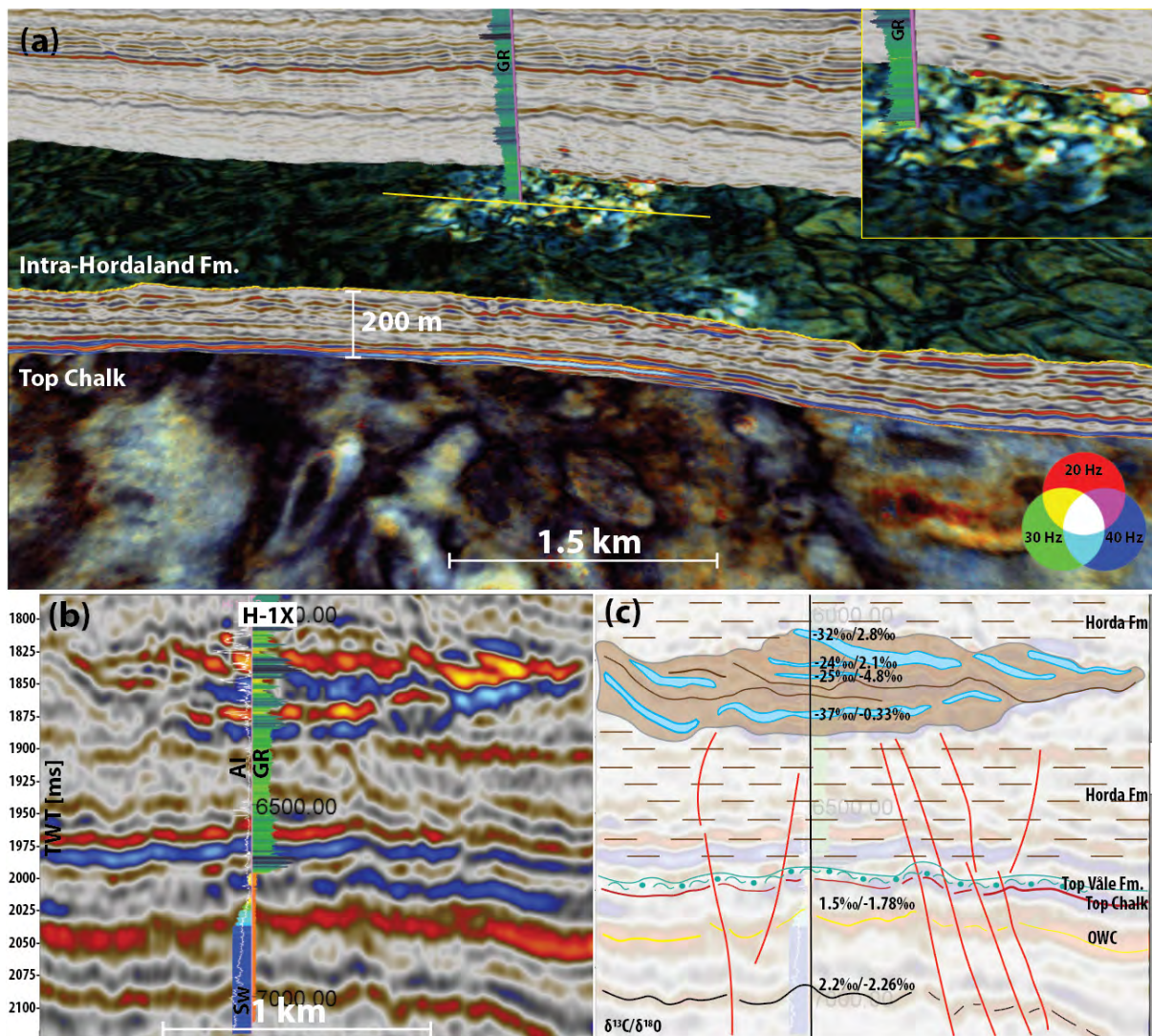


Figure 19. (a) Spatial distribution of a category 6 feature within the Eocene overburden above the Roar Gas Field (location in Fig. 1). They occur as high amplitude bright spots in spectral decomposition data (b) Seismic and wireline data, showing high amplitude reflective packages (HARPs). Well data from H-1X (Roar) shows at the high amplitude troughs (red) as compared to background: low GR readings (20 vs 80 API), high density (2.57 vs 2.11 g/cm³) and low transit times (65-85 vs. 140-160 ft/μs). Drill cutting material shows up to 100% grey, microcrystalline limestone. (c) Interpretation. The HARPs are interpreted as limestone lenses/stringers within clay. Carbon and oxygen isotope data shows very negative $\delta^{13}C$ values (-24 - -40‰) compared to the chalk (1.5 – 2.2‰). See also Figure 18 where all geochemical data is cross-plotted.

Seismic morphologies in the Upper Jurassic to Eocene succession – interpretation and origin

The interpretation of the seismic geomorphological features is summarized in Table 1. The majority of the observed features is believed to reflect processes linked to gas and fluid seepage and expulsion affecting the ancient sea floor, and their occurrence in the seismic stratigraphic framework can be used for dating and linkage to regional geological events (Fig. 4).

Category 1 features

The hill and valley morphology is mainly seen as continuous, elongated hills and valleys but also occurs as isolated rounded to rectangular shapes (Fig. 5, Table 1). The morphology seems not linked to fluid migration or expulsion but rather reflect either sedimentary or tectonic modification of the sea floor. In our view the morphology was formed initially from sediment remobilization (thin-skinned slumping) on the basin floor based on the slight normal offsets in 2D sections, the cusate shapes, and the occurrence of the features along sloping basin floors. Later modifications seem mainly to be of destructive character, and the sinuous shape of the valleys is likely the result of bottom current activity

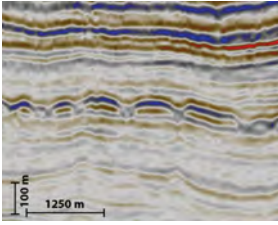
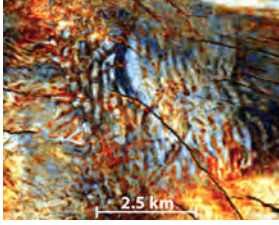
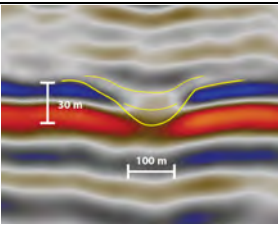
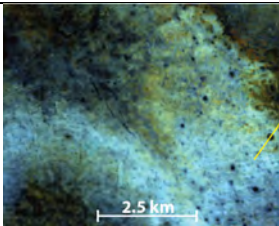
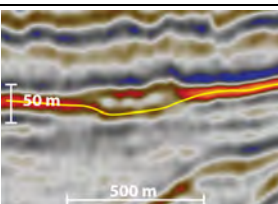
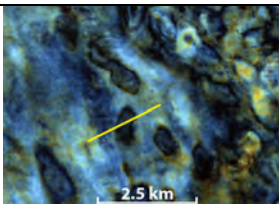
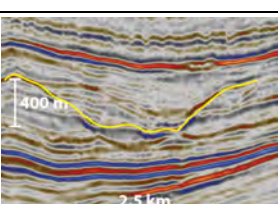
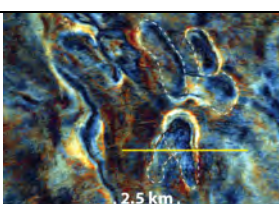
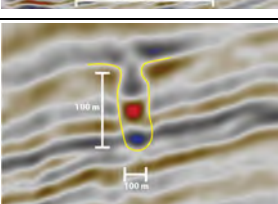
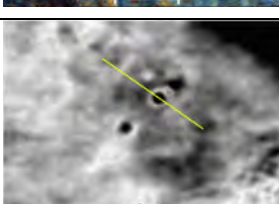
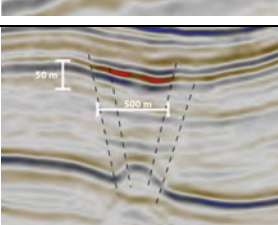
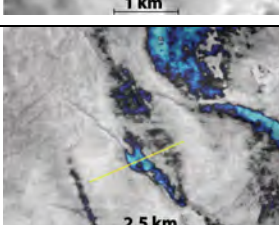
Cat.	2D seismic expression	Map view expression	Architecture	Dimensions	Stratigraphy	Interpretation
1			Hill and valley morphology Hills can be highly elongated and slightly sinusoidal, rectangular, squared, rounded or a complex combination. Valleys interrupt the hill topography, and depressions are elongated, or rounded. Doming underneath valley. Typically shows infilling younger packages	Hills: elongated (0.4 - 5 km by 0.1-0.4 km), rectangular (200-400 by 100 m), rounded (20-40 m), composite (50 - 300 m) Valleys: 20 m (rounded) to 3 km (elongated). Slopes are typically between 5-20°. Depth to valley floor (30 - 100 m).	Best expression at Base Cretaceous Unconformity reflector (BCU), where major Late Jurassic faults terminate (prior to Campanian inversion). Features are also found in Lower and earliest Upper Cretaceous strata.	Slumping and pockmark complex causing erosional depressions on basin floor. Driver of erosion is fluid expulsion following Late Jurassic faults and subsequent bottom current activity.
2			Small/medium depressions Mainly circular depressions with limited incisional depth. Infill thickest in depression centre, and wedges out to the side. Not necessarily clear link to fault systems, but found nested within larger depressions (e.g. cat. 3 and 4), hill and valley morphology (cat. 1), and within HARP's (cat. 6). Different from cat. 5 features due to gentle U-shape slopes (5-10°).	Depressions are between 10 to 200 m in radius, 10 - 40 m deep (e.g. 10 m is close to seismic detectability). Slopes are typically between 3-10°.	Occur throughout the Late Jurassic to Eocene strata.	Small to medium, round pockmarks due to fluid expulsion. Roundness indicates limited reworking by currents. Occurrence away from major fault systems indicate regional fluid expulsion from within the strata. Nested within larger depressions indicate smaller outbursts.
3			Giant depressions Circular, elliptical, and complex depressions with significant incisional depth. Often linked to fault systems and found above cat. 4 features. Ellipse and complex shapes likely due to amalgamation of single events.	Depressions are between 200 to 500 m wide (short axis), 200 - 1.5 km across (long axis), 20-60 m deep. Slopes are typically between 3-10°.	Occur within the Danian strata (Ekofisk Formation), incisions occur into the Maastrichtian Tor Formation.	Giant pockmarks with significant erosion into the underlying strata (up to 60 m). Occur on top of ridges where faults occur. The elongation is likely the result due to amalgamation of single pockmarks into more complex shapes, combined with possible bottom current reworking.
4			Mega depressions Round (rare) to elongated (common) large depressions, cutting deeply into strata causing several stratal terminations against surface. Seismic character of the infill comprise parallel reflectors onlapping onto surface, discontinuous to chaotic, and to transparent (low S/N) strata. Strong link to faults.	Depressions are between 0.5 to 4.0 km wide (short axis), 0.5 - 5.0 km across (long axis), 100 - 400 m deep. Slopes are typically between 5-15°.	Exclusively within Santonian - Campanian strata. Youngest incisional surface is Campanian in age (e.g. top 'intact' strata).	Mega pockmarks with very significant erosion into the underlying strata. Location strongly linked Late Jurassic faults underlying Roar Basin, and its position at the crest of the Mesozoic basin. Campanian inversion movement caused formation of these mega pockmarks.
5			Deep tube depressions Steeply dipping, round depressions, cutting deep into underlying strata causing stratal terminations. Widest at bottom, becoming narrower to the top (cone/tube shaped). High amplitude seismic reflectors occur within. Sometimes cross-cutting reflector can be observed above it. Strong link to faults.	Depressions are between 50 - 100 m wide at bottom, and become narrower at top (10-30 m). 20 - 100 m deep. Slopes are typically between 75-110° (near vertical to overhanging at top).	Observed within Hidra and Kraka Formations (Cenomanian to Santonian strata).	Interpretation 1: small pockmarks within semi-consolidated chalks. Interpretation 2: collapse structure due to hypogenic karst or fluidization of chalk. Interpretation 3: seep carbonate chimneys (favourite)
6			High amplitude reflector packages (HARP's) Strongly fault-bound hard beds within clays and chalks. Often in association with depressions, which occur above. Limestone material with highly negative $\delta^{13}C$ values (-1 to -40‰).	Reflectors show hardening between 0.1 - 5 km wide, 1 - 5 km in length. Well data shows individual beds are 1 - 7 meter thick.	Observed within Lower Cretaceous marls and chalks (Tuxen & Sola Formations), throughout Upper Cretaceous chalks, and within Paleogene and Neogene clays.	Hard beds reflect microbially mediated limestone precipitation from seeping methane to seafloor, utilized by sulphate-reducing bacteria just below seafloor. Pockmarks above may indicate short-lived explosive release of methane, causing erosion.

Table 1. Overview of the different morphological features.

and erosion, which enhanced the extensional topography further before it eventually disappeared due to differential sedimentation in the immediately overlying succession (Figs 5, 6, and 7). The isolated hills are believed to represent remnants of more elongated hills subjected to more severe sea floor erosion.

Category 2 features

The circular to slightly elliptical depressions of Category 2 are the smallest of the three depression

categories (Fig. 8, Table 1, 10-200 m in diameter). Circular depressions in the Chalk Group can represent hypogenic karst features (as meteoric karst is ruled out as it was never exposed subaerially in the Central Graben c.f. Gemmer *et al.*, 2002), but the shallow depressions show an atypical U- and V-shape, low-amplitudes, and are not always linked to faults. As these features also occur in marls and clays, this excludes a karst origin, and the depressions are interpreted as pockmarks formed by fluid expulsion on the sea floor in line with Masoumi

et al. (2014). Isolated depressions away from faults may have formed due to release of biogenic gas from biodegradation of organic material in the chalk (c.f. Betzler *et al.*, 2011; Masoumi *et al.*, 2014). The initial steep slopes of the craters were reworked by slumping as well as ocean bottom currents as evident from the wedged-shaped infill of the pockmarks (Fig. 8; Betzler *et al.*, 2011). Category 2 pockmarks affecting the hill and valley morphology (Category 1) created additional erosion and added to the complexity of the sea floor morphology (Fig. 5)

Category 3 features

The giant circular to highly elongated depressions of Category 3 mainly occur on top of inverted structural highs within the Kraka Formation (CK-2 to CK-3, Coniacian), Tor Formation (CK-5 to CK-6, Maastrichtian), and the mostly in the Ekofisk Formation (CK-6 to CK-7, Danian), where underlain by faults deeply rooted in Upper Jurassic strata (Figs 10, 12h and 13). The occurrence of merged circular depressions forming more elongated depression suggests that the morphology results from successive erosional events, and the Danian age of the infill of the youngest depressions in the Ekofisk Formation (cf. Henriksen *et al.*, (2009) suggests that they formed at the Danian seafloor, rather than being of post-depositional origin (diagenetic alteration). It is difficult to argue for syn-depositional hypogenic karst, as it would form steeply dipping ‘tube’-like features with overhangs or collapse structures, which are not observed. A simpler explanation is that the features represent giant pockmarks. Their sporadic occurrence within the Kraka Formation, closely associate to faults, suggests they formed during early inversion movements that reactivated faults and initiated fluid pathways (van Buchem *et al.*, 2018). Their frequent occurrence within the Ekofisk Formation on top of inverted structures suggests that wide-spread fluid expulsion occurred during the Danian. The coalesced pockmarks formed as successive expulsion events affected the sea floor in the same areas (e.g. see Fig. 10). The initial crater walls might have been steep but the angles were adjusted to match the angle of repose by mass movement and possible bottom current activity, processes that also tend to merge pockmarks (c.f.

Betzler *et al.*, 2011). The pockmarks cut down deep into the stratigraphy occasionally eroding the K/T boundary as the CK-6 marker often disappears below these depressions. The trough reflector at the bottom of the pockmark reflects the boundary from the softer infill sediments to clean chalks. As the lower Danian is often a barrier for fluid migration due to occurrence of argillaceous chalk, chalk with flint, and/or highly cemented chalks (Gennaro *et al.*, 2012)., the infill of the pockmarks might potentially create pathways for fluid flow, by-passing the dense zone.

Category 4 features

The U-shaped mega depressions of Category 4 cut deeply into the underlying stratigraphy and shallow up on all sides (Figs 11 and 12). Their infill often contains smaller pockmarks of category 2 and 3 as well as category 5 features, all related to fluid expulsion events. The depressions were originally interpreted to have formed purely from bottom current activity by Esmerode *et al.* (2008), but this is unlikely given their characteristics. The Category 4 mega depressions are all located above the thickest Upper Jurassic successions in the basin, which are deformed by normal faulting (Fig. 20), and above a Lower Cretaceous high separating the Tail End Graben to the east from the Rosa Basin to the west (Fig 21a-c). In this area, normal faults have roots in Lower to Middle Jurassic strata (Figs 3 and 12h). The location is where Campanian inversion movements were most extreme, as evident from the flattened reconstructions shown in Fig. 21b and c and isochores in Fig. 1a and b. Rapid uplift would have expanded trapped gas-rich fluids significantly, and coupled with fault reactivation that breaches seals in the Upper Jurassic to Lower Cretaceous strata, these trapped basinal fluids could escape towards the Campanian seafloor in explosive fashion. We therefore interpret these features as mega-scale pockmarks due to rapid uplift of the Roar Basin. While initial crater wall would be steep, mass movements and bottom current activity have adjusted the slope to match the angle of repose and fill in the depressions in the process (c.f. Betzler *et al.*, 2011) (Fig 11).

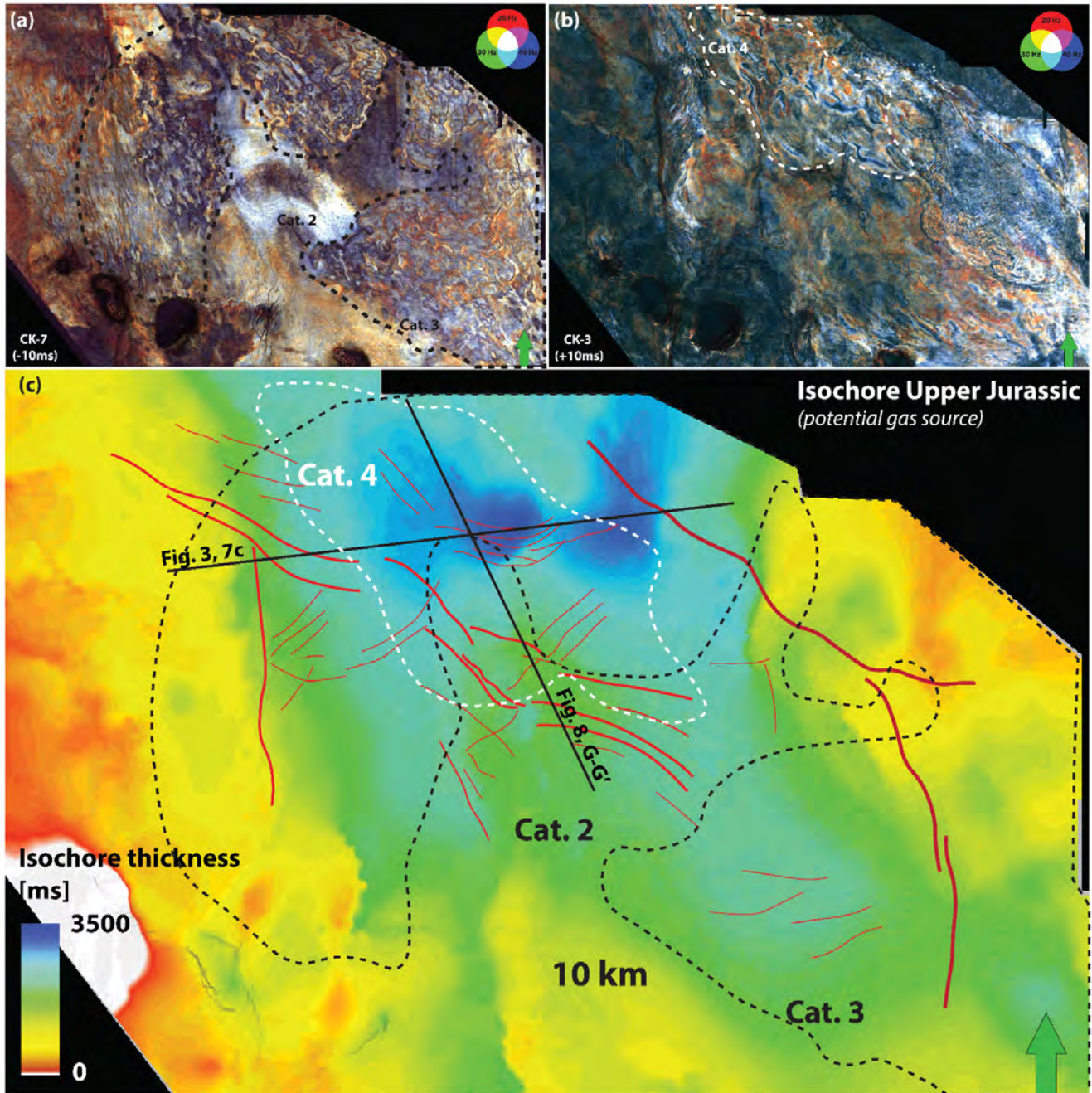


Figure 20. (a) Seismic stratigraphic horizon CK-7 (-10 ms) with spectral decomposition data in RGB blend. (b) Seismic stratigraphic horizon CK-3 (+10 ms) with spectral decomposition data in RGB blend. Spatial distribution of Category 4 features in white outline. (c) Isochore thickness of Upper Jurassic strata with main Late Jurassic faults in red outlines and Cat. 4 occurrence in white outlines. Corresponding seismic sections are indicated on black lines. A causal relationship is suggested between the occurrence of a thick Late Jurassic sedimentary package, deeply rooted faults, and the spatial occurrence of Category 4 features.

Category 5 features

The steep walls (75-90°) of the tube-shaped circular depressions of Category 5 make them different from the small pockmarks of Category 2 (3-10°) (Fig. 15). It is unlikely that these features formed

negative topography on the Cretaceous seafloor unless the chalk was consolidated, as mass movements and/or bottom currents would adjust the slope to the angle of repose. The seismic expression suggests that the strata are different from the surrounding chalks, and the downward shift from a

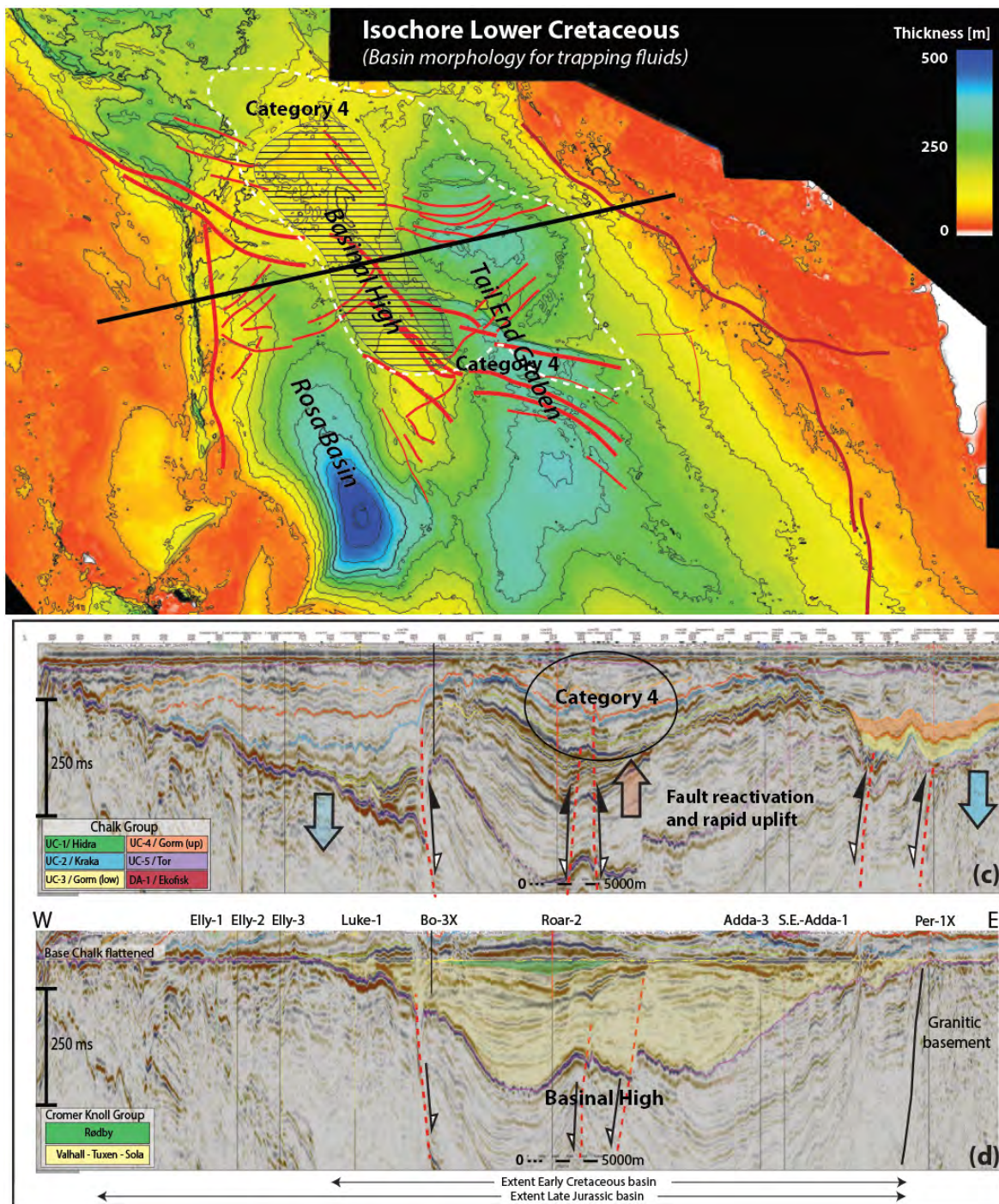


Fig. 21. (a) Spatial distribution Category 4 features (dashed area most pronounced and deepest) and faults at BCU level, projected on isochore of Lower Cretaceous. The isochore shows two depocenters (Rosa Basin and Tail End Graben), separated by a faulted basin high. Seismic section indicated with black line. (c-d) flattened seismic sections illustrating the basin inversion movement during Campanian times. At the basin high in the middle of the Lower Cretaceous basin, the most pronounced Category 4 features occur (see Figs 12a and h).

mid-amplitude peak to a high-amplitude trough and a basal high-amplitude peak suggests soft material at top, overlying hard material, until a downward transition to normal chalk (high-amplitude peak). Without well information, it is difficult to provide a solid interpretation. We see three options: 1) small pockmarks in consolidated chalk; 2) collapse

structures due to hypogenic karst; and 3) seep carbonate chimneys growing just below seafloor or in the water. Based on their steep-walled geometry, the occurrence around low-throw faults and in the vicinity of Category 6 features, we favour the last interpretation.

Category 6 features

The fault-bound high-acoustic impedance beds of Category 6 contain cryptocrystalline calcite that has very negative $\delta^{13}\text{C}$ (down to -40‰) (Figs 17 and 18). This is a good diagnostic feature to classify these as seep carbonate beds that form due to oxidation of methane (a highly negative $\delta^{13}\text{C}$ source) by sulphate reducing bacteria (Teichert *et al.*, 2005). They can occur as isolated beds in clays, or embedded in chalk (see examples Fig. 18). The methane can have a biogenic source (<-60‰), thermogenic source (>-60‰ for wet gas to -20‰ for dry gas), or a mix of both (Hitchman *et al.*, 1989; Stolper *et al.*, 2015). The purest beds in the Paleogene clays (H-1X, Fig 19) showed $\delta^{13}\text{C}$ values of -40 to -25‰, and could reflect a pure thermogenic source (wet and dry gas), or some mixing with a biogenic source. The occurrence of lateral seep carbonates beds in association with carbonate chimneys (Category 5) is common, as they share a similar formation origin (Bayon *et al.*, 2013).

Basin model and expulsion (biogenic gas and thermogenic)

The formation of Category 2 to 6 features are strongly linked to transportation of gas-bearing fluids along faults. In order to get a first order idea of possible sources of gas at the time of fluid expulsion, we have utilized a 3D basin model that predicts source rock thermal maturity (expressed in vitrinite reflectance) in the region over time. Three source rock levels are shown: Middle Jurassic coals, base Farsund Formation (start organic-rich interval), and Bo Member 'hot shale' at the top of the Farsund Formation (Fig. 22). Above 1.2% R_o dominantly gas is expelled from the source rocks. In addition, paleo-temperature maps at BCU level provides insight in the likelihood of biogenic gas formation (Fig. 23). Peak biogenic gas generation is assumed to occur at c. 40°C. The values given below reflect the variability in the area characterized by occurrence of Category 4 mega pockmarks (Fig. 9b).

During the Earliest Cretaceous (BCU level), Middle Jurassic coals show (modelled) vitrinite reflectance values between 1 and 3% R_o (Fig. 22a), the base of the Farsund Formation 0.2 to 0.5% R_o

(Fig. 22b), and Bo Member 0.2% R_o (Fig. 22c). The paleo-temperature at BCU level at this time was around 20°C (Fig. 23a). During chalk deposition in the earliest Late Cretaceous, modelled vitrinite reflectance values range from 2-4% R_o for the Middle Jurassic coals (Fig 22a'), to 0.5-2% R_o for the base Farsund Formation (Fig. 22b') and 0% for the Bo Member (Fig. 22c'). The paleo-temperature at the BCU at this time was between 30-50°C (Fig. 23b), increasing to 60-70°C at the time of the Campanian inversion (Fig. 23c).

During deposition of the youngest chalks (Danian), the Middle Jurassic coals have modelled vitrinite reflectance values of 2-5% R_o (Fig. 22a''), base Farsund Formation 1-2% R_o , and Bo Member 0.2-0.5% R_o . The paleo-temperature of the BCU at this time was 70-100°C (Fig. 23d).

The model thus indicates that candidates for triggering the formation of pockmarks at BCU level and in the Lower Cretaceous strata are thermogenic gas from the Middle Jurassic coals and biogenic gas from the organic-rich intervals of the Farsund Formation. The methane needed for the formation of seep carbonates in Lower Cretaceous strata was likely also sourced from these two intervals (Fig. 16b). The fluid expulsion and seep carbonates in the lowermost part of the Chalk Group (Fig. 15) could have been sourced by thermogenic gas from Middle Jurassic coals and organic-rich facies in the lower Farsund Formation. Biogenic gas from the upper sections of the Farsund Formation may have contributed (Fig. 22b'), but they were still immature for thermogenic gases (Fig. 22c'). The mega pockmarks therefore likely have formed by expulsion of gas accumulations of these combined sources. Biogenic gas from the Upper Jurassic strata likely stopped sometime after the Early Campanian as temperatures reached more than 60°C in the focus area (Fig. 23c).

During deposition of the youngest chalks (Danian), the lower Farsund Formation becomes much wider mature, and could have potentially formed an important source for the formation of the giant pockmarks found at the top of the Chalk Group (Figs 9a and 10), and might have also formed the methane source for the seep carbonates within the Paleogene and Neogene clays (Fig. 19).

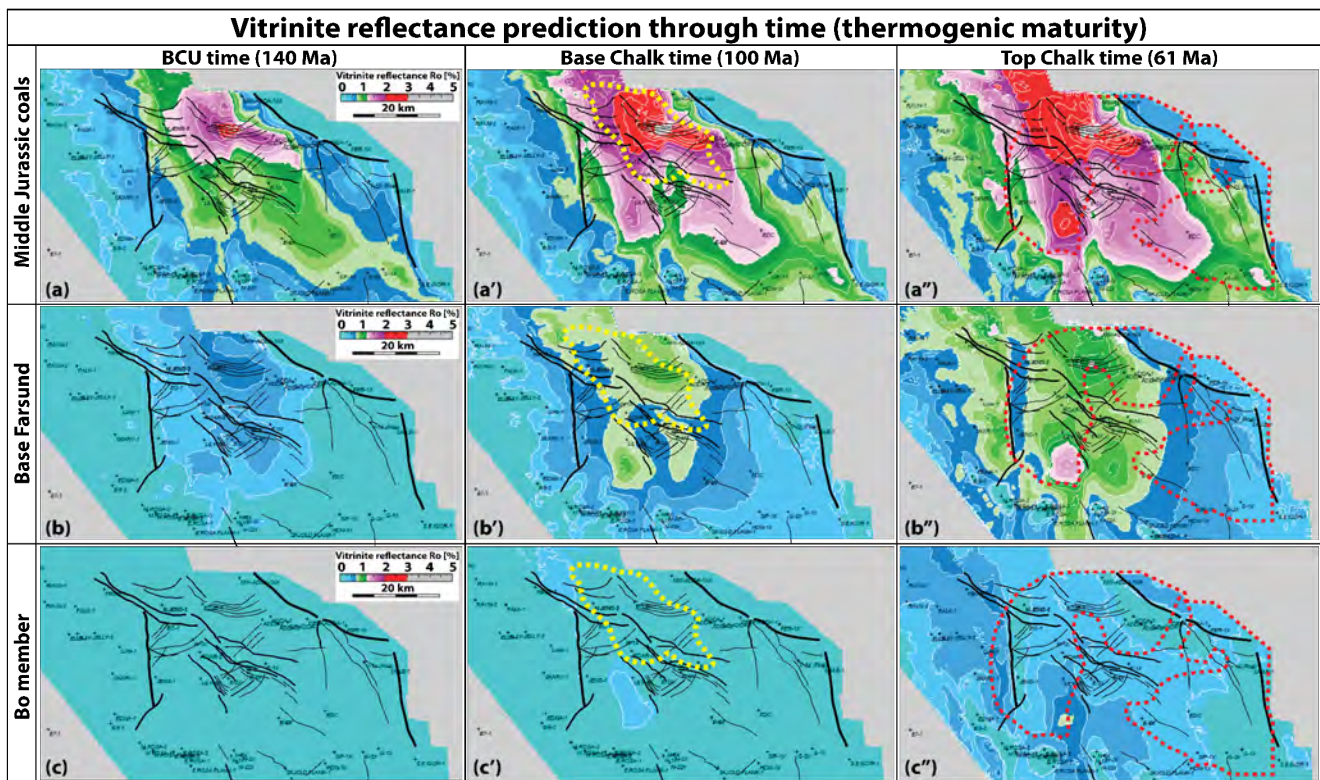


Figure 22. Modelled values of vitrinite reflectance (R_o in %) of three main source rocks in the study area at the start of the Cretaceous (BCU times, 140 Ma), start of the Cenomanian (base Chalk Group times, 100 Ma), end of the Danian (top Chalk Group times, 61 Ma). Dashed yellow outlines are Cat. 4 features (mega pockmarks), and dashed red outlines are Cat. 3 features (giant pockmarks) at top Chalk Group. (a-a'') Middle Jurassic coals of the Bryne Formation; (b-b'') Base Farsund Formation; (c-c'') Bo Member of the Farsund Formation ('hot shale' c.f. Ineson *et al.* 2003). Likely candidates for providing thermogenic gas-bearing fluids for the formation of mega pockmarks are the Middle Jurassic coals of the Bryne Formation, and lower parts of the organic rich Farsund Formation. The Bo member was immature at this time for providing thermogenically derived gas-bearing fluids.

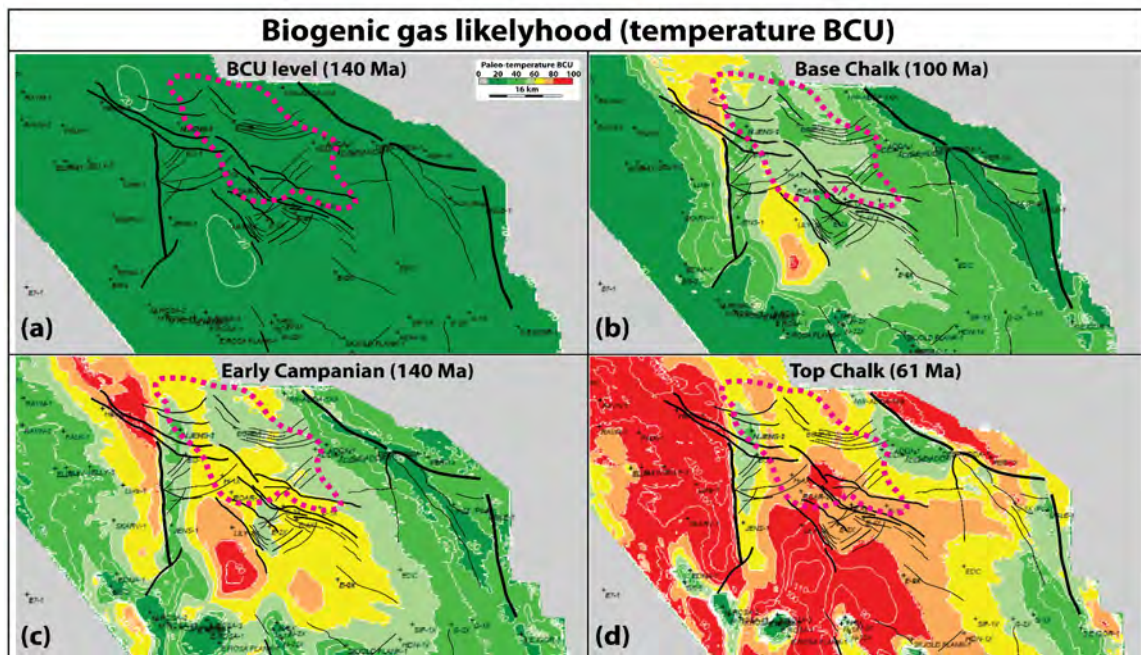


Figure 23. Modelled paleo-temperature of the BCU surface in the study area at (a) the start of the Cretaceous (BCU times, 140 Ma); (b) start of the Cenomanian (base Chalk Group times, 100 Ma); (c) time at the Campanian inversion (82 Ma); (d) end of the Danian (top Chalk Group times, 61 Ma). Dashed magenta outline reflects area of Cat. 4 features (mega pockmarks), while the black outline (d) reflects the area of Cat. 3 features (giant pockmarks). The palaeotemperatures in these regions depend on the burial history (e.g. rapid subsidence in the Rosa Basin led to fast increase in temperatures), and vary between 20 to 70 degrees. Following Schneider *et al.* (2016), with peak biogenic gas generation at 40°C (green colours) and termination at 65-70°C (yellow-orange), it is therefore likely that a biogenic source of gas-bearing fluids was possible for the formation of the fluid expulsion features.

Model for formation of the features

This paragraph will discuss our proposed model for the temporal formation of the features within the greater Roar Basin area, aided by the tectono-stratigraphic evolution described by van Buchem *et al.* (2018) as well as the basin modelling data (Fig. 22 and 23)

The earliest Cretaceous seafloor (BCU level) experienced thin-skinned slumping on the basin margins, causing extensional fault blocks to form (Category 1 features, Figs 5 and 7). Thermogenic gas from the Lower and Middle Jurassic strata had already commenced, as well as biogenic gas generation from Upper Jurassic strata (Fig. 22). The gas could migrate along Late Jurassic normal faults, and frequent fluid expulsion events created pockmarks within the slumped sediments (Fig 5c-d). These depressions would be further eroded by ocean currents to form long elongated depressions, as well as isolated hills and round valleys, which became filled in shortly after (Fig. 5, Table 1).

Deposition continued within the Early Cretaceous basin filling in the basin morphology (c.f. Vidalie *et al.*, 2014), while methane seepage occurred through Lower Cretaceous strata above major Late Jurassic faults, forming large-scale seep carbonate beds in the marls and chalks of the Tuxen and Sola Formation (Figs 16, 17, and 24a). This was most pronounced at the location of an Early Cretaceous basinal high, which potentially formed a focus point for ascending gas-bearing fluids (e.g. Figs 18b, 21a, and c).

During earliest chalk deposition in the Late Cretaceous, gas expulsions were not common, but methane seepage continued locally around faulted zones, where sulphate reducing bacteria formed seep carbonate chimneys and beds within and possibly above the chalk seafloor (Fig. 15, Category 5 features). Deposition continued uninterrupted until Coniacian times, when early basin inversion led to fault reactivation, followed by fluid expulsion that

created some giant pockmarks at CK-3 level (Figs 12h, 24b).

During the start of the Campanian, tectonic inversion was at its maximum, and caused rapid uplift of the Roar Basin, first by reactivation of basin bounding faults, followed by bulk uplift of the structure (Van Buchem *et al.*, 2018). The following scenario is envisaged: the uplift caused a rapid decrease in pressure, which caused an expansion of any accumulations of gas-bearing fluids contained within the Upper Jurassic to Lower Cretaceous strata. This caused large tensional forces on sealing packages, which consequently failed, and gas was funnelled towards the Campanian seafloor, facilitated by the newly reactivated faults. Enormous gas expulsions on the seafloor followed, causing mega-scale craters to form (Fig. 24c). Repetitive expulsions widened the craters further, while mass movements and bottom current activity adjusted the initial steep slope to more gentle U-shape slopes and filled in the depressions (Figs 11 and 12). The mega pockmarks cause disruption of the stratigraphy at a maximum of 250 m, reflected by many stratal terminations. Their spatial occurrence is restricted and is controlled by the following boundary conditions: 1) Above Late Jurassic depocenter (Fig. 20); 2) above an Early Cretaceous basinal high (Fig. 21); 3) faults that are deeply rooted in Late Jurassic strata (Figs 3 and 20). Together, the conditions favour a large drainage network, which is focussed towards the highest part in the basin, and pathways were guided by faults.

While tectonic activity waned during Late Campanian to Danian times, seals could be re-established, as indicated by the occurrence of smaller reactivation pockmarks (Category 2) and seep carbonates (Category 5) within the mega pockmarks (Fig. 14). A last phase of large-scale fluid expulsion occurred during Danian times, as giant pockmarks disrupt the top chalk surface significantly (Figs 9a and 24d). The spatial distribution of these giant pockmarks on post-inversion basinal highs that are

Figure 24. Temporal model for direct fluid migration indicators observed in the Jurassic to Eocene strata. See supplement 2 for a high-quality version. **(a)** Cenomanian. Methane derived from Bryne Formation and biogenic degradation from Upper Jurassic strata seeping along faults to form fault-bound seep carbonates formation within the Lower and earliest Upper Cretaceous strata **(b)** Santonian. Pre-inversion phase: earliest fluid migration event due to gas-mature Bryne Formation recorded at BCU level (latest Jurassic): fluidization structures and small pockmarks focused above Late Jurassic faults. Subsequently, seepage through Early Cretaceous strata led to pockmark formation and seep carbonate precipitation. Chalk deposition during Cenomanian – Santonian stages experienced local fluid expulsion events leading to small pockmarks, seep carbonate precipitation, both associated with Late Jurassic faults. Some larger pockmarks likely formed due to early inversion movements. **(c)** Campanian. Chalk deposition during the Campanian stage was characterized by mega pockmark formation as a result of major tectonic inversion movement along Late Jurassic faults, causing seal failure and rupturing of accumulated gas pockets within Late Jurassic to Early Cretaceous strata. Initially steep sloped, reworking by mass-movements and ocean currents likely created more U-shape depressions that are cup-shaped (e.g. different from contourite moats). **(d)** Paleogene. Chalk deposition during the Danian stage (Paleocene) was marked by giant pockmark formation and seep carbonate precipitation. Paleogene and Neogene mudstones covered the Chalk Group, but experienced syn-depositional polygonal faulting that affected its sealing capacity. Seep carbonates within the Paleocene – Eocene strata are evident that methane leaked out of the Chalk Group into the overburden.

faulted, suggests that fluids migration and expulsion was facilitated by the new basin morphology as well as structural pathways. The highly elongated morphology of these pockmarks is due to merging of individual depressions, caused by repetitive expulsion, mass wasting, and/or bottom current activity (Fig. 10). Finally, the Chalk Group was buried with Paleogene shales that became polygonal faulted at an early stage, forming a leaking seal (Cartwright *et al.*, 2003). While some gas accumulations formed in the chalk, at the highest points methane leaked out towards the Paleogene seafloor, resulting in the formation of pockmarks, as well as kilometre-scale seep carbonate beds (Figs 19 and 24d).

Discussion

An overlooked, early fluid expulsion phase

This study has made the case for direct fluid migration indicators from strata covering the latest Jurassic to Neogene time, and has shown how syn-sedimentary fluid expulsion has influenced stratigraphic architecture and created significant heterogeneities. Rapid burial of the organic-rich Fjerritslev Formation and coals of the Bryne Formation during the Late Jurassic rifting period, brought these source rocks rapidly into the hydrocarbon window, forming thermogenic gases. The rapid subsidence and sedimentation of the mainly marine mudstones of the Late Jurassic also facilitated generation of biogenic gases, which led to formation of the documented fluid expulsion features in this study. These events all pre-date the maturation of the Bo Member ('hot shale') of the Farsund Formation, which is considered the most important source rock for the petroleum plays in the Danish North Sea. Considering the spatial overlap between

the fluid expulsion features in the strata, and the present-day oil accumulation, it is likely that these fluid pathways were long-lived and re-used in subsequent hydrocarbon migration.

Thus, this 'forgotten' phase of fluid expulsion, anchored within the Late Jurassic to Eocene sediments and revealed with seismic geomorphological tools, provides us with important insights in the relationship between source rock maturation, fluid migration pathways, tectonic activity, and sedimentary response.

1. Late Jurassic faults form(ed) important hydrocarbon pathways into the Chalk Group during both hydrocarbon charging phases.
2. Eruptions of gas at the seafloor resulted in pockmarks, already observed at Earliest Cretaceous times. The gas was likely sourced from thermogenic source (Middle Jurassic coals) and biogenic source (degradation of organic-rich matter in Upper Jurassic strata).
3. Methane seepage resulted in microbially-mediated carbonate precipitates within Early Cretaceous strata, the Chalk Group, and within the Paleogene-Neogene polygonal faulted mudstones
4. Major tectonic inversion during the Campanian resulted in mega pockmark formation within the Chalk Group. While originally steep, slumping and bottom current activity generated more gentle slopes.
5. A renewed phase of tectonic activity led to formation of giant pockmarks at the top of the Chalk Group.
6. The polygonal faulted Paleogene – Neogene mudstones were likely semi-sealing until Mid-Miocene times, evident from the

occurrence of seep carbonates above the highest points in the chalk.

It provides us potentially with new ideas for exploration of hydrocarbons, as recognition of fluid expulsion features can indicate a (paleo-)source rock and fluid pathway. The high porosity of the chalk, which makes it an important reservoir, is often thought to originate from retardation of diagenesis by the establishment of overpressure and/or an early invasion of hydrocarbons. As the main expulsion of the Bo Member didn't start until the Late Miocene, the Chalk was already buried to around 1-1.5 km at this time. In the light of the observation that the polygonal faulted clays were perhaps not so sealing after all, the continuous hydrocarbon charge from the Bryne Formation and lower parts of the Farsund Formation might have been crucial to keep porosities high. Only after the second phase of rapid deposition during the Late Miocene: a) a better seal could form, as these strata were not polygonal faulted; b) the basin loading pushed the Late Jurassic source rocks into the hydrocarbon window, thereby invading the chalk for a second time and preserving the high porosity that we observe today.

Comparison to diagenetic geobodies in the Southern Central Graben

In a recent study, Smit *et al.* (2018) documented stratigraphy cross-cutting reflectors in chalk in the southern Central Graben (Ryan Anticline), and based on detailed petrographical and geochemical analysis, concluded that they represent fault-controlled diagenetic geobodies. While somewhat similar to the cross-cutting reflectors in the Roar Basin, there are marked differences between the two case studies.

First of all, the architecture of the features is markedly different. The cross-cutting reflectors in the Ryan case study have several seismic expressions (eight types, see Table 1 in Smit *et al.* 2018), and sections perpendicular to the long axis always show a V-shape. This reflects the strong coupling to low-thrust faults that are dictated by the underlying fault fabric and occur throughout the chalk with an angle between 45-55°. Seismic markers can often be traced

through the bodies, showing that the infill architecture is similar to outside. In the Roar Basin, the infill is significantly different from outside the features, indicating occurrence of different strata. Also, the 3D architecture follows an upside-down Christmas tree in the Ryan Anticline, reflecting the occurrence of intra-formational barriers and permeable vertical fractured zones. This is not observed in the Roar Basin, where it represents an upward widening zone reflecting the pockmark depositional profile.

Secondly, the petrography and geochemistry indicate a stronger diagenetic overprint of the strata within the cross-cuts than outside. This includes high Mn/Sr ratios, very negative $\delta^{18}O$ values, and occurrence of largely cemented zones with dolomite. This has not been observed in the Roar Basin.

Lastly, within the Ryan geobodies, no pockmarks have been recognized as has been in the Roar Basin (Fig. 14). This could be the result of a different basin morphology during the Jurassic between the two locations, where in the Roar area a deep Late Jurassic depocenter formed of organic-rich marine shales, but not in the Ryan area (Fig. 25). Therefore, limited burial occurred in the Ryan area, as well as occurrence of limited organic-rich Jurassic shales that could produce biogenic gas. The result is that in the Roar Basin syn-depositional fluid expulsion features occur (mega pockmarks), and in the Ryan area post-depositional diagenetic geobodies.

Summary of an updated chalk paradigm

The chalk depositional paradigm has significantly moved away from a pure pelagic rain of coccolith material forming pancake stratigraphy, to a highly dynamic seafloor recorded in the highly irregular geometries found within a typical seismic section through the Chalk Group. These architectural heterogeneities are caused by primary (syn-) depositional features and later post-depositional overprinting, and a general summary is given in Table 2. The first category encompasses pelagic chalks, well documented examples of moat and drift complexes from bottom current activity (Esmerode *et al.*, 2007; Lykke-Andersen and Surlyk, 2004), and

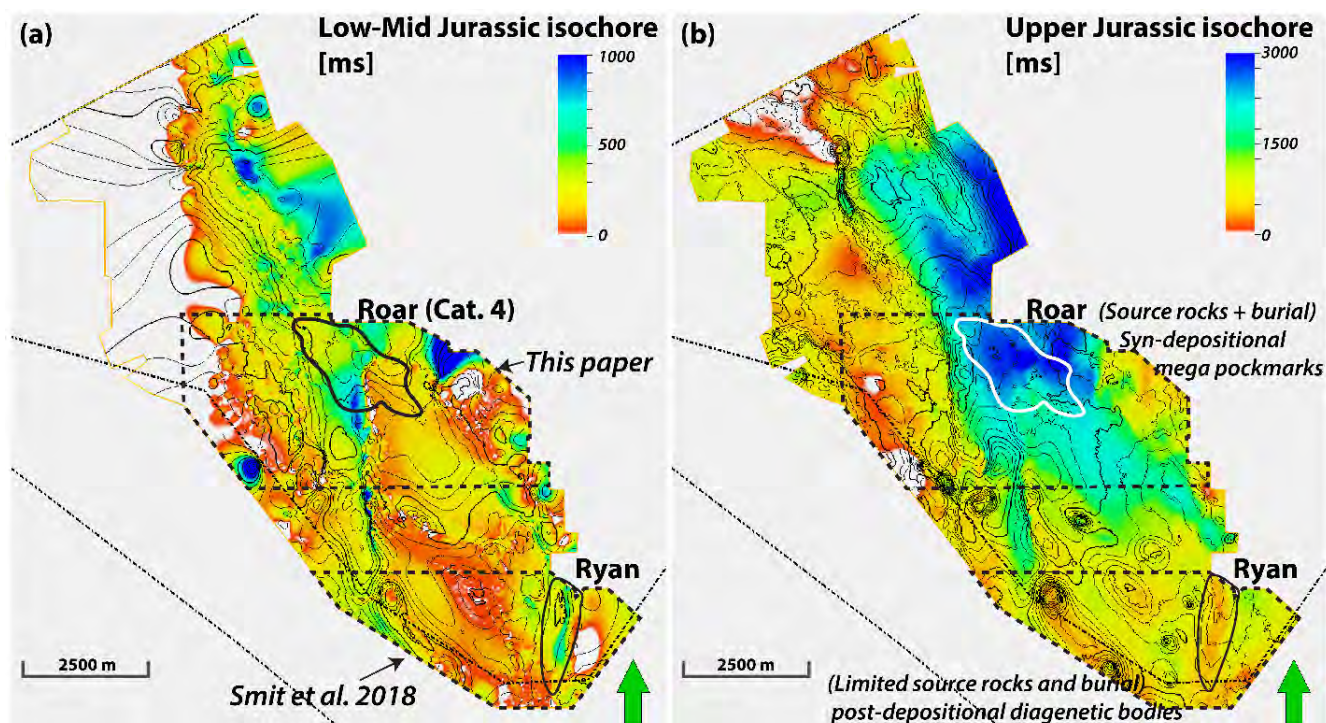


Figure 25. Basin-wide isochores with outlines of syn-depositional mega pockmarks in the Roar Basin and post-depositional diagenetic geobodies on the Ryan Anticline. Study areas indicated by dashed black line. Area of mega pockmarks in Roar indicated by black/white solid line, and diagenetic bodies on the Ryan Anticline by black solid lines. **(a)** Lower-Middle Jurassic isochore thickness. A deep N-S basin at Roar can be observed. A smaller basin formed at Ryan. **(b)** Upper Jurassic isochore thickness. A deep depocenter occurs at the Roar Basin location, which brings the Middle Jurassic coals into the hydrocarbon window, as well as stimulates formation of biogenic gas. At Ryan, limited accommodation is available due to the anticlinal structure, so that limited burial is possible. Thus at Roar there were likely significantly more source rocks present, as well as burial, resulting in larger amount of gas formation. These two conditions are not met at Ryan, which resulted in post-deposition basinal (non gas-bearing) fluids to cause diagenetic alteration

slope failures as a result of structural deformation (Gennaro et al., 2013; Smit et al., 2017; Van Buchem et al., 2018; van der Molen, 2004). This study has made the case for adding syn-depositional features caused by gas venting and related reworking of the chalk to the first category. These features are widespread on top of inverted structural highs, which also formed the main loci for hydrocarbon accumulations. Recognizing these new type of features within the Chalk Group is thus of significant importance for reservoir characterization. The second category encompasses post-depositional structural deformation to form fractured zones, and post-depositional diagenetic overprinting that generated seismic-scale geobodies as a result of compaction and precipitation of diagenetic calcite (Smit et al., 2018, 2017). To conclude, it has become clear that the Chalk Group has experienced several phases of both syn-depositional and post-depositional fluid

migration and expulsion (gas, oil, and water), which have become recorded in the stratigraphy. Depending on location with respect to thickness and burial of organic-rich Jurassic intervals, different types of fluid migration indicators have manifested itself. The spatial control of these features is strongly coupled to the underlying fault fabric as well as the tectonic history of the Late Cretaceous basin, and provide important insights in fluid migration pathways for the formation of the main hydrocarbon accumulations in the Danish Central Graben in the Early Miocene when the Bo Member became thermally mature.

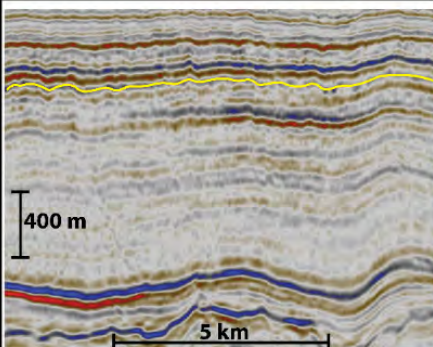
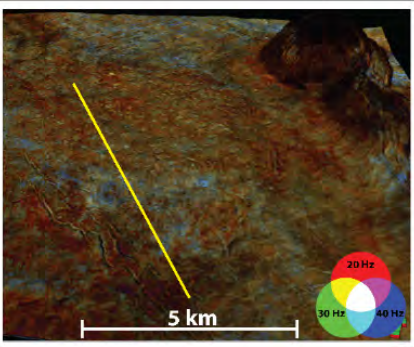
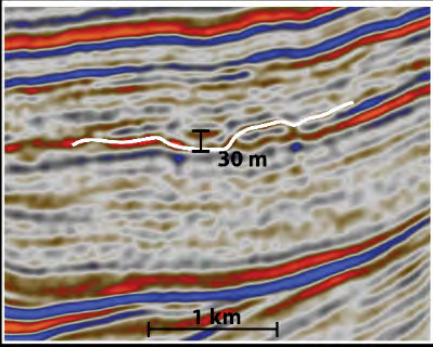
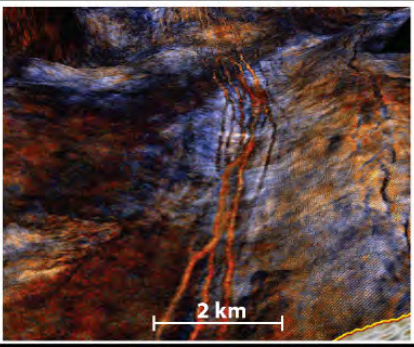
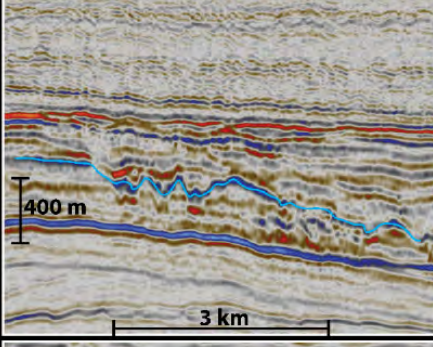
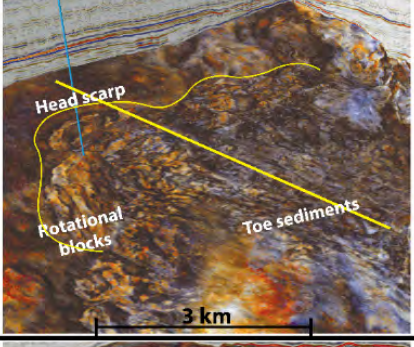
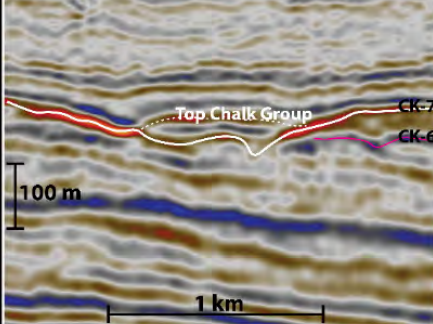
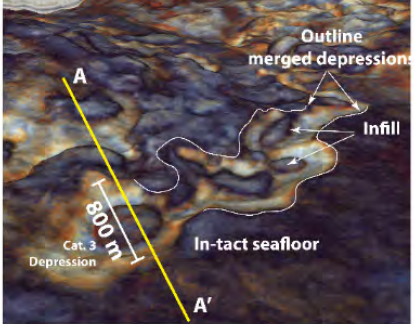
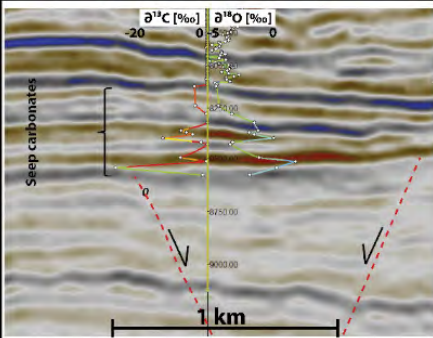
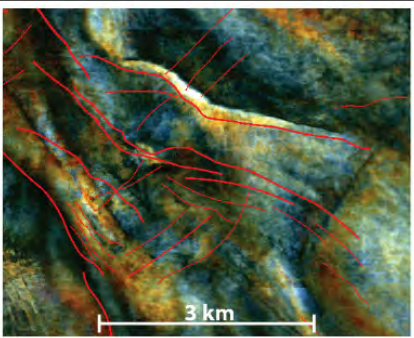
	Type	2D seismic example	3D seismic example
1. (syn-) depositional features	A. Pelagic deposition		
	B. Bottom current activity		
	C. Slope failure		
	D1. Gas venting (explosive)		
	D2. Gas venting (seepage)		

Table 2. Generalized overview of the different types of syn-depositional seismic facies in the Chalk Group. 1B from Smit *et al.* (2017)

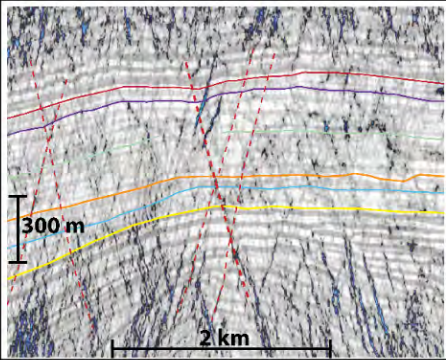
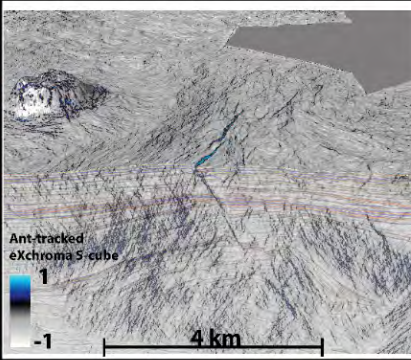
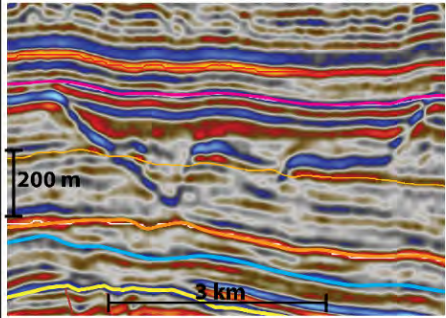
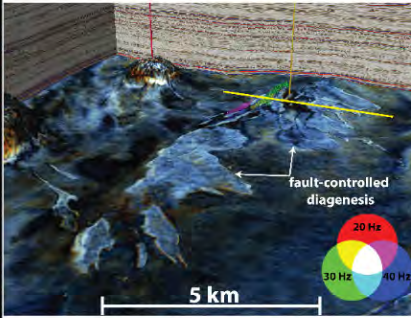
	Type	2D seismic example	3D seismic example
2. Post-depositional features	A. Structural deformation		
	B. Diagenetic overprint		

Table 3. Generalized overview of the different types of post-depositional seismic facies in the Chalk Group. 2B from Smit *et al.* (2018).

Conclusions

- This study documents direct fluid migration indicators in uppermost Jurassic to Neogene strata in the Roar Basin, Danish North Sea and thereby enable us to record an extended period of fluid expulsion events driven by maturation of coals of the Bryne Formation and biogenic gas from Upper Jurassic strata starting as early as the latest Jurassic.
- The fluid migration history distilled from the seismic sedimentary record starts with latest Jurassic slumping and pockmark formation at the Base Cretaceous Unconformity, is followed by Early Cretaceous pockmark formation and seep carbonate precipitation through fault-bound methanogenesis. During Late Cretaceous, pre-inversion time (Hydra and Kraka Formations) the first carbonate chimneys and small pockmark formed. During inversion (Gorm Formation) mega-pockmarks formed as a result of rapid uplift of the Roar Basin (fluid expansion), coupled with fault reactivation, causing explosive eruptions at the Campanian seafloor. Smaller reactivation pockmarks or carbonate chimneys occur within the

infill of the mega pockmarks. Following inversion (Tor and Ekofisk Formations) small reactivation pockmarks within Maastrichtian strata and giant pockmarks at the Top Chalk indicate renewed tectonic activity. The Paleogene and Neogene were affected by polygonal faulting, pockmark formation, and seep carbonate precipitation

- Likely sources for the fluid expulsion include thermogenic gas from Middle Jurassic coal and Jurassic shale of the Farsund formation, including Bo Member. Basin modelling indicates maturation of the Bryne Formation coals already during the latest Jurassic, lower Farsund shales during the Cenomanian whereas Bo Member was not matured until after deposition of the chalk.
- Biogenic sources include Upper Jurassic strata during Latest Jurassic to Danian times.
- The early charge of hydrocarbons from this phase might have played an important role in retardation of porosity reduction of the Chalk Group and maintaining overpressure, as a semi-leaking seal caused seepage out of the reservoir. This occurred before the Bo Member became mature and charged the reservoirs with present-day hydrocarbon accumulations.

- Lastly, the Roar and Ryan case studies both show stratigraphy cross-cutting reflectors. The Roar Basin reflectors are of syn-depositional origin, whereas the Ryan reflectors are of post-depositional origin. We suggest this is because of the limited burial of Middle Jurassic strata and limited Upper Jurassic depocenter in the Ryan area.

Acknowledgements

The authors kindly acknowledge the Danish Underground Consortium (Total, Shell, Chevron, and Nordsøfonden) for providing seismic and well data and the permission to publish the results. We kindly want to thank the follow software companies for providing academic licenses: Schlumberger is kindly thanked for providing Petrel E&P, Eliis is kindly thanked for providing PaleoScan™, and ffA GeoTeric is kindly thanked for GeoTeric. Peter Hillock, Niels Schodt, Peter Gelting, and Jorgen Toft, of Total Denmark are greatly thanked for their input during technical discussions. The research leading to these results has received funding from the Danish Hydrocarbon Research and Technology Centre under the Advanced Water Flooding program.

References

- Andresen, K. J., Huuse, M., & Clausen, O. R. (2008). Morphology and distribution of Oligocene and Miocene pockmarks in the Danish North Sea—implications for bottom current activity and fluid migration. *Basin Research*, 20(3), 445-466.
- Bayon, G., Dupré, S., Ponzevera, E., Etoubleau, J., Chéron, S., Pierre, C., Mascle, J., Boetius, A., Lange, G.J. De, 2013. Formation of carbonate chimneys in the Mediterranean Sea linked to deep-water oxygen depletion. *Nature Geoscience*, 6(9), 755
- Betzler, C., Lindhorst, S., Hübscher, C., Lüdmann, T., Fürstenau, J., & Reijmer, J. (2011). Giant pockmarks in a carbonate platform (Maldives, Indian Ocean). *Marine Geology*, 289(1-4), 1-16.
- Cartwright, J. A. (1989). The kinematics of inversion in the Danish Central Graben. Geological Society, London, Special Publications, 44(1), 153-175.
- Cartwright, J., James, D., & Bolton, A. (2003). The genesis of polygonal fault systems: a review. Geological Society, London, Special Publications, 216(1), 223-243.
- Cole, D., Stewart, S. A., & Cartwright, J. A. (2000). Giant irregular pockmark craters in the Palaeogene of the outer Moray Firth basin, UK North Sea. *Marine and Petroleum Geology*, 17(5), 563-577.
- Esmerode, E. V., Lykke-Andersen, H., & Surlyk, F. (2008). Interaction between bottom currents and slope failure in the Late Cretaceous of the southern Danish Central Graben, North Sea. *Journal of the Geological Society*, 165(1), 55-72.
- Esmerode, E. V., Lykke-Andersen, H., & Surlyk, F. (2007). Ridge and valley systems in the Upper Cretaceous chalk of the Danish Basin: contourites in an epeiric sea. Geological Society, London, Special Publications, 276(1), 265-282.
- Fehmers, G. C., Printz, B., & Febriany, G. (2012, June). Mapping of gas migration into, and out of, the Tyra Field in the Danish North Sea. In 74th EAGE Conference and Exhibition incorporating EUROPEC 2012.
- Gemmer, L., Huuse, M., Clausen, O. R., & Nielsen, S. B. (2002). Mid-Palaeocene palaeogeography of the eastern North Sea basin: integrating geological evidence and 3D geodynamic modelling. *Basin Research*, 14(3), 329-346.
- Gennaro, M., Wonham, J. P., Gawthorpe, R., & Sælen, G. (2013). Seismic stratigraphy of the chalk group in the Norwegian Central Graben, North Sea. *Marine and Petroleum Geology*, 45, 236-266.
- Gennaro, M., Wonham, J. P., Sælen, G., Walgenwitz, F., Caline, B., & Fay-Gomord, O. (2013). Characterization of dense zones within the Danian chalks of the Ekofisk Field, Norwegian North Sea. *Petroleum Geoscience*, 19(1), 39-64.
- Hancock, J. M. (1975). The petrology of the Chalk. *Proceedings of the Geologists' Association*, 86(4), 499-535.
- Heggland, R. (1997). Detection of gas migration from a deep source by the use of exploration 3D seismic data. *Marine Geology*, 137(1-2), 41-47.
- Henriksen, K., Gommessen, L., Hansen, H. P., Kistrup, J. P., & Steekelenburg, C. (2009, January). Optimizing Chalk Reservoir Development Using Detailed Geophysical Characterization: The Halfdan Northeast Field, Danish North Sea. In *Offshore Europe*. Society of Petroleum Engineers.
- Hitchman, S. P., Darling, W. G., & Williams, G. M. (1990). Stable isotope ratios in methane containing gases in the United Kingdom.
- Hovland, M., & Judd, A. (1988). Seabed pockmarks and seepages: impact on geology, biology, and the marine environment. Springer.
- Ineson, J. R., Bojesen-Koefoed, J. A., Dybkjær, K., & Nielsen, L. H. (2003). Volgian–Ryazanian ‘hot shales’ of the Bo Member (Farsund Formation) in the Danish Central Graben, North Sea: stratigraphy, facies and geochemistry. *The Jurassic of Denmark and Greenland*. Geological Survey of Denmark and Greenland Bulletin, 1, 403-436.

- Japsen, P., Britze, P., & Andersen, C. (2003). Upper Jurassic–Lower Cretaceous of the Danish Central Graben: structural framework and nomenclature. *The Jurassic of Denmark and Greenland. Geological Survey of Denmark and Greenland Bulletin*, 1, 233–246.
- Judd, A., & Hovland, M. (2009). *Seabed fluid flow: the impact on geology, biology and the marine environment*. Cambridge University Press.
- Kubala, M., Bastow, M., Thompson, S., Scotchman, I., Oygard, K., 2003. Geothermal regime, petroleum generation and migration, in: *The Millennium Atlas: Petroleum Geology of the Central and Northern North Sea*. Geological Society of London, pp. 289–315.
- Kyrkjebø, R., Gabrielsen, R. H., & Faleide, J. I. (2004). Unconformities related to the Jurassic–Cretaceous synrift–post-rift transition of the northern North Sea. *Journal of the Geological Society*, 161(1), 1–17.
- Loneragan, L., Cartwright, J., Laver, R., & Staffurth, J. (1998). Polygonal faulting in the Tertiary of the central North Sea: implications for reservoir geology. *Geological Society, London, Special Publications*, 127(1), 191–207.
- Lykke-Andersen, H., & Surlyk, F. (2004). The Cretaceous–Palaeogene boundary at Stevns Klint, Denmark: inversion tectonics or sea-floor topography?. *Journal of the Geological Society*, 161(3), 343–352.
- Masoumi, S., Reuning, L., Back, S., Sandrin, A., & Kukla, P. A. (2014). Buried pockmarks on the Top Chalk surface of the Danish North Sea and their potential significance for interpreting palaeocirculation patterns. *International Journal of Earth Sciences*, 103(2), 563–578.
- Møller, J. J., & Rasmussen, E. S. (2003). Middle Jurassic–Early Cretaceous rifting of the Danish Central Graben. *The Jurassic of Denmark and Greenland. Geological Survey of Denmark and Greenland Bulletin*, 1, 247–264.
- Petersen, H. I., & Nytoft, H. P. (2007). Are Carboniferous coals from the Danish North Sea oil-prone. *Geological Survey of Denmark and Greenland Bulletin*, 13, 13–16.
- Petersen, H. I., Andsbjerg, J., Bojesen-Koefoed, J. A., & Nytoft, H. P. (2000). Coal-generated oil: source rock evaluation and petroleum geochemistry of the Lulita oilfield, Danish North Sea. *Journal of Petroleum Geology*, 23(1), 55–90.
- Rasmussen, E.S., Vejbaek, O.V., Bidstrup, T., Piasecki, S., Dybkær, K., 2005. Late Cenozoic depositional history of the Danish North Sea Basin: implications for the petroleum systems in the Kraka, Halfdan, Siri and Nini fields, in: *Petroleum Geology: North-West Europe and Global Perspectives – Proceedings of the 6th Petroleum Geology Conference*. Geological Society of London, pp. 1347–1358.
- Schiøler, P., Andsbjerg, J., Clausen, O. R., Dam, G., Dybkær, K., Hamberg, L., ... & Rasmussen, J. A. (2007). Lithostratigraphy of the Palaeogene–Lower Neogene succession of the Danish North Sea (Vol. 12). Geological Survey of Denmark and Greenland.
- Schneider, F., Dubille, M., Montadert, L. (2016) Modeling of microbial gas generation: application to the eastern Mediterranean “Biogenic Play”. *Geologica Acta*, 14, issue 4, 403–417
- Smit, F.W.H., van Buchem, F.S.P., Schmidt, I., & Stemmerik, L. (2017). Updated seismic geomorphological workflow applied to the Chalk Group. In 2017 SEG International Exposition and Annual Meeting. Society of Exploration Geophysicists.
- Smit, F.W.H. (2014). Seismic stratigraphy, basin evolution and seismic geomorphology of the Late Cretaceous and earliest Paleocene Chalk Group in the Danish Central Graben. MSc thesis, Aarhus University, Denmark
- Smit, F. W. H., van Buchem, F. S. P., Holst, J. H., Lüthje, M., Anderskov, K., Thibault, N., ... & Welch, M. (2018). Seismic geomorphology and origin of diagenetic geobodies in the Upper Cretaceous Chalk of the North Sea Basin (Danish Central Graben). *Basin Research*.
- Stolper, D. A., Lawson, M., Davis, C. L., Ferreira, A. A., Neto, E. S., Ellis, G. S., ... & Sessions, A. L. (2014). Formation temperatures of thermogenic and biogenic methane. *Science*, 344(6191), 1500–1503.
- Strozyk, F., Reuning, L., Back, S., & Kukla, P. (2018). Giant pockmark formation from Cretaceous hydrocarbon expulsion in the western Lower Saxony Basin, The Netherlands. *Geological Society, London, Special Publications*, 469, SP469–6.
- Sun, Q., Wu, S., Hovland, M., Luo, P., Lu, Y., & Qu, T. (2011). The morphologies and genesis of mega-pockmarks near the Xisha Uplift, South China Sea. *Marine and Petroleum Geology*, 28(6), 1146–1156.
- Teichert, B. M., Bohrmann, G., & Suess, E. (2005). Chemohermes on Hydrate Ridge—Unique microbially-mediated carbonate build-ups growing into the water column. *Palaeogeography, Palaeoclimatology, Palaeoecology*, 227(1), 67–85.
- Van Buchem, F.S.P., Smit, F.W.H., Buijs, G.J.A., Trudgill, B., Larsen, P.H., Trudgil, B., Larsen, P.H., (2018). Tectonostratigraphic framework and depositional history of the Cretaceous – Danian succession of the Danish Central Graben (North Sea) – new light on a mature area, in: Bowman, M.B., Levell, B. (Eds.), *Petroleum Geology of NW Europe: 50 Years of Learning - Proceedings of the 8th Petroleum Geology Conference*. Geological Society of London, pp. 9–46.
- Van Der Molen, A. S. (2004). Sedimentary development, seismic stratigraphy and burial compaction of the Chalk Group in the Netherlands North Sea area. PhD dissertation, Department of Earth Sciences. University of Utrecht

- Vejbæk, O. V. (2002). Reservoir characterization of the Roar Gas Field, Danish North Sea. *Petroleum Geoscience*, 8(1), 71-87.
- Vejbæk, O. V., & Andersen, C. L. A. U. S. (2002). Post mid-Cretaceous inversion tectonics in the Danish Central Graben—regionally synchronous tectonic events. *Bulletin of the Geological Society of Denmark*, 49(2), 93-204.
- Vidalie, M., van Buchem, F.S.P., Schmidt, I., & Uldall, A. (2014). Seismic stratigraphy of the Lower Cretaceous Valhall Formation (Danish Graben, North Sea). *First Break*, 32(6), 71-80.

Chapter IV, Paper 3

Amalgamated pockmarks on the Danian seafloor caused by large-scale outbursts of gas-bearing fluids (Chalk Group, Greater Dan Region, Danish Central Graben)

F.W.H. Smit^{1*}, F.S.P. van Buchem², M. L  thje¹, P.K. Swart³, P.T. Staudigel³, L. Stemmerik⁴

Submission to Marine and Petroleum Geology

¹ Technical University of Denmark, Danish Hydrocarbon Research and Technology Centre, Elektrovej Building 375, 2800 Kongens Lyngby

² Halliburton-Landmark Exploration Insights, 97 Jubilee Avenue, Milton, Abingdon, OX14 4RW, UK.

³ Department of Marine Geosciences, University of Miami, Rosenstiel School for Marine and Atmospheric Sciences, 4600 Rickenbacker Causeway, Miami, FL 33149, USA

⁴ University of Copenhagen, Natural History Museum of Denmark, Øster Voldgade 5-7, 1350 Copenhagen K

* Corresponding author: fsmit@dtu.dk

Abstract

A large field of giant pockmarks is documented in Danian chalk of the hydrocarbon-bearing Ekofisk Formation on the Tyra-Igor-Emma Ridge in the Danish Central Graben. Integration of 3D seismic data, wireline logs and geochemical data shows round to highly elongated depressions 100-500 m across, 0.1 – 1.5 km long, and 25-75 m deep with Danian chalk or marl infill with $\delta^{13}\text{C}$ values different from the outside sediments. In addition, clumped isotope data show that the intact Danian seafloor and infill experienced similar closed-system burial diagenesis with increasing cementation temperatures reflected by increasingly more negative $\delta^{18}\text{O}$ values, which is common in normal burial diagenesis. The depressions are therefore interpreted to reflect seafloor topography rather than diagenetic overprinting. Close correlation between the occurrence of giant pockmarks and underlying Late Jurassic normal faults on inverted Campanian structures suggests that the faults formed the main fluid pathways towards highest parts of the basin, where expulsion of fluids created large craters on the Danian seafloor. Gas-bearing fluids originated from thermogenic (Middle Jurassic coals) or biogenic sources (degradation of organic material in Upper Jurassic source rocks) and the pockmarks therefore provide insights into the source rock maturity, tectonic evolution, and fluid migration during the Late Cretaceous. The pockmarks create reservoir heterogeneity that influences the position of the gas-water-contact and sweep efficiency in the Halfdan NE Gas Field. Therefore, understanding the distribution of these facies is of great importance for mapping reservoir quality, defining the top of the Chalk Group, and instrumental for future well planning. Giant pockmarks on top of inverted Campanian structures are firmly added to the catalogue of seismic features within the Chalk Group, as precursor fluid migration indicators (from an earlier expulsion phase) of the main hydrocarbon accumulations found at present.

Keywords: clumped isotope analysis, seismic geomorphology, fluid migration pathways, tectonic inversion, expulsion

Introduction

Fluid migration and charging are important elements of a petroleum play, yet are not possible to observe directly from static data (e.g. seismic and well data), but are rather inferred from dynamic data (e.g. charge simulations in basin modelling studies). This means that we can only *infer* fluid migration from static data if these events leave behind traces in the (seismic) sedimentary record. Syn-depositional fluid migration or expulsion can lead to formation of seismic-scale pockmarks, furrows, and seep carbonates (Andresen *et al.*, 2008; Andresen and Huuse, 2011; Betzler *et al.*, 2011; Teichert *et al.*, 2005), while post-deposition fluid migration and expulsion can alter rocks properties by dolomitization and porosity-reducing compaction (see for a seismic-scale example in chalk: Smit *et al.*, 2018). Such features can be visualized using seismic geomorphological workflows, and further characterized through integration with petrographic and geochemical data from wells (Smit *et al.*, 2017). In addition to recording events, they can highly influence reservoir quality that may influence recovery factor and/or sweep efficiency (Henriksen *et al.*, 2009). It is therefore key to recognize these features in reservoirs for exploration purposes (indicating early expulsion), as well as production purposes and well planning (reservoir quality).

Pockmarks are seafloor depressions that form during catastrophic outbursts of fluids, which leave behind steep-walled V-shaped craters that subsequently become modified by reworking and bottom current activity to form more U-shaped morphologies (Betzler *et al.*, 2011). Importantly, reworking processes in a large field can create a very complex morphology that can be difficult to interpret.

In this study, we investigate features in the hydrocarbon-bearing Ekofisk Formation at the top of the Upper Cretaceous to lowermost Paleocene Chalk Group in the Tyra, Halfdan, and Dan gas fields in the Danish North Sea (Figs 1 and 2a). We describe their morphology and stratigraphy, and investigate their spatial distribution with respect to the underlying Late Jurassic fault fabric. The spatial and temporal

occurrences of these features are placed in the tectono-stratigraphic framework of van Buchem *et al.* (2018), and are linked to maturation of potential Jurassic source rocks. Finally, we will conclude on their origin and propose a model for their formation. A discussion will follow on the significance of the features within the Chalk Group for exploration purposes, as well as implications for production and well planning within the hydrocarbon-bearing formations.

Geological Setting

The study area is located in the central portions of the Danish Central Graben on top of the Igor-Emma Ridge (Fig. 1). It encompasses the Greater Dan Region, including the Dan, Halfdan Main, Halfdan NE, and Tyra SE hydrocarbon fields (Fig. 2). The Igor-Emma Ridge formed in response to compressional forces during a Mid-Cretaceous inversion event, which caused former Late Jurassic basin to be uplifted (van Buchem *et al.*, 2018) (Fig. 2). First the tectonostratigraphic evolution of the Danish Central Graben is discussed, followed by a brief description of relevant stratigraphy.

Tectonostratigraphic evolution

The Danish Central Graben forms the southernmost branch of the North Sea Central Graben (Fig. 1a, inset). It comprises a complex set of half-grabens bounded to the south and east by the Ringkøbing-Fyn High, and to the west by the Mid North Sea High (Figs 1 and 2). The half-grabens formed during two major tectonic rifting phases, (Japsen *et al.* 2003; Fig. 3 for an overview of lithostratigraphic units and major tectonic events). During the Permo-Triassic, an E–W oriented stress regime led to N–S oriented half-grabens (Glennie *et al.*, 2003; Goldsmith *et al.*, 2003), whereas Late Jurassic rifting occurred in a NE–SW oriented stress regime, leading to generally NW–SE oriented half-grabens (Fraser *et al.*, 2002). In the study area substantial creation of accommodation combined with high sedimentation rates led to deposition of thick Upper Jurassic siliciclastic successions (up to 2.5 km thick) below the Chalk Group (Fig. 2b).

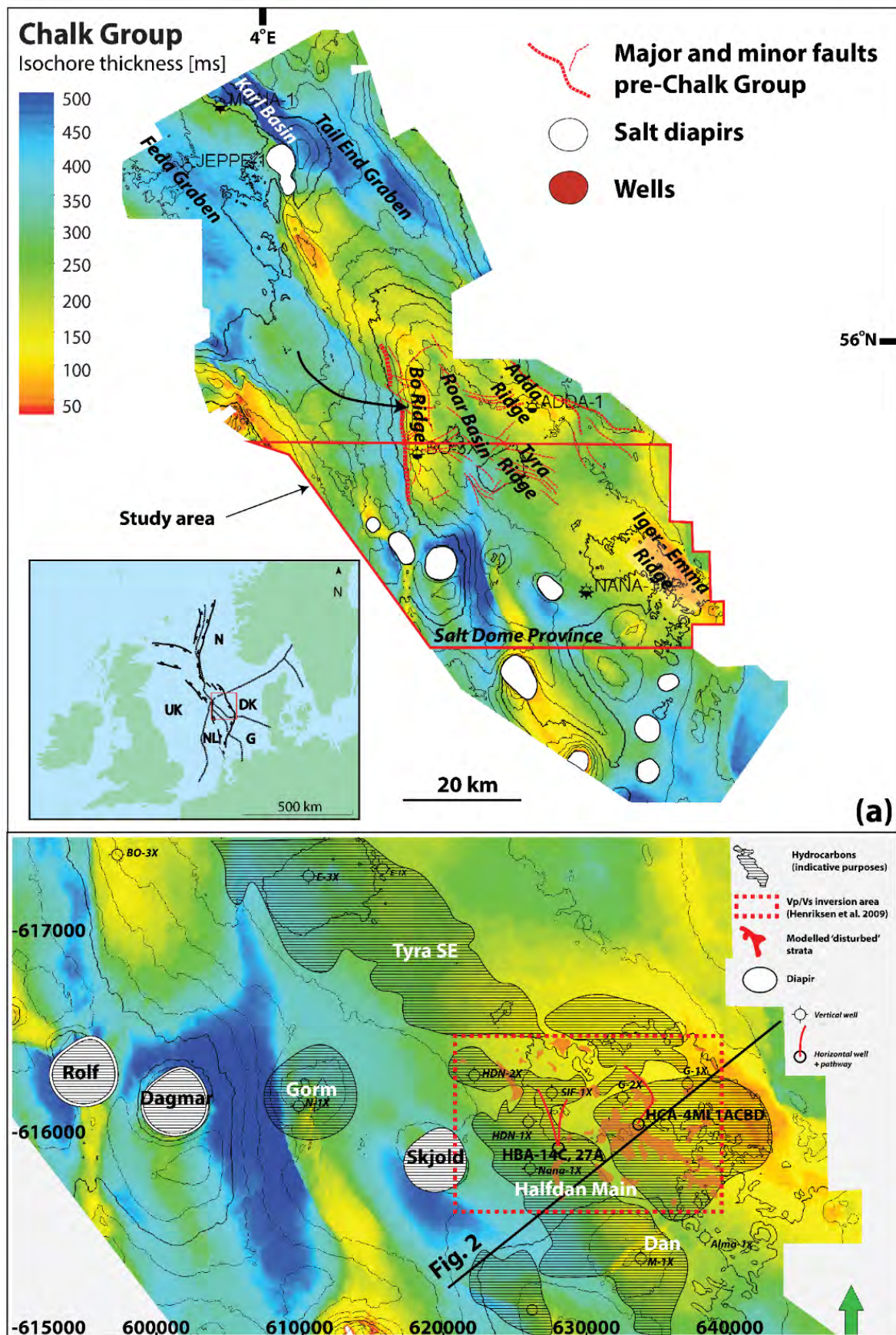


Figure 1. (a) Chalk Group isochore (Late Cretaceous – Paleocene) and its location within the North Sea Basin (inset), where UK = United Kingdom; NL = Netherlands; G = Germany; DK = Denmark; N = Norway. Contours mark the present-day top Chalk Group structure ((b) Close-up of the study area showing major fault systems in the pre-chalk strata. Relevant wells are displayed as well as orientation of seismic transects. Hydrocarbons in Lower Cretaceous chalks as black outlines with dots, in Upper Cretaceous chalks as white outlines with stripes. (a-d) from van Buchem *et al.* 2018

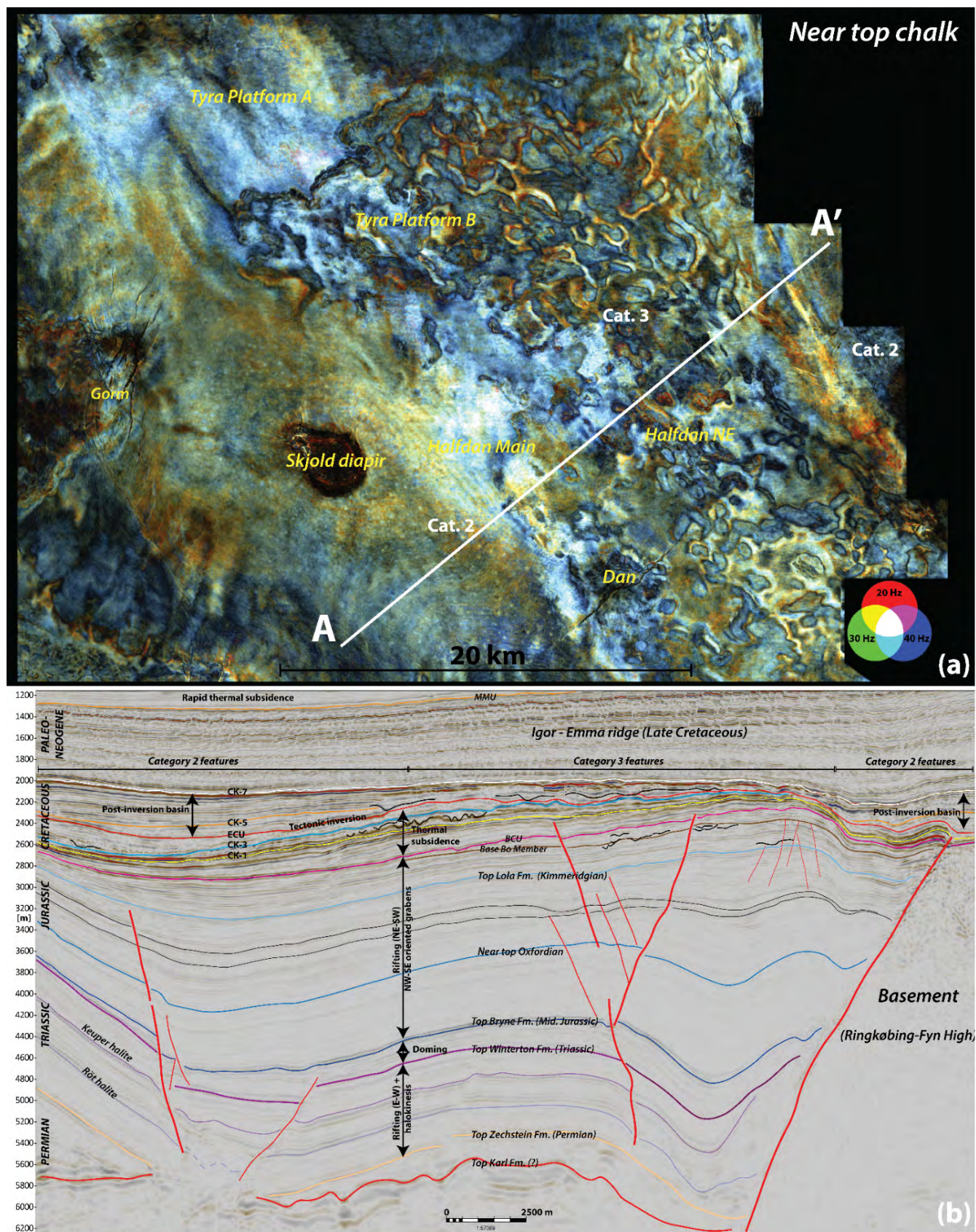


Figure 2. (a) Spectral decomposition RGB blend (20, 30, 40 Hz) on horizon slice at near top Chalk Group. A highly complex canyon morphology is observed in this stratigraphic level (Cat. 3 features), while smaller round depressions on both sides (Cat. 2 features). (b) Regional seismic line A-A' over the Igor-Emma Ridge.

The Base Cretaceous Unconformity (BCU) is a basin-wide diachronous surface that marks the end of active rifting and start of thermal subsidence, which prevailed throughout most of the Cretaceous period (Kyrkjebø *et al.*, 2004; Vidalie *et al.*, 2014). It was interrupted by a distinct compressional phase in the Late Cretaceous beginning with early inversion during Coniacian times, and reaching a climax during the early Campanian. This resulted in reactivation and movements along older faults and facilitated a major re-arrangement of depocenters and sediment remobilization along newly formed highs (Cartwright, 1989; Smit, 2014; van Buchem *et al.*, 2018; Vejgård and Andersen, 2002). Shift in depocenters is illustrated in the seismic section in Fig. 2: pre-inversion strata (CK-1 to CK-3) follow the Late Jurassic basin morphology (e.g. thin to the east and west), while the post-inversion strata (ECU to CK-7) show the opposite trend being thickest in the east and west. From the late Campanian and onward thermal subsidence prevailed, and chalk sedimentation continued into the Maastrichtian within the new basin configuration, only influenced locally by halokinesis and some smaller earliest Paleocene inversion movements (Vejgård and Andersen, 2002).

Chalk deposition came to an end in the mid-Danian and was replaced by marine shale deposition, which continued until Mid-Miocene times. The Paleogene – Neogene strata show polygonal features throughout, likely due to a combination of soft sediment deformation, density inversion, and syneresis, making their sealing capacity questionable (Cartwright *et al.*, 2003; Lonergan *et al.*, 1998). Rapid sediment loading of the basin started during the Late Miocene causing fault reactivation as a result of differential compaction and halokinesis, and leaking hydrocarbons were expelled to the seafloor causing pockmark formation (Andersen *et al.*, 2008).

Stratigraphy

We provide a brief summary of the Jurassic to Paleocene stratigraphy. For a more complete description, please see Smit *et al.* (Paper 2).

Lower to Middle Jurassic strata comprise open-marine mudstones of the Fjerritslev Formation, that are separated by a hiatus from the paralic and

non-marine sandstones, siltstones, mudstones and coal of the Middle Jurassic Bryne Formation (Fig. 3) (Møller and Rasmussen, 2003). The coals form a source rock in other parts of the Danish Central Graben (Petersen *et al.*, 2008), and gas chimneys are observed below the Tyra Field (Fehmers *et al.*, 2012).

The Upper Jurassic syn-rift strata comprise open-marine mudstones and siltstones of the Lola Formation (Oxfordian – Kimmeridgian) and Farsund Formation (Kimmeridgian – Volghian) (Møller and Rasmussen, 2003). The organic-rich facies of the Farsund Formation (including the Bo Member) form important source rocks for present-day hydrocarbon accumulations (Ineson *et al.*, 2003).

The Lower Cretaceous post-rift strata comprise grey calcareous claystones of the Valhall Formation (Hauterivian – Barremian), chalk of the Tuxen Formation (Barremian – Aptian), marls of the Sola Formation (Aptian – Albian), and marls and marly chinks of the Rødby Formation (van Buchem *et al.*, 2018).

The Upper Cretaceous Chalk Group forms the main hydrocarbon reservoir in the Danish North Sea. The stratigraphic nomenclature for the Chalk Group follows the tectono-stratigraphic framework of van Buchem *et al.* (2018), which separates pre-inversion formations from post-inversion formations based on the occurrence of a 5-10 Myr hiatus (Early Campanian Unconformity, ECU, see inset Fig. 3). Pre-inversion strata consist of white to light-grey chalk of the Hydra (Cenomanian) and Kraka (Turonian – Santonian) formations. The syn-inversion strata of the Gorm Formation (Campanian) show a distinctly different depocenter distribution and frequent occurrence of slumped deposits illustrating the impact of the basin inversion (van Buchem *et al.*, 2018). The post-inversion strata comprise the hydrocarbon-bearing Tor (Maastrichtian) and Ekofisk (Danian) formations.

The Chalk Group is overlain by Upper Paleocene marlstones of the Selandian Våle Formation and Thanethian hemipelagic mudstones of the Lista Formation, which include a lower Æbelø Clay Member, and upper Holmehus Clay Member (Schiøler *et al.*, 2008).

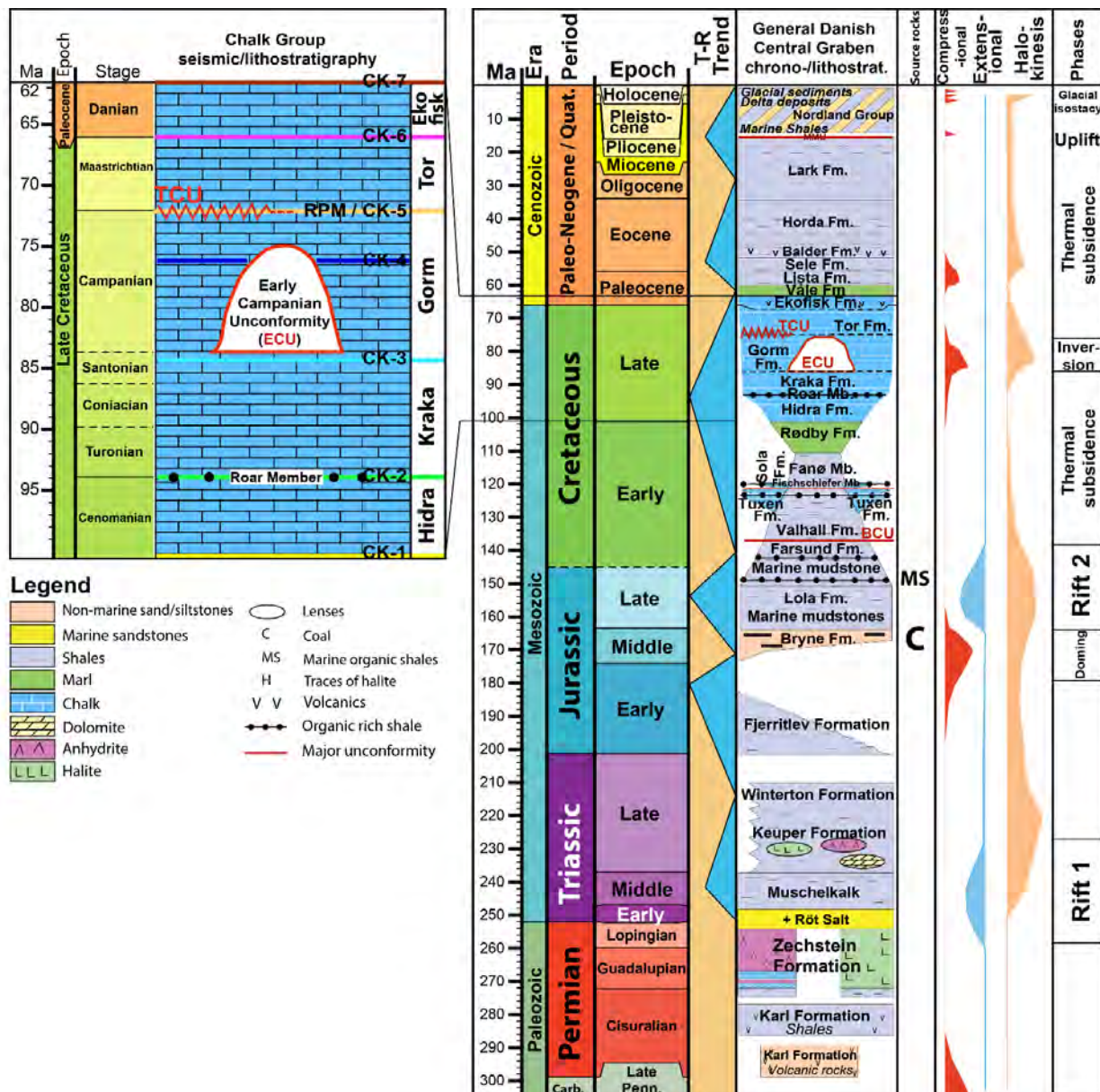


Figure 3. Chrono-/lithostratigraphic subdivision of the Danish North Sea. Stratigraphic units and tectono-sedimentary phases based on a literature synthesis. Coward *et al.* (2003) for Permian – Middle Jurassic, Rasmussen and Møller (2003) for the Middle Jurassic – Lower Cretaceous, Michelsen *et al.* (2003) for Jurassic, Japsen *et al.* (2003) for Late Jurassic and Lower Cretaceous, Ineson *et al.* (2003) for Late Jurassic, and Van Buchem *et al.* (2017) for the Lower and Upper Cretaceous, Schiøler *et al.* 2008 for Early Cenozoic, and Rasmussen *et al.* (2010) for Late Cenozoic. Tectonic phases are simplified and serve as broad tectonic framework for this study. Time scale generated with Geological Time Scale Creator, conform Ogg *et al.* (2016).

Data and methods

Seismic data

A 1500 km² subcrop of a regional seismic data set (pre-stack depth migrated) has been used (Fig. 1). The quality of the data is in general very

good in the Late Jurassic basin, but deteriorates towards the margins (basement) and in salt influenced zones (Fig. 2). The polarity follows North Sea convention, with a downward increase in acoustic impedance reflected by a trough (red). The dominant frequency in the Chalk Group is approximately 30 Hz, average acoustic velocity is

around 3400 m/s, leading to an average vertical resolution of 28.3 m as a quarter of the wavelength of the dominant frequency (Sheriff, 1980).

A neural network methodology has been applied for seismic interpretation (PaleoScan™, c.f. Pauget *et al.*, 2009) in order to create, in a time-efficient manner, the large number of stratigraphy consistent horizon slices through the Chalk Group. To increase the information extracted from the stratal horizons, spectral decomposition data revealed information in the frequency domain. Based on a dominant frequency of 30 Hz, three spectral frequency cubes (20, 30, 40 Hz) were calculated using a matching pursue algorithm in GeoTeric 2016.2 (c.f. Morozov *et al.*, 2013). Image processing of seismic data (c.f. Laake 2013), and using ‘swarm intelligence’ of artificial ants on the structural output of the workflow highlights possible near sub-seismic faults and fractured zones (Smit *et al.*, 2017).

Well data

The well data consist of wireline logs from 10 vertical wells for seismic-to-well tie of Top Chalk, as well as three horizontal wells that penetrated the features of interest (Fig. 1). Drill cutting material was analysed for stable carbon and oxygen isotopes at Iso-Analytical (UK) using continuous flow isotope ratio mass spectrometry (CF-IRMS), and values are reported as $\delta^{13}\text{C}$ and $\delta^{18}\text{O}$, deviations in parts per thousand relative to the V-PDB and V-SMOW standard. Analyses were performed on every drill cutting sample (10 m interval) from three horizontal wells (HCA-4ML1ABCD, HBA-14C, and HBA-27A) that penetrated the depressions.

In order to constrain diagenesis further, this study has utilized for the first time for chalks in the North Sea Basin, an absolute carbonate palaeothermometer, clumped isotope analysis on 34 chalk samples with a general spacing of 120 m (Ghosh *et al.*, 2006; Schauble *et al.*, 2006; Swart, 2015). Samples were chosen based on their position with respect to the seismic depressions. Sample preparation and $\Delta 47$ measurements were done in the Stable Isotope Laboratory at University of Miami and follow the procedures as outlined by Staudigel *et al.* (2018) and Swart *et al.* (2016).

This method measures the amounts of isotopologues of CO_2 (e.g. same molecule, different isotope configurations) in an adjusted mass spectrometer (Thermo-Fischer Scientific, MAT 253). There are six different isotopologues (44-49), the amount of isotopologue 47 ($\Delta 47$, $\text{C}^{13}\text{O}^{16}\text{O}^{18}$ is by far the most common) is a function of absolute precipitation temperature (Ghosh *et al.*, 2006). With increasing temperature, the amount of $\Delta 47$ will become smaller, and by comparison to reference materials that precipitated at known temperatures, the absolute temperature can be estimated. As bulk $\delta^{18}\text{O}$ is measured at the same time, two of the three unknowns in the classic palaeothermometer (equation 1, 2, c.f. Kim and O'Neill, 1997) are known (e.g. bulk $\delta^{18}\text{O}_{\text{calcite}}$ and temperature T), and the last unknown (fluid $\delta^{18}\text{O}_{\text{H}_2\text{O}}$) can be estimated.

$$1000 \ln \alpha(\text{calcite} - \text{H}_2\text{O}) = 18.03 \left(\frac{10^3}{T} \right) - 32.42 \quad (1)$$

$$\text{With } \alpha(\text{calcite} - \text{H}_2\text{O}) = \frac{1000 + \delta^{18}\text{O}_{\text{calcite}}}{1000 + \delta^{18}\text{O}_{\text{H}_2\text{O}}} \quad (2)$$

Basin model

The formation of several features in the Chalk Group are strongly linked to transportation of gas-bearing fluids along faults. In order to get a first order idea of possible sources of gas at the time of fluid expulsion, a 3D basin model was provided by M. Hertle (Total) that predicts source rock thermal maturity (expressed in vitrinite reflectance) in the region over time. In addition, paleo-temperature maps at BCU level provides insight in the likelihood of biogenic gas formation, with peak generation assumed to occur at c. 40°C and ceases at temperatures higher than 65/70°C (c.f. Schneider *et al.* 2016).

Seismic morphologies at top of the Chalk Group

In this paragraph the features at the top of the Chalk Group are described in terms of morphology and spatial distribution. Seismic geomorphological studies of chalk have identified a number of internal heterogeneities including, channels, stratigraphy cross-cutting reflectors, and pockmarks (e.g. Back *et al.*, 2011; Smit *et al.*, 2018; Surlyk *et al.*, 2008). Smit

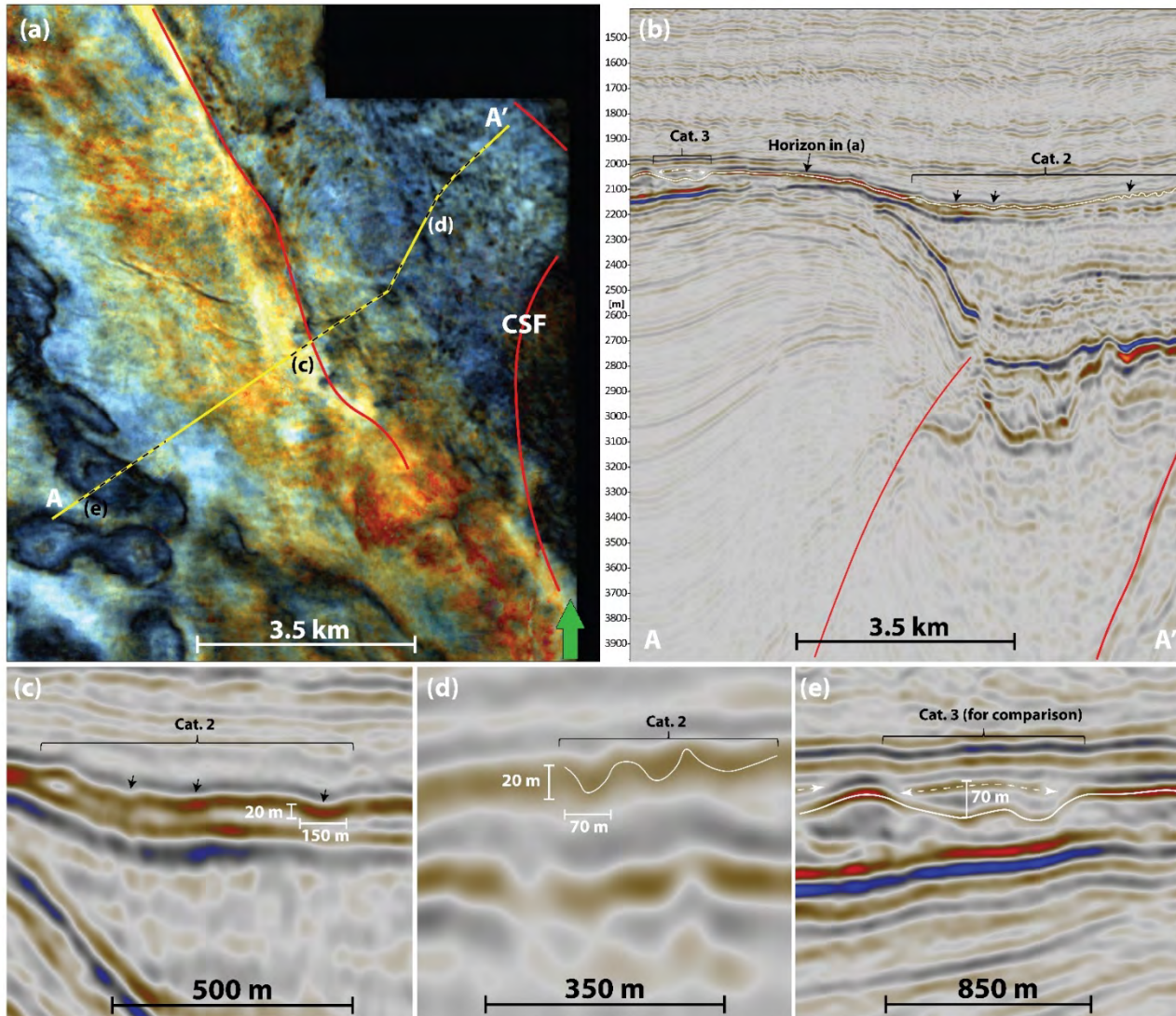


Figure 4. (a) Top Chalk Group surface morphology as seen on a seismic horizon RGB blend of spectral decomposition data (20, 30, 40 Hz). Round to elliptical small depressions (black) are observed in the north-eastern side (bluish region), 20 to 150 m in diameter. Larger, Cat. 3 features are observed on the western side, corresponding to the Igor-Emma Ridge. (b) Seismic amplitude section A-A' at the eastern edge of the Igor-Emma Ridge, where a Cat. 3 feature is observed, and to the east Cat. 2 features. The bluer colours (higher frequencies) in the north eastern region is due to the occurrence of high-frequency reflectors at this level. On the slope of the Igor-Emma Ridge, a high-amplitude low-frequency reflector occurs, creating more red colours in (a). Vertical exaggeration of 3x the horizontal scale. (c) Close-up section of Cat. 2 depressions, 100-150 m across, and 10-20 m deep. The infill is low-amplitude high-frequency (dark blue colours in a). The unaltered sections consist of high-amplitude low-frequency reflectors which show up as green-reddish colours (dominancy in 20 to 30 Hz) in (a). (d) Cat. 2 depressions with smaller dimensions, 20-70 m across, 20 m deep. (e) An example of Cat. 3 feature for scale comparison. These features are discussed in Fig.

et al. (Paper 2) developed a classification scheme for 6 different types of features (Cat. 1-6) observed within the Jurassic to Eocene strata in the Roar Basin. We utilize the same scheme, but note that Cat. 1 and 4-6 are not observed in the considered stratigraphic interval in the study area. As well data is available for Cat. 3 features, these will be addressed in detail.

Category 2 features

At the top of the Chalk Group, small round to slight elliptical depressions, 20 – 150 m in diameter, 10 – 20 m deep (near sub-seismic resolution) with gentle slopes (3-10°) occur along the flanks of the Igor – Emma ridge. Their infill consists of low-

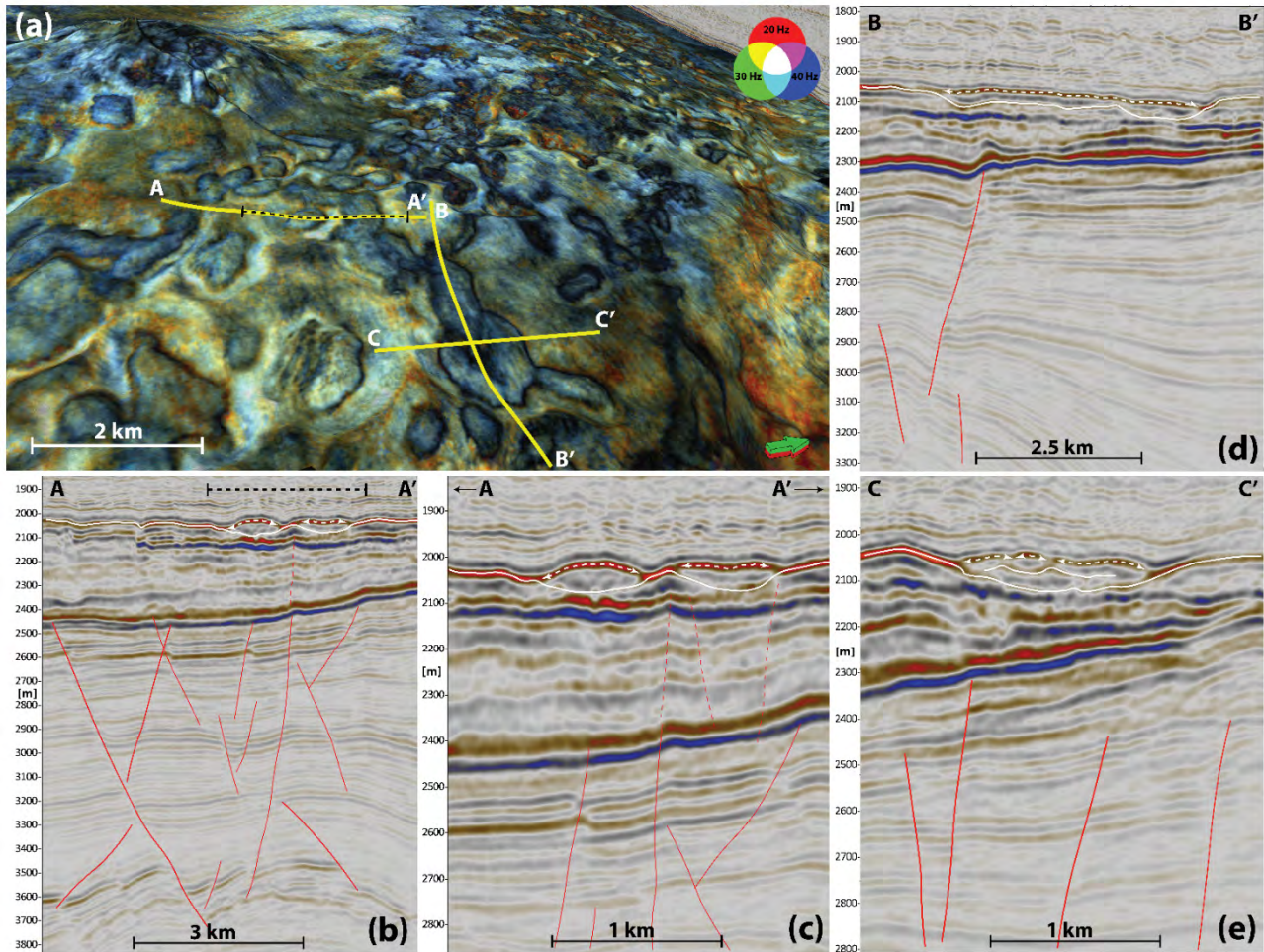


Figure 5. (a) Top Chalk Group surface morphology as seen on a seismic horizon RGB blend of spectral decomposition data (20, 30, 40 Hz). The surface follows the solid white in the areas where Cat. 3 depressions do not occur, and the dashed white line where the Cat. 3 features occur. This is due to the seismic similarity of the unaltered trough reflector (near Top Chalk) and top ‘infill’ of the depression. (b) Seismic amplitude section A-A’ through a round depression and more elongated depression. Vertical exaggeration of 3x the horizontal scale. (c) Close-up section of the depressions, which are 700-800 m across, and 50-70 m deep. Late Jurassic normal faults are found below these features. Note low to mid-amplitude, high-frequency infill which results in more bluish colours in spectral decomposition (e.g. 40 Hz) in (a). The unaltered sections consist of high-amplitude low-frequency reflectors which show up as green-reddish colours (dominance in 20 to 30 Hz) in (a). (d) Longitudinal section B-B’ through elongated depression, 3 to 3.5 km long. The basal reflector of the depression shows three individual depressions, which seem to have merged into one larger depression. A large Late Jurassic fault can be observed, which also folded the basal Chalk Group reflector. (e) Cross-section C-C’ through last part of section B-B’ where a 1 km wide, 75 m deep depression can be observed with low- to mid-amplitude high-frequency infilling reflectors.

amplitude, high-frequency packages (dark blue in Fig. 4a). They are not necessarily linked to the underlying fault systems (Fig 2b).

Similar features have previously been observed by Smit *et al.* (Paper 2) in the Roar and Tyra areas, and are interpreted as small pockmarks. Their size indicates relative smaller expulsion events in line with their location away from the Igor-Emma Ridge and main Late Jurassic faults. Since they are not necessarily associated with low-throw faults, it is

possible that both intra-formational fluids (e.g. biogenic gas) and extra-formational fluids (biogenic and thermogenic gas) caused their formation (c.f. Masoumi *et al.*, 2014).

Category 3 features

The top of the Chalk Group shows a highly complex canyon morphology, consisting of round to highly elongated depressions 200 to 850 m across, 0.2 – 2.5 km in length and 20-100 m deep (Figs 2a and 5a).

The slopes of the bounding walls are between 3 to 10° to the normal (Fig. 5b – e). The infill consists of low- to mid-amplitude high-frequency reflectors, which is reflected in more bluish colours in spectral decomposition slice (Fig. 5a). Dipping seismic reflectors within the infill suggest that beds are not horizontal but are inclined, though no borehole imaging or dipmeter data are available to confirm (Fig. 6b). Comparable depressions were described by Smit *et al.* (Paper 2) from the Roar and Tyra areas and their origin interpreted solely based on seismic geomorphological data. On the Igor-Emma ridge several horizontal wells penetrate these features providing information about infill lithologies and material for geochemical analyses to better constrain their origin. From Fig. 6 it is evident that well HCA-4ML1 and side tracks penetrate three seismically defined depressions and surrounding host rock, including the surfaces that seismically define the depressions. The initial well HCA-ML1, and sidetrack A, penetrate the upper part of depression 1, and a sharp transition in gamma-ray (GR) values is observed, from 5-10 API to 30-40 API as it enters the depression, to 60-70 at the end of the sidetrack (Fig. 6b). Drill cuttings from this boundary show a change from Danian chalks, to Danian marls, to marls of the Våle Formation and Æbelø Clay of the Lista Fm. at the end of the sidetrack (Fig. 6b, c, Final Well Report). While sidetrack A starts in the Danian marl, it does not encounter marls of the Våle Fm., while located just 50 m from the initial horizontal well. Instead, younger strata (Æbelø Clay of the Lista Formation) are overlain by older Danian marls (Ekofisk Fm.), suggesting remobilization occurred (Fig. 6c). In seismic section, the Top Chalk Group trough is here replaced with a peak, outlining a 10-15 m deep Cat. 2 depression, suggesting that the Våle Formation is eroded away.

Sidetrack 1B is deflected down due to the occurrence of a thick chert layer (Fig. 6c ‘chert layer deflects hole down’), which causes the well to penetrate the infill lower in depression 1. Slightly raised GR values (10-15 API) are found throughout the lower part of the depression. The interval in between depression 1 and 2 is also characterized by low GR values (5-10 API), as well as the entire depression 2 (Fig. 6b). Drill cuttings show 10-60%

chert just before sidetrack 1B is deflected downhole with the remainder being clean chalk (with no visible porosity). As it enters depression 1, chert content goes down to trace levels, but goes up to towards the depression 1 surface (10-40%), the remainder being clean chalk with rare argillaceous laminations. From the depression 2 surface to the middle part of depression 2, chert amounts to 10-70% of the drill cuttings in sidetrack 1C, and the remainder tight chalk with argillaceous laminations. From the middle part onwards, only trace levels of chert are found, while the remainder is clean chalk.

Sidetrack 1D starts in the section between depressions 2 and 3, where GR values are low (5-10 API) and drill cuttings show 100% clean chalk. Increased amounts of chert (10-50%) forces sidetrack 1D into depression 3 (Fig. 6c, ‘chert layer deflects hole down’). The infill shows GR values of 5-10 API, and drill cuttings show mainly clean chalks with trace to 10% chert. As sidetrack 1D moves out of the infill, chert amount increases to 30% with the remainder being chalk. Summarizing, increased amounts of chert are found towards the surfaces of the depressions, on top of the host rock, and within the infill. In addition, the infill also contains Danian chalk, marl, and Paleocene marls and clays (Fig. 6c).

Stable carbon and oxygen isotope analysis of drill cutting material from well HCA-4ML1 (and sidetracks A-D) show $\delta^{13}\text{C}$ values between 0 and 2‰ and $\delta^{18}\text{O}$ values between -5 and -2‰ (Fig. 7a). There is no obvious difference between the infill and the host rock, but material from the host rock between depression 1 and 2 shows the most negative $\delta^{18}\text{O}$ values. Clumped isotope data from 23 points along the well path indicate bulk temperatures between 22-55°C and bulk fluid $\delta^{18}\text{O}$ values from -1.7 to 3‰ (Fig. 7b). Temperatures obtained from material inside the depressions fall towards the lower end of the measured temperatures (26-36°C), while warmer temperatures occur in the host rock segments outside the depressions (e.g. see section HCA-4ML1C).

Well HBA-14C penetrates a 450m wide and 40 m deep depression (Fig. 7c). The infill has slightly lower $\delta^{13}\text{C}$ values compared to the host rock (‘infill’ in Fig. 7c). Clumped isotope data show a very

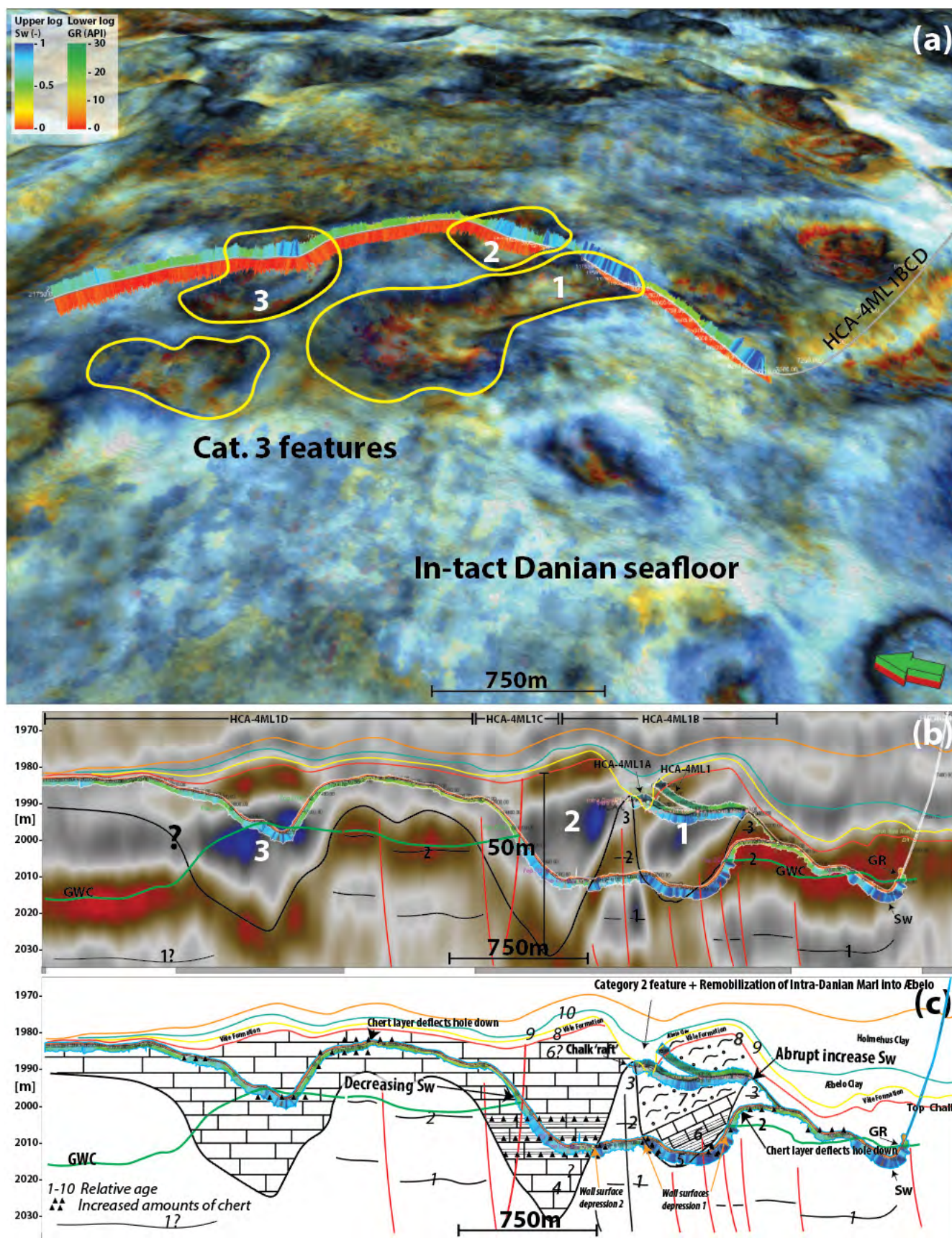


Figure 6. (a) Spectral decomposition RGB blend on near top Chalk Group surface. Examples of Cat. 3 features that are penetrated by a horizontal well with several side-tracks (HCA-4ML1BCD). The upper log shows water saturation and lower log gamma-ray. The water saturations are generally higher within the pockmarks (0.8 – 1.0) compared to outside (0.2 – 0.5). This has partly to do with the well trajectory moving up and down the gas column, but also with the lithology of the infill. (b) Well section showing the different side-tracks (GR log is top log, Sw lower log). Interpreted low-throw faults in red outlines. (c) Cartoon of the Cat. 3 depression. Interpretation of the lithologies based on horizontal well penetrations. Depression wall penetrations indicated with orange arrows. Note the rapid shifting water saturation, likely due to differences in lithology and position relative to the gas-water-contact. See text for further description.

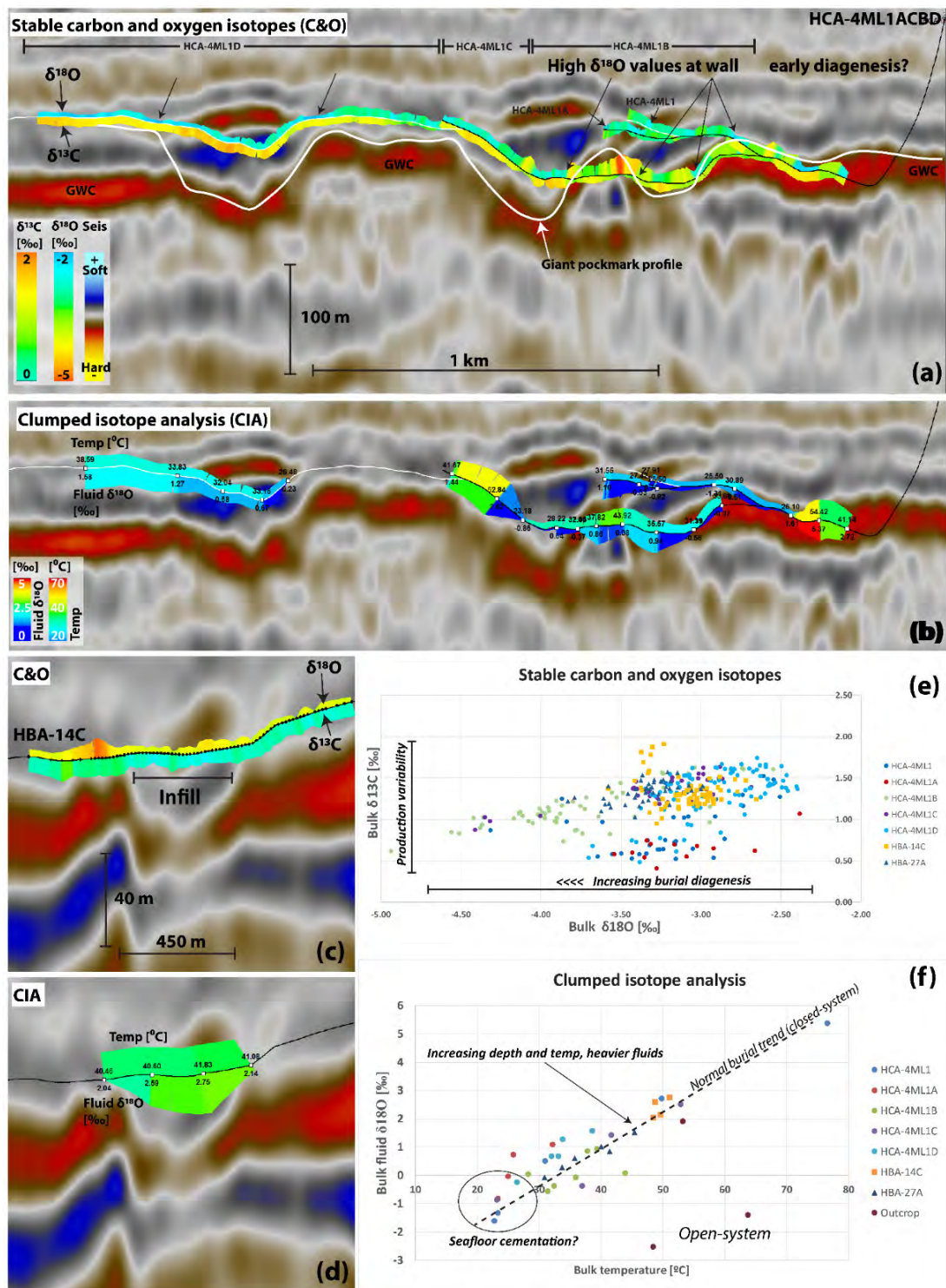


Figure 7. Seismic sections through category 3 features with geochemical data displayed along the well paths. **(a)** Well section of HCA-4ML1 with sidetracks ABCD (black lines) with stable carbon and oxygen isotope data. Profile of the depression shown in white. While difficult to see a distinct trend between depression and intact seafloor, $\delta^{13}\text{C}$ values (lower log) fluctuate between 0-1.7‰ likely due to differences in production of algae (reflecting availability of lighter C^{12}), while $\delta^{18}\text{O}$ values fluctuates between -2.3 to -4.9‰, reflecting increasing burial diagenesis. Large outliers are not seen (e.g. -10‰ as in Smit *et al.* 2018). **(b)** Same well section, showing clumped isotope data (23 data points, bulk temperature and bulk $\delta^{18}\text{O}$ of the fluid). Measured temperatures range from 22 to 55°C, while $\delta^{18}\text{O}$ range from -1.7 to 3‰. There is no clear trend to be observed between depression and intact seafloor. **(c)** Seismic section through HBA-14C with stable carbon and oxygen isotopes. Slightly lower $\delta^{13}\text{C}$ values are observed within the depression infill, likely marking chalk of a different age (due to temporal production variability causing differences in $\delta^{13}\text{C}$ values). **(d)** Clumped isotope data shows very constant temperature of 41°C, and $\delta^{18}\text{O}$ between 2.04 to 2.75‰. **(e)** Cross-plot of carbon and oxygen isotope data. The spread in $\delta^{13}\text{C}$ values reflects temporal variability in production, while the spread in $\delta^{18}\text{O}$ reflects differences in burial diagenesis. **(f)** Cross-plot of temperature vs fluid $\delta^{18}\text{O}$ measured from clumped isotope analysis, which are two independent variables. The data from the horizontals that run through the depressions shows that there is a general positive correlation. With increasing temperature, the fluid from which the calcite precipitated becomes heavier. This is a typical closed-system diagenetic signature (c.f. Swart *et al.* 2015). In contrast, data from an outcrop that contains large calcite veins along a fault plane plots off the line, reflecting an extra-formational source that has a different temperature. We conclude that the depressions experienced the same diagenesis (e.g. closed-system) as the intact chalks, and thus were seafloor depressions.

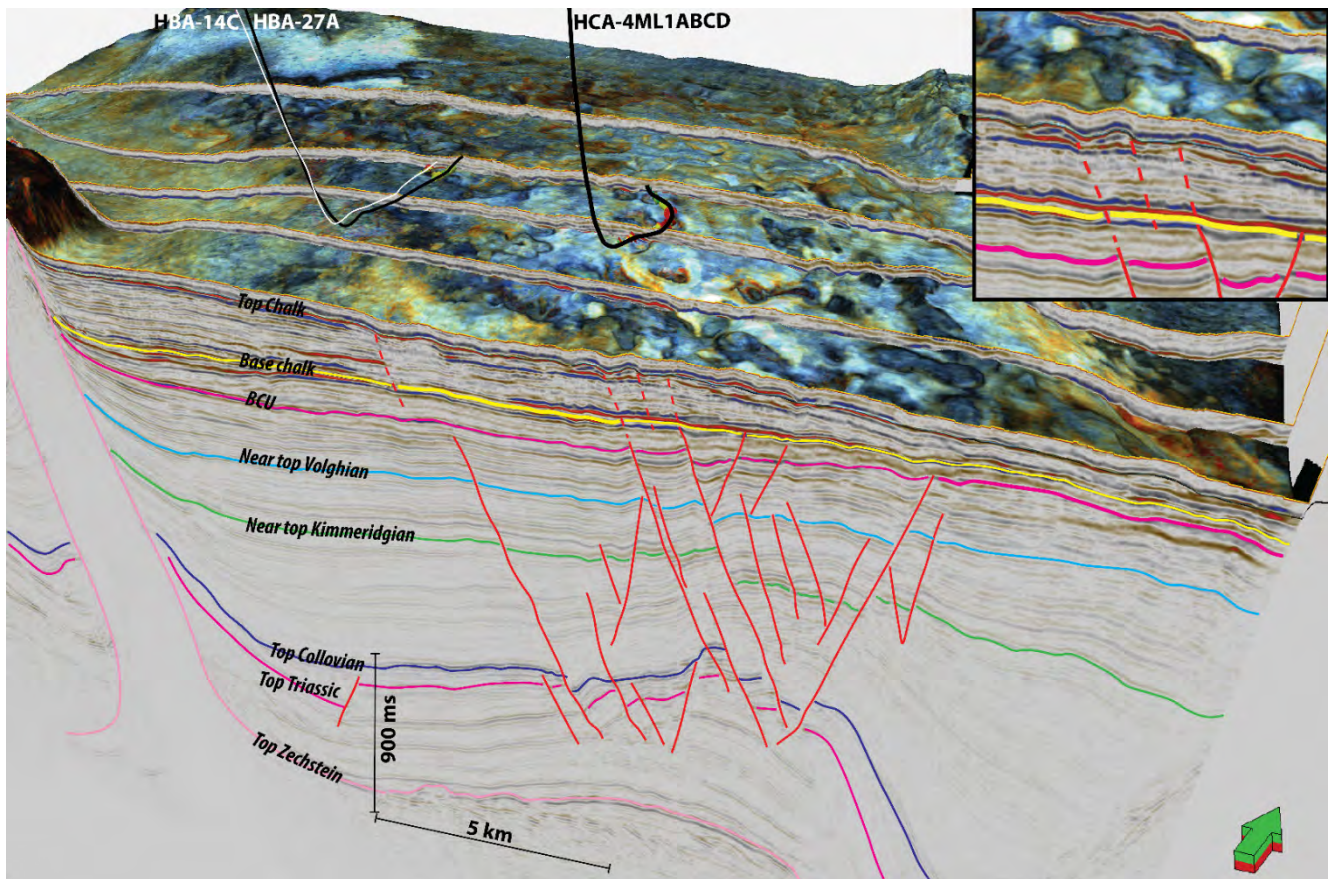


Figure 9. Juxtaposition of the Late Jurassic faults at the crest of the inverted Igor-Emma Ridge, and the occurrence of category 3 features. Category 3 features occur mainly on the inverted structures, which are underlain by Late Jurassic normal faults that root even root into Lower to Middle Jurassic strata. The inset shows the correlation between the faults and the occurrence of depressions within the Danian Ekofisk Formation.

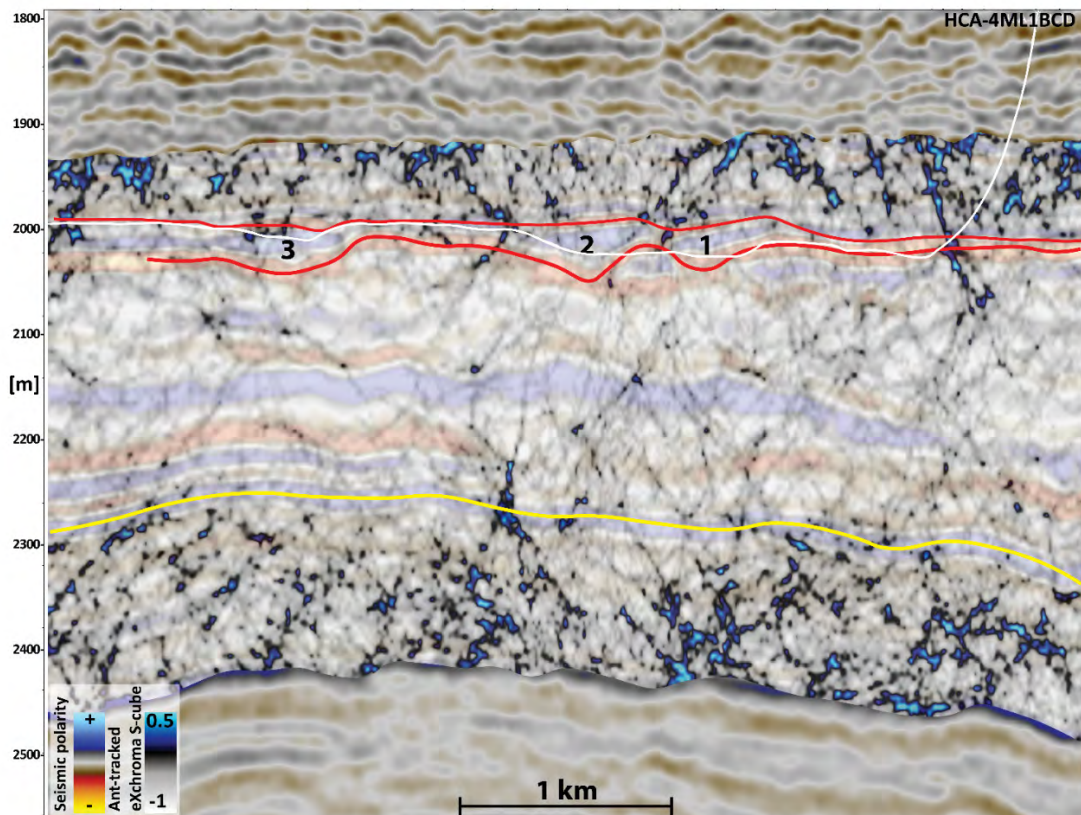


Figure 10. Well section through HCA-4ML1ABCD with seismic amplitude blended with ant-tracked eXchroma structural cube. The lineations observed within the ant-tracked data are in the extension of faults that offset strata slightly below the Chalk Group. We propose that the lineations within the Chalk Group are reactivated Late Jurassic normal faults to form low-throw faults and fractured zones

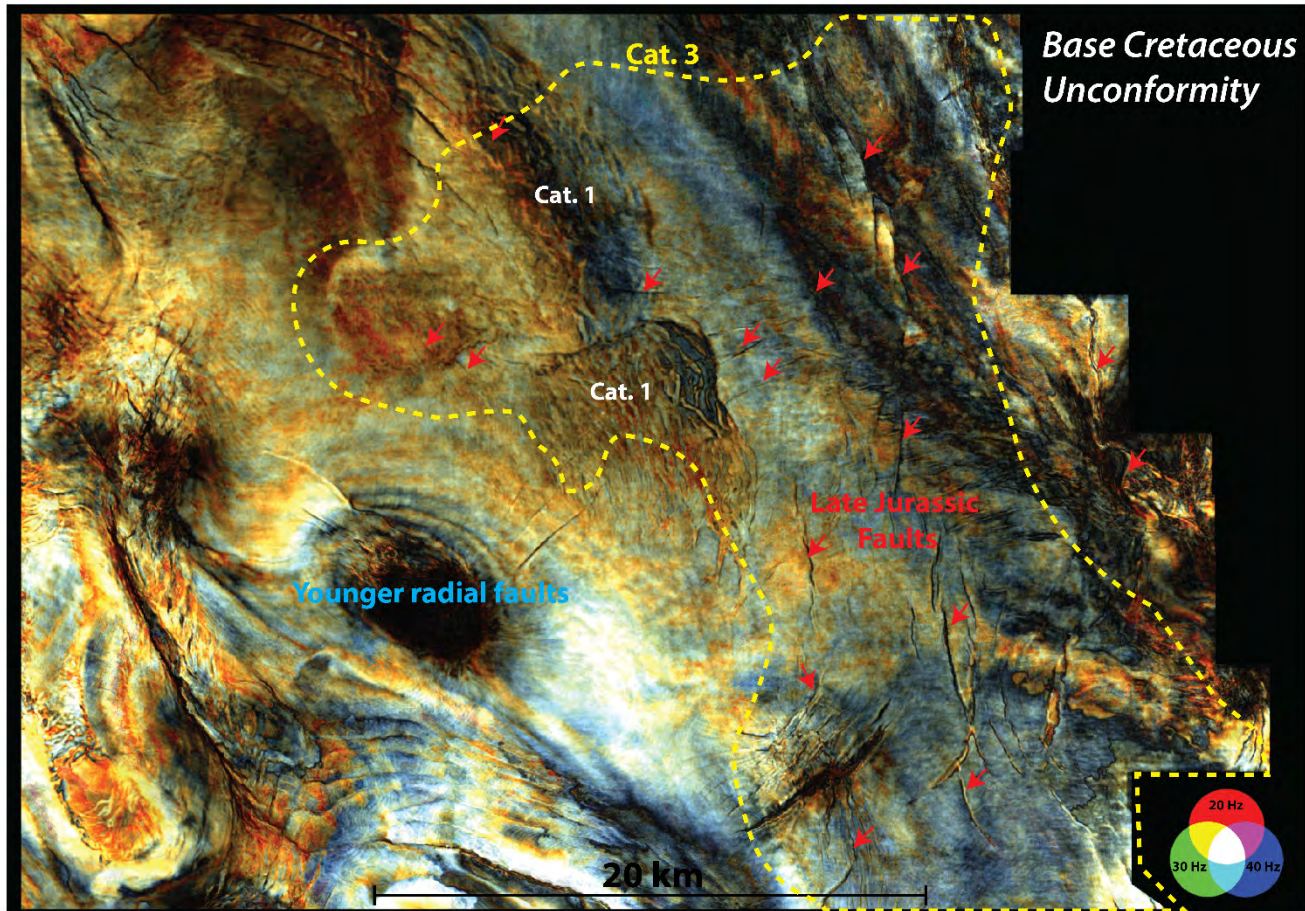


Figure 11. Horizon slice on the Base Cretaceous Unconformity (BCU), with RGB display of spectral decomposition data (20, 30, 40 Hz). Deeply rooted inverted Late Jurassic normal faults are observed at this slice (red arrows). The yellow dotted line shows the spatial distribution of category 3 features, which shows that these mainly occur above the Late Jurassic faults on top of the inverted Igor-Emma Ridge, but not around possibly younger radial faults around the diapirs. Thin-skinned slumping is observed as cusped features (Cat. 1 features c.f. Smit *et al.* –Roar).

9, inset). Image processing of seismic data followed by ant-tracking of the edge detected volume, reveal these lineaments quite well and they most likely represent structural damaged zones within the chalk as a result of folding and fault reactivation (Fig. 10)(c.f. Smit *et al.*, 2017). Juxtaposition of the spatial occurrences of Category 3 depressions on the BCU horizon slice shows good correlation between the N-S oriented faults and the depressions (Fig. 11). They do not occur along the radial faults of the nearby salt diapir (Skjold diapir)

Interpretation of Cat. 3 features

The U-shape reflectors outline 700-800 m wide, 20-80 m deep depressions that are filled with chalk, marl, and clay of Danian age (Figs 5 and 6).

This suggests that the depressions formed during the last stage of chalk deposition in the Mid-Danian, and rather than reflecting post-depositional diagenesis. Clumped isotope data show a positive trend between bulk cementation temperature and fluid $\delta^{18}O$ of the chalk in both the infill and the intact seafloor (Fig. 7f). The positive trend is typical for normal, closed-system burial diagenesis, as with increasing burial depth (and temperature), preferentially the lighter O^{16} goes into the crystal lattice and the heavier O^{18} stays behind in the formation water (Swart *et al.*, 2016). Since both the infill and the intact seafloor sediments experienced similar closed-system burial diagenesis, post-depositional open-system diagenetic overprinting was not involved in shaping the

depressions. The geochemical data are thus in line with a syn-depositional depression interpretation.

The linkage to underlying inverted Late Jurassic faults and occurrence on top of the inverted Igor-Emma Ridge suggest that the features are strongly connected to the structural fabric (Figs 9 and 10). We therefore interpret these features as giant pockmarks, formed due to large outbursts of gas-bearing fluids funnelled to the seafloor by inverted Late Jurassic faults.

The highly complex canyon morphology and the different types of infill suggests that the pockmarks did not form at the same time, and were time-transgressive (Fig. 5). While initially steep-walled, later remobilization by gravity movements and bottom current activity must have adjusted the slope to the angle of repose forming the more U-shaped depressions (Betzler *et al.*, 2011). The time-transgressive nature and reworking led to amalgamation of the depressions resulting in the highly complex morphology and infill patterns (Fig. 5). Erosion of North Sea Marl and remobilization in the post-chalk depression between depression 1 and 2 (penetrated by HCA-4ML1A), indicate that smaller expulsions still occurred after chalk deposition stopped (Fig. 6). The smaller size suggests that expulsion of fluids became smaller, possibly as pressures were adjusted.

GWC surfaces

Well HCA-4ML1 (and sidetracks) shows the complexity of the water saturation and associated GWC surface, as a result of the disturbance of the host rock (clean chalks) (Fig. 9). Possibly, the crater wall and infill experienced early cementation and seep carbonate formation, which would create tight zones (c.f. Betzler *et al.*, 2011). Faults and fractures that formed pathways for the pockmark formation could be re-used during subsequent charge to form localized low water saturated zones (Fig. 9). Cherty intervals, possibly associated with depression outlining surfaces and infill, are not only pore reservoir quality, it also forced the drill bit down dip below the GWC. Locally however, cherty intervals can act as sealing rock, as is seen in sidetrack 1B in depression 2, leading to localized lower water

saturations. Understanding the spatial distribution of these lithologies and the surfaces is therefore key in well planning.

Modelled vitrinite reflectance data and palaeotemperature BCU

A small Early-Middle Jurassic depocenter is present underneath the Igor-Emma Ridge, and strata are between 50 to 500 ms thick (Fig. 12a). In addition, a deep Late Jurassic depocenter is present in the study area, and strata (with thick organic-rich intervals) are between 750 and 2000 ms thick (Fig. 12b). In order to evaluate possible sources for the gas-bearing fluids that caused the generation of the giant pockmarks during the Danian, we have utilized temporal estimates of the vitrinite reflectance (thermal maturity) of three main source rock intervals. These are: 1) Middle Jurassic Bryne Formation (coals); 2) the base of the Upper Jurassic Farsund Formation (base organic-rich shales); and 3) the Bo Member of the Farsund Formation ('hot shale' c.f. Ineson *et al.* 2003) (Fig. 13a-c). In addition, we have evaluated the likelihood of an Upper Jurassic biogenic source by juxtaposing a paleo-temperature map at BCU level during the end of the Danian (Fig. 13d). The dashed line in Fig. 13d marks the spatial occurrence of the giant pockmarks (category 3 features). As category 3 features occur both in the study area and Roar Basin, we briefly describe them both (see for a more detailed treatment of the Roar Basin, Smit *et al.*) The Middle Jurassic coals show vitrinite reflectance values between 0.5 to 1.5 % Ro within the study area increasing to 2-4% Ro in the Roar Basin (Fig. 13a). The Base Farsund shows values from 0 to 0.5% Ro in the study area compared to 1-1.5% Ro in the Roar Basin (Fig. 13b). The Bo Member shows values between 0 to 0.75% Ro in both study area and Roar Basin (Fig. 13c). The paleo-temperature of the BCU during Danian times was 30 to 70°C in the study area increasing to 40 to 100°C in the Roar Basin (Fig. 13d).

Middle Jurassic coals seems to be the most likely thermogenic source in the study area, while the lower organic-rich intervals of the Farsund might have contributed in the Roar Basin. Thermogenic contribution from the Bo Member is unlikely as it is

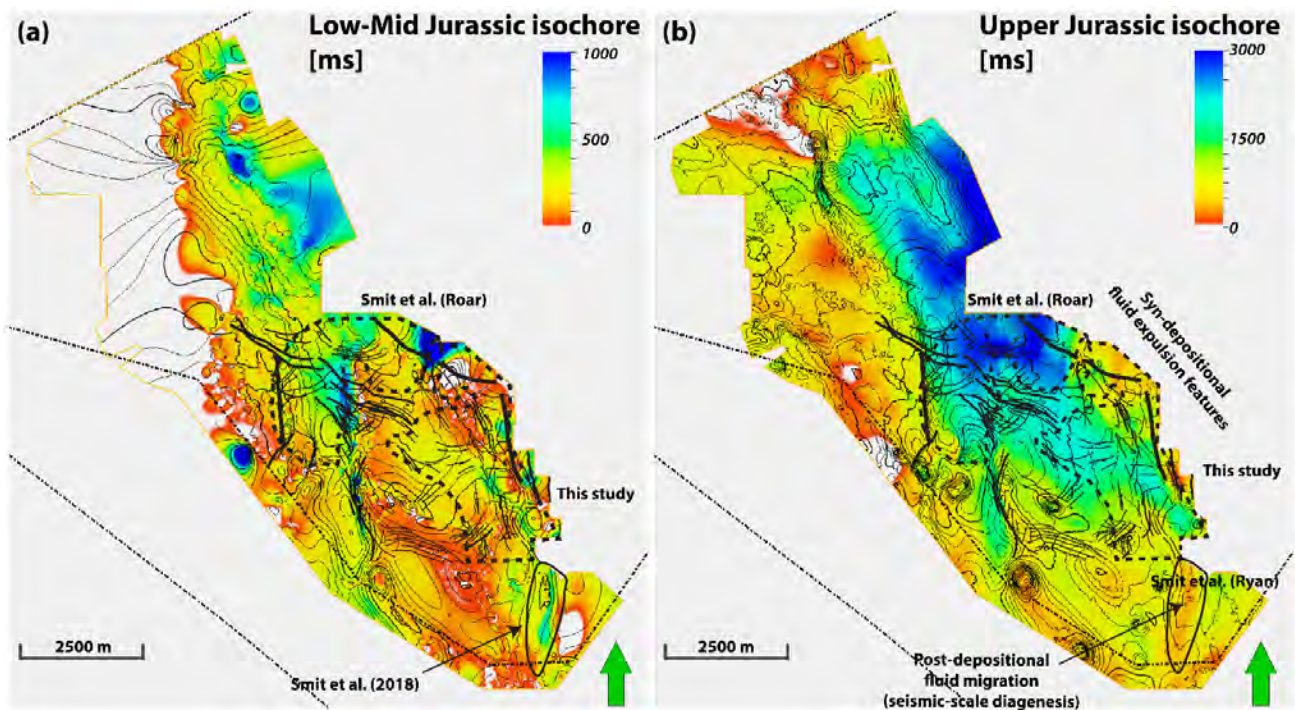


Figure 12. (a) Lower to Middle Jurassic isochore. The dotted black line shows the spatial occurrence of category 3 features. Thick solid black lines represent faults that root into these strata. Within the study area, Lower to Middle Jurassic strata are between 50 to 500 ms thick. Especially underneath the inverted Igor-Emma Ridge. (b) Upper Jurassic isochore. Within the study area, thicknesses between 750 – 2000 ms occur, reflecting the occurrence of a Late Jurassic depocenter at the location of category 3 features.

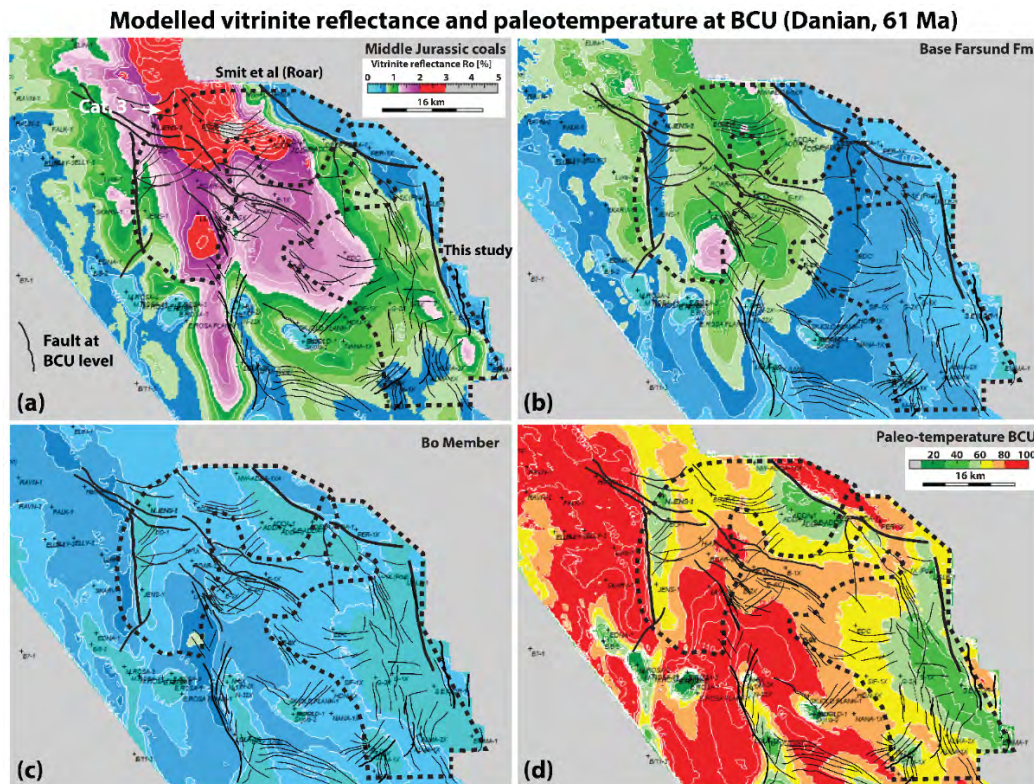


Figure 13. Modelled vitrinite reflectance data within the Greater Dan Area at 61 Ma (e.g. end of Danian times) (a-c). Palaeotemperature of BCU at top Chalk times in d. Dotted black line shows the spatial occurrence of category 3 features. The solid lines reflect faults at BCU level (see Fig 10). (a) Coals of the Middle Jurassic Bryne Formation show vitrinite reflectance values between 0.5 to 1.5 % Ro in the study area, while in the Roar Basin values of 2 to 3.5% Ro are observed. It shows that the source rock was thermally mature at this time in the Greater Dan Area. (b) Organic-rich intervals at the base of the Upper Jurassic Farsund Formation show vitrinite reflectance values between 0 to 0.5% Ro in the study area, while in the Roar Basin values of 0.5 to 1.5% are observed. These source rock strata were not yet thermally mature in the study area, while early mature in the Roar Basin. (c) The Bo Member of the Farsund Formation ('hot shale') shows throughout the Greater Dan area values between 0 and 0.5% Ro. It was immature during the formation of the category 3 features. (d) Palaeotemperature at BCU level at end of the Danian. Within the study area temperatures range from 30 to 60°C, while in the Roar basin higher temperatures are observed. Generation of biogenic gas from organic degradation was thus possible from the upper parts of the Farsund Formation.

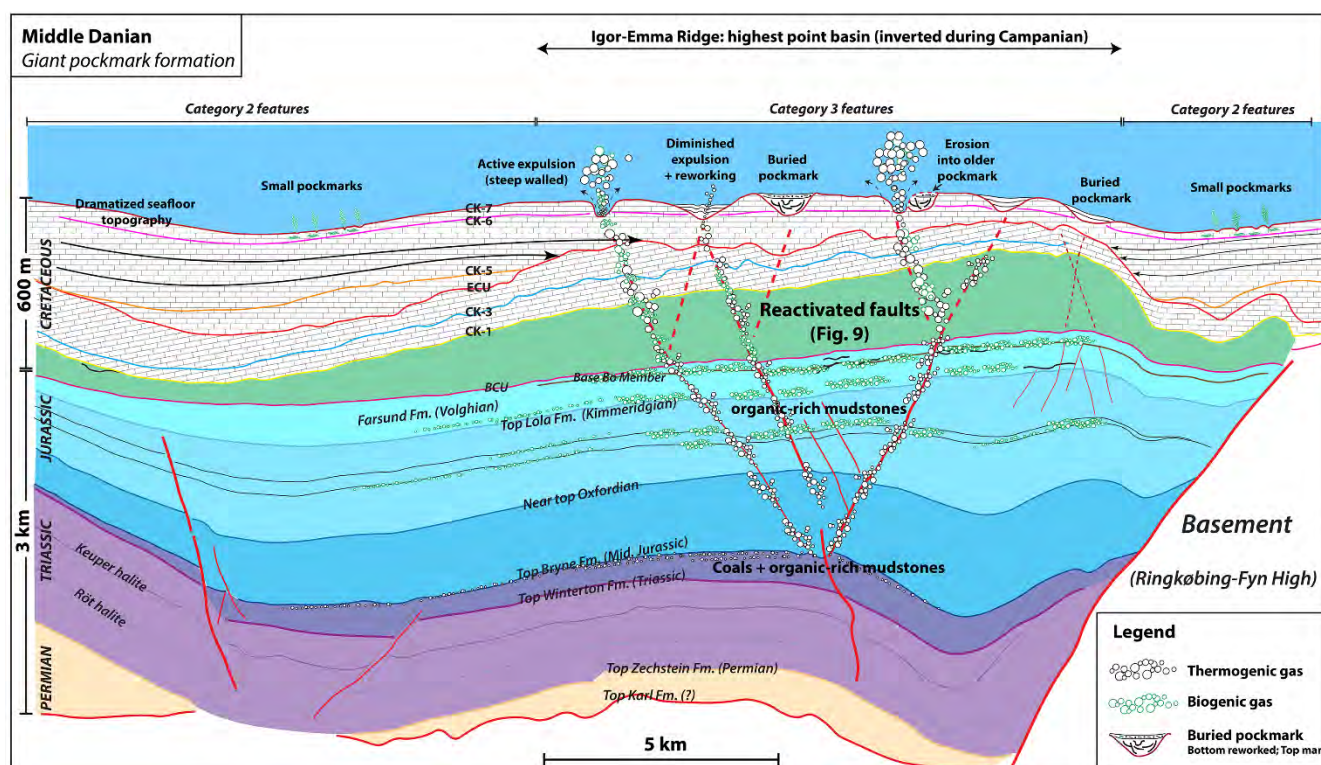


Figure 14. Model for the formation of giant pockmarks within the Ekofisk Formation (Danian). See supplement 3 for a high-quality version. During Campanian inversion event basin that existed at the Igor-Emma Ridge became tilted to form an asymmetric anticlinal structure. Renewed deposition of chalk led to an angular unconformity seen as seismic onlaps onto the structure (black arrows). During the Middle Danian, gas-bearing fluids from both thermogenic and biogenic sources started to become expelled violently, leading to the formation of giant pockmarks. They formed on top of the basinal high (Igor-Emma Ridge), as inverted Late Jurassic faults are present here, and because it formed the locus for expelling fluids (e.g. highest point in the basin). While depressions initially were steep sloped, reworking by gravity movements and bottom current activity led to more U-shape reflectors. In addition, together with renewed expulsion phases that eroded into previously formed depressions, the highly elongated canyon morphology started to form within the Ekofisk Formation. Some depressions became filled in with chalk, others with marls and clays. Smaller pockmarks formed along the side of the structure, and their occurrence away from main faults could suggest that they formed mainly from biogenic gas expelled from organic-rich intervals within the Chalk Group.

mostly thermally immature across the region. The paleo-temperatures at the BCU show that organic degradation of organic-rich material was possible in the study area, and in places in the Roar basin. It is thus likely that both thermogenic and biogenic sources provided gas-bearing fluids for the formation of the giant pockmarks.

Model for formation of the giant pockmarks

We propose the following formation mechanism for the giant pockmarks formed during the latest stages of chalk deposition. During the Danian, gas-bearing fluids were expelled from organic-rich Jurassic strata (both thermogenic and

biogenic c.f. Fig. 13) and migration occurred along inverted Late Jurassic faults towards the highest points in the basin, which were the structures created during Campanian inversion (Figs 9 and 14). They include the Igor-Emma Ridge, Adda Ridge, and Bo-Valdemar Ridge, all characterized by condensed chalk sections (Fig. 1, limited thickness in isochores). Lower Cretaceous mud-grade strata and possibly also the lower part of the Chalk Group formed an effective seal, until pore pressures exceeded the sealing capacity, and the gas-bearing fluids were funnelled towards the Danian seafloor to form giant pockmarks (Figs 9 and 10). The spatial distribution of the giant pockmarks was controlled by the basin morphology, and the occurrence of weak zones within the Upper Jurassic and Cretaceous strata (e.g. faults and fractured zones).

While initially steep-walled, reworking by mass movements and bottom current activity would adjust the slope to the angle of repose (3- 10°), and fill the depressions with 'disturbed' facies (c.f. Henriksen *et al.*, 2009) (Fig. 14). The differences in infill of the depressions (e.g. marl vs chalk) indicate the time-transgressive nature of the pockmark formation (Fig. 6). The infill sequence of depression 1 where Danian marl is conformably overlain by the Våle Fm. reflects the last phases of Danian chalk/marl deposition and this depression is thus younger than depression 2 and 3 (Fig. 14, compare buried pockmarks with actively forming pockmarks). Here, the infill is composed entirely of chalk, suggesting a slightly older fluid expulsion event prior the expulsion event that created depression 1 (Fig. 6b-c). It also shows that renewed expulsion events could cause cannibalization of older pockmarks (Fig. 14). The removal of the Våle Fm. in a category 2 pockmark between depression 1 and 2 indicates that gas-bearing fluids were still funnelled towards the seafloor in (smaller) explosive events after chalk deposition has stopped.

Discussion

Significance of pockmarks at the top of the Chalk Group

The pockmarks form a direct indicator of fluid migration and expulsion *during* deposition of the Ekofisk Formation chalk, where yet no top seal had formed (e.g. Paleo- and Neogene clays). Both biogenic and thermogenic sources provided gas-bearing fluids that leaked out of the present-day reservoir before they could be trapped (Fig. 14). The migration predates thermal maturation of the most prolific source rock, the Bo Member, which is thought to have contributed volumetrically the most to present-day accumulations (Andresen *et al.*, 2008; Ineson *et al.*, 2003; Vejbæk *et al.*, 2005). The giant pockmarks thus provide a snapshot of fluid migration pathways and early expulsion events. We might not be able to resolve the pathways directly from the seismic amplitude data (e.g. low-throw faults), but the giant pockmarks are clearly evidence that such pathways did exist. New technologies make it possible to investigate near sub-seismic features,

such as image processing seismic data (Laake, 2013), which helps to visualize potential pathways that might not stand-out with conventional seismic attributes (Fig. 10).

The spatial distribution of the giant pockmarks with respect to smaller pockmarks shows that larger outbursts occurred at the higher parts of the ridge (e.g. the inverted structures) (Fig. 14). Due to the limited accommodation on top of the structures (see Fig. 1, isochore), the chalk is thinner and more complex with evidence of early cementation due to non-deposition (Smit *et al.*, 2018; van Buchem *et al.*, 2018), bottom current activity (Esmerode *et al.*, 2008), and fluid expulsion features (Smit *et al.* Paper 2). As these inverted structures remained basinal highs during subsequent thermal subsidence (with only slight tilting in the Late Miocene), the present-day hydrocarbon accumulations are found here.

Applications for petroleum geological studies

The giant pockmarks cause variability in reservoir quality (e.g. marls and cherts are found in between clean chalk), and have generated depositional profiles through the main reservoir, which may be sealing due to early cementation (as a result of non-deposition) or seep carbonate formation. In contrast, it might have cut through tighter zones within the Ekofisk Formation (e.g. Danian dense zone Gennaro *et al.*, 2013) to establish pathways with more porous sections of the Chalk Group (e.g. Tor Formation) (Fig. 14). Therefore, future (exploration) studies could attempt to model fluid migration of present-day accumulations to incorporate these kilometre-wide disturbances in the reservoir that existed already from Danian times. Indeed, the giant pockmarks are direct indicators that gas-bearing fluids were generated, and able to migrate through the Chalk Group towards the seafloor before a seal was present. After a seal was established, there might have formed economic accumulations.

The highly variable infill and surfaces seem to influence the position of the GWC, which becomes a challenge to model, and makes data availability from pockmarks penetrations crucial (Fig. 8). Marly infill has lower acoustic impedance, which could be

mistaken in seismic inversion porosity data to be a porous reservoir filled with hydrocarbons. Henriksen *et al.* (2009) made a good attempt to find physical properties to model disturbed facies within the pockmarks, and found that V_p/V_s ratios provided the best differentiation. 4D seismic data potentially also provide meaningful input, as they will show zones of low gas extraction. Together with the horizontal well database, and available geophysical and petrophysical data, a machine-learning approach could provide a way forward (Liu, 2017). The recognition of giant pockmarks with a variable infill is a step forward to better reservoir models, and improved predictability of reservoir quality (chalk, low water saturations) will indeed help future well planning through the Halfdan Gas Field.

Seismic geometries in the Chalk Group

A large variety of 2D internal seismic expressions are found within the Chalk Group, which can be challenging to interpret if the focus area is constraint to the hydrocarbon accumulations. By using the regional megamerge and tectono-stratigraphic surfaces as defined by van Buchem *et al.* (2018), spatial patterns of certain features are more easily obtained, which can be placed within the regional geological context. Combining an integrated seismic geomorphological method where palaeoreconstructions of the seafloor are integrated with other proxies (e.g. petrographical and geochemical data, including clumped isotope analysis), interpretations can be made more intuitively and conclusively. This has already led to the documentation of the first example of seismic-scale diagenesis within the Chalk Group (Smit *et al.* 2018), as well as the occurrence of a large variety of fluid expulsion features (e.g. mega pockmarks and seep carbonates) (Smit *et al.* Paper 2). This case study firmly adds giant pockmarks on top of inverted Campanian structures to the catalogue of features, as precursor fluid migration indicators (from an earlier expulsion phase) of the main hydrocarbon accumulations found at present.

Conclusions

- A large field of giant pockmarks (category 3 features) is documented in the gas-bearing Danian Ekofisk Formation of the Chalk Group in the Halfdan and Tyra area of the Danish Central Graben. The dimensions range from 200 to 1000 m across, 0.2 to 3 km in length due to amalgamation, and 20 – 100 m deep. The pockmarks formed as a result of large outburst of gas-bearing fluids, which originated from Jurassic thermogenic sources as well as degradation of organic-rich shales.
- Stable isotope data combined with clumped isotope analysis of material from the infill and the intact seafloor indicate closed-system diagenetic behaviour, with increasing bulk cementation temperature, calcite precipitated from fluids with more positive $\delta^{18}O$ values. A post-depositional origin is therefore ruled-out, and the depressions were syn-depositional relief on the Danian seafloor.
- This study utilizes for the first time in chalks of the North Sea Basin, the absolute clumped isotope carbonate palaeothermometer.
- The spatial distribution of the giant pockmarks reveals that Late Jurassic faults formed the main pathway for the gas-bearing fluids, and that they are focussed in the highest parts of the basin due to Campanian inversion. Smaller pockmarks (category 2 features) along the flanks of these structures represent smaller outbursts.
- Pockmark formation was a time-transgressive process as reflected by a variable and highly complex infill with chalk, marl, and clay. Initial steep walls became remobilized by gravity movements and bottom current activity, which also caused amalgamation of individual depressions into kilometre-wide elongated depressions. Renewed expulsion could lead to cannibalization of older pockmarks and contribute to the complex morphology.
- The variable infill and the depositional surfaces of the giant pockmarks might have influenced hydrocarbon charge pathways when the main source rock became mature (Bo Member) during the Miocene. In order to predict the type of infill, and thus extraction potential of the pockmarked reservoir, a type of machine learning could help.

This will indeed help optimize future planning of horizontal wells in the Halfdan region.

- Giant pockmarks on top of inverted Campanian structures are firmly added to the catalogue of seismic features within the Chalk Group, as precursor fluid migration indicators (from an earlier expulsion phase) of the main hydrocarbon accumulations found at present.

Acknowledgements

The authors kindly acknowledge the Danish Underground Consortium (Total, Shell, Chevron, and Nordsøfonden) for providing seismic and well data and the permission to publish the results. Andrew Hoover and Katherine Lauriks (Total) are kindly thanked for their input during technical discussions on the features. Michael Hertle (Total) is kindly thanked for providing modelled vitrinite reflectance data. We kindly thank our colleagues at the Stable Isotope Laboratory at University of Miami for their warm welcome, their help, and for hosting the clumped isotope research project in summer of 2017. We kindly want to thank the follow software companies for providing academic licenses: Schlumberger for providing Petrel E&P, Eliis for providing PaleoScan™, and ffA GeoTeric for providing GeoTeric. The research leading to these results has received funding from the Danish Hydrocarbon Research and Technology Centre under the Advanced Water Flooding program.

References

- Andresen, K. J., & Huuse, M. (2011). 'Bulls-eye' pockmarks and polygonal faulting in the Lower Congo Basin: relative timing and implications for fluid expulsion during shallow burial. *Marine Geology*, 279(1-4), 111-127.
- Andresen, K. J., Huuse, M., & Clausen, O. R. (2008). Morphology and distribution of Oligocene and Miocene pockmarks in the Danish North Sea—implications for bottom current activity and fluid migration. *Basin Research*, 20(3), 445-466.
- Back, S., Van Gent, H., Reuning, L., Grötsch, J., Niederau, J., & Kukla, P. (2011). 3D seismic geomorphology and sedimentology of the Chalk Group, southern Danish North Sea. *Journal of the Geological Society*, 168(2), 393-406.
- Back, S., Van Gent, H., Reuning, L., Grötsch, J., Niederau, J., & Kukla, P. (2011). 3D seismic geomorphology and sedimentology of the Chalk Group, southern Danish North Sea. *Journal of the Geological Society*, 168(2), 393-406.
- Cartwright, J. A. (1989). The kinematics of inversion in the Danish Central Graben. Geological Society, London, Special Publications, 44(1), 153-175.
- Cartwright, J., James, D., & Bolton, A. (2003). The genesis of polygonal fault systems: a review. Geological Society, London, Special Publications, 216(1), 223-243.
- Esmerode, E. V., Lykke-Andersen, H., & Surlyk, F. (2008). Interaction between bottom currents and slope failure in the Late Cretaceous of the southern Danish Central Graben, North Sea. *Journal of the Geological Society*, 165(1), 55-72.
- Fehmers, G. C., Printz, B., & Febriany, G. (2012, June). Mapping of gas migration into, and out of, the Tyra Field in the Danish North Sea. In 74th EAGE Conference and Exhibition incorporating EUROPEC 2012.
- Gennaro, M., Wonham, J. P., Sælen, G., Walgenwitz, F., Caline, B., & Fay-Gomord, O. (2013). Characterization of dense zones within the Danian chalks of the Ekofisk Field, Norwegian North Sea. *Petroleum Geoscience*, 19(1), 39-64.
- Ghosh, P., Adkins, J., Affek, H., Balta, B., Guo, W., Schauble, E. A., ... & Eiler, J. M. (2006). 13C–18O bonds in carbonate minerals: a new kind of paleothermometer. *Geochimica et Cosmochimica Acta*, 70(6), 1439-1456.
- Henriksen, K., Gommessen, L., Hansen, H. P., Kistrup, J. P., & Steekelenburg, C. (2009, January). Optimizing Chalk Reservoir Development Using Detailed Geophysical Characterization: The Halfdan Northeast Field, Danish North Sea. In Offshore Europe. Society of Petroleum Engineers.
- Ineson, J. R., Bojesen-Koefoed, J. A., Dybkjær, K., & Nielsen, L. H. (2003). Volgian–Ryazanian 'hot shales' of the Bo Member (Farsund Formation) in the Danish Central Graben, North Sea: stratigraphy, facies and geochemistry. The Jurassic of Denmark and Greenland. Geological Survey of Denmark and Greenland Bulletin, 1, 403-436.
- Japsen, P., Britze, P., & Andersen, C. (2003). Upper Jurassic–Lower Cretaceous of the Danish Central Graben: structural framework and nomenclature. The Jurassic of Denmark and Greenland. Geological Survey of Denmark and Greenland Bulletin, 1, 233-246.
- Kim, S. T., & O'Neil, J. R. (1997). Equilibrium and nonequilibrium oxygen isotope effects in synthetic carbonates. *Geochimica et Cosmochimica Acta*, 61(16), 3461-3475.
- Kyrkjebø, R., Gabrielsen, R. H., & Faleide, J. I. (2004). Unconformities related to the Jurassic–Cretaceous synrift–post-rift transition of the northern North Sea. *Journal of the Geological Society*, 161(1), 1-17.

- Liu, Y., 2017. Applications of Machine Learning for Seismic Quantitative Interpretation, in: *GeoConvention*. Calgary, Canada, pp. 1–5
- Lonergan, L., Cartwright, J., Laver, R., & Staffurth, J. (1998). Polygonal faulting in the Tertiary of the central North Sea: implications for reservoir geology. *Geological Society, London, Special Publications*, 127(1), 191–207.
- Laake, A., 2013. Structural interpretation in color—A new RGB processing technique for extracting geological structures from seismic data, in: *SEG Technical Program Expanded Abstracts 2013*. Society of Exploration Geophysicists, pp. 1472–1476.
- Masoumi, S., Reuning, L., Back, S., Sandrin, A., & Kukla, P. A. (2014). Buried pockmarks on the Top Chalk surface of the Danish North Sea and their potential significance for interpreting palaeocirculation patterns. *International Journal of Earth Sciences*, 103(2), 563–578.
- Møller, J. J., & Rasmussen, E. S. (2003). Middle Jurassic–Early Cretaceous rifting of the Danish Central Graben. *The Jurassic of Denmark and Greenland. Geological Survey of Denmark and Greenland Bulletin*, 1, 247–264.
- Petersen, H., Nielsen, L., Bojesen-Koefoed, J. A., Mathiesen, A., Kristensen, L., & Dalhoff, F. (2008). Evaluation of the quality, thermal maturity and distribution of potential source rocks in the Danish part of the Norwegian–Danish Basin. *Geological Survey of Denmark and Greenland Bulletin*, 16, 1–27.
- Schauble, E. A., Ghosh, P., & Eiler, J. M. (2006). Preferential formation of ^{13}C – ^{18}O bonds in carbonate minerals, estimated using first-principles lattice dynamics. *Geochimica et Cosmochimica Acta*, 70(10), 2510–2529.
- Schiøler, P., Andsbjerg, J., Clausen, O. R., Dam, G., Dybkjær, K., Hamberg, L., ... & Rasmussen, J. A. (2007). Lithostratigraphy of the palaeogene-lower neogene succession of the Danish North Sea (Vol. 12). *Geological Survey of Denmark and Greenland*.
- Schneider, F., Dubille, M., Montadert, L. (2016) Modeling of microbial gas generation: application to the eastern Mediterranean “Biogenic Play”. *Geologica Acta*, 14, issue 4, 403–417
- Smit, F.W.H. (2014). Seismic stratigraphy, basin evolution and seismic geomorphology of the Late Cretaceous and earliest Paleocene Chalk Group in the Danish Central Graben. MSc thesis, Aarhus University, Denmark
- Smit, F.W.H., van Buchem, F.S.P., Schmidt, I., & Stemmerik, L. (2017). Updated seismic geomorphological workflow applied to the Chalk Group. In 2017 SEG International Exposition and Annual Meeting. Society of Exploration Geophysicists.
- Smit, F. W. H., van Buchem, F. S. P., Holst, J. H., Lüthje, M., Anderskov, K., Thibault, N., ... & Welch, M. (2018). Seismic geomorphology and origin of diagenetic geobodies in the Upper Cretaceous Chalk of the North Sea Basin (Danish Central Graben). *Basin Research*.
- Staudigel, P. T., Murray, S., Dunham, D. P., Frank, T. D., Fielding, C. R., & Swart, P. K. (2018). Cryogenic Brines as Diagenetic Fluids: Reconstructing the Diagenetic History of the Victoria Land Basin using Clumped Isotopes. *Geochimica et Cosmochimica Acta*.
- Surlyk, F., Jensen, S. K., & Engkilde, M. (2008). Deep channels in the Cenomanian–Danian Chalk Group of the German North Sea sector: Evidence of strong constructional and erosional bottom currents and effect on reservoir quality distribution. *AAPG bulletin*, 92(11), 1565–1586.
- Swart, P. K. (2015). The geochemistry of carbonate diagenesis: The past, present and future. *Sedimentology*, 62(5), 1233–1304.
- Swart, P. K., Cantrell, D. L., Arienzo, M. M., & Murray, S. T. (2016). Evidence for high temperature and ^{18}O -enriched fluids in the Arab-D of the Ghawar Field, Saudi Arabia. *Sedimentology*, 63(6), 1739–1752.
- Teichert, B. M., Bohrmann, G., & Suess, E. (2005). Chemohermes on Hydrate Ridge—Unique microbially-mediated carbonate build-ups growing into the water column. *Palaeogeography, Palaeoclimatology, Palaeoecology*, 227(1), 67–85.
- Van Buchem, F.S.P., Smit, F.W.H., Buijs, G.J.A., Trudgill, B., Larsen, P.H., Trudgil, B., Larsen, P.H., (2018). Tectonostratigraphic framework and depositional history of the Cretaceous – Danian succession of the Danish Central Graben (North Sea) – new light on a mature area, in: Bowman, M.B., Levell, B. (Eds.), *Petroleum Geology of NW Europe: 50 Years of Learning - Proceedings of the 8th Petroleum Geology Conference*. Geological Society of London, pp. 9–46.
- Vejbæk, O. V., & Andersen, C. L. A. U. S. (2002). Post mid-Cretaceous inversion tectonics in the Danish Central Graben—regionally synchronous tectonic events. *Bulletin of the Geological Society of Denmark*, 49(2), 93–204.
- Vejbæk, O. V., Frykman, P., Bech, N., & Nielsen, C. M. (2005, January). The history of hydrocarbon filling of Danish chalk fields. In *Geological Society, London, Petroleum Geology Conference series* (Vol. 6, No. 1, pp. 1331–1345). Geological Society of London.
- Vidalie, M., van Buchem, F.S.P., Schmidt, I., & Uldall, A. (2014). Seismic stratigraphy of the Lower Cretaceous Valhall Formation (Danish Graben, North Sea). *First Break*, 32(6), 71–80

Chapter V, Paper 4

Distinguishing syn- and post-depositional fluid migration in the Chalk Group using clumped isotope analysis and seismic geomorphology (Upper Cretaceous, Danish Central Graben and onshore United Kingdom)

F.W.H. Smit^{1*}, P.K. Swart², P.T. Staudigel², van Buchem, F.S.P., L. Stemmerik³

Submission to Marine and Petroleum Geology

¹ Technical University of Denmark, Danish Hydrocarbon Research and Technology Centre, Elektrovej Building 375, 2800 Kongens Lyngby

² Department of Marine Geosciences, University of Miami, Rosenstiel School for Marine and Atmospheric Sciences, 4600 Rickenbacker Causeway, Miami, FL 33149, USA

³ University of Copenhagen, Natural History Museum of Denmark, Øster Voldgade 5-7, 1350 Copenhagen K

Abstract

This study combines seismic geomorphology and clumped isotope analysis of chalk in order to reveal the origin of fluids involved in the formation of distinctive geobodies in the Upper Cretaceous chalk of the Danish Central Graben. The results from the clumped isotope analysis provide key information about the diagenetic regime associated with different seismic-scale geometries and help to distinguish between depositional and diagenetic anomalies. Clumped isotope analyses were performed on material from three different settings: 1) A field of syn-depositional giant pockmarks in the Danian Ekofisk Formation; 2) stratigraphically cross-cutting diagenetic geobodies in the Upper Cretaceous chalk on the Ryan Anticline; and 3) heavily deformed chalk with calcite veins outcropping at Selwicks Bay (UK). Cross plotting of (bulk) temperature versus fluid $\delta^{18}O$ data were used to differentiate closed-system diagenesis from open-system diagenesis involving extra-formational fluids. Closed-system diagenesis is characterized by a positive, linear trend of temperature and fluid $\delta^{18}O$ reflecting that with increasing burial depth (and temperature), lighter ^{16}O isotopes will preferentially go into the calcite cement, whereas the heavier ^{18}O isotopes will remain within the formation water. Bulk temperatures in this trend range from 22 to 85 °C ($\pm 15^\circ\text{C}$, 1 SE), and the corresponding fluid $\delta^{18}O$ values from -1.60 to 6.7‰. Cold temperatures and negative fluid $\delta^{18}O$ likely represent early cementation near the seafloor or highly-porous chalks that have not undergone burial diagenesis. Material that has undergone open-system diagenesis deviates from this trend, having bulk temperatures between 48 to 104°C and fluid $\delta^{18}O$ values from -2.5 to -0.1‰. These samples originate from calcite veins and surrounding chalk at Selwicks Bay and the stratigraphically cross-cutting geobodies on the Ryan Anticline, and suggest that these represent cementation by external fluids migration up along faults and fracture zones. Chalk host rock at the Ryan Anticline and all samples from the Ekofisk pockmark field are characterized by closed-system diagenesis indicating that the outburst of gas was not affecting the diagenesis of the chalk. Temperature and fluid $\delta^{18}O$ data used in combination with basin modelling can provide insights in timing of fluid migration.

Keywords: closed-system and open-system diagenesis, faults, fractures, calcite veins, geochemical analysis, geochemistry, fluid expulsion, pockmarks

Introduction

Fluid migration indicators, if properly understood, provide important insights in aspects of fluid expulsion during basin history usually obtained in basin modelling workflows (Smit *et al.*, Papers 2 and 3). This includes factors crucial in hydrocarbon exploration like evaluation of source rock maturity, timing of biogenic gas formation, and mapping of fluid migration pathways. In the Danish sector of the North Sea recognition of seismic anomalies in the Upper Cretaceous Chalk Group has helped to identify syn- and post-depositional fluid migration and to reconstruct timing of fluid expulsion events. Syn-depositional expulsion of pressurized (gas-bearing) fluids has created pockmarks (explosive style) and seep carbonates (seepage style) whereas post-depositional fluid migration has caused diagenetic reactions (Smit *et al.*, 2018), or importantly, hydrocarbon accumulations if sealing strata are present.

The aim of this study is to combine seismic geomorphology and clumped isotope analysis of chalk in order to reveal the origin of fluids involved in the formation of these distinctive geobodies, and based on the trends in the clumped isotope data, we provide a theoretical model for the relationship between burial depth and $\delta^{18}O$ values of cement, bulk sample, and fluid. The results from the clumped isotope analysis also provide key information about the diagenetic regime associated with different seismic-scale geometries and help to distinguish between depositional and diagenetic anomalies. We build on three case studies by Smit *et al.* (2018, Papers 2 and 3) and supplement with data from onshore UK (Fig. 1a). Integrated seismic geomorphological workflow is a powerful tool to investigate possible fluid migration indicator features as it provides the sedimentary geological framework for other investigations (petrography, petrophysics, and geochemistry). By coupling these different disciplines, a novel example of fault-bound seismic-scale diagenesis was documented within the Danish Central Graben (Smit *et al.*, 2018).

In this paper we take advantage of recent developments in stable isotope geochemistry that have provided a solid carbonate palaeothermometer

independent of the fluid $\delta^{18}O$: clumped isotope analysis (Ghosh *et al.*, 2007; Schauble *et al.*, 2006). Rather than measuring bulk amounts of $C^{12}, C^{13}, O^{16}, O^{17}, O^{18}$ isotopes, it measures the ‘isotopologues’ of CO_2 (same molecule, different isotopic composition) with mass 44 to 49 (Ghosh *et al.*, 2006). The amount of isotopologue 47 (mainly $O^{16}C^{13}O^{18}$), expressed as $\Delta 47$, decreases with increasing temperature and can be used to estimate the (bulk) precipitation temperature. Since bulk $\delta^{18}O$ and $\delta^{13}C$ can be inferred from mass 45/44 and 46/44 (Murray *et al.*, 2016) fluid $\delta^{18}O$ can be obtained from the palaeothermometer function of Craig, (1965). This is thus a very effective method to obtain absolute precipitation temperature and fluid $\delta^{18}O$, which are very useful variables in fluid migration indicators.

Geological setting

Chalk Group in the North Sea (three locations)

The three case studies cover different parts of the Upper Cretaceous and early Paleocene Chalk Group in the North Sea Basin (Figs 1b and 2). During the Late Cretaceous, an epeiric sea was established in NW Europe due to a combination of high eustatic sea level, thermal subsidence, and low topographic relief (Surlyk *et al.*, 2003). Thick successions of pelagic cool carbonates, up to 3 km, accumulated in the North Sea area, giving the rock a widespread occurrence (Fig. 1a, b). The thickest successions were deposited within the Central Graben, a Late Jurassic failed rift system in the central sections of the North Sea (Fig. 1b). Subsequent Tertiary uplift at the basin margins gave rise to well-known outcrops in the UK and Denmark, while the chalk in the Central Graben remained buried underneath 1 to 4 km of Cenozoic sediments (Vejbæk *et al.*, 2010) (Fig. 1b).

Case study 1 and 2 are located within the Danish North Sea, and encompass Danian-aged strata of the Ekofisk Formation and the entire Chalk Group respectively (Figs 1b and 2, case study column). Case study 3 is an outcrop study located onshore UK (Selwicks Bay at Flamborough Head),

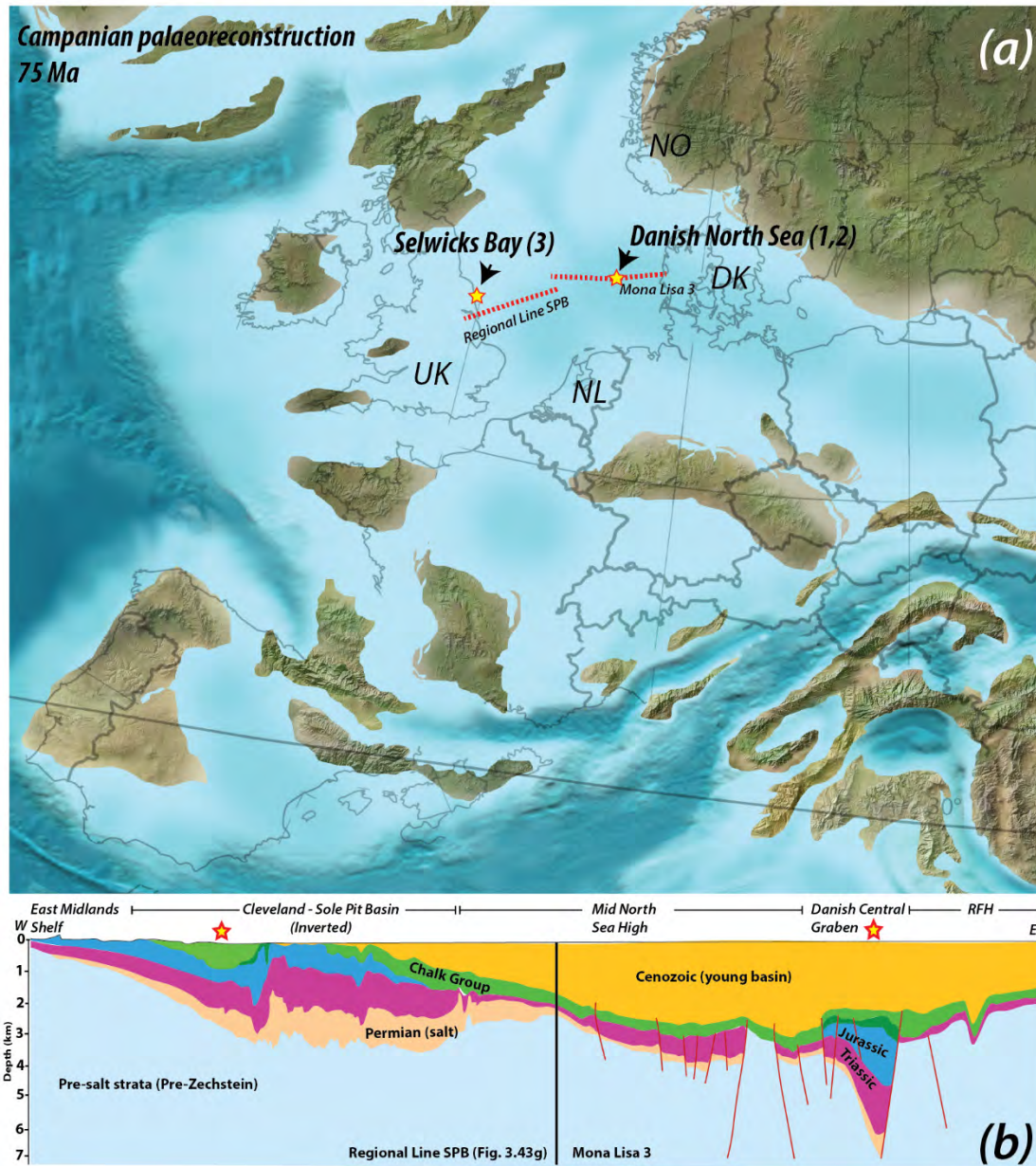


Figure 1. (a) Palaeogeographic reconstruction at Mid-Cretaceous times (Campanian, 75 Ma) showing location of study areas. Study area 1 (giant pockmarks) and 2 (diagenetic geobodies) within Danish North Sea, and study area 3 in Selwicks Bay, Flamborough Head, onshore UK. Location of regional lines indicated by red dotted line. (b) Compilation of two regional lines: Mona Lisa 3 in Danish sector to Mid North Sea High (Abramovitz and Thybo, 1999), and regional line from (Pharaoh *et al.*, 2010, Fig. 3.43g), indicating the regional correlation through the North Sea Basin. Map credits: © 2011 Colorado Plateau Geosystems Inc. and licensed for publication.

and the exposed stratigraphy is of Upper Santonian to Lower Campanian age (Figs 1b and 2).

Case study 1: Giant pockmarks

Case study 1 is located within the central section of the Danish Central Graben, where

Campanian (Mid-Cretaceous) basin inversion had profound impact on depocenter locations (Van Buchem *et al.*, 2018). The features of interest are located on top of the inverted Igor-Emma Ridge, where several hydrocarbon accumulations are present (e.g. Tyra, Halfdan, and Dan) (Fig. 3a). The Chalk Group is underlain by 400 m thick organic-rich

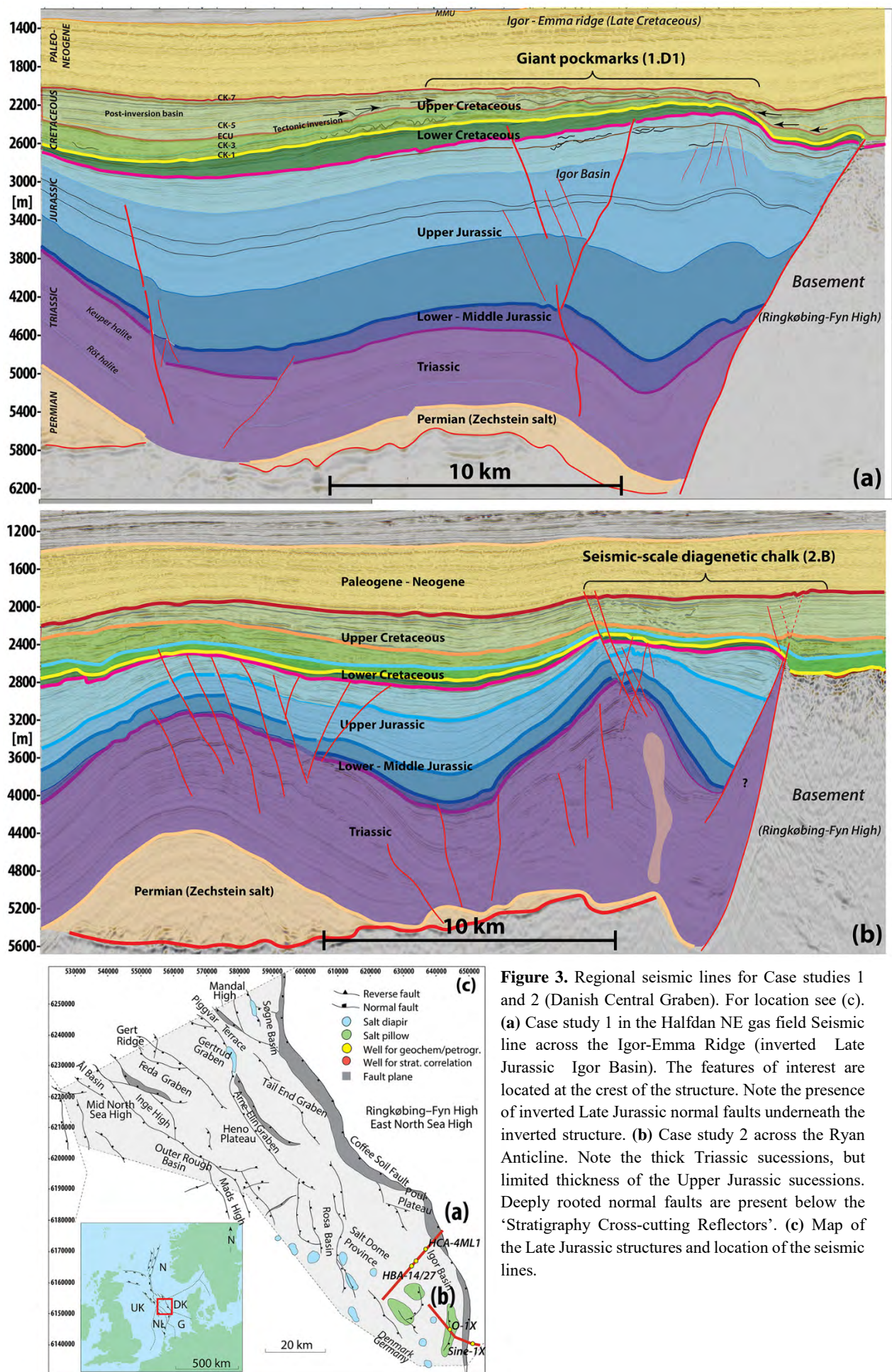


Figure 3. Regional seismic lines for Case studies 1 and 2 (Danish Central Graben). For location see (c). **(a)** Case study 1 in the Halfdan NE gas field Seismic line across the Igor-Emma Ridge (inverted Late Jurassic Igor Basin). The features of interest are located at the crest of the structure. Note the presence of inverted Late Jurassic normal faults underneath the inverted structure. **(b)** Case study 2 across the Ryan Anticline. Note the thick Triassic successions, but limited thickness of the Upper Jurassic successions. Deeply rooted normal faults are present below the 'Stratigraphy Cross-cutting Reflectors'. **(c)** Map of the Late Jurassic structures and location of the seismic lines.

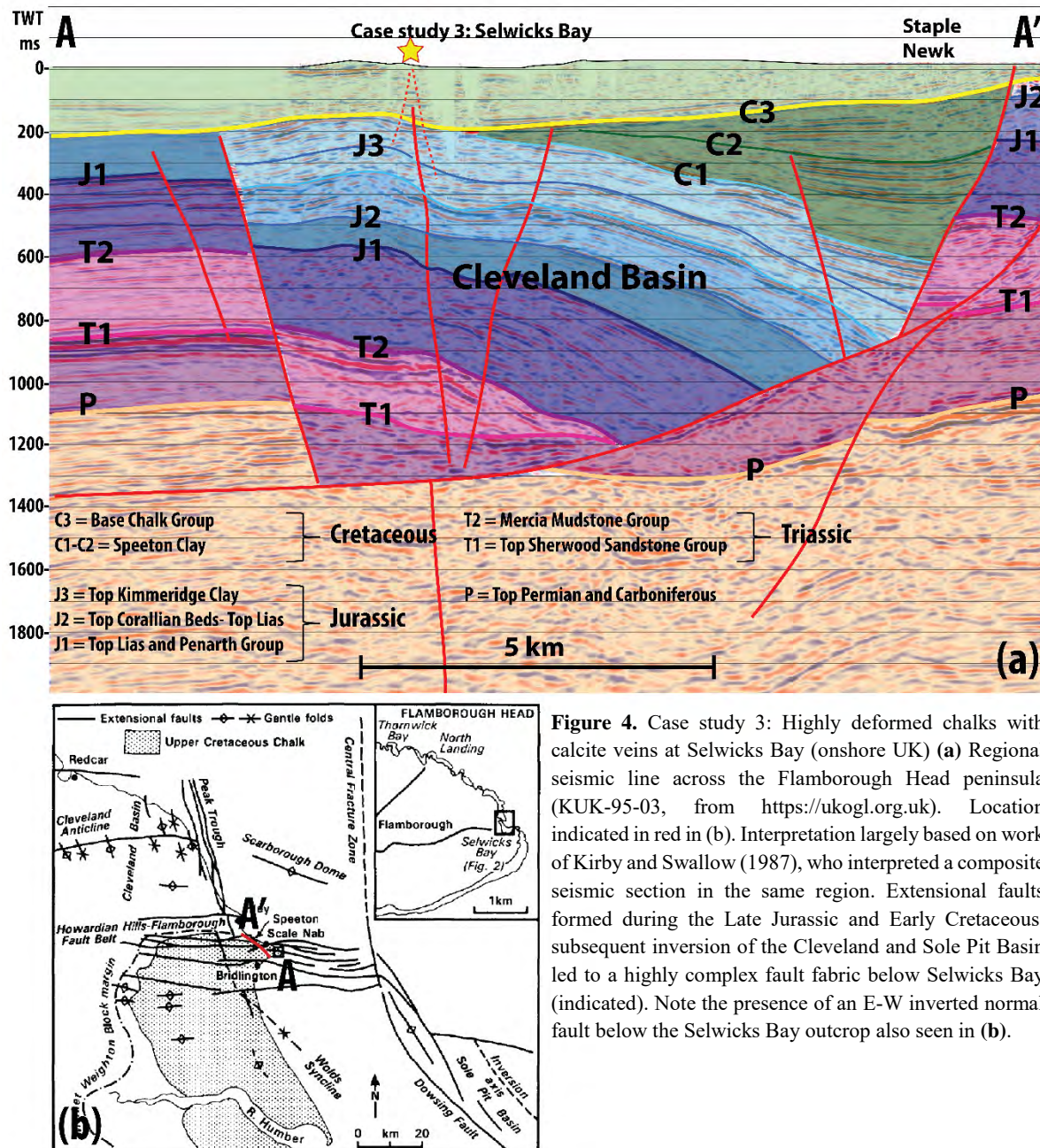


Figure 4. Case study 3: Highly deformed chinks with calcite veins at Selwicks Bay (onshore UK) (a) Regional seismic line across the Flamborough Head peninsula (KUK-95-03, from <https://ukogl.org.uk>). Location indicated in red in (b). Interpretation largely based on work of Kirby and Swallow (1987), who interpreted a composite seismic section in the same region. Extensional faults formed during the Late Jurassic and Early Cretaceous, subsequent inversion of the Cleveland and Sole Pit Basin led to a highly complex fault fabric below Selwicks Bay (indicated). Note the presence of an E-W inverted normal fault below the Selwicks Bay outcrop also seen in (b).

Case study 3: Highly deformed strata

Case study 3 is located in Flamborough Head, central United Kingdom (Fig. 4). Regional seismic sections across the area reveal a complex structural history that involves extension during the Late Jurassic and Early Cretaceous to form E-W oriented grabens (Cleveland Basin) (Fig. 4). A deeply rooted listric fault formed during Early Cretaceous, which accommodated deposition of

Lower Cretaceous shales in the basin centre, while erosion occurred at the basin margins (Kirby and Swallow, 1987). During the Late Cretaceous, chinks were deposited on top of the complex fault fabric, which subsequently became buried to ca. 2 km depth before it was brought back to the surface by post-Cretaceous inversion movements (Starmer, 1995).

Data and methods

Seismic data and interpretation techniques

A 3000 km² subcrop of a regional seismic data set (pre-stack depth migrated) is available for Case study 1 and 2 in the Danish Central Graben (Fig. 3c). The quality of the data is in general very good, though it deteriorates around salt diapirs. The polarity follows North Sea convention, with a downward increase in acoustic impedance represented by a trough (shown in red). The dominant frequency in the Chalk Group is approximately 30 Hz, and average acoustic velocity is around 3400 m/s, leading to an average vertical resolution of 28.3 m as a quarter of the wavelength of the dominant frequency (Sheriff, 1979). For Case study 3 at Flamborough Head, onshore 2D seismic line KUK-95-03 (recorded in 1995) is available to provide geological context. Seismic interpretation is largely based on work by Kirby and Swallow (1987) on similar composite seismic sections over the Flamborough Head area.

A neural network methodology is applied for seismic interpretation (PaleoScan™, c.f. Pauget *et al.*, 2009) in order to create a stack of stratigraphy consistent horizon slices in the Chalk Group. To increase the information extracted from the stratal horizons, spectral decomposition data reveals information in the frequency domain. Based on a dominant frequency of 30 Hz, three spectral frequency cubes (20, 30, 40 Hz) were calculated using a matching pursue algorithm in GeoTeric 2016.2 (c.f. Morozov *et al.*, 2013).

Well material and logs

In total, five wells were used in this study (3 horizontal, 2 vertical), all in the Danish sector. Full log suites were available for the three horizontal wells (Case study 1: HCA-4ML1, HBA-14C, HBA-27A) and one vertical well (Sine-1X), while O-1X (Case study 2) only has gamma-ray and deep resistivity logs.

Geochemical analysis

Material for stable carbon and oxygen isotope analysis comprise drill cuttings and a 10 m core in O-1X. Spacing of cuttings is 10 m in the horizontal wells and O-1X, and 3 m in Sine-1X. Carbonates were analysed at Iso-Analytical (UK) using continuous flow isotope ratio mass spectrometry (CF-IRMS). Values are reported as $\delta^{13}\text{C}$ and $\delta^{18}\text{O}$, deviations in parts per thousand relative to the V-PDB and V-SMOW standard. Standard deviations are reported to be better than 0.08‰ for $\delta^{13}\text{C}$ and 0.02‰ for $\delta^{18}\text{O}$.

In order to constrain diagenesis further, this study has utilized for the first time for chalks in the North Sea Basin, an absolute carbonate palaeothermometer, clumped isotope analysis (Ghosh *et al.*, 2006; Schauble *et al.*, 2006; Swart, 2015). Samples for clumped isotope analysis were selected in Case study 1 (n=34) based on location with respect to seismic identified depressions, while in Case study 2 sampling is based on observed trends in $\delta^{18}\text{O}$ that make up three zones (c.f. Smit *et al.*, 2018) and cover the entire stratigraphy (n=26). Sampling in Case study 3 was done based on outcrop architecture, and one chalk sample and two calcite veins were selected for analysis. Sample preparation and $\Delta 47$ measurements were done in the Stable Isotope Laboratory at University of Miami and follow the procedures as outlined by Staudigel *et al.* (2018) and Swart *et al.* (2016). Average standard errors are $\pm 7^\circ\text{C}$ for temperature, and $\pm 1.4\text{‰}$ for fluid $\delta^{18}\text{O}$.

This method measures the amounts of isotopologues of CO₂ (e.g. same molecule, different isotope configurations) in an adjusted mass spectrometer (Thermo-Fischer Scientific, MAT 253). There are six different isotopologues (44-49), and the amount of isotopologue 47 ($\Delta 47$, $\text{C}^{13}\text{O}^{16}\text{O}^{18}$ is by far the most common) is a function of absolute precipitation temperature (Ghosh *et al.*, 2006). With increasing temperature, the amount of $\Delta 47$ will become smaller, and by comparison to reference materials that precipitated at known temperatures, the absolute temperature can be estimated. As bulk $\delta^{18}\text{O}$ is measured at the same time, two of the three

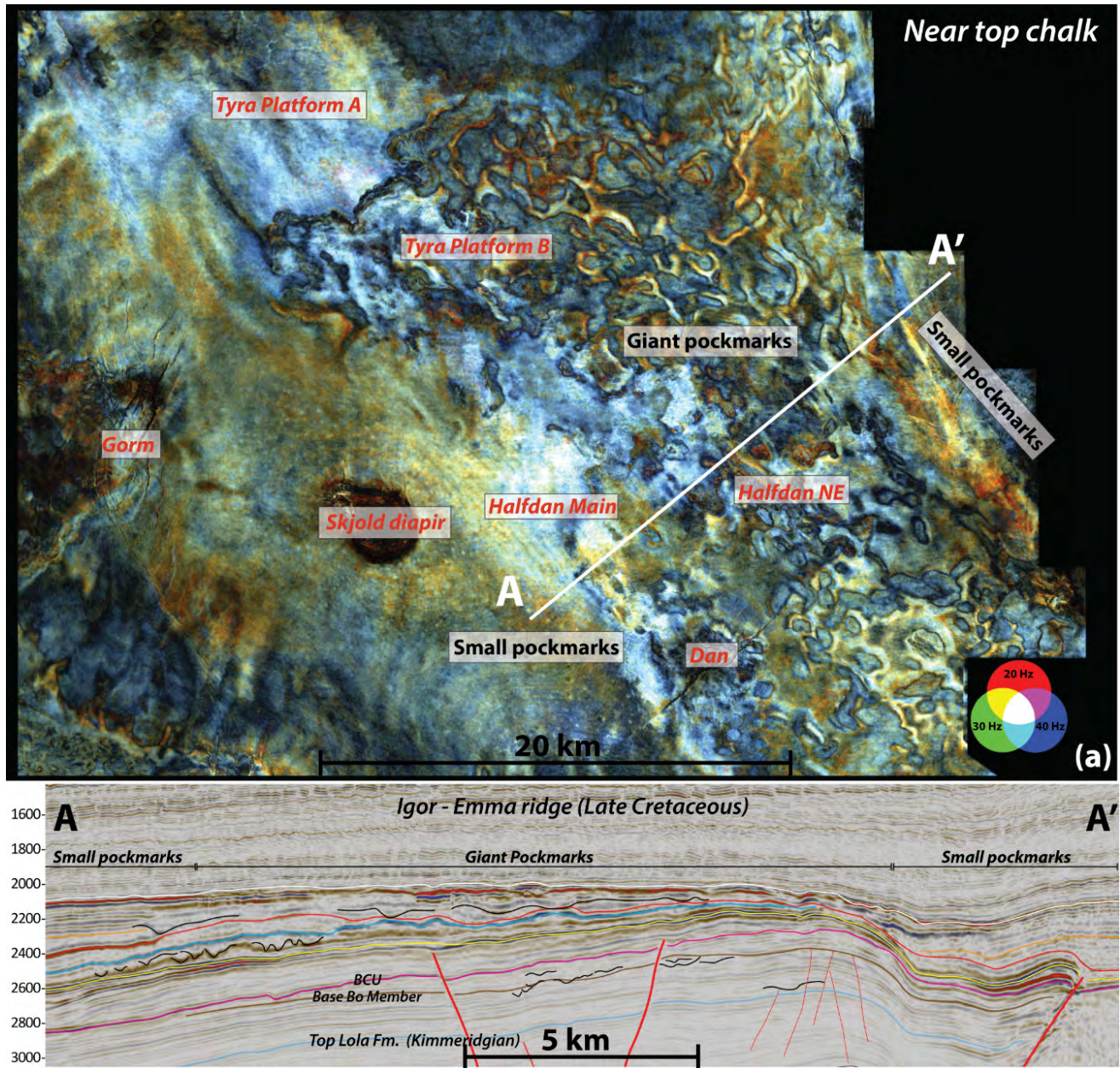


Figure 5. (a) Spectral decomposition data in RGB blend upon near top Chalk seismic horizons. Hydrocarbon fields indicated in red font. Two type of features are observed: a) small circular features, with a radius of 20-100 m, which are interpreted as small pockmarks; b) the highly irregular pattern observed within the Halfdan NE gas field and Tyra Platform B are 100 – 800 m wide, 20 – 80 m deep depressions (see b), and interpreted as amalgamated giant pockmarks that occur on top of the Igor-Emma Ridge. **(b)** The former basin became inverted during the Campanian, and deeply rooted normal faults are present that provided pathways for gas-bearing fluids from Jurassic source rocks.

unknowns in the classic palaeothermometer (equation 1, 2, c.f. Kim and O'Neill, 1997) are known (e.g. bulk $\delta^{18}O_{calcite}$ and temperature T), and the last unknown (fluid $\delta^{18}O_{H_2O}$) can be estimated.

$$1000 \ln \alpha(\text{calcite} - H_2O) = 18.03 \left(\frac{10^3}{T} \right) - 32.42 \quad (1)$$

$$\text{With } \alpha(\text{calcite} - H_2O) = \frac{1000 + \delta^{18}O_{calcite}}{1000 + \delta^{18}O_{H_2O}} \quad (2)$$

Results

Case study 1: Halfdan

At the top of the Igor-Emma Ridge, a highly complex morphology characterize the Danian Ekofisk Formation at the top of the Chalk Group

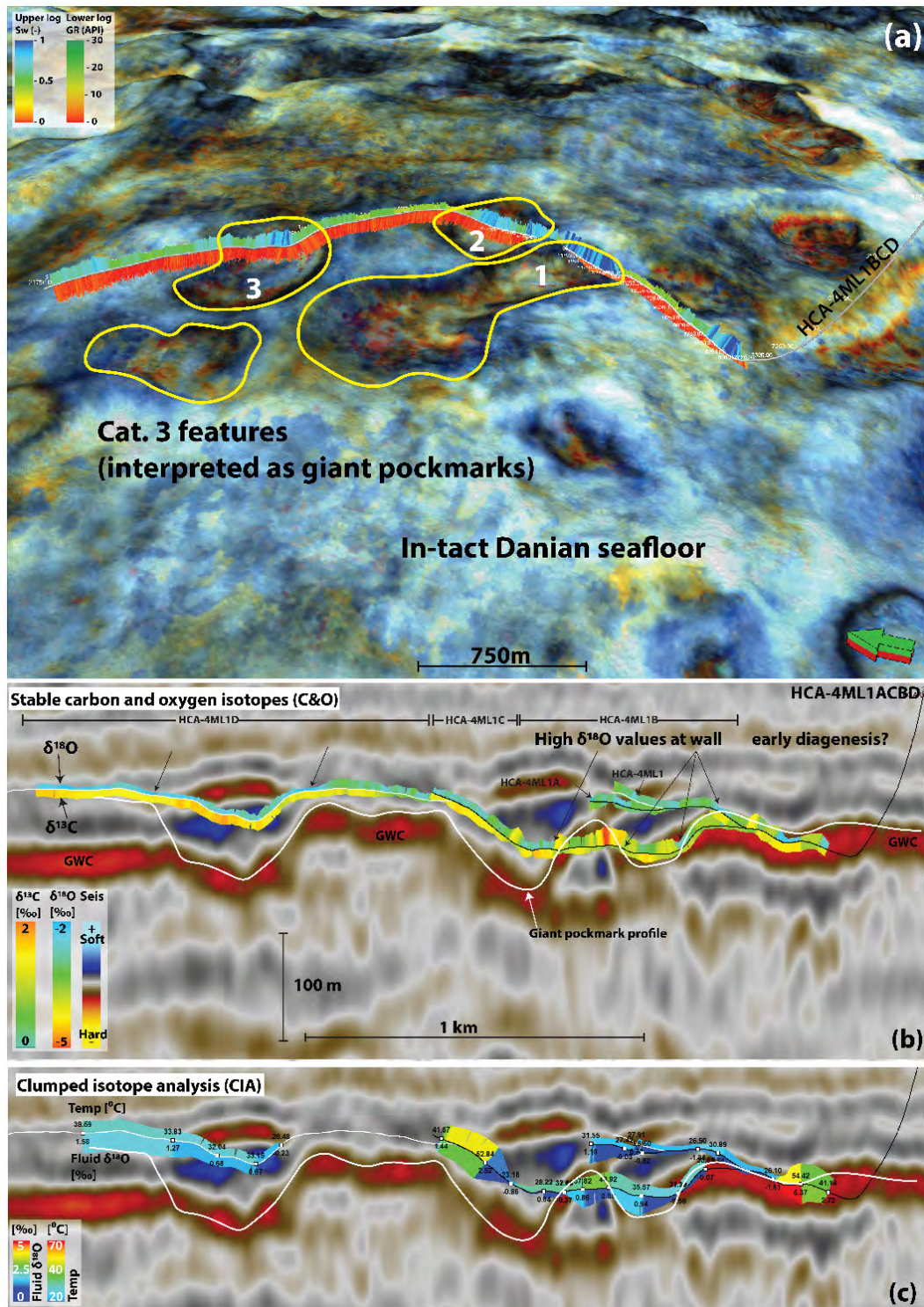


Figure 6. (a) Seismic horizon with spectral decomposition data in RGB blend (20, 30, 40 Hz). (b) Detailed seismic line through giant pockmark depressions in the Halfdan NE Gas Field. Well HCA-4ML1 (and sidetracks A-D) penetrate the depressions in which clays, marls, and chinks of Danian age are found. The upper log reflects bulk $\delta^{18}\text{O}$ values while the lower log reflects bulk $\delta^{13}\text{C}$ values. (c) Same seismic section, with clumped isotope results projected upon the well trajectory. Upper log represents bulk temperature, lower log represents bulk $\delta^{18}\text{O}$ of the fluid from which the material precipitated (coccoliths and cements). From Smit *et al.* (submitted).

(Fig. 5a). These features are 100 – 800 m wide, 20 - 80 m deep depressions observed within 2D sections (Fig. 5b). Their position at the highest points of the

Danian Basin, as well as their close link to underlying normal faults connecting organic-rich intervals, led

Smit *et al.* (Paper 3) to interpret these features as amalgamated giant pockmarks.

The giant pockmarks occur within a hydrocarbon-bearing interval of the Ekofisk Formation, and are penetrated by several horizontal wells. Well HCA-4ML1 (and sidetracks ABCD) penetrates three individual depressions (1-3), and wireline data and drill cuttings show significant variations in the infill of the depressions being composed of Danian chalk, marl, and chert, and younger Paleocene clay (Fig. 6, and Fig. 6c in Smit *et al.* Paper 3).

Bulk $\delta^{13}\text{C}$ values vary between 0.5 and 1.9‰ and bulk $\delta^{18}\text{O}$ are in the range -4.8 to -2.4‰ (Figs 6b and 7a). The bulk $\delta^{13}\text{C}$ values vary stratigraphically, which can be observed when the horizontal well moves up or down relative to the seismic bedding (Fig. 6b). Values are rather constant when the well follows the seismic stratigraphic bedding (e.g. more horizontal). Bulk $\delta^{18}\text{O}$ values seem to reach most positive values close to the surface separating the unaffected Danian sea floor from the pockmark fill (inner side of the infill) (Fig. 6b, black arrows). A cross-plot of the bulk $\delta^{13}\text{C}$ and

$\delta^{18}\text{O}$ values, color-coded for location within infill or seafloor, shows a large spread with no clear distinction between the two groups (Fig. 7a).

Bulk absolute temperature and fluid $\delta^{18}\text{O}$ values from clumped isotope analysis (CIA) of samples of both infill and intact seafloor chalk, range between 23 to 77°C ($\pm\text{SE}$, 7°C), and -1.6 to 5.4‰ ($\pm\text{SE}$, 1.4‰) respectively (Fig. 7b). A positive trend (slope 7.5°C/‰, $R^2=0.83$) can be observed between the two independent variables: with increasing temperature, fluid $\delta^{18}\text{O}$ becomes more positive. There is no clear zonation between the samples from the infill or from the intact seafloor. One point might be off this trend, and occurs within depression 2 (HCA-4ML1C, 14160 ft MD).

We interpret the observed positive trend as a normal burial diagenetic trend in a closed system. With increasing burial depth (and increasing temperature), lighter ^{16}O isotopes will preferentially be taken up into the crystal lattice of the chalk cement, and heavier ^{18}O isotopes will remain in the formation water. Therefore, with increasing burial diagenesis, higher temperatures and heavier fluids are observed (Swart *et al.*, 2016).

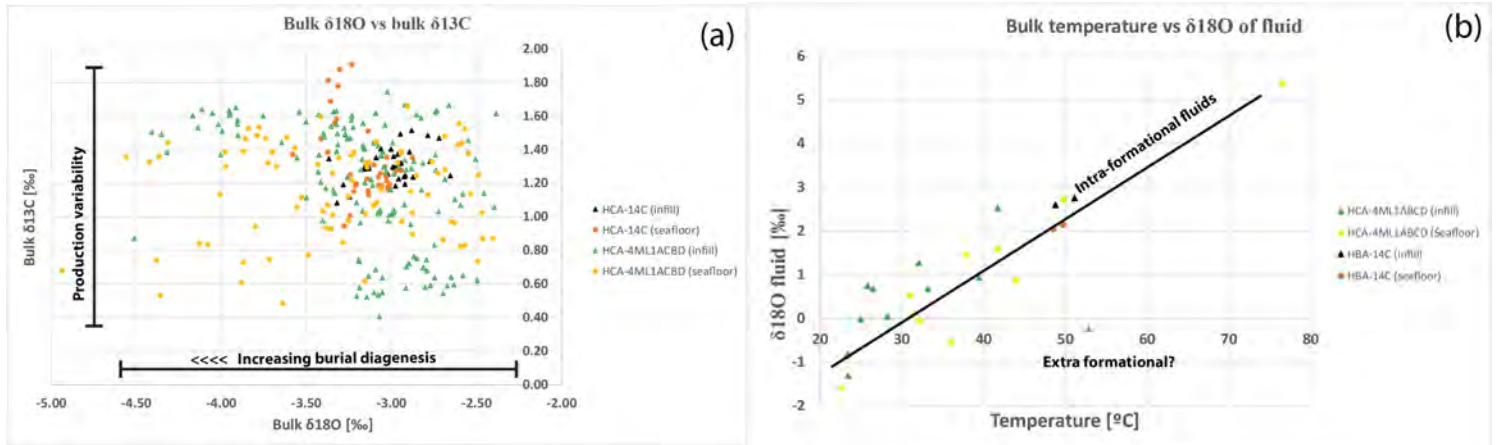


Figure 7. (a) Bulk $\delta^{18}\text{O}$ and $\delta^{13}\text{C}$ of the rock. Samples are divided by their occurrence within the infill or on the intact seafloor (see Fig 6a). The variability in $\delta^{13}\text{C}$ values (0.50 to 1.90 ‰) reflects primary production variability through time, and thus sampling from different stratigraphic intervals in the Danian. The variability in $\delta^{18}\text{O}$ values (-2.4 to -4.8‰) reflects increasing amounts of burial diagenetic cement. A large spread occurs within the samples, but no clear zonation between infill and intact seafloor is observed. **(b)** Independent variables bulk temperature of the rock, and bulk $\delta^{18}\text{O}$ of the precipitating fluid are cross-plotted for the Halfdan wells. Temperatures range from 23 to 77°C, fluid $\delta^{18}\text{O}$ between -1.6 to 5.4‰. A convincing positive correlation (slope 11°C/‰) is observed between the two independently acquired parameters. With increasing temperature (or burial depth), the $\delta^{18}\text{O}$ values of the formation fluids become more positive. This is reflecting normal burial diagenesis in a closed system. One point, within the infill of depression 2, deviates from this trend, which could reflect some extra-formational fluid – which is rather light (0‰) and hot (54°C).

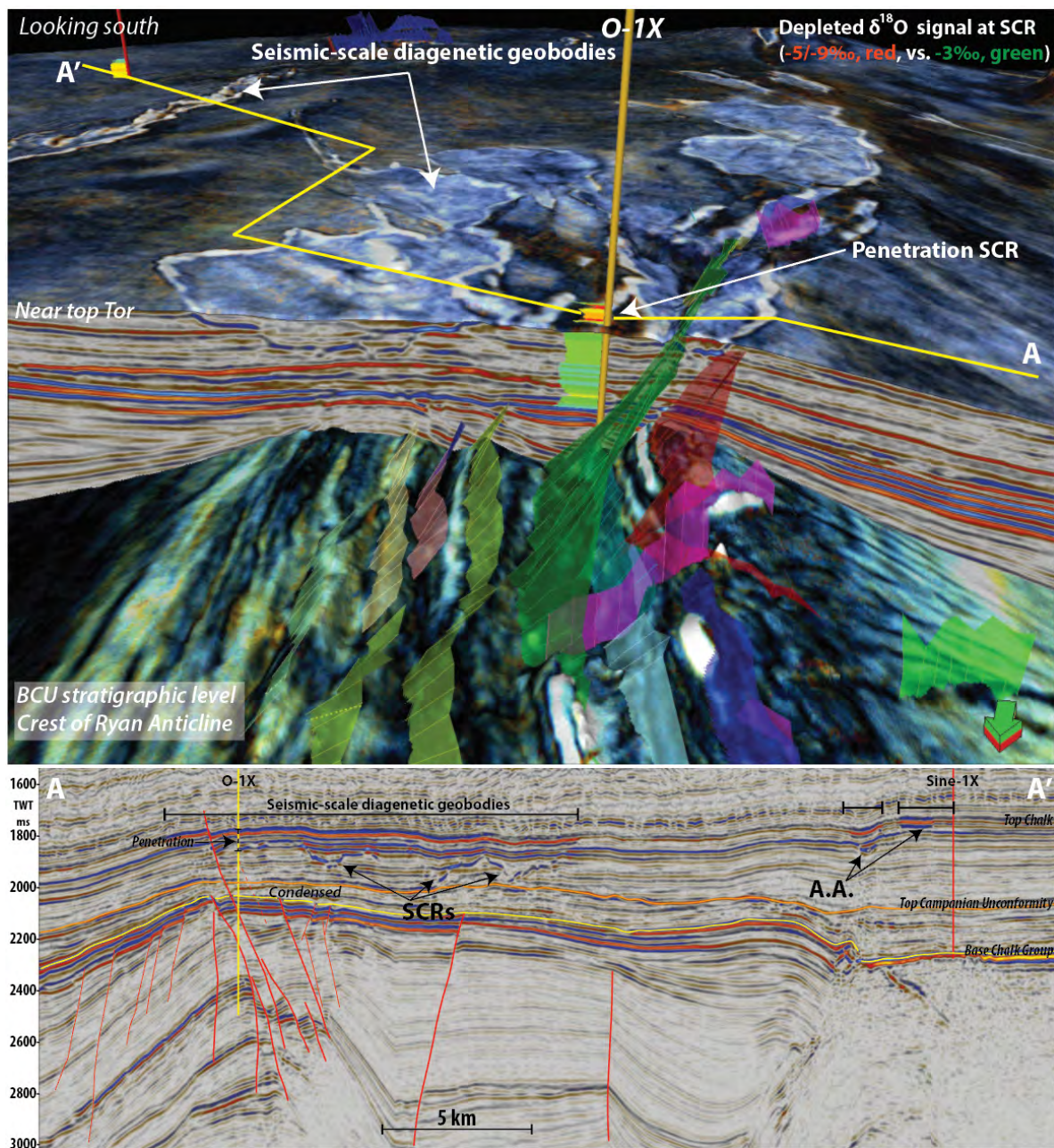


Figure 8. (a) Chair diagram with two seismic horizons (bottom: BCU; top: Near top Tor Formation) with spectral decomposition data (20, 30, 40 Hz). The high-density chinks outlined by the peak reflectors (boundary to low-density chinks), and occur as lobate and irregular high-frequency features (bluish colour). Note the penetration of O-1X into the anomaly upon the bulk $\delta^{18}\text{O}$ values decrease. Seismic line A-A' indicated with yellow line. **(b)** Regional seismic line over the Ryan Anticline. Seismic-scale diagenetic geobodies are outlined by Stratigraphy Cross-cutting Reflectors (SCRs) and seismic Amplitude Anomalies (A.A.), and occur as high-amplitude reflectors. Modified from Smit *et al.* (2018)

Case Study 2: Ryan Anticline

On top of the Ryan Anticline, in the southern Danish Central Graben, Stratigraphy Cross-cutting Reflectors (SCRs) and Amplitude Anomalies (A.A.) are observed within the Tor and Ekofisk Formations (Fig. 8a and b). The features represent dense zones within the Chalk Group that formed as a result of compaction due to overpressure leak-off, and

cementation due to introduction of manganese-rich fluids into the chalk, dictated by the underlying Late Jurassic fault fabric (Smit *et al.*, 2018). Wells O-1X and Sine-1X occur within the affected area and bulk $\delta^{18}\text{O}$ values generally show a decrease from -2‰ in high-porous chinks, to -9‰ within the dense chinks (SCRs affected stratigraphy) (Fig. 8a). In addition, the Regional Porosity Marker separates low-porous chinks and the upper high-porosity chinks, and $\delta^{18}\text{O}$ values decrease from -3.2‰ to -5.6‰ (Fig. 9a).

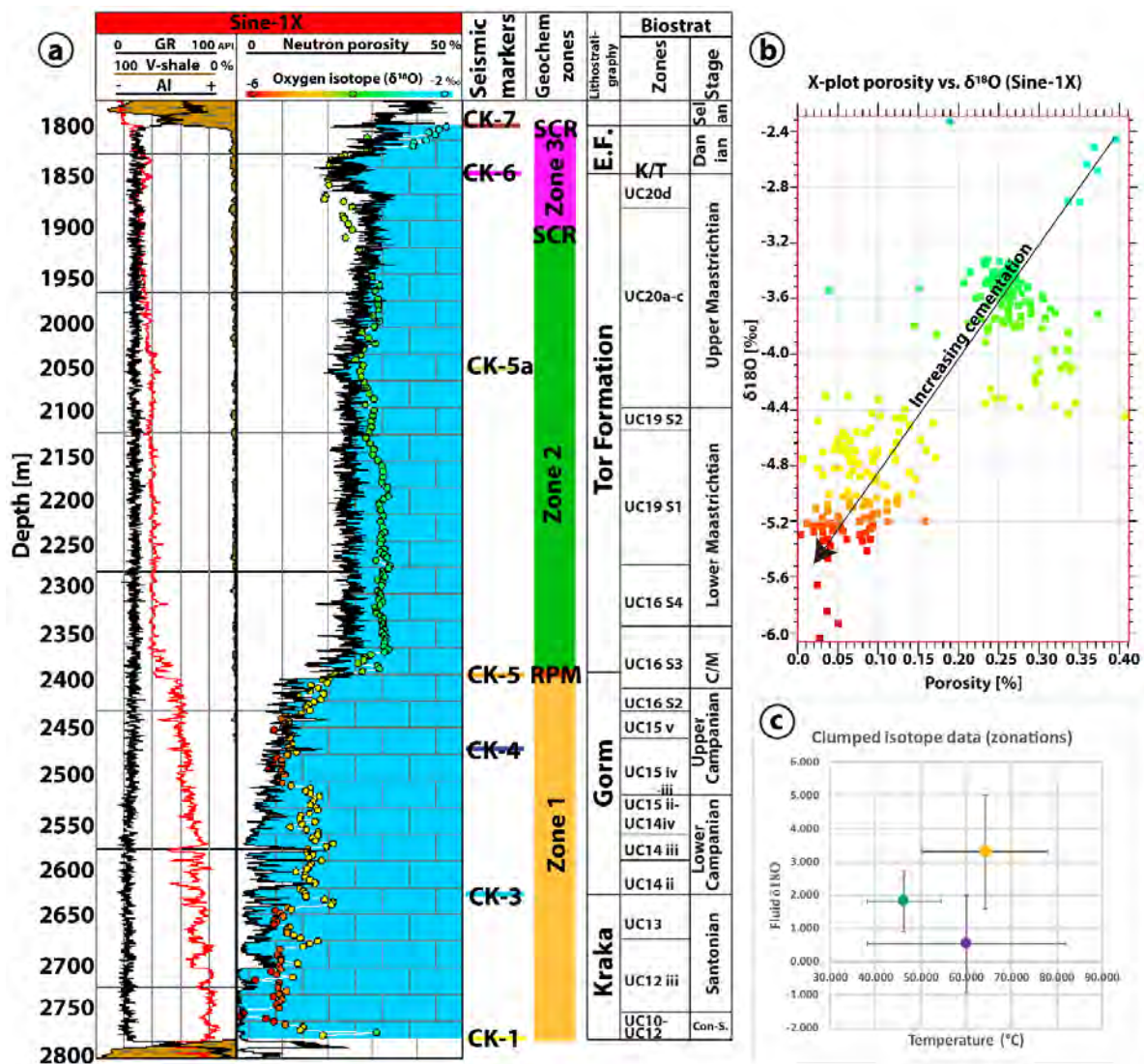


Figure 9. (a) Petrophysical logs from Sine-1X (gamma ray, sonic, and neutron-derived porosity), bulk $\delta^{18}O$ values as dots. Seismic markers, formations, and biostratigraphy indicated. A clear break in porosity is observed at the Regional Porosity Marker (RPM), which also marks a decrease in $\delta^{18}O$ values (b) cross-plot between neutron-derived porosity and $\delta^{18}O$ values from same interval. A general positive trend can be observed, where $\delta^{18}O$ decrease with decreasing porosity. (c) Clumped isotope analysis results with respect to the differentiation in three zones. The samples from each zone can be differentiated in bulk temperature and fluid $\delta^{18}O$ as well. Reprinted from Smit *et al.* (2018)

There is therefore a general positive relationship between bulk $\delta^{18}O$ values and porosity (Fig. 9b).

CIA was done on 23 samples selected from below the RPM (Zone 1), within the high-porous chalks (Zone 2), and from the dense chalk zones outlined by the SCRs (Zone 3) (Fig. 10). Bulk temperatures vary between 29 to 104°C (\pm SE, 7°C), and bulk fluid $\delta^{18}O$ vary between -2.5 to 6.7‰ (\pm SE, 1.4‰). In both wells, the RPM marks a significant deviation of temperatures and fluid $\delta^{18}O$ values (Fig. 10a, b). Chalks within Zone 1 in O-1X have temperatures between 39 and 51°C, and fluid $\delta^{18}O$ between 1.5 to 4.0‰ (Figs 10a). In Sine 1X,

temperatures are between 58 and 85°C, and fluid $\delta^{18}O$ between 1.9 to 6.7‰ (Fig. 10b). Chalks from Zone 2 show temperatures between 29 to 54°C and fluid $\delta^{18}O$ between 0.3 to 3.1‰ (Fig. 10a, b). Chalks from Zone 3 show temperatures between 38 and 104°C and fluid $\delta^{18}O$ values between -2.4 to 4.4‰ (Fig. 10a, b). The highest temperatures are measured in a translucent calcite vein and surrounding chalk within the core of O-1X, recovered within the dense zone (Fig. 10c). These samples also show negative fluid $\delta^{18}O$ values, whereby the vein has the lowest value (-2.4‰ vs 0.0‰ for the surrounding chalk). Two meter down the stratigraphy, away from veins, the chalk shows a temperature of 54°C

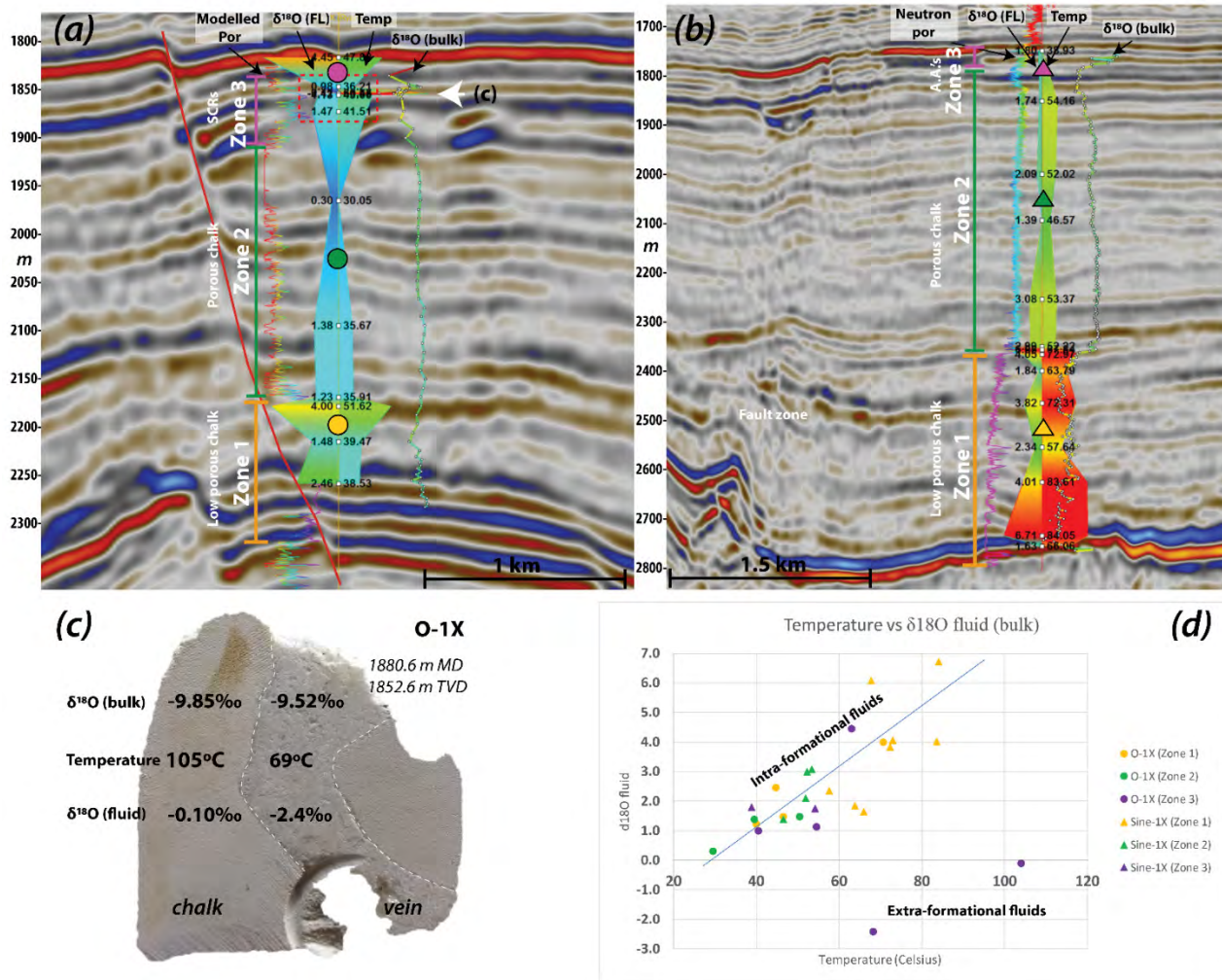


Figure 10. Detail seismic well sections and clumped isotope data. Depths in seismic sections in TVD. Zones indicated with corresponding colours and symbols with respect to d. **(a)** Well section O-1X. In Zone 1, in chalks below the Regional Porosity Marker (RPM), temperatures are between 38 to 52°C, and fluid $\delta^{18}\text{O}$ between 1.5 to 4.0‰. The boundary to Zone 2 (high-porous chalks) is sharp and defined by the RPM, where relatively cold temperatures (30 to 36°C) are measured, and fluid $\delta^{18}\text{O}$ values are low (0.3 to 1.4‰). O-1X penetrates a seismic anomalies associated with the SCRs, starting from 1910 m TVD (Zone 3). Bulk $\delta^{18}\text{O}$ values decrease upward, as well as the modelled porosity (from 35% to 25%). Bulk chalk samples show similar values as in Zone 2, though at the top of the chalk, the sample shows a rather positive (4.6‰) and hot temperature (62°C). **(b)** Seismic section at Sine-1X. The chalks in Zone 1 (low-porous chalk) shows higher temperatures compared to O-1X (e.g. 58 to 84°C), and more positive fluid $\delta^{18}\text{O}$ (1.8 to 6.7‰). The boundary to Zone 2 is sharp and defined by the RPM. Temperatures are lower (46 to 54°C) and fluids less positive (1.4 to 3.0‰). Zone 3 shows similar values as in Zone 2. **(c)** Hand specimen from O-1X core within Zone 3, showing a 3 mm thick, 5 cm wide calcite vein (1880.6 m MD). Both the chalk and calcite vein show highly negative $\delta^{18}\text{O}$ values of -9.52 to -9.85‰. Clumped isotope measurement indicates a temperature of the vein of 69°C and chalk 105°C, and fluid $\delta^{18}\text{O}$ of -2.4 and -0.1‰ respectively. **(d)** Cross-plot of the data used above. Samples from Zone 1 show hot and most positive fluid $\delta^{18}\text{O}$ values, Zone 2 coldest and less positive $\delta^{18}\text{O}$ values, while Zone 3 contains two samples that are clear outliers with hot and negative fluid $\delta^{18}\text{O}$ values. A linear trend can be observed within the bulk of the samples, which is interpreted to represent diagenesis within a closed-system, while the outliers from the core specimen reflect diagenesis from open-system diagenesis.

and fluid of 1.1‰. A cross-plot of temperature versus fluid $\delta^{18}\text{O}$ shows also a positive trend (slope 7.07°C/‰, $R^2=0.64$) for the bulk of the data, though the spread is larger than in the Halfdan case study (resulting in the lower R^2 -value). The chalks below the RPM (Zone 1) show larger deviations off the

positive trend. We interpret the positive trend as reflecting normal burial diagenesis in a closed system, similar to the Halfdan case study. Clear deviations from this trend occur in the analysed core material from O-1X indicates migration of extra-formational fluids through the chalk, and thus

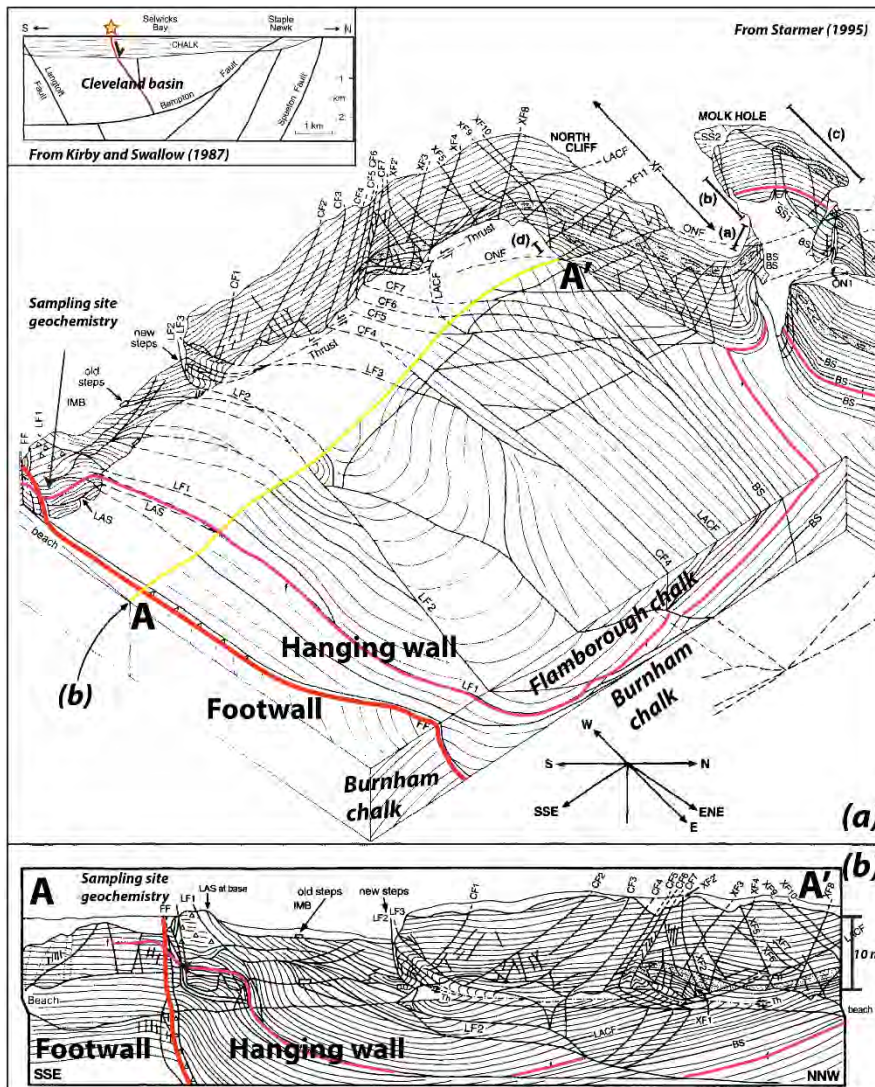


Figure 11. (a) Structural interpretation of Selwicks Bay (Flamborough Head, UK) modified from Starmer (1995). Note the fault plane (red) and the last flint band (purple) separating the Burnham Chalk from the Flamborough Chalk. The chalk is heavily deformed due to the occurrence of a deeply rooted normal fault (see inset for regional cross-section from Kirby and Swallow (1987), outcrop location at yellow star). (b) Orthogonal section A-A' (indicated in a) of the outcrop showing the complex deformation pattern. Associated with these zones, calcite veins occur, which have been sampled for geochemical analysis. At this location the chalk has been buried to 2 km, and subsequently been uplifted during Tertiary compressional phases, as well as glacial tectonic uplift (Starmer, 1995).

open-system diagenesis. It is possible that the chalk host rock was affected by open-system diagenesis to lesser degree since data show a relative larger spread in the normal burial trend than seen in the Halfdan case. In addition, the temperature and fluid $\delta^{18}O$ are distinctively different between the three zones, indicating different styles and degrees of diagenesis. (Fig. 9c)

Case study 3: Flamborough Head

The N-S oriented outcrop at Selwicks Bay shows heavily deformed chalk around an E-W oriented normal fault, which potentially is rooted deeply into Jurassic and Triassic strata (Figs 4 and 11a, Cleveland Basin). On the south side, the footwall shows horizontally oriented chalk beds, while at the fault the chalk beds dip nearly vertical

towards the North (Figs 11b and 12a). The complex deformation is the result of multiple tectonic (inversion) phases (Starmer, 1995).

At the fault plane, a 1 m thick master vein is observed with coarse calcite crystals, as well as secondary smaller veins branch off into the surrounding chalks of the footwall and hanging wall (Fig 12b). Bulk $\delta^{13}C$ and $\delta^{18}O$ values of the chalk ($n=2$) are 2.35‰ and -3.90‰ respectively, while the veins ($n=3$) show values of 1.59‰ and -8.00‰ respectively. CIA was done on one chalk and two vein samples. The temperature for the chalk is 53°C and fluid $\delta^{18}O$ values 1.92‰. The temperature of the veins is between 49 and 64°C, while fluid $\delta^{18}O$ is between -2.50 to -1.40‰. The data thus shows that the bulk chalk material precipitated from fluids with positive $\delta^{18}O$ value, while the veins precipitated

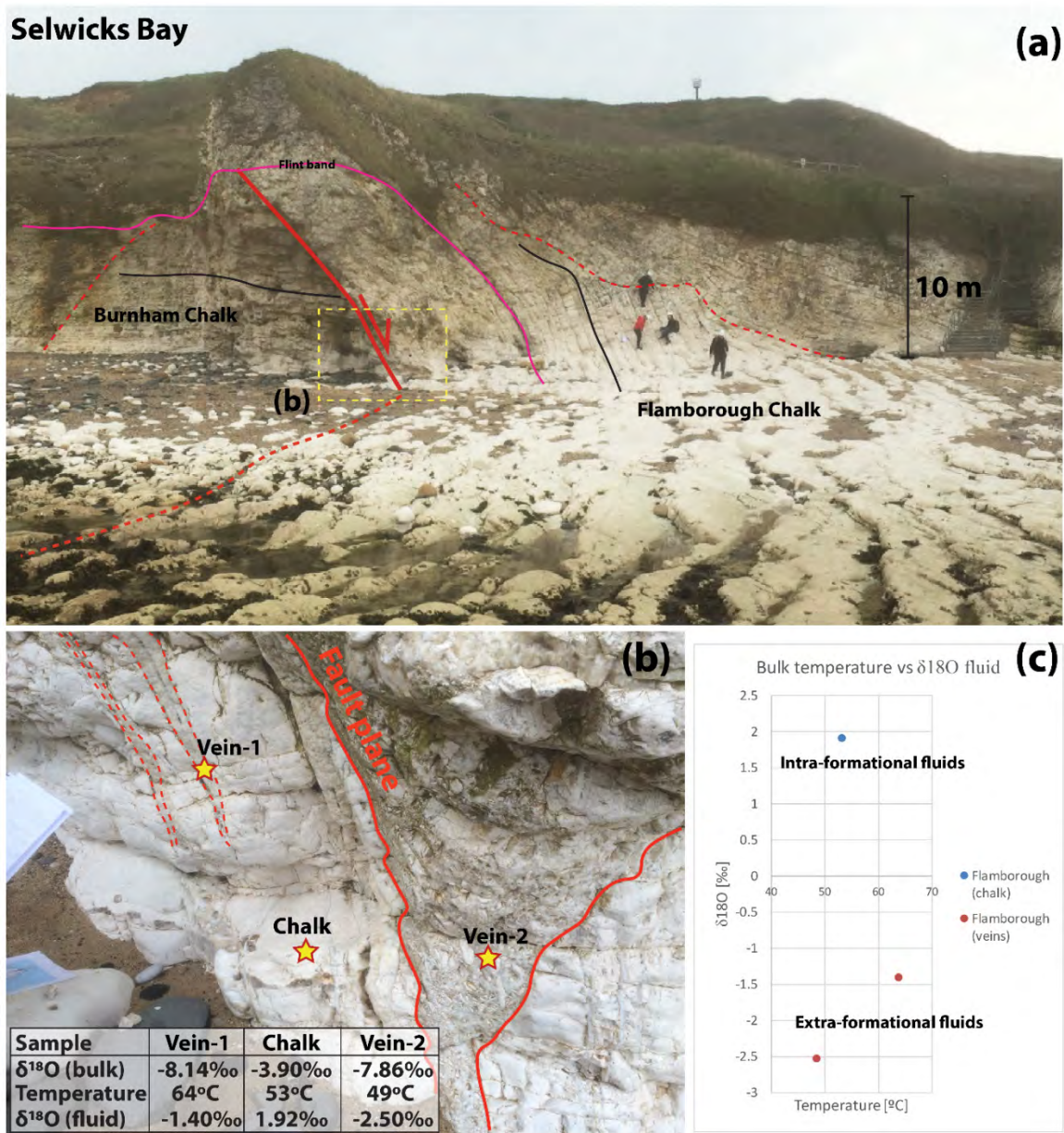


Figure 12. (a) Outcrop photo at Selwicks Bay showing the heavily deformed strata around the fault plane. (b) At the fault plane, large calcite veins occur that contain brittle chalk and translucent calcite crystals. Several smaller veins are splitting off the master vein. Sample locations are indicated with stars. Vein-1 contained very pure, coarse grained, translucent calcite crystals. Vein-2 also contained coarse grained calcite material, but was less pure (e.g. milkier). A chalk sample was taken directly adjacent to the major fault plane. (c) cross-plot.

from fluids with negative $\delta^{18}\text{O}$ value. Had the veins precipitated from formation water in the Chalk Group (e.g. Late Cretaceous seawater), it would have become more positive due to burial diagenesis of the chalk and therefore have a positive $\delta^{18}\text{O}$ value.

We interpret the chalk to have undergone some burial diagenesis, causing a raised temperature and positive fluid $\delta^{18}\text{O}$ value. The calcite veins

formed as a result of extra-formational fluids migrating through the chalk along fault planes. The fluids would have originated from strata in the underlying Cleveland Basin (Fig. 4). The smaller secondary veins are likely forming within the damage zone (in smaller faults and fractures), and might reflect some new phases of fluid migration as the master vein becomes clogged up with calcite.

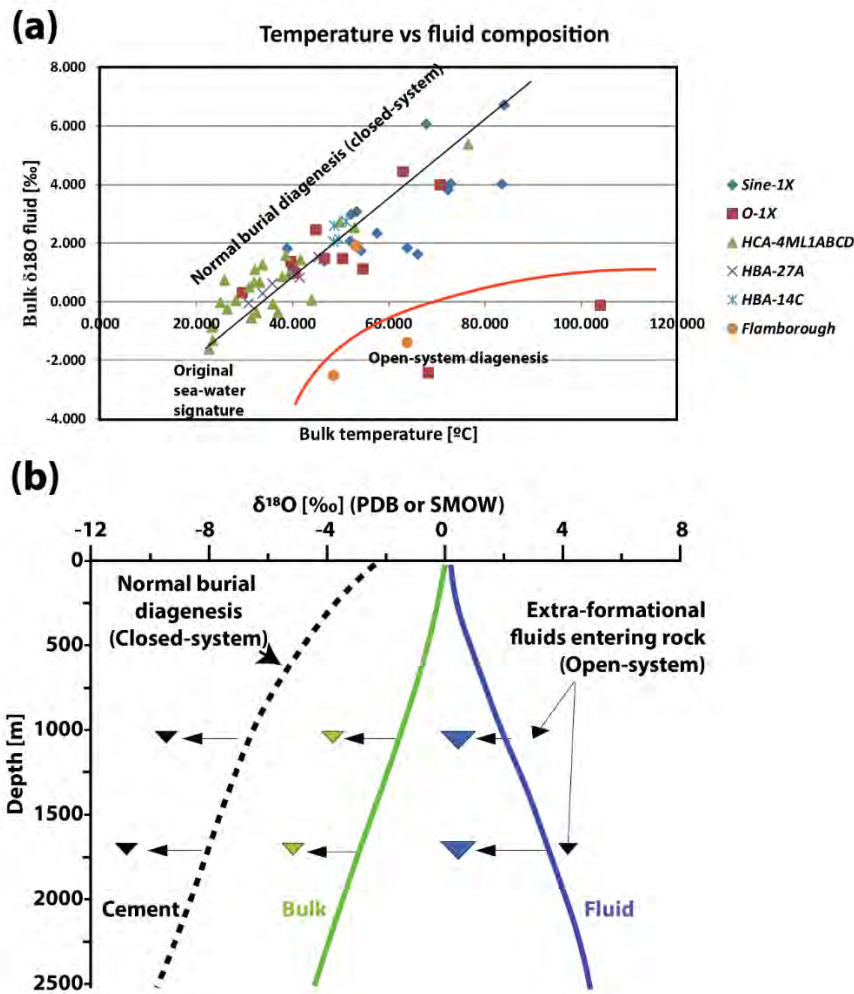


Figure 13. (a) Summarizing results of clumped isotope analysis. The linear trend between independent variables bulk temperature and fluid $\delta^{18}O$ shows that with increasing temperature (burial depth), the formation fluids become more enriched with heavier O^{18} , while O^{16} is preferentially taken up in the crystal lattice. This means that the bulk calcite sample $\delta^{18}O$ becomes more negative, which is a function of original $\delta^{18}O$ of the depositional material, and subsequent cements (that become more negative with depth). The coolest measurements occur in chalks that: 1) did not undergo burial diagenesis and are still highly porous (early establishment diagenetic retardation); 2) or reflect seafloor cementation. It might therefore provide a good estimate of seawater temperatures and compositions. Where points deviate significantly from this trend, likely the material precipitated from extra-formational fluids that had different temperature and/or fluid $\delta^{18}O$ value. **(b)** Proposed model: in the case of normal burial diagenesis, the $\delta^{18}O$ value of the cement and bulk sample become more negative with depth, while the fluid $\delta^{18}O$ becomes more positive. Deviations of this trend occur where extra-formational fluids enter the host rock and from which a cement precipitates that is anomalous in the trend. Model modified from Swart (2015).

Model for closed- and open-system diagenetic behaviour

Based on the three case studies, a model is proposed to explain the variability in temperature and fluid $\delta^{18}O$ obtained from clumped isotope analysis. The positive correlation between absolute temperature and fluid $\delta^{18}O$ reflects the enrichment of formation water with respect to ^{18}O as the lighter ^{16}O is preferentially taken up in the crystal lattice of the burial cement as temperature increases (Fig. 13a) (c.f. Swart *et al.*, 2016). Thus, with increasing temperature (or burial depth), the $\delta^{18}O$ value of the cement becomes more negative, shifting the bulk $\delta^{18}O$ value of the sample to negative values, while the $\delta^{18}O$ value of the fluid becomes more positive

(Fig. 13b). This assumes a closed-system, where formation water remains within more or less similar stratigraphic intervals. The positive slope therefore indicates that these samples underwent normal burial diagenesis in a closed-system (Fig. 13a).

Samples that have cold (e.g. 20-25°C) and slightly negative $\delta^{18}O$ values can reflect two situations: 1) chalks with no or limited burial cement; 2) early cemented chalk (of the first hundreds of metres) (Fig. 13a). The first situation could occur if sedimentation rates are so high, that trapped fluids do not have the time to escape, and almost immediate overpressure would form (such in a dense mass movement). The second situation may relate to extended periods of non-deposition (Gale *et al.*, 2013), followed by limited early burial cement. In

both cases, with minor alterations, it would capture seawater temperature and seawater $\delta^{18}\text{O}$ values.

Outliers from this trend being relatively hot or characterized by negative $\delta^{18}\text{O}$ values represent precipitation from fluids with different geochemical characteristics than the formation fluid within the chalk (which would have been enriched with respect to ^{18}O at that temperature/depth). These points originate from calcite veins and immediately surrounding chalk in the vicinity of faults (Figs 8 and 12). We therefore interpret these fluids to be extra-formational and to have migrated from pre-Chalk Group strata along faults and fractures (Figs 12b and 13b). The deviation off the positive trend in Zone 1 chalks below the RPM (yellow dots and triangles in Fig. 10d) in Case study 2 towards the outliers (e.g. hot and negative fluids) could indicate that some extra-formational fluids created cement. This is in line with the conclusion of Smit *et al.* (2018), who characterized the chalks below the RPM to have experienced only limited open-system diagenesis due to early cementation.

Discussion

Syn- and post-depositional fluid migration indicators

The case studies presented here were chosen to test the power of the clumped isotope palaeothermometer to differentiate seismically identified syn- and post-depositional fluid migration features in chalk in the North Sea Basin. Smit *et al.* (Paper 3) showed the first time usage of clumped isotope on North Sea chalks, while this study adds two more important examples (Case study 2 and 3) illustrating the usage of this promising method. The main learning from using clumped isotope analysis is that most of the Chalk Group has undergone normal burial diagenesis in a closed-system (e.g. cement from trapped formation water). Even in geobodies reflecting seismic-scale diagenesis (e.g. SCRs), most of the chalk seem to be dominated by normal burial diagenesis (Fig. 10d), though some influence by external fluids might be indicated by the larger spread of values (Fig. 10d).

This study therefore confirms the interpretation of Smit *et al.* (2018) that the SCRs reflect high-density chalk that formed due to compaction and due to open-system diagenesis. They also interpreted the chalks below the RPM to have experienced limited open-system diagenesis due to early cementation. This is likely true for O-1X, where colder temperatures and less positive fluid $\delta^{18}\text{O}$ values were observed. For chalks below the RPM at Sine-1X, the relative high temperature and heavy fluids indicate that burial diagenesis continued to be the porosity reducing mechanism. Possibly, only limited amount of lighter fluids penetrated these chalks, indicated by the slight deviation from the positive trend (Fig. 10d, Zone 1).

The outcrop case study shows that even within 1 meter, the chalk and two veins showed very different geochemical signatures, and similarly core material from O-1X shows that chalk 2 m away from calcite veins are almost unaffected by external fluids. Given the extremely low matrix permeability of chalk it is not a huge surprise that most diagenesis is in closed systems and open-system diagenesis is limited to narrow zones along high permeability fairways and areas with high pressure gradients.

The relationship between temperature and fluid composition is very similar in the two areas of the North Sea studied here, 7.1-7.7°C/‰ of fluid $\delta^{18}\text{O}$ (Fig. 13a). This indicates that the amount isotope exchange between formation fluid and cement is constant with increasing temperature. It is likely that formation water in chalk (90-100% CaCO_3) is more easily saturated with respect to calcite than in the case of formation water in a carbonate-barren sandstone, and therefore the relationship possibly will change according to the lithology. Also, the temperature of the formation water (in a closed-system) is not only a function of depth, but also the geothermal gradient, which can fluctuate through time and in space. Differences in geothermal gradients (in place and in time) will influence the temperature of the formation water with depth, which in turn will influence the fractionation with depth. The slope is therefore possibly valid for the Chalk Group with similar geothermal gradient. The fact that the chalk sample

in Flamborough Head falls close to the observed slope, suggest that the geothermal gradient was comparable in the two regions (orange dot within closed-system diagenesis in Fig. 10a). At present, they are in the same order of magnitude (65-75mW/m², c.f. Guterch *et al.*, 2010), but this should be assessed throughout burial history.

An efficient workflow to arrive at better temperature estimates

The correlation between temperature (or burial depth) and fluid $\delta^{18}O$ values provides interesting insights in the exchange of oxygen isotopes between formation water and precipitating cement (c.f. Swart *et al.*, 2016). This observation implies that using Upper Cretaceous seawater (often taken as -1‰) in a classical carbonate palaeothermometers (such as Craig, 1965) for chalks that underwent burial diagenesis (e.g. North Sea chalks) is rather wrong. The range of fluid $\delta^{18}O$ values found in this study with CIA is in the order of 8‰, which would reflect a maximum deviation of 50°C of the bulk carbonate temperature if one was not using the correct fluid $\delta^{18}O$ value in the classical palaeothermometer (Craig, 1965). CIA therefore also shows the need for good control points for fluid $\delta^{18}O$ values.

While CIA provides unambiguous answers, it is a labour-intensive and time-consuming procedure (e.g. 4-5 hours per sample, including preparation and analysis, and the need to do so twice or thrice). To cover large stratigraphic sections, an efficient workflow would be to get bulk $\delta^{13}C$ and $\delta^{18}O$ values from rather inexpensive automated carbon and oxygen isotope analysis for the whole stratigraphy, and select a limited amount of samples that represent the main trends. The obtained temperature and fluid $\delta^{18}O$ value would form control points for sections in the stratigraphy in order to better constrain $\delta^{18}O$ of the fluid in the classical carbonate palaeothermometer. Together, a better constraint temperature curve can be produced reflecting the average rock temperature (original material and cements).

Other applications of a combined CIA and seismic geomorphology workflow

The promise of CIA is that it provides unambiguous estimates of temperature and fluid $\delta^{18}O$ of a rock sample (P. K. Swart, 2015). This is very useful when reconstructing seawater temperatures and $\delta^{18}O$ values through time. Based on petrography, samples can be selected that did not experience (much) burial diagenesis, and represent rather pristine material from a certain time interval. CIA then provides better estimates of seawater temperature and $\delta^{18}O$ that can help to refine palaeoclimatic curves that are based on classical paleocarbonate thermometers and/or biogenic material (Miller *et al.*, 2005).

Recognizing meteoric or hypogenic karst is also possible with a combination of CIA and seismic geomorphology. Seismic geomorphology provides a geological context in which specific samples can be selected. Bulk $\delta^{18}O$ values of the sample could be very negative in both cases, though one it is the result of the fluid (highly negative $\delta^{18}O$ values) and the other due to possible high temperatures (hypogenic karst). In case of meteoric karst, rather cold temperatures and highly negative $\delta^{18}O$ values would be obtained from CIA, while hypogenic karst would be warm and could have a range of $\delta^{18}O$ values depending on the origin of the water.

Conclusions

- This paper showed the second application of clumped isotope analysis (CIA) on chalks from the North Sea Basin, and provided seismic geomorphological context or outcrop architecture for the samples that were analysed. This workflow provides a powerful coupling or integration method to understand the geochemical signals better.
- The following relationships have been obtained from the CIA data (absolute temperature and fluid $\delta^{18}O$):
 - The positive correlation between increasing temperature and more positive $\delta^{18}O$ reflects increasing enrichment of the formation water with respect to ¹⁸O as the lighter ¹⁶O are

preferentially taken up into the crystal lattice of the burial cement with increasing temperature. It thus reflects normal burial diagenesis in a closed-system.

- The slope (7.1-7.7°C per ‰ of fluid $\delta^{18}O$) is possibly a variable that is lithology (Chalk Group) and thermal gradient dependent (in time and space).
- The points that deviate from the positive trend, reflect that this material precipitated from extra-formational fluids that had different fluid $\delta^{18}O$ values and temperature than the formation water in the Chalk Group. The material originates from calcite veins and surrounding chalk, in association with deeply rooted faults. It thus reflects open-system diagenesis.
- CIA thus provides a good proxy for open- and closed-system diagenesis.
- Most of the chalk experienced closed-system diagenesis, and open-system diagenesis only occurred in narrow zones associated with high porosity/permeability and/or high pressure gradients, such as in fault damage zones.
- Closed-system diagenetic behaviour is even found to be the most common style of diagenesis in a clear open-system diagenetic case studies, reflecting the extremely low matrix permeability.
- To cover large sections of the stratigraphic column, an efficient workflow is proposed whereby first bulk $\delta^{13}C$ and $\delta^{18}O$ values are obtained from inexpensive automated stable isotope workflows. Subsequently, samples are selected for CIA that cover the major trends observed in the bulk analysis.
- Other possible applications include refining palaeoclimatic curves due to the unambiguous temperature and fluid $\delta^{18}O$ estimate, as well as differentiating between meteoric and hypogenic karst.

Acknowledgements

The authors kindly acknowledge the Danish Underground Consortium (Total, Shell, Chevron, and Nordsøfonden) for providing seismic and well data and the permission to publish the results. Colleagues at the Stable Isotope Laboratory at University of Miami (Peter Swart, Gregor Eberli, Philip Staudigel, Amel Saied, Sevag Mehterian, Sharm Giri, Megan Smith, and Evan Moore) are kindly thanked for hosting the clumped isotope project as part of the Research Stay Abroad, their warm welcome, and their help with obtaining the results. We kindly want to thank the follow software companies for providing academic licenses: Schlumberger is kindly thanked for providing Petrel E&P, Eliis is kindly thanked for providing PaleoScan™, and FFA GeoTeric is kindly thanked for GeoTeric. The research leading to these results has received funding from the Danish Hydrocarbon Research and Technology Centre under the Advanced Water Flooding program.

References

- Abramovitz, T. A. N. I., & Thybo, H. (1999). Pre-Zechstein structures around the MONA LISA deep seismic lines in the southern Horn Graben area. *Bulletin of the Geological Society of Denmark*, 45, 99-116.
- Craig, H. (1965). The measurement of oxygen isotope paleotemperatures. *Stable isotopes in oceanographic studies and paleotemperatures: Consiglio Nazionale delle Ricerche*, 161-182.
- Gale, A. S., Surlyk, F., & Anderskov, K. (2013). Channelling versus inversion: origin of condensed Upper Cretaceous chalks, eastern Isle of Wight, UK. *Journal of the Geological Society*, 170(2), 281-290.
- Ghosh, P., Adkins, J., Affek, H., Balta, B., Guo, W., Schauble, E. A., ... & Eiler, J. M. (2006). ^{13}C - ^{18}O bonds in carbonate minerals: a new kind of paleothermometer. *Geochimica et Cosmochimica Acta*, 70(6), 1439-1456.
- Ghosh, P., Eiler, J., Campana, S. E., & Feeney, R. F. (2007). Calibration of the carbonate 'clumped isotope' paleothermometer for otoliths. *Geochimica et Cosmochimica Acta*, 71(11), 2736-2744.
- Guterch, A., Wybraniec, S., Grad, M., Chadwick, A., Krawczyk, C., Ziegler, P., Thybo, H., de Vos, W.M., 2010. Crustal structure and structural framework, in: *Petroleum Geological Atlas of the Southern Permian Basin Area*. pp. 11-23.
- Kim, S. T., & O'Neil, J. R. (1997). Equilibrium and nonequilibrium oxygen isotope effects in synthetic

- carbonates. *Geochimica et Cosmochimica Acta*, 61(16), 3461-3475.
- Kirby, G. A., & Swallow, P. W. (1987). Tectonism and sedimentation in the Flamborough Head region of north-east England. *Proceedings of the Yorkshire Geological Society*, 46(4), 301-309.
- Miller, K. G., Kominz, M. A., Browning, J. V., Wright, J. D., Mountain, G. S., Katz, M. E., ... & Pekar, S. F. (2005). The Phanerozoic record of global sea-level change. *science*, 310(5752), 1293-1298.
- Murray, S. T., Arienzo, M. M., & Swart, P. K. (2016). Determining the $\Delta 47$ acid fractionation in dolomites. *Geochimica et Cosmochimica Acta*, 174, 42-53.
- Pharaoh, T.C., Dusaar, M., Geluk, M.C., Kockel, F., Krawczyk, C., Krzywiec, P., Scheck-Wenderoth, M., Thybo, H., Vejbaek, O.V., van Wees, J.D., 2010. Tectonic Evolution, in: Doornenbal, J.C., Stevenson, A.G. (Eds.), *Petroleum Geological Atlas of the Southern Permian Basin Area*. EAGE Publications, Houten, pp. 25–57.
- Schauble, E. A., Ghosh, P., & Eiler, J. M. (2006). Preferential formation of ^{13}C – ^{18}O bonds in carbonate minerals, estimated using first-principles lattice dynamics. *Geochimica et Cosmochimica Acta*, 70(10), 2510-2529.
- Sheriff, R. E. (1980). Nomogram for Fresnel-zone calculation. *Geophysics*, 45(5), 968-972.
- Smit, F. W. H., van Buchem, F. S. P., Holst, J. H., Lüthje, M., Anderskov, K., Thibault, N., Welch, M. & L. Stemmerik (2018). Seismic geomorphology and origin of diagenetic geobodies in the Upper Cretaceous Chalk of the North Sea Basin (Danish Central Graben). *Basin Research*.
- Starmer, I. C. (1995). Deformation of the Upper Cretaceous Chalk at Selwicks Bay, Flamborough Head, Yorkshire: its significance in the structural evolution of north-east England and the North Sea Basin. *Proceedings of the Yorkshire Geological Society*, 50(3), 213-228.
- Staudigel, P. T., Murray, S., Dunham, D. P., Frank, T. D., Fielding, C. R., & Swart, P. K. (2018). Cryogenic Brines as Diagenetic Fluids: Reconstructing the Diagenetic History of the Victoria Land Basin using Clumped Isotopes. *Geochimica et Cosmochimica Acta*.
- Surlyk, F., Dons, T., Clausen, C.K., Higham, J., 2003. Upper Cretaceous, in: *The Millennium Atlas: Petroleum Geology of the Central and Northern North Sea*. pp. 213–233.
- Swart, P. K. (2015). The geochemistry of carbonate diagenesis: The past, present and future. *Sedimentology*, 62(5), 1233-1304.
- Swart, P. K., Cantrell, D. L., Arienzo, M. M., & Murray, S. T. (2016). Evidence for high temperature and ^{18}O -enriched fluids in the Arab-D of the Ghawar Field, Saudi Arabia. *Sedimentology*, 63(6), 1739-1752.
- Van Buchem, F.S.P., Smit, F.W.H., Buijs, G.J.A., Trudgill, B., Larsen, P.H., Trudgil, B., Larsen, P.H., (2018). Tectonostratigraphic framework and depositional history of the Cretaceous – Danian succession of the Danish Central Graben (North Sea) – new light on a mature area, in: Bowman, M.B., Levell, B. (Eds.), *Petroleum Geology of NW Europe: 50 Years of Learning - Proceedings of the 8th Petroleum Geology Conference*. Geological Society of London, pp. 9–46.
- Vejbaek, O.V., Andersen, C., Dusaar, M., Herngeen, W., Krabbe, H., Leszczynski, K., Lott, G.K., Mutterlose, J., van der molen, A.S., 2010. Cretaceous, in: *Petroleum Geological Atlas of the Southern Permian Basin Area*. pp. 195–209.

(a)

Near top Chalk Group



Source rock presence + burial =
Syn-depositional gas venting

(b)

20 km

Absence of source rocks + limited burial =
Post-depositional diagenesis

(c)

(b)

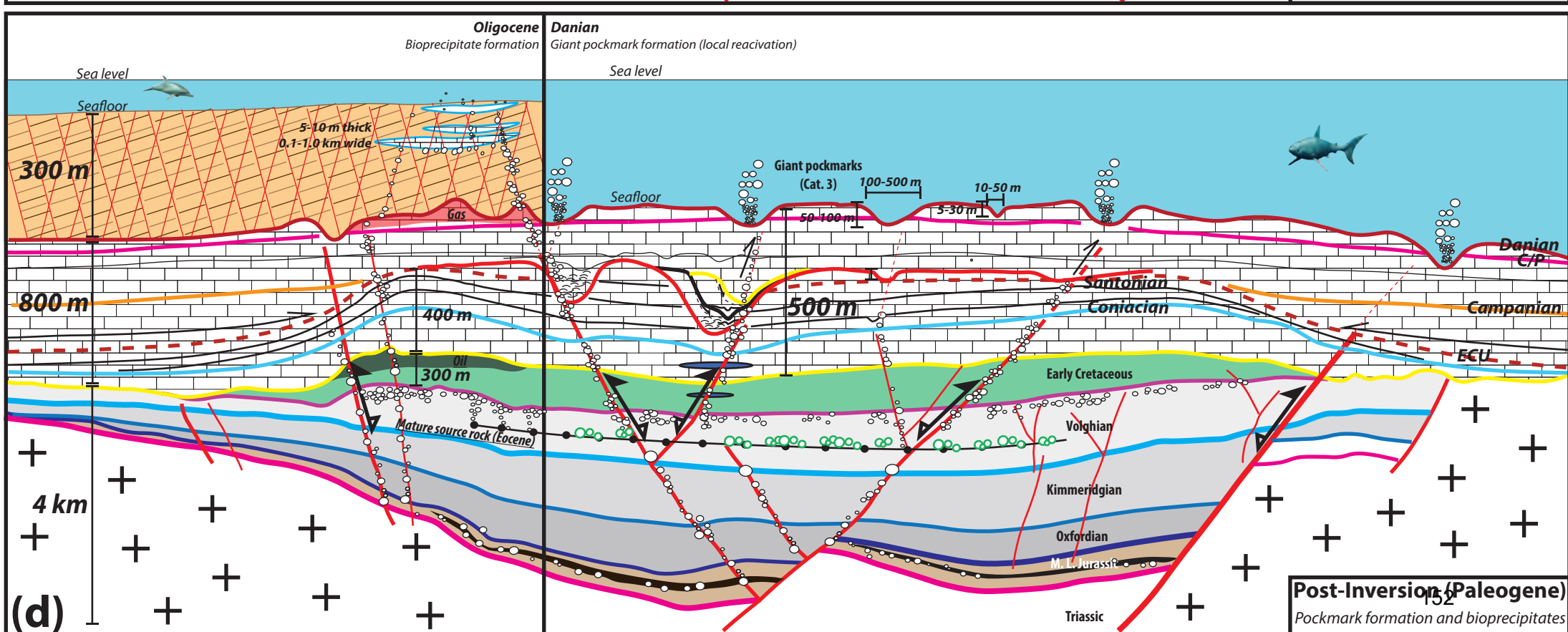
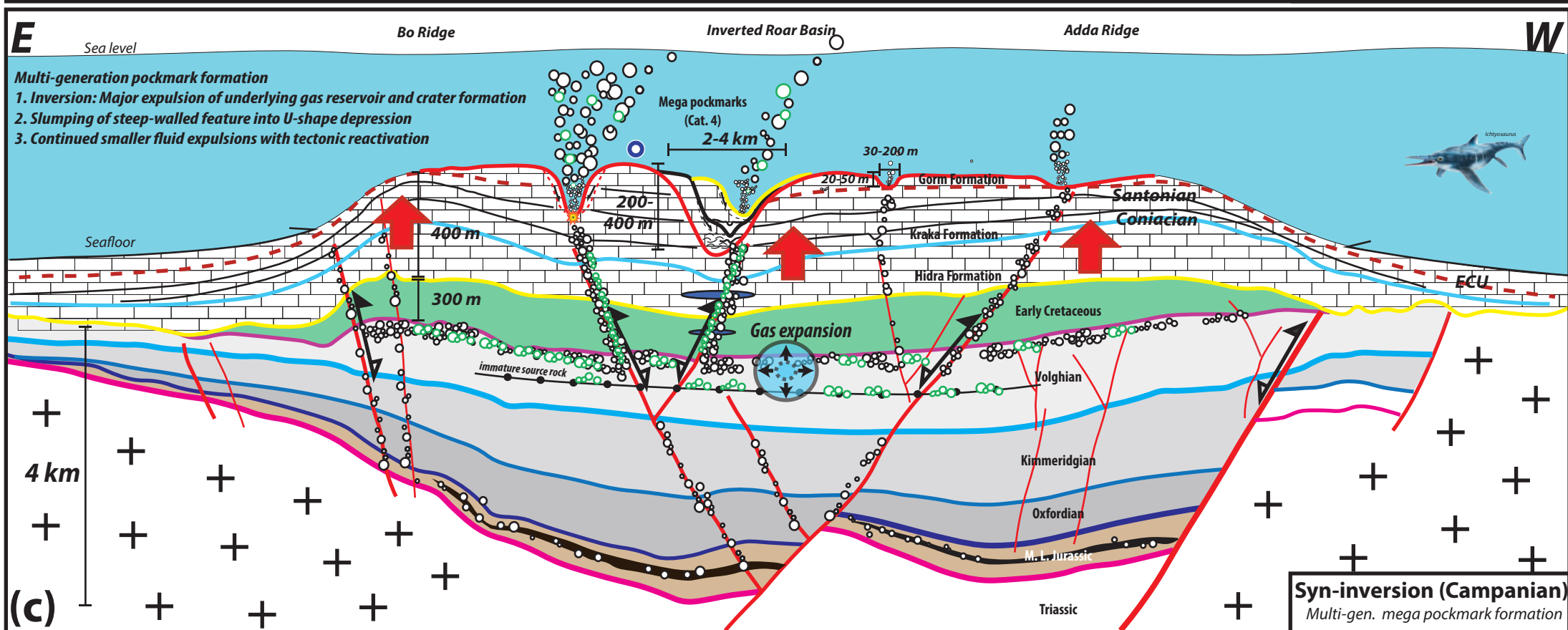
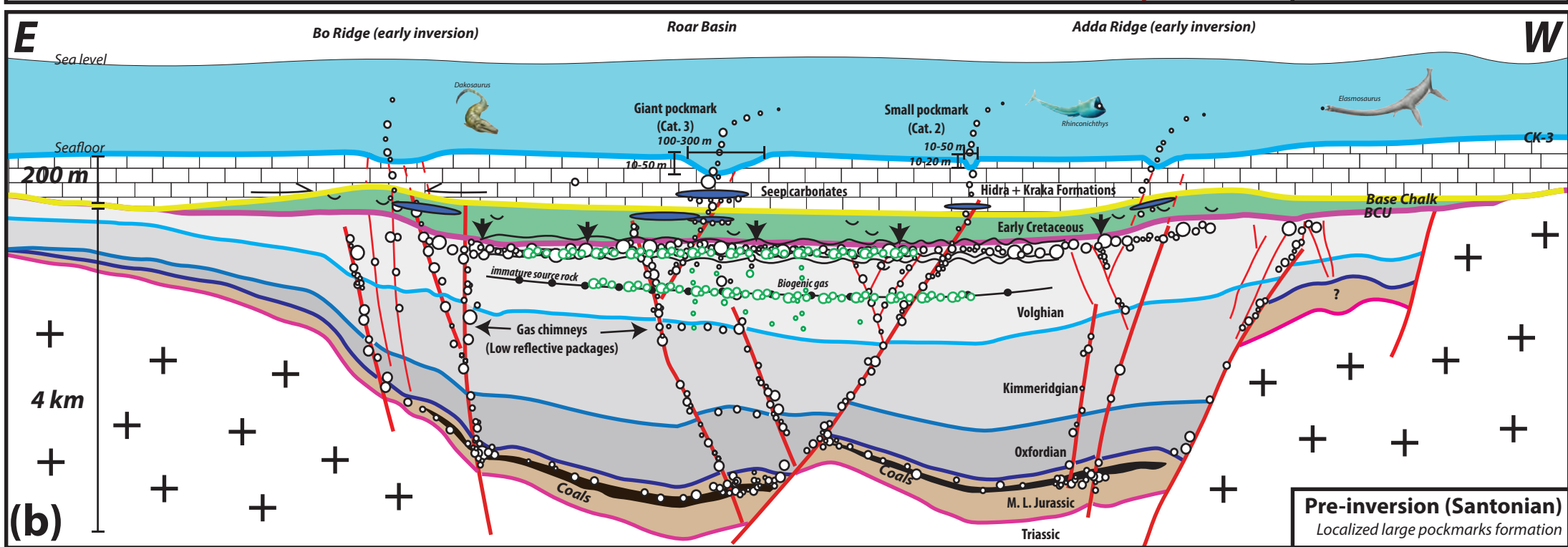
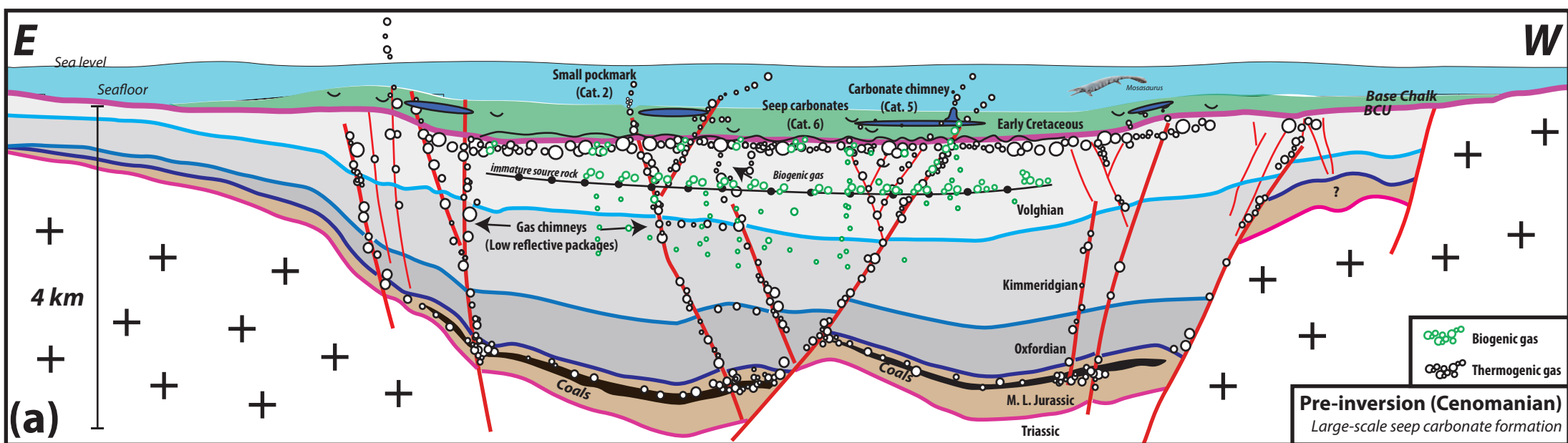
Giant
pockmarks

10 km

(c)

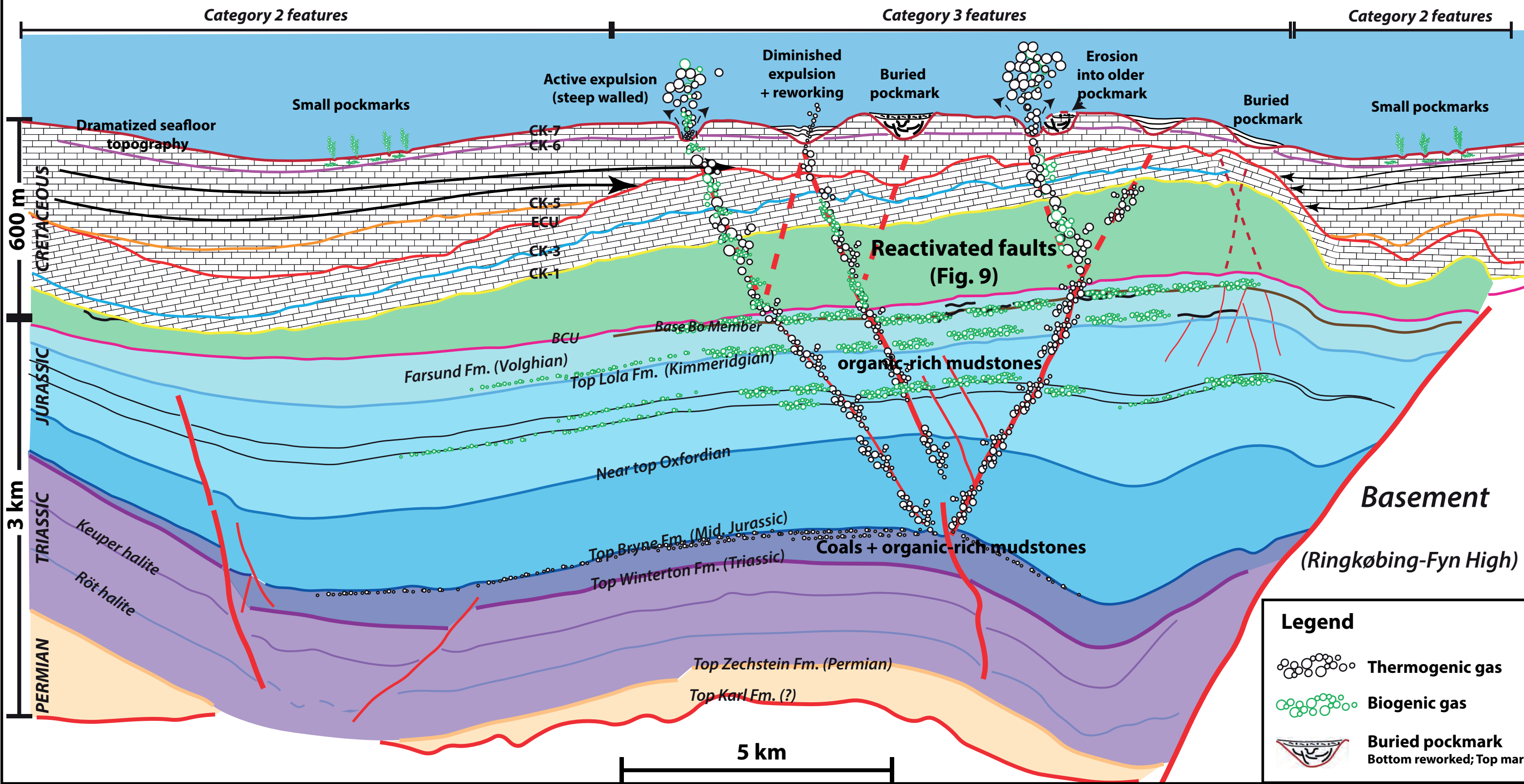
Seismic-scale
diagenesis

10 km



Middle Danian
Giant pockmark formation

← Igor-Emma Ridge: highest point basin (inverted during Campanian) →



Legend

- Thermogenic gas
- Biogenic gas
- Buried pockmark
Bottom reworked; Top marl

Updated seismic geomorphological workflow applied to the Chalk Group

Florian Smit*, Technical University of Denmark; Frans van Buchem, Maersk Oil and Gas (present Haliburton-Landmark Exploration Insights); Ingelise Schmidt, Maersk Oil and Gas; Lars Stemmerik, University of Copenhagen

Summary

An updated seismic geomorphological methodology has led to improved visualization of seismic-scale heterogeneities in the Chalk Group in the Danish Central Graben. The promise of the workflow is that it prepares a spatial framework for integration with other disciplines working at different scales. Such integration would lead to better predictions of reservoir quality away from the wells.

The computation of a large amount of stratal slices that follows a 3D Relative Geological Time Model allows, consistent 'scanning' through the seismic stratigraphy. This revealed more subtle seismic geomorphological features than obtained with volumetric averaging. In addition, by using the latest spectral decomposition methods, projected upon these stratal slices, details that normally would be difficult to distinguish with classical attributes became apparent. Lastly, a new methodology that image processes seismic data, has revealed subtle linear features that are difficult to observe in normal seismic amplitude data. These can well present low-throw faults and fracture swarms as known from chalk outcrops with a similar burial history.

Introduction

Chalk is a pure biogenic sediment made up by 90-100% calcium carbonate. It is mainly composed of the remnants of micron-size eukaryotic phytoplankton (coccolithophorids), with a minor addition of microfossils (i.e. foraminifera, calcispheres, and siliceous sponge spicules) (e.g. Hancock 1975; Scholle & Halley 1985; Fabricius 2007). It is of large economic importance in the North Sea, as it forms the main hydrocarbon reservoir in the Danish North Sea, as well as parts of the Norwegian, UK and Dutch North Sea.

From outcrop and 2D seismic sections, the chalk might seem like a layer-cake. However, sedimentological, petrological, and petrophysical studies at micro- and core-scale have shown heterogeneities that are controlled by sedimentary processes (most notably bottom currents and mass-wasting processes) (e.g. Anderskov & Surlyk 2012), deformation (fractures) (e.g. Gaviglio et al. 2009), and diagenetic overprinting (e.g. Fabricius & Borre 2007). The heterogeneities can be both beneficial and detrimental for reservoir quality (perm/por) and challenging for reservoir

characterization outside of the control points obtained in discrete cored intervals.

Due to the general purity of the chalk in the Danish North Sea, e.g. 90-100% CaCO_3 (calcite) with rather constant density and seismic velocity, the acoustic impedance is mainly a function of the porosity (e.g. Japsen, 1998). Seismic data are therefore a good starting point for studying large-scale heterogeneities in porosity, and several studies based on interpretation of 2D geometries and by volumetric slicing have addressed sedimentary and structural heterogeneities in the Chalk Group (e.g. Esmerode et al. 2008; Back et al. 2011; Gennaro et al. 2013). Though only used with classical attributes (RMS amplitude), Smit (2014) showed how the usage of a 3D Relative Time Model was very beneficial for understanding seismic-scale heterogeneities within the Chalk Group. This approach is taken a step further by visualizing spectral decomposition data onto the stratal slices. In addition, image processing of the seismic data has helped to highlight structural features within the chalk. The different methodologies are here introduced and examples from the Chalk Group are shown.

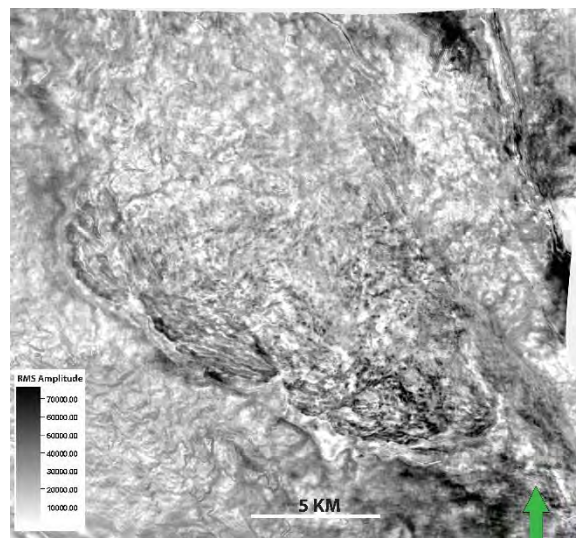


Figure 1. Classical volumetric attribute (RMS amplitude) between two horizons to show heterogeneities within the Chalk Group as used by Back et al. (2011).

Data and methods

The seismic dataset consists of 6000 km² regional data from fourteen merged surveys (pre-stack depth migrated) of various vintages (1996 – 2011). The signal to noise ratio within the Chalk Group is generally very good, though limited around salt diapirs and around platforms. The dominant frequency within the chalk interval is 25 Hz and average acoustic velocity is 3500 m/s, resulting in a vertical resolution of 35 m.

The usage of a 3D Relative Time Model (c.f. Pauget et al. 2009), which generates a large amount of consistent stratal horizons, has shown to be very beneficial in ‘scanning’ the seismic data. It uses the principle of a neural network, by minimizing the cost of automatically connecting nodes generated for every peak, trough and zero-crossing within the seismic data while following user-constraint interpretation. High-definition spectral decomposition data (c.f. Morozov et al. 2013) were generated to display upon the stratal slices. A seismic spectrum was made for the Chalk Group interval, and three synthetic wavelets were defined with a matching pursue algorithm: low-frequency (20 Hz, red), mid-frequency (30 Hz, green), high-frequency (40 Hz, blue).

In addition, a seismic image processing algorithm was used to generate chromatic (seismic) geological data, which could be used for RGB display of seismic heterogeneities and structural information (c.f. Laake, 2013). Here we use the structural cube (S-cube) output, which is the result of

edge-detection on of the saturation component of the chromatic seismic data, to highlight heterogeneities between three adjacent seismic time slices calculated for the entire seismic cube. By applying ‘swarm intelligence’ of artificial ants (c.f. Pedersen *et al.* 2003) on the S-cube, consistent vertical heterogeneities can be visualized upon the 2D sections and stratal slices.

Volumetric averaging vs. high density stratal slicing

If bulk changes in the acoustic impedance of the rock are above the detectability threshold, a seismic signal may result. When volumetric averaging is used between two horizons (e.g. Back et al. 2011), such as an RMS amplitude extraction, these subtle changes in the rock properties might be too small to be seen. In Figure 1, a large feature in the Chalk Group can be seen, in data obtained through RMS extraction between two stratigraphic horizons (approximately 100 ms TWT thick volume). A sharp NW-SE discontinuity, some elongated discontinuities adjacent, and a more homogenous signal to the NE are evident. It is interpreted as a large crestal collapse.

By using a small RMS window (4 ms) around a stratigraphy consistent stratal slice, these features will stand out more clear (e.g. Smit 2014; Figure 2), and can be used in 3D for geological more realistic interpretations. With a continuous set of consistent stratal slices with RMS amplitude projected upon, throughout the interval of interest (e.g. the Chalk Group), it becomes possible to quickly ‘scan’ for seismic-scale heterogeneities.

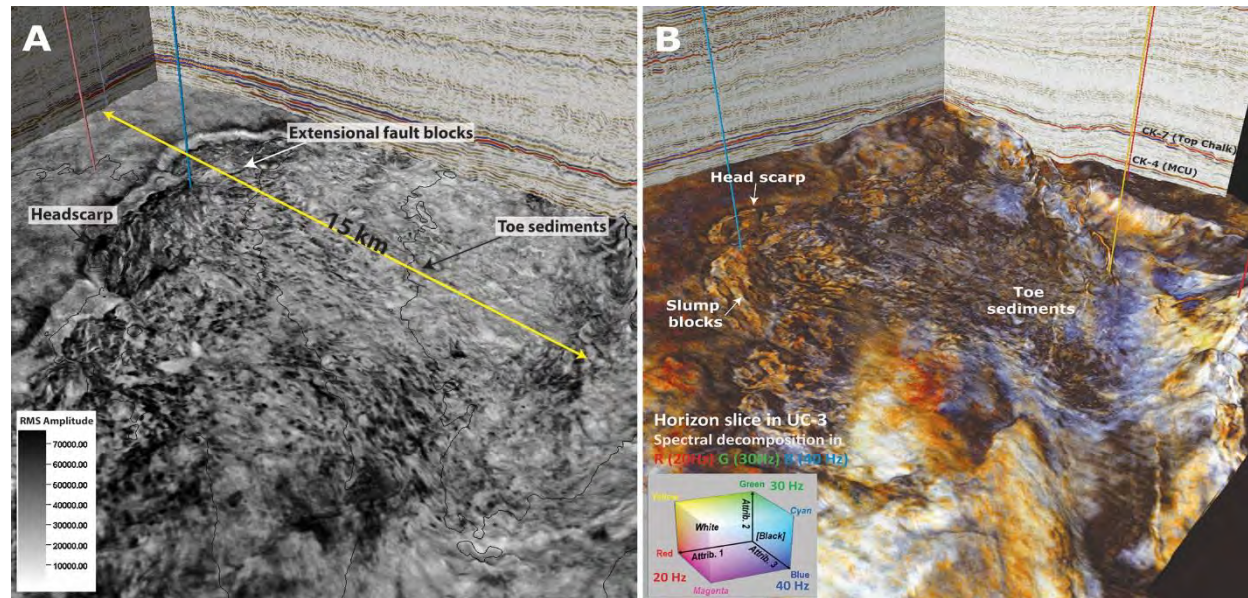


Figure 2. A) Stratal slice generated with the 3D Relative Geological Time Model methodology (c.f. Pauget et al. 2009) draped with a RMS amplitude attribute (from van Buchem et al. 2017), note the scale bar; B) the same stratal slice with high-definition spectral decomposition data (c.f. Morozov et al. 2013).

Updated seismic geomorphological workflow

Another advantage of stratal slicing over volumetric slicing is that the data points extracted from the seismic data are made on a smaller window, and are following the stratigraphy. This leads to more consistent ‘seascapes’, and makes comparison of the seismic feature to well data less ambiguous. Interpreting the feature as a large remobilization feature is now rather obvious (Figure 2A).

Spectral decomposition data in the Chalk Group

Figure 2B shows the same horizon, but now projected upon high-definition spectral decomposition data (c.f. Morozov et al. 2013). Whereas amplitude data can provide information on changing acoustic impedance, spectral decomposition data provide extra information on the changes in frequencies within the seascape. The intact platform to the left shows rather reddish colors, suggesting that low-frequency packages dominate the seismic signal. Beyond the head

scarp, down-dip of the collapse, colors are more bluish indicating that higher-frequency packages dominate.

It is however difficult, if not impossible, to interpret what happens to the chalk facies in the different regions based on frequency data alone. High-resolution well data provide key information to understand such seismic seascapes, and integration of different scales (seismic to nanoscale) and disciplines (sedimentology, petrophysics, petrology, and geochemistry), is instrumental in order to better understand the type of facies associated with the different elements on the seascape and making predictions away from wells.

Lastly, another advantage of such 3D images is that it becomes easier to find potential analogues, both from present-day and other seismic geomorphological studies, although caution is needed when evaluating the compatibility of such analogues.

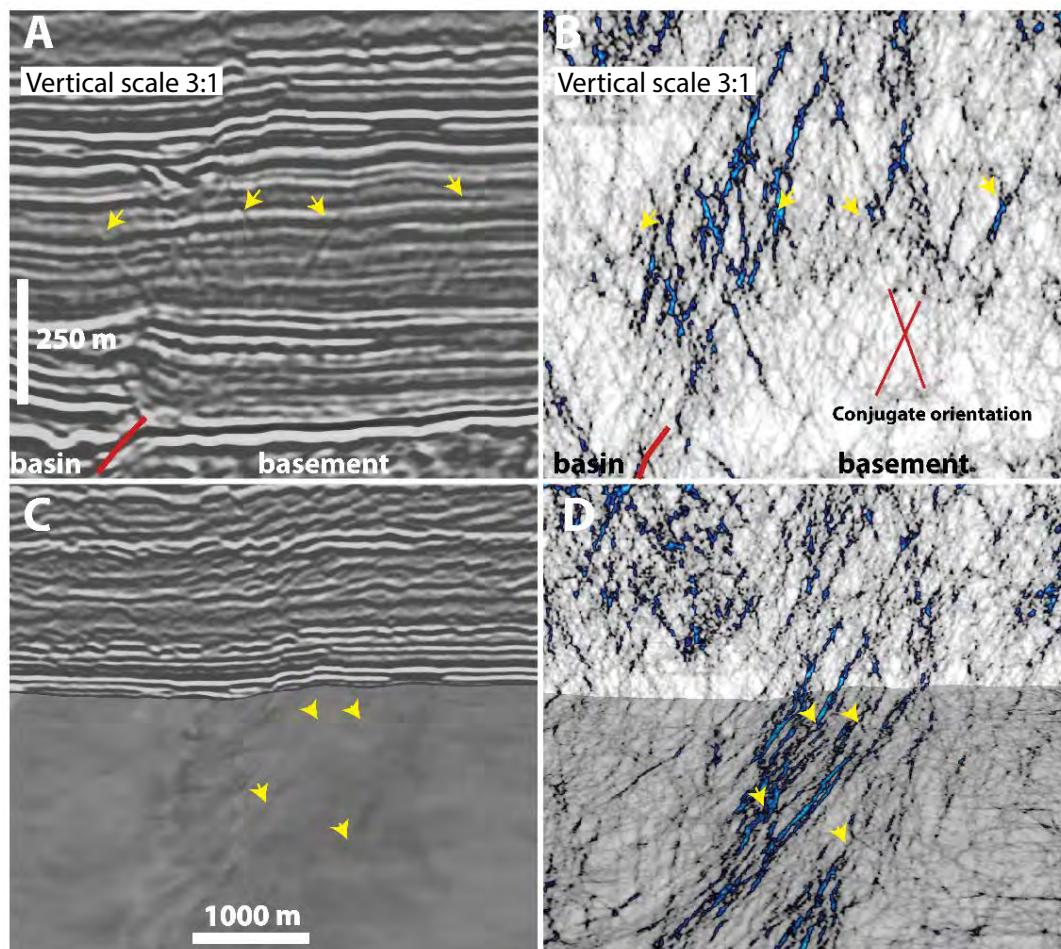


Figure 3. A) Seismic amplitude section. Note the ‘pseudo-reflectors’ (white arrows). B) Same 2D section with ant-tracked image processed structural data. Note how the pseudo-reflectors are highlighted through this procedure. C) Chair diagram, with seismic amplitude, pseudo-reflectors occur as subtle elongated lineations. D) Chair diagram same as (C), but with ant-tracked image processed structural data. The pseudo-reflectors are well connected, and occur at the transition from the basin to the basement.

Image processing of seismic data

Laaque (2013) introduced a new seismic processing technique that image processes seismic data in such a way that heterogeneities are emphasized and homogeneities diminished. The output is suitable for RGB display of heterogeneities, similar to spectral decomposition, but due to time-slice based processing instead of wavelet, has a much higher resolution (e.g. 1.5x the sampling rate). Another output of this process is the 'structural cube', which here has been ant-tracked (c.f. Pedersen et al. 2002) and shown in Figure 3. Within the chalk, some subtle pseudo-reflectors can be observed to have a conjugated geometry (Figure 3A). The ant-tracking of the S-cube has attenuated the homogeneities (seismic reflectors) and highlighted the subtle consistent conjugated pseudo-reflectors (Figure 3B). In map view, these reflectors are consistent elongated discontinuities and occur at the boundary between the basin to the left, and basement to the right (Figure 3C and D). A likely explanation for these features is that differential subsidence between basin and basement has created enough stress in the chalk that it resulted in brittle deformation, such as low-throw faults and fracture swarms. The geometries and angles of these features as observed in the seismic, are consistent with fault geometries in chalk outcrops at Flamborough Head (UK), which have been buried to similar depths as the Danish chalk (Starmer 1995). The fact that it can be seen within the chalk must mean that there is an acoustic impedance change associated with these faults. It is not unlikely that fluids have passed through the fault plane and have (partly) cemented it. In order to understand these conjugated pseudo-reflectors better, information from wells that penetrate these features is crucial (e.g. borehole imaging, core etc.).

Discussion and conclusions

The 'seascapes', as illustrated here, can provide a well-needed spatial geological framework for well studies. The promise of the seismic geomorphological workflow is that prediction of chalk facies and reservoir quality away from the wells can be improved. In order to achieve this, e.g. understand the seismic geomorphological 'seascapes', integration of different scales, disciplines and datasets (seismic to nanoscale; petrology, geology, geomechanics, and geochemistry) is crucial.

Here, we present an updated seismic geomorphological workflow that has been applied to the Chalk Group in the Danish Central Graben.

1. High-density stratal slicing allows swift scanning of the seismic data for (subtle) seismic features.
2. The combination of high-density stratal slicing with high-definition spectral decomposition data provides very clear seascapes within the chalk, due to the general purity of the rock (90-100% calcite matrix).
3. The structural output from an image processing technique for seismic data, has shown to be promising

for identifying potential low-throw faults and fracture swarms within the chalk.

4. It is crucial in understanding the seascapes that close integration occurs, both in terms of scales and with disciplines.

Acknowledgements

The DUC partners Maersk Oil, Shell, Chevron and Nordsoefonden are kindly thanked for providing seismic and well data, and the permission to publish these results. Schlumberger is kindly thanked for providing Petrel E&P software suite and the eXchroma plugin. Eliis is kindly thanked for providing PaleoScan™ software to generate a 3D Relative Geological Time Model. FfA GeoTeriC is kindly thanked for providing GeoTeriC software for generating high-definition spectral decomposition data. This work is part of the PhD project of the first author, hosted at the Centre for Oil and Gas – DTU.

EDITED REFERENCES

Note: This reference list is a copyedited version of the reference list submitted by the author. Reference lists for the 2017 SEG Technical Program Expanded Abstracts have been copyedited so that references provided with the online metadata for each paper will achieve a high degree of linking to cited sources that appear on the Web.

REFERENCES

- Anderskov, K., and F. Surlyk, 2012, The influence of depositional processes on the porosity of chalk: *Journal of the Geological Society*, **169**, 311–25, <http://doi.org/10.1144/0016-76492011-079>.
- Back, S., H. Van Gent, L. Reuning, J. Grottsch, J. Niederau, and P. Kukla, 2011, 3D seismic geomorphology and sedimentology of the chalk group, Southern Danish North Sea: *Journal of the Geological Society*, **168**, 393–405, <http://doi.org/10.1144/0016-76492010-047>.
- Esmerode, E. V., H. Lykke-Andersen, and F. Surlyk, 2008, Interaction between bottom currents and slope failure in the late cretaceous of the Southern Danish Central Graben, North Sea: *Journal of the Geological Society*, **165**, 55–72, <http://doi.org/10.1144/0016-76492006-138>.
- Fabricius, I. L., 2007, Chalk: Composition, diagenesis and physical properties: *Bulletin of the Geological Society of Denmark*, **55**, 97–128.
- Fabricius, I. L., and M. K. Borre, 2007, Stylolites, porosity, depositional texture, and silicates in chalk facies sediments. Ontong Java Plateau - Gorm and Tyra Fields, North Sea: *Sedimentology*, **54**, 183–205, <http://doi.org/10.1111/j.1365-3091.2006.00828.x>.
- Gaviglio, P., S. Bekri, S. Vandycke, P. M. Adler, C. Schroeder, F. Bergerat, A. Darquennes, and M. Coulon, 2009, Faulting and deformation in chalk: *Journal of Structural Geology*, **31**, 194–207, <http://doi.org/10.1016/j.jsg.2008.11.011>.
- Gennaro, M., J. P. Wonham, R. Gawthorpe, and G. Sælen, 2013, Seismic stratigraphy of the chalk group in the Norwegian Central Graben, North Sea: *Marine and Petroleum Geology*, **45**, 236–66, <http://doi.org/10.1016/j.marpetgeo.2013.04.010>.
- Hancock, J. M., 1975, The petrology of the chalk: *Proceedings of the Geologists' Association*, **86**, 499–535, [http://doi.org/10.1016/S0016-7878\(75\)80061-7](http://doi.org/10.1016/S0016-7878(75)80061-7).
- Laake, A., 2013, Structural interpretation in color—A new RGB processing technique for extracting geological structures from seismic data: 83rd Annual International Meeting, SEG, Expanded Abstracts, 1472–1476, <http://doi.org/10.1190/segam2013-0079.1>.
- Morozov, P., G. Paton, A. M. Milyushkin, V. V. Kiselev, D. N. Myasoedov, 2013, Application of high definition frequency decomposition techniques on Western Siberia Reservoirs: 75th Annual International Conference and Exhibition, EAGE, Extended Abstracts, <http://doi.org/10.3997/2214-4609.20142716>.
- Pauget, F., S. Lacaze, and T. Valding, 2009, A global approach in seismic interpretation based on cost function minimization: 79th Annual International Meeting, SEG, Expanded Abstracts, 2592–2596, <http://doi.org/10.1190/1.3255384>.
- Pedersen, S. I., T. Randen, L. Sonneland, and Ø. Steen, 2002, Automatic fault extraction using artificial ants: 72nd Annual International Meeting, SEG, Expanded Abstracts, 512–515, <http://doi.org/10.1190/1.1817297>.
- Scholle, P. A., and R. B. Halley, 1985, Burial diagenesis: Out of sight, out of mind!, in *Carbonate Sedimentology and Petrology*, **36**, 135–60, <http://doi.org/10.1029/SC004p0135>.
- Smit, F. W. H., 2014, Seismic stratigraphy, basin evolution and seismic geomorphology of the late cretaceous and earliest paleocene chalk group in the Danish Central Graben: M.S. thesis, Aarhus University.
- Starmer, I. C., 1995, Deformation of the upper cretaceous chalk at Selwicks Bay, Flamborough Head, Yorkshire: Its significance in the structural evolution of North-East England and the North Sea

Basin: Proceedings of the Yorkshire Geological Society, **50**, 213–28,
<http://doi.org/10.1144/pygs.50.3.213>.

van Buchem, F. S. P., F. W. H. Smit, G. J. A. Buijs, B. Trudgill, and P.H. Larsen, 2017,
Tectonostratigraphic framework and depositional history of the Cretaceous–Danian Succession of
the Danish Central Graben (North Sea) – New light on a mature area: Petroleum Geology
Conference Series, <http://doi.org/10.1144/PGC8.24>.

Cordilleran Section - 113th Annual Meeting - 2017

Paper No. 56-4

Presentation Time: 2:35 PM

BASINAL FLUID FLOW THROUGH THE CHALK GROUP IN THE SOUTHERN DANISH CENTRAL GRABEN AS SEEN ON 3D SEISMIC DATA – ANCIENT EXAMPLES OF LARGE SCALE FLUID SEEPAGES

SMIT, Florian W.H.¹, VAN BUCHEM, Frans S.P.², HOLST, Jesper H.¹, LÜTHJE, Mikael¹, ANDERSKOUV, Kresten³, BUIJS, Govert A.J.⁴, WELCH, Michael¹ and STEMMERIK, Lars⁵, (1)Centre for Oil and Gas, Technical University of Denmark, Elektrovej, Building 375, Lyngby, 2800, Denmark, (2)Neftekh, Halliburton, 92 Park Drive, Milton, , Abingdon, OX14 4RY, United Kingdom; Maersk Oil and Gas, Esplanaden 50, Copenhagen, 1365, Denmark, (3)Department of Geoscience and Natural Resource Management, University of Copenhagen, Østervoldgade 10, Copenhagen, 1350, Denmark; Natural History Museum, University of Copenhagen, Østervoldgade 5-7, Copenhagen, 1350, Denmark, (4)Maersk Oil and Gas, Esplanaden 50, Copenhagen, 1365, Denmark, (5)Natural History Museum of Denmark, University of Copenhagen, Copenhagen, DK-1350, Denmark, fsmit@dtu.dk

An integrated seismic geomorphologic, petrophysical, and geochemical analysis has led to the recognition of seismic features of diagenetic origin in the Chalk Group in the Danish Central Graben. A close correlation between the occurrence of the seismic features and the underlying fault systems suggest a genetic relationship, where fluids could ascend along fault planes into the chalk, leading to diagenetic reactions. As a result of tectonic movement and/or high pore pressures, the top seal failed, resulting in an escape of pore fluids into the overburden and subsequent compaction of the chalk. A lower-than-average seismic velocity anomaly atop these seismic features could well indicate: 1) presence of localized high overpressure compartments as a result of fluid seepage and 2) stretching of the overburden due to the compaction of the underlying chalk. Interestingly, large pockmark fields are observed at two stratigraphic levels: firstly, at the top of the Chalk Group, which could represent large-scale syn-sedimentary fluid escape; secondly, within the top seal, gigantic pockmarks are observed which could be related to major basinal fluid expulsion event(s). The findings of this study provide important new insights into the relationships between basinal fluid flow, faults, and diagenesis in chalk. In addition, it shows how fluid seepages affected the seafloor topography.

Acknowledgements

The Danish Underground Consortium partners (Shell, Maersk Oil, Chevron, Nordsøfonden) are kindly thanked for providing seismic and well data and allowing to present this work. This presentation is part of a larger publication as a result of the PhD project.

Session No. 56

[T12. Fluid Flow, Submarine Seeps, and Gas Hydrate Systems: Implications for the Global Carbon Cycle and Seafloor Stability](#)
Thursday, 25 May 2017: 1:30 PM-4:50 PM

Room 319B (Hawai'i Convention Center)

Geological Society of America Abstracts with Programs. Vol. 49, No. 4
doi: 10.1130/abs/2017CD-292534

© Copyright 2017 The Geological Society of America (GSA), all rights reserved. Permission is hereby granted to the author(s) of this abstract to reproduce and distribute it freely, for noncommercial purposes. Permission is hereby granted to any individual scientist to download a single copy of this electronic file and reproduce up to 20 paper copies for noncommercial purposes advancing science and education, including classroom use, providing all reproductions include the complete content shown here, including the author information. All other forms of reproduction and/or transmittal are prohibited without written permission from GSA Copyright Permissions.

Back to: [T12. Fluid Flow, Submarine Seeps, and Gas Hydrate Systems: Implications for the Global Carbon Cycle and Seafloor Stability](#)

[<< Previous Abstract](#) | [Next Abstract](#)

Mega pockmarks within the Upper Cretaceous Chalk Group in the Danish Central Graben: evidence for large-scale outburst of fluids

Florian W.H. Smit^{1*}, Frans S.P. van Buchem^{2**}, M. Lühje¹, M. Hertle², and Lars Stemmerik³

1. Technical University of Denmark, Danish Hydrocarbon Research and Technology Centre, Elektrovej Building 375, 2800 Kongens Lyngby, Denmark
2. Total Denmark, Amerika Plads 29, 2100 Copenhagen Ø, Denmark
3. University of Copenhagen, Natural History Museum of Denmark, Øster Voldgade 5-7, 1350 Copenhagen K, Denmark

* Corresponding author: fsmit@dtu.dk

** Now at Halliburton-Landmark, 97 Jubilee Avenue, Milton Park, Abingdon, OX14 4RW, UK.

A field of mega pockmarks has been documented within Campanian strata of the Upper Cretaceous Chalk Group in the Danish Central Graben. They are recognized as 1-3 km wide U-shaped reflectors, 100 – 250 m deep, that shallow up on all sides, forming several cup-shaped depressions within the Roar Basin. Within the infill, chaotic packages, smaller pockmarks, and possibly seep carbonates are observed. The spatial location of the mega pockmarks is constrained on top of deep Late Jurassic depocenters, as well as deeply rooted normal faults that offset Jurassic strata. It is at this location that Campanian inversion tectonics was at its maximum, and we propose that trapped gas-bearing fluids within the Late Jurassic strata rapidly expanded, causing seal failure and funneling of gases to the Campanian seafloor along the inverted faults. Explosive release of these fluids caused enormous craters to form, which subsequently became reworked by gravity movements, bottom current activity, and renewed expulsion events. This phase clearly predates thermal maturity of the main source rock for present-day hydrocarbon accumulations, the Bo Member of the Farsund Formation, which became mature during the Late Eocene. We therefore suggest that the fluids originated from a combination of thermogenic gas from Lower to Middle Jurassic strata, as well as biogenic gas from organic-rich facies of the Upper Jurassic. This study shows present-day accumulations occur in close vicinity of these expulsion features, and therefore suggest that fluid migration pathways were long-lived.

Acknowledgements

The authors kindly acknowledge the Danish Underground Consortium (Total, Shell, Chevron, and Nordsøfonden) for providing seismic and well data, and the permission to publish these results. The research leading to these results has received funding from the Danish Hydrocarbon Research and Technology Centre under the Advanced Water Flooding program.